MODELING OF CRACK AND CREVICE CHEMISTRY IN LIGHT WATER REACTOR ENVIRONMENTS

by

MAUREEN J. PSAILA-DOMBROWSKI

B.S. Wheaton College
(1982)

S.M. Massachusetts Institute of Technology
(1986)

Submitted in Partial Fulfillment of the
Requirements for the Degree of

DOCTOR OF PHILOSOPHY

at the

MASSACHUSETTS INSTITUTE OF TECHNOLOGY
February 1990

Signature of Author : _____
Department of Nuclear Engineering
January 24, 1990

Certified by : _____
Dr. Ronald G. Ballinger
Thesis Supervisor

Accepted by : _____
Dr. Allan F. Henry
Chairman, Departmental Committee of Graduate Students

MODELING OF CRACK AND CREVICE CHEMISTRY IN LIGHT WATER REACTOR ENVIRONMENTS

by

Maureen J. Psaila-Dombrowski

Submitted to the Department of Nuclear Engineering on the 24th of January 1990, in partial fulfillment of the requirements for the Degree of Doctor of Philosophy in Nuclear Engineering.

ABSTRACT

A mathematical model has been developed that can predict the time-evolution of solution chemistry and electrode potential within cracks and crevices, in any alloy system, exposed to light water reactor (LWR) environments (i.e. dilute solutions and low conductivity) and other systems. Specific processes modeled include : transport due to diffusion, ion migration, and convection (induced by cyclic displacement of the crack walls); homogeneous reactions including equilibrium reactions and radiolysis; heterogeneous reactions, occurring on the walls of the cavity, including anodic and cathodic reactions, precipitation, and chemical dissolution. In relation to cracks, enhanced electrode reaction rates associated with crack tip straining is also incorporated. The number of species or reactions the model is limited only by computing memory and speed. The model has been verified by comparison with simple analytic solutions and other numerical models for more limited systems.

The model has been used to predict the evolution of electrochemical conditions within a crevice exposed to Boiling Water Reactor (BWR) environments for a range of material and environmental variables. The practical goal, in this case, was to evaluate the material and bulk conditions leading to the development of crevice chemistry conducive to stress corrosion cracking (SCC). The crevice was modeled as parallel sided plates constructed of 304 stainless steel and Inconel 600 typical of a piping safe end. It was found that the inclusion of both internal cathodic reactions and solubility limits on metallic ions were necessary for accurate prediction of the electrochemical conditions that develop within the crevice. The dissolution of the major alloying elements (Ni^{2+}, Fe^{2+}, and Cr^{3+}) and minor element Mn^{2+}, was not sufficient to cause polarization or acidification in the crevice because of the low solubility of these elements. Indeed, the conditions developed within the crevice corresponds to alkaline pH and a relatively low potential, equivalent to the corrosion potential of the alloy in the localized environment. These conditions are relatively benign in relation to SCC. The modeling results compare favorably with experimental crevice measurements. However it was shown that under appropriate conditions, chemical dissolution of manganese sulfide (MnS) inclusions to form H_2S could cause a rise in potential without lowering the pH. This is the result of enhancement of cathodic processes within the crevice by the reduction of H_2S, a feature not previously considered in high temperature electrochemistry. The induced change in local chemistry was reversible once the MnS inclusions were consumed. For this case the effect is transient and will not have long-lasting implications. Excursions in bulk conductivity drastically changed the electrochemistry within the crevice causing polarization, acidification and

a large increase in crevice conductivity. Using realistic reduction kinetics, these conditions were maintained even after the excursion was over and the bulk conductivity was restored to its original condition. Thus, new steady state conditions were established within the crevice. The irreversibility of local conditions has two important implications. First, the aggressive environment developed during the excursion may persist despite remedies to bulk coolant. Second, the existence of multiple steady states raises questions concerning the application of steady state analysis to the evaluation of local crack or crevice electrochemistry exposed to LWR environments. The application of hydrogen water chemistry reduced the severity of the conditions generated in the crevice during and after an excursion, but did not completely prevent polarization and acidification from occurring. The chemistry developed during the excursion did not necessarily revert to the original conditions after the excursion was over.

Cracking has been observed to occur within the crevice when the potential and/or conductivity is raised above critical levels. Based on these modeling results, these conditions will be achieved under the following circumstances : as the result of chemical dissolution of MnS inclusions or as the consequence of excursions in bulk conductivity. Additionally, the dissolution of a more soluble minor species could, in principle, induce significant chemistry changes. This latter aspect could not be evaluated fully because of a lack of necessary input data for all the minor elements. In the case of a BWR recirculation inlet nozzle ,which creates a very long crevice, the first two effects are not likely to initiate cracking because : (1) inclusions will be consumed shortly after the initial immersion of the component and the driving force for cracking is not sustained, and (2) the length of excursions in operating reactors is short and aggressive electrochemical conditions does not have sufficient time to develop. However, the dissolution of more soluble species could play a role in the initiation of cracking in this safe end region. Another important factor could be a decrease in temperature (such as during an outage) which would increase the solubility of the cations produced and, thereby, raise the local conductivity within the crevice during the outage period. These conditions may not be reversible with the return to operating temperature.

The investigations carried out in this thesis have lead to some important concerns. In particular, it is necessary to establish : (a)whether the cracking associated with the recirculation safe end is actually due to specific chemistry changes in the crevice, (2) the role of crevice geometry in crevice stress corrosion testing, (3) the role of manganese sulfide inclusions, and (4) the effect of long term plant outages on cracking behavior and the reversibility of the conditions developed during plant outages. It is also necessary to assess the amount and nature of crud buildup in safe ends and to evaluate the effect of this crud on flow in these regions. In addition, this work has stressed the importance and need of basic high temperature experimental data (eg. anodic and cathodic kinetic parameters, diffusion coefficients, equilibrium constants, solubility limits, and stress corrosion cracking susceptibility curves for the relevant alloy/environment systems).

Thesis Supervisor : Ronald G. Ballinger
Title : Associate Professor of Nuclear Engineering and Materials Science and Engineering

ACKNOWLEDGEMENTS

There are a number of people who have helped me during my stay at MIT that I would like to acknowledge. First, I would like to thank Alan Turnbull, a visiting scientist at MIT during 1989, for the aid and support he gave during his stay. His advice and encouragement have been critical in the development of my thesis and my development as a scientist. I have particularly appreciated and benefitted from the numerous discussions that typified our interactions. I have been greatly enriched by our collaboration.

I am deeply grateful to my family for their constant encouragement and help. I would like to thank my husband, David Dombrowski, who provided me with the support I needed to finish this thesis. Not only did he type most of this document, he also put up with the frequent expressions of frustration and discouragement that were part of the process. I would like to thank my parents, Dr. Justin Psaila and Gemma Psaila, for the support and encouragement they have given me throughout my life and, particularly, during these last few months. They have always provided me with a living example of what can be accomplished if one works at it.

I am also grateful to my advisor, Prof. R. Ballinger, for supporting me during my stay at MIT and for his advice and encouragement. He always belived I could do it even when I didn't. Also, I would like to thank Prof. N. Rasmussen for always being available to talk and for introducing me to the difference between a pigeon and a rock dove. I have also benefitted from numerous discussions with Il Soon Hwang.

Cameron Haase-Pettingell, a dear friend, was also very helpful with the thesis preparation and showed her encouragement through numerous care packages and phone calls. Susan Cooper and Margarita Crocker also showed their support also showed their support.

A number of people on the staff of the Nuclear Engineering Department have also been very helpful. Jennifer Gwinn provided invaluable support at a critical time. Clare Egan was always available to answer questions and provide encouragement. Also, Paula Cornelio and Laura Miltner provided word processing aid and advice during the thesis preparation processes.

TABLE OF CONTENTS

LIST OF FIGURES

LIST OF TABLES

Chapter 1

INTRODUCTION

1.1 INTRODUCTORY REMARKS

The cost of corrosion and corrosion protection is extremely high (*1,2*). In the United States alone it is estimated to be over 200 billion dollars per year (*1*). Thus corrosion results in an enormous waste of resources and money. The tremendous cost of corrosion is understandable when one considers that corrosion is probable whenever metals are used in an application. Environmental degradation is common for all alloy systems in many environments. Corrosion phenomena can be divided into two general categories. The first group encompasses general corrosion processes which occur on the bulk metal surface. It includes uniform corrosion, galvanic corrosion, erosion corrosion, and selective leaching. The second group of corrosion processes are localized phenomena that act at specific sites on the metals surface. These processes include crevice attack, intergranular attack, stress corrosion cracking, corrosion fatigue, and pitting.

In this thesis we are concerned primarily with the characterization of the environment and, in particular, the modeling of corrosion and electrochemical processes which develop in the restricted geometries of crevices and cracks. These processes can promote the development of an environments that results in the premature failure by one or more of the above processes. In general, the materials involved may be metals or non-metals. Environments include aqueous with inorganic

or organic solutes, gaseous, or liquid metals (*3*). However, in this work, the primary application will be to alloys exposed to aqueous environments and, in particular, environments typical of Light Water Reactor (LWR) systems

Crevice chemistry is usually different from the bulk environment because mass transport of dissolved species is restricted and little or no convective mixing occurs within the occluded region (*1,2*). Since there is no mixing, the concentration of all dissolved species is controlled by their transport within the region, due to diffusion and ion migration, and the production and consumption of these species either in solution or on the walls. If these changes result in the production of a sufficiently aggressive environment, localized attack may occur and lead to environmentally enhanced cracking (EAC). In either case, prediction of cracking and localized attack within crevices requires a knowledge of the local electrochemical conditions within the crevice (i.e., pH, electrode potential, concentration of dissolved ions, etc.). This information would be used, in conjunction with experimental data defining the environmental conditions necessary to initiate and propagate cracking, to identify regimes of susceptibility or risk.

Stress corrosion cracking (SCC) and corrosion fatigue (CF) are forms of environmentally assisted cracking which result from the synergistic interaction of the mechanical environment (stress) and the chemical environment, often in combination with certain microstructural features. As with the crevice, the chemical environment within the crack is affected by transport of dissolved species, electrochemical processes on the tip and walls of the crack, homogeneous chemical reactions, and precipitation. The distinction is that localized straining at the crack tip can disrupt protective or partially protective films. The mechanical stresses can be present as the result of residual stresses from fabrication and installation and/or stresses resulting from operation. SCC refers to an environmentally assisted cracking process that is

generally considered to occur as the result of a combination of "static" tensile stress, applied or residual, a particular environment and a susceptible material. CF refers to a similar cracking process that involves cyclic loading. It is considered by some that CF is not mechanistically distinctive from SCC (*4*). The stress results in the accumulation of strain at the crack tip which eventually leads to film rupture and crack propagation. The removal of either the chemical environment or mechanical stress often results in the cessation of cracking. Environmentally assisted cracking in aqueous solutions can be promoted by either anodic reaction processes or by hydrogen embrittlement. There are various mechanisms by which the crack is considered to propagate, at least in part, by anodic dissolution mechanisms. The two most popular mechanisms are : (1) film rupture/slip dissolution (as proposed by Ford et al. (*3*)) in which cracking is directly related to the oxidation charge density passed between the film rupture events; and, (2) film-induced cleavage (proposed by Sieradzki and Newman (*5*)) in which cracks initiate in the anodic reaction film and propagate into the metal substrate by a cleavage process. In relation to hydrogen embrittlement the major mechanisms proposed include : (1) hydrogen induced local plasticity in which the normal ductile slip processes are enhanced by absorbed hydrogen; (2) decohesion in which hydrogen acts to lower the fracture strength of atom-atom bonds at the crack tip; and, (3) the formation of brittle hydride phases at the crack tip (*4*). Whichever detailed mechanism is appropriate, knowledge of the local crack tip environment is necessary to predict crack propagation rate since this will determine both the hydrogen supply rate and the anodic reaction rate.

In the nuclear industry, EAC has been a major problem for at least the last fifteen years (*6,7,8,9*). SCC and CF have been the major cause of failures (*5,6*). Crevices have been identified as important sites for SCC initiation in some cases. Premature failures of structural components have occurred in both the primary and

the secondary systems. Components affected include vessel clad and internals, nozzle safe ends, control rod drives, piping valves, fuel cladding, steam generators, turbines, fittings, and heat exchangers (*8,9,10*). These failures have delayed plant startups, caused extensive downtime, and proven expensive to the nuclear industry as a result of the costs of equipment repair, replacement costs, and lost power (*3,7*). Figure 1-1 shows the loss of capacity due to various corrosion and cracking problems. This area under this curve represents a loss of capacity of billions of dollars (*10*). This cost does not include the cost of replacement or repair, nor the cost due to other forms of corrosion that occur in nuclear reactors. These premature failures have resulted in the loss of structural integrity of components and have raised questions regarding the present safety evaluation codes used to predict component life. It is because of these economic and safety concerns that considerable scientific effort has been focused on finding ways to understand, predict, and prevent these forms of localized attack.

Much of this effort has been directed towards the development of a fundamental understanding of the complex interactions involving the material, environment, stress, temperature, and time. With the appropriate use of a quantitative crack growth model, it would be possible to anticipate component failure situations and more effectively deal with and understand any failures that might occur (*1*). As previously discussed, such a crack growth model must include the capability of accurately predicting the local electrochemistry in occluded regions such as cracks and crevices. In order to predict the chemistry within these regions, a model must be developed which can accurately describe the interrelation between the local environment with the bulk environment, and metal that forms the occluded region through the modeling of the transport processes and reactions involving dissolved species within these regions. The development and application of a model that predicts local chemistry based on rigorous mass transport and electrochemical theory is presented in this thesis.

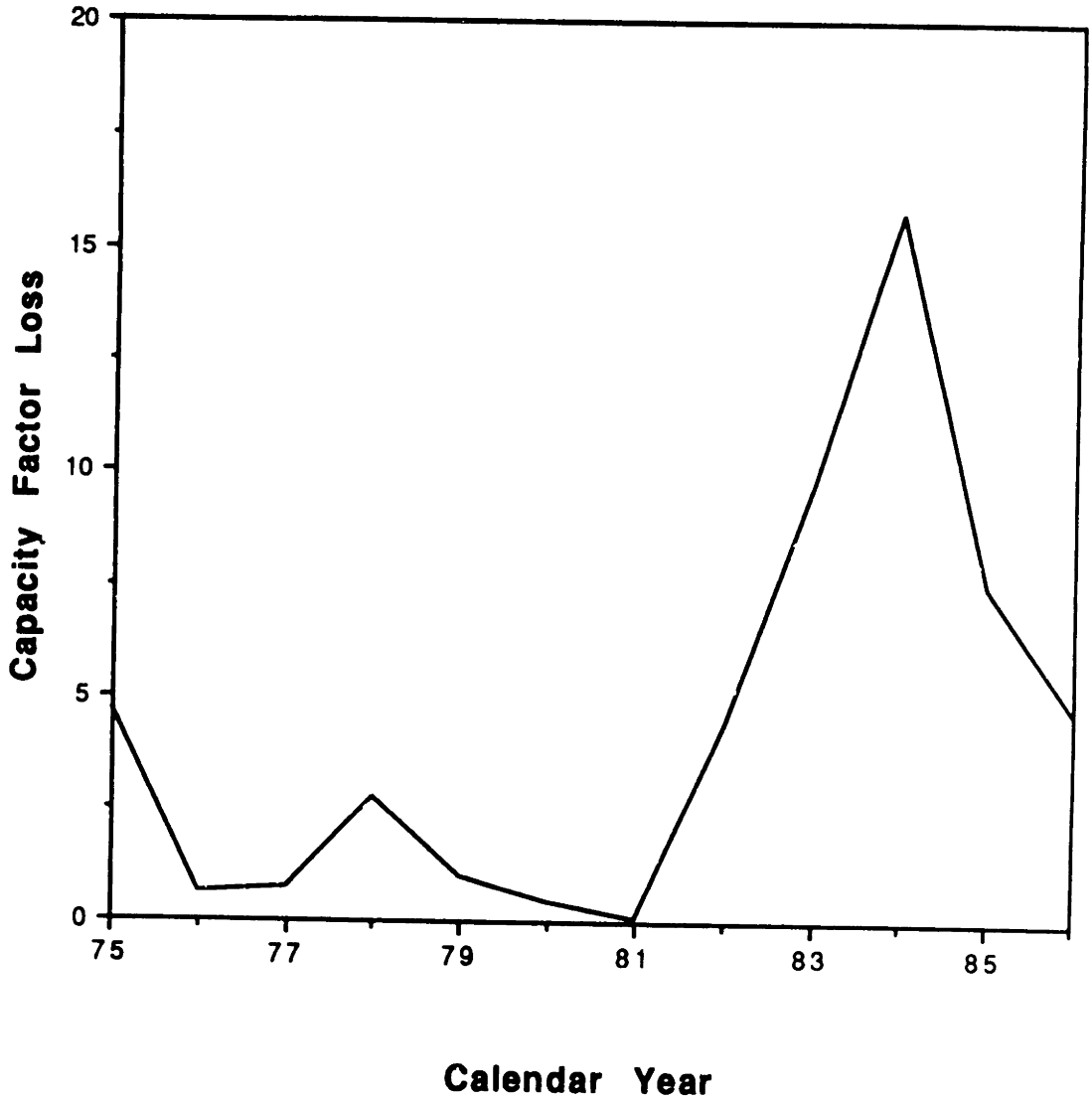

Figure 1-1. Capacity factor loss by calendar year due to pipe cracking (*9*).

1.2 THESIS DESCRIPTION

The goal of the research project was to develop a model which can accurately predict the local chemistry within cracks and crevices in any alloy systems exposed to light water reactor environments. This required a model that is both fundamentally rigorous but flexible. Rigor is essential to ensure confidence in its predictions and because too many simplifications or assumptions would impose serious limitations on the applicability of the model and thus limit its application. The model must be flexible in order to be able to model cracks or crevices in different alloy systems which may involve different dissolved species and different reactions processes.

The model that has been developed and is presented in this thesis has the following features:

- It is a transient model. Thus the time dependent concentration and potential profiles within the cavity region can be analysed as well as the effect of changes in bulk conductivity and potential on these profiles.

- Transport modes included in the model are:
  - -- diffusion,
  - -- ion migration,
  - -- convection induced by cyclic pumping of crack walls.

- Parallel sided or tapered geometries may be used.

- Any number of species may be used limited only by computer memory and speed.

- Any number of homogeneous reactions may be incorporated.

- Any number of anodic and cathodic reactions at the crack tip or on the walls may be used. These reactions may be dependent on the local concentration of species or potential.

- Solubility limits may be applied to any dissolved species.

- The production of species by radiolysis of water may be included.

- Chemical dissolution of inclusions may also be incorporated.

The inclusion all these transport and reaction processes should result in a model capable of accurately predicting the environment within cracks and crevices exposed to reactor environments. However, the accuracy of the predictions made by this model is limited by the accuracy of the necessary input data.

In the following chapters the model is described in detail and a particular application of the model is presented. Chapter 2 presents a literature review which allows one to distinguish this model from other models which have been developed. Chapter 3 presents a detailed mathematical description of the model, the numerical solution of this mathematical model, and its verification. Chapter 4 describes the application of the model to assessment of the chemistry developed within a crevice for a variety of environmental and material variables. Two important variables considered

are the dissolution of soluble or partially soluble species from the metal and excursions in bulk conductivity. The implications of these results to the cracking susceptibility of a typical BWR recirculation inlet safe-end crevice are described in Chapter 5. In Chapter 6, the importance of the results and the broad implications of these results in understanding environmentally enhanced cracking is discussed. Some details of the proposed applications of the model to these cracking problems are also presented. Conclusions and future work are described in Chapter 7.

1.3 REFERENCES

(1) M.G. Fontana and N.D.Greene, Corrosion Engineering, McGraw-Hill, New York, 1978.

(2) J.C. Scully, The Fundamentals of Corrosion, Pergamon Press, New York, 1975.

(3) F.P. Ford, Mechanisms of Environmental Cracking in Systems Peculiar to the Power-Generation Industry, EPRI, NP-2589, Sept. 1982.

(4) F.P. Ford, "The Crack-Tip System and Its Relevance to the Prediction of Environmentally-Assisted Cracking", International Conference on Environment-Induced Cracking of Metals, ASM Int., NACE and AIME,Kohler, Wisconsin, Oct. 1988.

(5) K. Sieradzki and R.C. Newman, Phil. Mag., vol. 51, pp. 45-132, 1985.

(6) L.G. Ljungberg and D. Cubicciotti, Corrosion, 41, pp 290-295, May 1985.

(7) S.H. Bush and R.L. Dillon, in Stress Corrosion Cracking and Hydrogen Embrittlement in Iron-Base Alloys, Uniew-Firminy, France, pp 61-79, June 1973.

(8) J.J.A. Roberts, Structural Materials in Nuclear Power Systems, Plenum Press, New York.

(9) D.W. LeShey, et al., Nuclear Unit Operating Experience : 1985-1986 Update, EPRI, NP-5544, 1987.

(10) R. Jones, Seminar at M.I.T., November 13, 1989.

Chapter 2

LITERATURE REVIEW OF CRACK AND CREVICE MODELING

2.1 INTRODUCTION

A critical review of the literature on the mathematical modeling of crack, crevice, and pit electrochemistry is presented in this chapter. Two extensive literature reviews have already been done giving a detailed description of each modeler's work (*1,2*). Unlike these reviews, this chapter examines previous modeling efforts in order to evaluate whether the models developed are sufficiently rigorous and flexible for specific application to the crevices and cracks in a nuclear power station. A number of the models developed were appropriate for the specific case for which they were developed, but are not appropriate for the environment or alloy systems of interest in this thesis. The purpose of this review is to establish the current state of modeling and to present the model in this context.

The aim of most models of crevice, crack, and pit electrochemistry is to predict the solution chemistry and potential within the occluded region of interest. This information, coupled with "known" separately determined electrochemical behavior of the material under these conditions, can be used as input into crack growth models and in predicting localized corrosion. Specifically, models ideally try to predict the concentration of dissolved species and/or electrode potential as a function of position and, possibly, time within the cavity region. These variables will be a function of bulk solution composition, occluded region geometry, external electrode potential, kinetics

of electrochemical reactions, homogeneous reactions, etc. The development of an appropriate model for a particular application is nontrivial and requires a great amount of information during the model development (in order to construct an accurate model) and in its the application. A complete description of the information necessary to develop, formulate, and apply a mathematical model to predict localized chemistry within cavities is presented in Appendix A. As described there, the accuracy and appropriateness of a model depends to a large extent on the assumptions and approximations which are made in its development. Indeed, the model is inherently limited by these assumptions and in many cases the assumptions are so significant as to make the model inappropriate for application to the problem for which it was designed. In order to better understand some of the assumptions made and thus gain an appreciation of the validity and relevance of previous models, a general description of the theory used will be presented here. A more detailed description is presented in Chapter 3.

The models that have been developed range from very simple to the very complex, requiring analytic solutions or rigorous numerical schemes respectively. Though the models vary greatly, they are all derived from the same fundamental governing theory. This theory describes the mass transport, production, and consumption of solute species in dilute electrolyte solutions. The transport of dissolved aqueous species is controlled by diffusion, ion migration, and convection. This is mathematically detailed in the flux equation., The flux of species i, J_i , is given by

$$J_i = C_i v - D_i \frac{\partial C_i}{\partial x} - \frac{z_i D_i F}{RT} C_i \frac{\partial \phi}{\partial x} \qquad (2-1)$$

where D_i = diffusion coefficient of species i

C_i = concentration of species i

z_i = charge of species i

μ_i = ionic mobility of species i

F = Faraday's constant

ϕ = electrostatic potential

V = velocity of solution

R = gas constant

T = temperature (K)

The first term represents convection which represents transport due to motion of the solvent fluid. The second term is the diffusion term which represents transport as the result of a gradient in concentration. Ion migration, mathematically represented by the third term, is the transport of charged species due to a gradient in potential. The one dimensional form of the equation is given here since that is the form typically used by modelers.

Mass is conserved within the cavity, and for a species i this is described by

$$\frac{\partial C_i}{\partial t} = -\frac{\partial J_i}{\partial x} + \sum_j R_{i,j} \qquad (2-2)$$

where t = time

R_i = rate of production or consumption of species i by reactions occurring in solution

Substituting Equation 2-1 into Equation 2-2 results in the full form of the mass balance equation

$$\frac{\partial C_i}{\partial t} = D_i \frac{\partial^2 C_i}{\partial x^2} + \frac{z_i D_i F}{RT} \frac{\partial}{\partial x}\left(C_i \frac{\partial \phi}{\partial x}\right) - \frac{\partial}{\partial x}(C_i v) + \sum_j R_{i,j} \qquad (2-3)$$

Where $\partial C/\partial t$ is the time rate of change of species i at any position within the region. The reaction rate term normally represents homogeneous reactions occurring in the solution. Reactions such as electrochemical reactions, precipitation, and chemical dissolution which occur on the walls of the cavity normally constitute the boundary conditions in the appropriate dimension. However, in principle, they can be incorporated into the one-dimensional model by averaging over the width of the cavity region. The resulting term is implicitly represented by R_i in Equation 2-3 The inclusion of homogeneous and heterogeneous reactions are important in many modeling applications because these reactions can significantly alter the local electrochemistry.

The potential is governed by Poisson's equation which can be described by

$$\nabla^2 \phi = \frac{F}{\varepsilon} \sum_i z_i C_i \qquad (2-4)$$

where ε is the permitivity of the solution. The permitivity is a very small number and therefore F/ε is very large. This implies that slight deviations from electrically neutral solution (i.e., $\Sigma_i z_i C_i = 0$) are restored by very large forces. Thus, Poisson's equation is usually approximated by the electroneutrality equation

$$\sum_i z_i C_i = 0 \qquad (2-5)$$

in most models. An additional equation frequently used by modelers is that for the current density in electrochemical solutions. The current density in the solution is proportional to the fluxes of the species in solution and is given by

$$I = F \sum_i z_i J_i \qquad (2-6)$$

where I is the current density.

Equations 2-1 through 2-6 provide a complete description of the transport, production, and consumption of dissolved species within a crack, crevice, or pit. When used with appropriate boundary conditions and initial conditions, where appropriate, they provide a consistent set of equations that can be used by modelers. Although it is not intrinsically difficult to construct models based on the above equations, the solution of the stiff, nonlinear set of equations that result is not trivial and requires advanced numerical techniques. Indeed, it is the difficulty of numerical solution that is often the limiting factor in model development. Since these governing equations have been known for decades, the development of crack and crevice modeling primarily reflects advances in computing power readily available to the modeler.

A lack of computing power often results in a series of approximations to the fundamental equations some of which have validity but which in many other cases introduce significant uncertainties. In making any assumptions that would simplify the solution of the problem, the limitations in applicability of the model developed with these assumptions must be clearly understood. In general, the approximations made include : (1) a reduction in dimensionality of the problem from three dimensions to one dimension; (2) steady-state analysis of electrochemistry in cavity; (3) simplification or exclusion of certain transport processes; and (4) exclusion of various reaction processes. Often a number of these simplifications are made in combination. While the simplification in dimensionality and the use of steady-state analysis can be appropriate in many cases, the exclusion of transport (especially diffusion and ion migration) and reaction processes often is not. When metal is immersed in water, electrode reactions

(both anodic and cathodic) occur on its surface. In occluded regions, these reactions, combined with poor mixing, result in chemistry changes (i.e., deaeration, acidification, etc) (*3,4*). The establishment of a concentration and/or a potential gradient within these regions will lead to transport due to diffusion **and** ion migration. Reactions, both electrode and homogeneous, occur in the cavity region. While simplification concerning these processes may have been justifiable in the past due either to a lack of understanding of the importance of different processes or lack of computing power it is unnecessary now. It is clear that, in order for a model to be rigorous and of wide applicability it must include, in general, at least transport due to diffusion and ion migration (as long as convective effects within the cavity are negligible), homogeneous reactions, and anodic and cathodic reactions.

In this literature review, the models are grouped according to the transport modes included and time dependence of the model. This grouping broadly follows the historical progression of modeling as computing power has increased and interest in this problem has grown.

2.2 LITERATURE REVIEW

As discussed in the last section, models have been developed with a range of different assumptions and approximations. Indeed, it is possible to classify a model according to its complexity and the approximations made during its development. In this section, the previous modeling efforts are reviewed. They have been classified into four groups. The first group of models discussed are simple steady-state models which are usually based on one form of transport (i.e., diffusion, ion migration, or convection) or very simple coupled transport. Usually no homogeneous reactions were

incorporated into these models. The second group of models incl advanced steady state models and simple transient models. Steady state models generally incorporated multiple homogeneous reactions. Transient models incorporated a few reaction terms but added and subtracted the transport equations to remove the homogeneous reaction rate terms from these equations in order to make the system of equations less stiff. For example, if the system of interest involves two dissolved species (A and B) which react with one another, the governing mass transport equations (given by Equation 2-3) can be added together or subtracted from one another in order to remove the homogeneous reaction rate terms (given by $R_{i,j}$ in Equation 2-3). A single mass transport equation would result involving transport of both species A and B and the equilibrium relationship must be used as the additional equation necessary to solve for the unknown concentrations. This addition or subtraction of the transport equations limits the application of the model to systems involving the **same** homogeneous reactions. The third group of models include advanced transient models involving convection. The convective term is the result of pumping due to movement of the crack wall. In the last part of the review, the most recent modeling efforts are reviewed in order to more clearly set the model presented in this thesis in the appropriate context.

2.2.1 Simple Steady-State Models Involving One or Two Modes of Transport

Early efforts to model crack, crevice, or pit electrochemistry appeared in the 1960's and early 1970's. These models were very simple and usually incorporated only one mode of transport, such as diffusion, ion migration, or convection, or were in very simplified cases involving both diffusion and ion migration (*5-30*). Rarely were

homogeneous reactions, solubility limits, and cathodic reactions considered. These types of transport problems were numerically straightforward to solve. This simplified type of modeling continued until about 1980. The next few paragraphs will detail a few models typical of each simplified approach. The models will be present and a critique of the general approach will be made at the end of each section.

Migration Models

A number of steady state models have been developed that assume that mass transport within the cavity regions occurs only by ion migration (*5-14*). This assumes that there are no concentration gradients within the cavity and the fluid velocity is zero everywhere. Hence, no diffusion or convection occur within the occluded region. Substituting Equation 2-1 into Equation 2-6 and removing the diffusion and convection terms yields the governing equations that are generally used in these models

$$I = \left[- \frac{F^2}{RT} \sum_i z_i^2 D_i C_i \right] \frac{\partial \phi}{\partial x} \qquad (2-7)$$

or

$$I = \kappa \frac{\partial \phi}{\partial x} \qquad (2-8)$$

This is simply a form of Ohm's law. Laplace's equation is used to solve for the potential distributions. Laplace's equation, in one dimension, is given by

$$\frac{\partial^2 \phi}{\partial x^2} = 0 \qquad (2-9)$$

The current density within the cavity is considered to be a function of position in many migration models. The goal of these models was, usually, to predict the potential distribution within the crack or crevice region.

The first of the migration models was developed by Hines (*5*). In this model it was assumed that anodic dissolution occurred at the tip and on the walls of a wedge-shaped crack. The crack tip was rounded with a radius dependent on crack length. All cathodic reactions occurred on the external surface outside the crack. The model was used to predict the potential drop down a stress corrosion crack as a function of the anodic current, crack depth and radius of the crack tip, and crack mouth opening.

Two later migration models, developed by Gutman (*6*) and by Bignold (*7*), considered migration in a paralleled sided crack where anodic dissolution occurred at the tip and cathodic processes occurred on the walls. It was assumed that no homogeneous reactions occurred within the crack region. Gutman used his model to predict the type of polarization (anodic or cathodic) that occurred within the crack when the external surface is at the free corrosion potential and under cathodic polarization. Bignold considered the cases of free corrosion potential and anodic polarization.

Vicentini et al. developed a model to predict the potential distribution and current density variation along a cylindrical crevice (*8*). Ohm's law was used to develop this one dimensional model in which current was averaged over the width of the crevice. In this case, the current density at the crevice tip was ignored. The resulting equations were solved numerically.

Two models were developed to predict the potential distribution within pits. Newman et al. developed a model based on Laplace's equation in an effort to predict the potential within a hemispherical corroding pit (*9*). The equations were solved numerically to give equipotential and flux curves within the model pit. Nisancioglu and Holtan developed a model based on Ohm's law to predict the potential drop within a cylindrical pit (*10*). The walls of the pit were assumed to be inert. An analytic solution was developed for the potential drop down the pit.

Doig and Flewitt developed a model to predict the distribution of potential and electrode reactions within a parallel-sided stress corrosion crack (*11,12*). Their model assumed that anodic dissolution reactions occurred only at the tip and that only cathodic reactions occurred on the walls of the crack. Ohm's law was used as the basic transport equation with Tafel expressions for the anodic and cathodic current densities. Tafel equations relate potential to the log of the current density for a particular electrode reaction. A quasi-analytic/numerical approach was taken to solve the resulting differential equations. An important step in the solution processes was the assumption that the slope of the potential approached zero as the potential approached the free corrosion potential. Melville criticized this assumption suggesting that it is valid only for semi infinite cracks (*13,14*).

Melville developed (in his opinion) a more appropriate analytic model (within the constraints of the assumption of Ohm's law) which predicted the potential distribution within a stress corrosion crack (*13,14*). The model incorporated a corrosion current density that was a function of potential along the walls of the crack. The width of crack could be varied linearly with crack length. The potential distribution within the crack was described by modified Bessel functions of the first and third kind of orders zero and one.

The key assumption in all of these models is that concentration gradients within an occluded region are negligible and, therefore, diffusion can be ignored. This is only valid at short times when the solution within the cavity will be similar to the bulk concentration, such as when a pre-cracked specimen is initially immersed. However, the potential gradient and the resulting ion migration and electrochemical reactions will cause a rapid change in the concentration of species within the cavity region resulting in concentration gradients. In this case Ohm's law is no longer valid. Thus, these simple migration models cannot accurately predict electrochemical conditions within cavities.

Diffusion Models

A number of models have been developed which incorporate transport due only to diffusion (*15-21*). This reduced the flux, as given in Equation 2-1, to

$$J_i = - D_i \frac{\partial C_i}{\partial x} \qquad (2-10)$$

in one dimension. The simplified mass balance equation, derived from Equation 2-3 under steady state conditions is

$$D_i \frac{\partial^2 C_i}{\partial x^2} + \sum_j R_{i,j} = 0 \qquad (2-11)$$

In the early diffusion-based models developed by Falta et al. (*15*), Tester and Isaacs (*16*), and Galvele (*17,18*), Equation 2-10 was used as the governing transport

equation. Since this equation was used, homogeneous reactions occurring within the crevice could not be accounted for in any mathematically correct way. Indeed, Faita et al., and, Tester and Isaacs made no attempt to account for any homogeneous reactions occurring in their transport models. Galvele attempted to account for homogeneous reactions by incorporating the equilibrium relations as part of the system of equations used to solve for the concentration of species. Of the models developed that incorporated diffusion as the only mode of transport, the model developed by Turnbull (*19*) is the most advanced because it incorporated both homogeneous and electrochemical reactions occurring along the walls and tip of the parallel-sided crack or crevice (*19*). Steady-state transport equations were used for each of the four species, Fe^{2+}, $FeOH^{+}$, H^{+}, and OH^{-}, including reaction terms appropriate for the hydrolysis of Fe^{2+} to $FeOH^{+}$. The electrochemical reactions included dissolution of Fe to form Fe^{2+} and cathodic reduction of water and H^{+}. In order to remove some of the reaction terms the system of equations was simplified by adding and subtracting the mass balance equations (Equation 2-11 for each species) and assuming equilibrium, as described earlier in this chapter. The system of equations was solved numerically. The model was extended to take into account the effects of alloying elements and the buffering action of sea water.

These diffusion models assume that the potential drop down the model crack or crevice is small and thus ion migration terms can be neglected. The potential drop in a cavity depends on a number of variables including the conductivity of the solution in the bulk and the cavity, the geometry of the cavity, and, of course, the current within the cavity. This would only be valid when the conductivity of the solution is very high or when the current density within the crevice is extremely low. These factors, the conductivity and the current, are dependent on the conditions that develop within the cavity region and it is therefore impossible to establish general criterion for when

these conditions would occur. The validity of the assumption can only be tested by solving the relevant mass transport equations with both diffusion and ion migration or by experimental measurement of potentials within the cavity.

Convective Models With No Homogeneous Reactions

Few models have been developed that incorporate only convection as a mode of transport within the occluded region (*22-25*). There has been no generalized approach to convective transport models. Hartt et al. (*22*) attempted to evaluate how fatigue variables might influence mixing between the crack and bulk solutions. This evaluation consisted of calculating the average velocity of the fluid at the crack mouth . This calculated velocity was **not** the velocity of the fluid in the crack but the fluid velocity generated at the mouth of a corrosion crack due to the cyclic displacement of the crack walls. The velocity was used to calculate the net momentum of the fluid during crack wall displacement. Hartt et al. considered that the net momentum should influence the amount of mixing that occurs at the crack mouth. The momentum was found to be a function of the crack opening angle, frequency, mean stress, and crack length. The importance of the calculated fluid momentum on the chemistry within the crack would depend on the amount of external flow past the mouth of the crack. The model does not attempt to predict the chemistry within a fatigue crack. It's purpose is to predict what factors may be important in the development of electrochemistry within the crack.

Taunt and Charnock (*23,24*) developed a model to predict the concentration of a reactant within a corrosion fatigue crack based on convective transport. The model assumes that there is perfect turbulent mixing within the crack, resulting in uniform composition, and that the bulk solution is fast flowing past the mouth so that each load

cycle draws fresh fluid into the crack. Expressions used to calculate the opening at the crack tip and mouth as a function of time allowed calculation of the average displacement and the amount of fluid expelled and replaced. The effects of specimen type, crack length, stress ratio, maximum stress intensity factor, and frequency on the concentration of the reactant was evaluated.

This assumption of turbulent mixing is only valid if the Reynold's number, as given by

$$Re = \frac{(velocity)(width)}{kinematic\ \ viscosity} \qquad (2\text{-}12)$$

within the cavity is greater than 1000 (for parallel plates) (*25*). Assuming a crack width of approximately 10 μm and a kinematic viscosity of 10^{-5} m^2/s (air at room temperature) the velocity of fluid within the crack would have to be 10^3 m/s or three times the speed of sound in air. A similar calculation can be done for water, where the kinematic viscosity is 10^{-3} m^2/s, resulting in velocities greater than 100 m/s being necessary for turbulent flow. These velocities are unrealistic within a crack. Therefore, the flow within a crack is laminar and the electrochemistry developed within this region cannot be modelled by convective transport alone.

Diffusion and Migration Models With No Homogeneous Reactions

The last group of models that will be presented in this section are the first attempts at combining the transport processes of diffusion and ion migration in a steady state model (*26-30*). These models were generally simple transport models that ignore any homogeneous reactions that might take place. The steady state model is

developed by using the flux equation, as described by Equation 2-1, in one dimension without the convection term. Thus the governing transport equation is

$$J_i = - D_i \frac{\partial C_i}{\partial x} - \frac{z_i D_i F}{RT} C_i \frac{\partial \phi}{\partial x} \qquad (2-13)$$

There are two different types of models that fall in this group.

The first type, developed by Oldfield and Sutton (*26,27*), separated the effects of transport due to diffusion and ion migration to model the electrochemistry within a crevice. The model is based on a four stage mechanism for crevice corrosion. The four stages include : (1) oxygen depletion within the crevice; (2) anodic dissolution resulting in eventual acidification within the crevice; (3) breakdown of the passive film resulting in rapid corrosion; (4) propagation of crevice corrosion. The model uses the first three stages of this crevice corrosion mechanism separately to try to identify parameters associated with the alloy, environment, and crevice geometry that might control crevice corrosion. In the first stage, the time necessary to deplete the oxygen within the crevice (t_d) and the distance which oxygen can diffuse into the crevice in this time (δ_d) are calculated. Modeling of the second stage of crevice corrosion is more complicated. The time to decrease the pH from its initial bulk value to the critical value for passivity breakdown (pH_c) is determined by calculating the time necessary to change the pH a small amount, ΔpH. To do this it is necessary to calculate the rate of production of various ions in the crevice (using Faraday's law) and the amount of acidification resulting from the precipitation of chromate ions which is necessary to produce the necessary change in pH. Thus a time for the ΔpH can be calculated. The effect of migration on this value is taken into account and an estimate of diffusion effects is calculated. These effects are used to make corrections on the pH change that occurs in a certain time and, therefore, alter the time necessary to change

the pH by ΔpH. The third stage, passivity breakdown, is accounted for by assuming that the critical solution chemistry (i.e., pH) for breakdown and propagation of corrosion is known. The model does not give an accurate representation of behavior within a crevice since the transport and reaction processes are separated. In the real crevice situation transport and reaction processes occur on a continual basis. Also, some important reactions which greatly affect the pH (i.e., reduction of water or H^+ ions and water equilibrium) are not included. Since the model is based on the calculation of pH, the lack of these reaction processes is a serious limitation.

The other general type of steady-state diffusion/migration model developed tried to solve the coupled diffusion/ion migration equations. These equations were solved, in part, analytically. The flux equation as given by Equation 2-12 was assumed to be linear for **non-reacting** species (i.e., ϕ is not a function of the concentration of species in solution). The equation was then integrated for these **non-reacting** species (*28-30*). The resulting analytic expression for these **non-reacting** species is the Boltzman's distribution given by

$$C_i = C_{i,bulk} \exp\left[- \frac{z_i F \phi}{RT} \right] \qquad (2-14)$$

The major fault with these models (based on Boltzman's distribution) is that the assumption of linearity of the flux equation is incorrect. The error in this assumption is explained in detail in Appendix B. To summarize, this assumption is incorrect because the potential is a complex function of all the charged species in solution. Thus, the flux equation is **nonlinear**. Since the flux equation is nonlinear it cannot be directly integrated and, therefore, the Boltzman's distribution that results from this equation is incorrect. Also, in these models no homogeneous reactions are allowed to occur.

Vermilyea and Tedmon (*28*) developed such a model to predict the concentration and potential variation in a crevice. In this model, the current is carried by a cation and an anion is included to balance charge. The concentration of the anion is assumed to be given by Boltzman's distribution. Because of charge neutrality, the concentration of each of the charge carrying ions is assumed to be equal. The potential distribution is derived from Ohm's law. The Boltzman's distribution is substituted into this potential gradient and the resulting equation integrated to get the potential distribution. This model is mathematically and physically unsound because of the use of Boltzman's distribution, Ohm's law, and the lack of homogeneous reactions, cathodic reactions and the assumption of inert walls.

Ateya and Pickering (*29*) developed a model to predict the electrochemical conditions within a crack undergoing cathodic hydrogen charging. H^+ ions and an anion are considered. The Boltzman distribution was assumed for the non-reacting anion. Since there are only two ions and electroneutrality must hold the flux equation (Equation 2.-12) for the non-reacting ion was used to derive an expression for the potential. This model is invalid because of its use of Boltzman's relationship, lack of homogeneous reactions, and the lack of any other electrochemical reaction other than H^+ reduction (e.g., water reduction, anodic processes, etc.).

The most advanced example of these models was developed by Beck and Grens II (*30*). This steady state model predicted the concentration of three dissolved species (an anion, a cation, and H^+) and the potential within a stress corrosion crack. The concentration profile of the non-reactive cation is obtained using the approach described above. The concentration of the other species and the potential were solved numerically using iterative techniques. Because of the lack of homogeneous reactions and the assumption of a linear flux equation this model was generally invalid, but

considering that this model was published in 1969, these modelers were obviously ahead of their time.

2.2.2 Advanced Steady-State Models and Transient Models Involving Diffusion and/or Migration

In the previous section the simple steady-state transport models which first appeared in the literature were reviewed. These models were often based on only one transport process (i.e., diffusion, ion migration, or convection). Those coupled diffusion/ion migration models that did appear involved either the separation of these transport processes or an unjustified assumption in order to simplify the equations for solution. Also, homogeneous reactions were generally ignored as well as many of the electrochemical processes that occur. Though these models were generally not comprehensive enough to accurately predict the electrochemistry, they represent a first attempt at such predictions. In the mid 1970's and 1980's as modeling of transport in cavity regions became more prevalent as the desire for the accurate prediction of local electrochemistry within cracks and crevices increased, more advanced steady state and simple transient models were developed (*31-46*). The governing equation used in the simple transient diffusion models is given by

$$\frac{\partial C_i}{\partial t} = D_i \nabla^2 C_i + \sum_j R_{i,j} \qquad (2\text{-}15)$$

For the two dimensional diffusion model that was developed, only homogeneous reactions were included. In the case of a one dimensional model, reactions occurring on the walls were included. Turnbull developed a series of analytic solutions to simplified forms of

Equation 2-15 (*31*). These solutions involved only oxygen in solution in the model crack and were a prelude to more elaborate and accurate models that were developed later.

Alkire et al. also developed an analytic diffusion model (*32*). This model involved one species being transported by one dimensional diffusion but without any homogeneous reactions. A more elaborate diffusion model was later developed by Alkire and Siitari in which the electrochemistry within a crevice was modeled assuming transport by diffusion but the electrochemical reactions that occurred on the walls were potential dependent (*33*). The potential was calculated using Ohm's law. It should be recalled that Ohm's law is inherently invalid because concentration gradients are present. Other limiting factors of these models are the fact that transport due to ion migration and homogeneous reactions are ignored.

More advanced steady state models were developed which incorporated the transport of many species as the result of diffusion and ion migration as well as homogeneous and heterogeneous reactions involving these species (*34-38*). The governing equation in this case is derived from Equation 2-3 for steady state diffusion and ion migration in one dimension. Thus, the equation used in these models is

$$D_i \frac{\partial^2 C_i}{\partial x^2} + \frac{z_i D_i F}{RT} \frac{\partial}{\partial x}\left(C_i \frac{\partial \phi}{\partial x}\right) + \sum_j R_{i,j} = 0 \qquad (2\text{-}16)$$

Gravano and Galvele developed a model to predict the electrochemical conditions within pits (*34*). The pit walls were assumed to be inert. This is not an accurate approximation unless the passive current on the walls of the pit is many orders of magnitude less than the current at the bottom surface of the pit. Also, cathodic reactions were ignored in the model pit. The transport equations for the dissolved

species were added and subtracted in order to remove the reaction rate terms from the equations thus making the system of equations less stiff. Boltzman's distribution (Equation 2-14) was used for the concentration of non-reacting species. The system of equations was solved numerically. The limitations of this model stem from the omission of electrochemical reactions occurring on the walls and the use of Boltzman's distribution for non-reacting species. The application of the model to other systems is restricted because of the addition and subtraction of transport equation. Despite these limitations this model did provide some important insights into pit behavior.

The models developed by Turnbull and by Danielson to predict the electrochemistry within parallel-sided cracks were very similar (*35-38*). The steady-state transport equations incorporated diffusion and ion migration with homogeneous reactions and heterogeneous electrochemical potential dependent fluxes occurring on the walls and averaged over the width of the crack. These equations were added and subtracted in order to remove the homogeneous reaction rate terms from the transport equations resulting in multiple species transport equations. Electroneutrality was used as the equation to solve for potential. The equilibrium relationships were substituted as equations for unknown concentrations. For non-reacting species, an exact analytic solution (Boltzman's distribution) was used which was derived assuming that the flux equation was linear. The implications of this and reasons for its invalidity were explained briefly in Section 2.2.1 and are explained in detail in Appendix A. Thus, a system of transport equations, equilibrium equations, and analytic type equations was solved numerically.

The models described in the previous paragraph were greatly advanced compared to other models developed in the same period. They were relatively rigorous since they included the transport effects of both diffusion and ion migration along with both homogeneous reactions occurring in the crack solution and anodic and cathodic reactions

at the crack tip and on the walls. The assumption of Boltzman's distribution (Equation 2-14) for the non-reacting species is the only part of these models that is not rigorous. The development of these complex, many species, models was a big step in understanding the complexity of electrochemistry within occluded regions.

A few simple transient diffusion/migration models were developed during this period of time. These models were all one dimensional. The governing transport equation for these models could be derived from Equation 2-3 by ignoring the convective transport term. The resulting transport equations that was used is given by

$$\frac{\partial C_i}{\partial t} = D_i \frac{\partial^2 C_i}{\partial x^2} + \frac{z_i D_i F}{RT} \frac{\partial}{\partial x}\left(C_i \frac{\partial \phi}{\partial x}\right) \qquad (2-17)$$

The first transient model incorporating the effects of both diffusion and ion migration was developed by Shuck and Swedlow (*39,40*). This model incorporated only three species : hydrogen ions, hydroxide ions, and chloride ions. Hydrogen ions were electrochemically produced on the walls and presumably the crack tip at a constant rate by oxide formation. The effect of crack geometry on the concentration of species was examined for three specific cases : rectangular, hyperbolic, and pie-shaped. The model showed some differences in local electrochemistries initially for these different geometries, but there was little difference at steady state. This model ignored cathodic reactions occurring within the crack and the lack of potential dependence of electrochemical reactions. The model was applied to very simple systems involving only two or three species.

A more rigorous transient model was developed by Herbert and Alkire (*41*) for predicting the electrochemistry in crevices in aluminum alloys. This model incorporated diffusion, ion migration, homogeneous equilibrium reaction, and potential

dependent heterogeneous reactions (both anodic and cathodic). In this case, some of the transport equations were added and subtracted (as described earlier in this chapter) and an equilibrium relationship was used. Not all charged species were allowed to migrate under the influence of the potential field; only the inert ions such as Cl^- and Na^+. This is a curious assumption considering that the H^+ and Al^{3+} ions which are considered are very likely to migrate because of high mobility and large charge, respectively. This assumption is inherently not valid but the effect on the accuracy of the predictions is unknown.

Another transient diffusion and ion migration model was developed by Fu and Chan (*42*). This model assumed that the walls of the crack were inert and that no homogeneous reactions occurred within the region of interest. Also, Ohm's law was assumed valid and used to calculate the potential distribution in the cavity region. These assumptions make the model unrealistic.

A few of the models that were developed during the mid 1980's seemed overly simplistic relative to the other models developed during this period. The model developed by Bertocci (*43*) assumed that the walls of the model crack were inert and no cathodic reactions were allowed to occur. It is unclear from the paper whether homogeneous reactions were included. Even if homogeneous reactions were included, they could not have been incorporated correctly since the flux equations (as shown in Equation 2-10) were used as governing equations in this model; homogeneous reactions cannot be incorporated correctly using the flux equation, the mass balance equation (given in Equation 2-3) must be used. The model is more typical of models developed in the mid 1970's. Another model developed by Edwards (*44*) also ignored homogeneous reaction and electrochemical reactions occurring on the walls. Lastly, a model developed by Alkire, Tomasson, and Hebert (*45*) assumed transport of species only by diffusion and calculated the potential distribution using Ohm's law. Both of

these assumptions lack rigor, as discussed in the previous section, and create uncertainty in the prediction. This latter work is particularly surprising, since just three years before this, the same authors presented a very detailed transient diffusion and ion migration model which included homogeneous reactions and potential dependent reactions occurring at the tip and on the walls!

In summary, a number of advanced steady-state diffusion migration models have been developed incorporating homogeneous and heterogeneous reaction. The most complete of these models used a Boltzman's distribution (Equation 2-14) for the concentration distribution of non-reacting species. The equation for the concentration is derived using the invalid assumption of linearity of the flux equation (see Appendix B). Thus, the concentrations of these species cannot be calculated using this distribution. A few simple transient diffusion/ion migration models were developed which in general did not incorporate homogeneous reactions or did not allow charged species to migrate.

2.2.3 Advanced Transport Models Involving Convection And Reactions

Convection within occluded regions such as cracks or crevices can develop by several mechanisms : (1) natural convection due to bubble formation or density gradients, (2) motion of the fluid in the bulk solution, (3) movement of the crack front, and, (4) cyclic displacement of the walls of the region such as in corrosion fatigue. No models have been developed to date which account for transport of dissolved species due to natural convection within cracks, crevices, or pits. However, some work

has been done in which the convection within these regions is induced by bulk fluid motion or displacement of the walls of the occluded region. This work will be reviewed here.

The flow of the bulk fluid external to the crack, crevice, or pit may occur in many directions relative to the cavity orientation (*47*). Flow may occur parallel to the metal surface. In the case of a crack, this type of flow may occur across the crack mouth, along a crack mouth with closed sides, or at some angle between these two orientations. Flow may also occur perpendicular to the metal surface. In this case, flow may be directly into the cavity region, or, in the case of compact tension specimens which are open on the sides, through the crack.

Some work has been done on the flow induced within a cavity by flow past the mouth of this cavity and parallel to the external surface of the metal (*48-52*). Most of these models have concentrated on the flow patterns which develop within cavity regions and do not incorporate this induced flow into a transport model to predict the concentration of species within the cavity region. These hydrodynamic models are not of direct interest and have been reviewed in detail elsewhere (*47*).

The model developed by Alkire et al. makes a first attempt at incorporating the effect of convective transport (induced by flow past a semi-spherical cavity parallel to the external metal surface) on the concentration of dissolved species within the cavity (53). The model is a diffusion/convection model in which dissolution occurs only from the surfaces of the cavity and without any homogeneous reaction. The two-dimensional steady-state velocity profile developed within the cavity was calculated using the equation for incompressible Stokes flow as given by

$$\nabla^2 v = \frac{1}{\nu\rho} \nabla P \qquad (2\text{-}18)$$

where V = velocity

ν = kinematic viscosity

ρ = fluid density

P = pressure

The velocity profile was used in the steady state diffusion convection transport equation which can be derived from Equation 2-3 and is given by

$$D\nabla^2 C_i = v\nabla C_i \qquad (2-19)$$

The model was used to calculate the steady state two dimension/concentration profiles that developed within the cavity as a function of external fluid velocity. The model does not incorporate the effects of ion migration and homogeneous reactions. Nevertheless, it is important because it has been the only attempt to assess the influence of this type of induced flow within occluded regions on the concentrations developed within those regions.

No model has been developed to predict the velocity profile developed within a cavity induced by external fluid flow perpendicular to the external metal surface (be it into the opening of a cavity or through a crack). Thus, the effect of this type of flow on the concentration of dissolved species within the cavity has not been quantitatively assessed. Some qualitative analysis of the possible affects of various parameters (width, length, external fluid velocity, etc.) on crack chemistry has been done by Easthope and Turnbull (*47*).

The lack of modeling in the area of flow induced by external fluid flow is potentially serious. Most of the laboratory experiments are carried out using "two dimensional" specimens (i.e., with no side plates) often with external fluid flow. The

results of these experiments are used to predict the behavior of these metals in practical applications. Cracks in service do not have this "two-dimensional" shape, but are usually semi-elliptical. Hence, in real cracks through flow cannot occur. Without accurate modeling to predict the significance of induced flow, no direct comparison can be made between the conditions that develop within "laboratory" cracks and "real" cracks that develop in service. Without this direct comparison a degree of uncertainty in prediction of practical behavior with laboratory specimens is inevitable.

Fluid flow within a cavity, particularly a crack, can be induced by the movement of the tip of the cavity region. Models developed to predict the concentration of dissolved species within ignore the effect of ion migration. The governing mass transport equation used in this case is generally given by

$$\frac{\partial C_i}{\partial t} = D\nabla^2 C_i - \nabla \cdot (C_i v) + \sum_j R_{i,j} \qquad (2\text{-}20)$$

Steady state models simply use the same governing equation setting $\partial C_i/\partial t$ equal to zero. This equation can be derived from Equation 2-3 assuming no potential gradients are present within the model crack.

Shuck and Swedlow developed a very simple model of the diffusion convection type assuming that the sides of the crack are displaced vertically and that the crack angle does not change (*39,40*). This simulates crack growth. Thus, the velocity is constant over the entire length of the crack. H^+ ions dissolved at a constant flux from the crack walls. No cathodic or homogeneous reactions were accounted for. Two very similar models were developed by Newman and Smyrl to predict the velocity and the concentration of dilute species in propagating cracks (*54,55*). The first model predicted the velocity profile within a propagating crack using the Navier-Stokes momentum equation and the continuity equation for a fluid of uniform density. The

second model incorporated the velocity profile developed within the crack in a steady-state diffusion/convection model. In this case the walls were inert and no electrochemical or homogeneous reactions occurred in the model crack. Both groups of modelers ignored transport by ion migration. No homogeneous or cathodic reactions were allowed to occur within the model regions. These assumptions lead to serious limitations on application of the models, and, indeed, are unrealistic. Another factor of importance concerning these models is that for significant convection to be induced by crack growth, the crack propagation must be so fast that the structure is already failing. Therefore this type of modeling is not relevant practically.

The last type of induced convective motion that is considered in this review, is that induced by the opening and closing of the crack walls. This type of flow was considered earlier by Hartt et al. and by Taunt et al. (*22-24*). In this group of models, however, the effect of this type of induced convection on the electrochemistry within the cavity region was not quantitatively evaluated. The governing equation in this case was similar to that given in Equation 2-20. While this may be valid for transport of uncharged species, since they are not influenced by potential gradients, it is not valid for the case of charged species. Shuck and Swedlow also modeled the convective effect of crack opening (not cyclic opening and closing) on the concentration profile. The crack angle increases in a wedge shaped model with no change in crack length; the crack was allowed only to open, drawing in fluid from the bulk. Crack closure was not incorporated into the model. Thus pumping of the crack wall did not occur. The velocity of the fluid in the crack increased linearly with distance from the crack tip. The opening of the crack was not related in any way to normal mechanical stress parameters such as stress intensity factors, yield strength, etc.. Again H^+ ions were allowed to dissolve at a constant rate from the crack walls. No homogeneous reactions or cathodic

reactions were incorporated. The assumptions made in this model make it inapplicable to real crack situations.

A more advanced diffusion convection model was developed by Turnbull (*56-59*). The model tried to predict the oxygen concentration within a tapered corrosion fatigue crack with a blunt tip. Thus, flow within the crack is the result of opening and closing of the crack and results in an influx and efflux of fluid. (The cathodic reduction of oxygen is considered to be a function of oxygen concentration and external electrode potential). Cycling of the crack walls is a function of stress intensity factor, stress ratio, and specimen geometry. The crack tip opening displacement is calculated using Dugdale's model of crack tip plasticity. Using the displacement at the load line and the crack tip opening displacement, the width of the crack as a function of position and time was calculated. The average velocity at any position within the crack was calculated using

$$\bar{v} = -\frac{\dot{h}(x,t)\,x}{h(x,t)} \qquad (2\text{-}21)$$

where $h(x,t)$ = crack half width at position x and time t

$\dot{h}x,t)$ =

x = position from crack tip

v-bar = average velocity

The velocity is used in the governing transport equation that is obtained by integrating the flux over the width and averaging. The resulting equation is

$$\frac{\partial C_i}{\partial t} + \frac{\dot{h}(x,t)C_i}{h(x,t)} = -\frac{\partial J_i}{\partial x} - \frac{I'}{h(t)} \qquad (2\text{-}22)$$

where J_i' = flux (due to diffusion and convection)

I' = flux of oxygen consumed on walls

This equation was solved numerically. The model is limited by the lack of ion migration and homogeneous reactions. Though oxygen is not a dissolved species, and, therefore, does not migrate in a potential field, the reduction kinetics is potential dependent and will vary with changes in potential down the crack. Nevertheless, the model provided insight into the effect of mechanical variables and crack depth on transport within a corrosion fatigue crack.

Turnbull and Ferris developed a much more elaborate transient model involving convection induced by cyclic pumping of crack walls (*60-64*). The cyclic opening and closing of the crack is modeled in the same way as with their previous model. The model includes the effects of transport by diffusion, ion migration and convection as well as homogeneous reactions in the solution and potential dependent electrode reactions on the crack walls. This model is the most rigorous model developed to date.

2.2.4 Recent Work

A number of modeling papers have appeared in the literature in the last two years. Many of these models have not included important transport and reaction processes. Of this recent work, the crevice modeling done by Sharland et al. has been the most rigorous (*65,66*). In this case crevice was modeled as both a passive (inert) walled crevice (no electrode reactions on walls) and an active wall crevice. The inert

wall model is invalid since the walls are important, especially in a crevice, because of the large surface area of wall as compared to tip. The first model developed was a steady state model. The governing transport equation was similar to that in Equation 2-3. Homogeneous reactions were included in the model. Solubility reactions were included but as equilibrium type reactions with a forward and backward in this model. This type of approach could easily lead to spurious source terms which would be strongly dependent on the value of the rate chosen for the precipitate dissolution. In order to use this approach accurately, one must account for how much precipitate is produced as a function of position and ensure that the precipitate dissolution process does not exceed this amount. In this model, the amount of precipitate produced is not monitored and, therefore, a spurious source term may be present. A better approach is to consider the precipitation process as occurring in one direction and without precipitate dissolution. Indeed, the kinetics of metal oxide dissolution are very slow and it is likely that other processes (i.e., anodic dissolution) would supply metal ions at a much faster rate. The equations were added and subtracted (as discussed in the beginning of Section 2.2) to remove the reaction rate terms, thus making the system of equations easier to solve but limiting the applicability of the model to other systems.

A transient model has recently been published by Sharland et al. in the literature (*67*). It is difficult to comment on this model since the equations used were not fully documented in the paper. It is clear that if precipitation processes were incorporated in the transient form of the model that they would have been incorporated as in the previous model and the danger of spurious terms would still be present.

The latest paper by Bertocci is very similar to the earlier work which has been previously discussed (*68*). The model is steady state with inert crack walls. No cathodic reactions or homogeneous reactions were incorporated into the model. Apparently no homogeneous reactions or solubility limits were incorporated. The flux

equation incorporating diffusion and ion migration were used as the governing transport equation. It was unclear how the problem is solved. In any case, the assumptions made are limiting for general application.

Another recent model was developed by Alkire and Lott to predict the electrochemistry in stainless steel crevices exposed to room temperature, high conductivity NaCl solutions (*69*). This transient model incorporates transport by diffusion and ion migration. Homogeneous reactions, cathodic reactions and solubility limits are ignored. The walls of the crevice are anodically active without any potential dependence and the crack tip is inert. Manganese sulfide inclusions are allowed to dissolve to produce Mn^{2+} and $S_2O_3^{2-}$ at a rate dependent on the potential. H^+ ions are not included in this model. The system of equations is solved numerically. The lack of homogeneous reactions and cathodic reactions is invalid. The fact that the pH within the crevice is not calculated is curious since the onset of crevice corrosion is usually pH dependent.

The most recent model by MacDonald and Urquidi-MacDonald is the only model to date which has attempted to predict the electrochemistry within an occluded region exposed to high temperature, low conductivity solutions (i.e., BWR water chemistry) (*70*). This a steady-state crack model which assumes that the crack walls are inert, that there are no cathodic reactions, and that no homogeneous reactions occur within the crack and that the metal ion concentration is not limited by solubility limits. Another assumption is that Laplace's equation is valid within the crack. The anodic crack tip reaction has no potential dependence. The assumptions made in this model are unrealistic. The crack walls cannot be assumed inert unless the crack tip current density is many orders of magnitude higher than the wall current density. In low conductivity (or high resistivity) media cathodic reactions cannot be ignored within the crack (as shown in Chapter 4 of this thesis). In all likelihood, some of the anodic

current will be satisfied within the crack region. Homogeneous reactions occur everywhere in solution and are always important. In high conductivity water, metal ions have a very low solubility (except in very acidic conditions). The assumption that Laplace's equation can be used is intrinsically invalid when concentration gradients are present as in this case.

2.3 DISCUSSION

The development of a mathematical model to predict the local electrochemistry within a cavity which considers transport, and, production and consumption of species within this region is not intrinsically difficult. The necessary governing equations have been known for some time. The limitation on the development of the model is the solution of the system of equations that results from the development of a rigorous model. The system of equations obtained consist of a set of stiff, non-linear, differential equations which in their full form are three dimensional. By using approximations and assumptions to the full set of transport based equations, it is possible to simplify the system of equations and make their solution tractable. The approximations and assumptions which are made will in some way limit the applications of these models. The question is whether these limitations are appropriate for realistic situations such as a crack, crevice, or pit. As described earlier, to completely model the electrochemical conditions within cracks and crevices, the transport effect of diffusion and ion migration (and convection if fluid flow into the occluded region is significant) must be included. Homogenoous and potential dependent anodic and cathodic reactions should be incorporated. If the solubility of any species in the model is limited, the possibility of precipitation should be incorporated. By

ignoring the possible effects of these important factors when developing a model it is possible that the results from the model may be misleading. Approximations and assumptions should be made only in cases where the limitations imposed by these assumptions does not prohibit application to the problem of interest.

Earlier modelers used many approximations after reducing the transport equation to one type of transport or simplified diffusion/ion migration models at steady state. Homogeneous reactions, equilibrium reactions, wall reactions, and cathodic reactions were generally ignored. Modeling work progressed to much more complicated steady state models and simple transient models. The steady-state models included transport by diffusion and ion migration as well as homogeneous reactions and in some cases cathodic reaction within the occluded region. Simple transient models incorporating diffusion and ion migration were developed. These models incorporated neither homogeneous reactions nor cathodic reaction within the cavity region. Also the anodic electrode reactions were not potential dependent.

More rigorous models were developed culminating with the work of Turnbull and Ferris. (*60-64*). Turnbull developed a crack model which was rigorous in approach, incorporating transport by diffusion, ion migration, and convection (due to pumping of the crack walls). Also incorporated were homogeneous reactions, precipitation of species on the walls, potential dependent electrode reactions. The model is very rigorous but is somewhat limited in flexibility because of the addition and subtraction of transport equations. This limits the application of the model to other systems of interest.

No model has been developed that can rigorously model electrochemistry within cavities exposed to nuclear reactor environments incorporating all the necessary transport terms, homogeneous reactions, potential dependent electrode reactions on the tip and on the walls, solubility reactions, production of species by radiolysis, and the

low conductivity conditions present within BWR's (*71*). The only model that purports to describe the electrochemistry in an occluded region in BWR water is that of MacDonald and Urquidi-MacDonald (*70*). As already discussed, this model is not a rigorous one and contains invalid and inappropriate approximations which cast doubt on the predictions.

The model presented in this thesis was developed to rigorously and flexibly model the transient electrochemistry within occluded regions exposed to nuclear reactor aqueous environments. The transport modes of diffusion and ion migration are included, and, when appropriate, convection due to pumping can be included. Any number of homogeneous equilibrium reactions and potential dependent electrode reactions at the tip and on the wall can also be included. Since the transport equations are <u>not</u> added and subtracted from one another, as done in other models in order to remove the homogeneous reaction reaction rates, the model is general and flexible. It can be applied to a crack or crevice in any system as long as the necessary input data (equilibrium constants,diffusion coefficients, electrode reaction kinetic parameters, etc.) are known. Solubility reactions (occurring along the walls of the cavity) can be applied to any of the species being modeled. Also, the possibility of chemical dissolution of inclusions from the wall and the tip is accounted for. Production of species, such as oxygen or peroxide by radiolysis of water, can be incorporated. Radiolysis production is possible due to both neutron and gamma radiation and is dose dependent. The model also allows for transients in bulk (boundary) conditions such as concentrations of species or external potential during the run to account for transients that normally occur during reactor operation. The model was developed for nuclear reactor environments and therefore is able to handle very dilute solutions (10^{-6} M) which tend to make the system of equations more difficult to solve than usual. Thus, the model developed is very rigorous by the standards set in previous modeling work and

incorporates the effects of all the important types of reactions that could occur. The model is not all embracing. Indeed, convection induced by flow past the mouth of the cavity and natural convection are not considered. Nevertheless, the model developed is a significant step in the general progression of predicting the local electrochemistry within cavity regions.

2.4. REFERENCES

(1) A. Turnbull, Reviews on Coatings and Corrosion, vol. 5(3), p. 43, 1982.

(2) S.H. Sharland, Corrosion Science, vol. 27(3), pp. 289-323, 1987.

(3) M.G. Fontana and N.DD.Greene, Corrosion Engineering, McGraw-Hill, New York, 1978.

(4) J.C. Scully, The Fundamentals of Corrosion, Pergamon Press, New York, 1975.

(5) J.G. Hines, Corrosion Sci., vol. 1, p. 21, 1961.

(6) E. M. Gutman, Proc. of Third Int. Cong. on Metallic Corrosion, Moscow, vol.2, pp. 377-384, NACE, 1966.

(7) G.J. Bignold, Corrosion, vol. 28(8), pp. 307-312, 1972.

(8) Vicentini, D. Sinigaglia, and G. Taccani, Werks U. Korr., vol. 22, pp. 916-924, 1971.

(9) J. Newman, D.N. Hanson, and K.J. Vetter, Electrochim. Acta, vol. 22, pp. 829-831, 1977.

(10) K. Nisancioglu and H. Holton, Electrochim. Acta, vol. 23, pp. 251-253, 1978.

(11) P. Doig and P.E.J. Flewitt, Proc. R. Soc. Lond. A., vol. 357, pp. 439-452, 1977.

(12) P. Doig and P.E.J. Flewitt, Met. Trans. A., vol. 9A, pp. 357-362, 1978.

(13) P.H. Melville, Br. Corr. J., vol. 14(1), pp. 15-19, 1980.

(14) P.H. Melville, Br. Corr. J., vol. 14(1), pp. 26-30, 1980.

(15) G. Faita, F. Mazza, and G. Bianchi, in Localized Corrosion,B.F. Brown, J. Kruger, and R.W. Staehle, eds., pp. 34-44, NACE, 1974.

(16) J.W. Tester and H.S. Isaacs, J. Electrochem. Soc., vol. 122, p. 1438, 1975.

(17) J.R. Galvele, J. Electrochem. Soc., vol. 123(4), pp. 464-474, 1976.

(18) J.R. Galvele, Corrosion Sci., vol. 21(8), pp. 551-579, 1981.

(19) A. Turnbull, J.G.N. Thomas, NPL Report DMA A(11), 1979.

(20) D.H. Ferriss, NPL Report DNACS 14/79, 1979.

(21) K.J. Vetter and H. Strenblow, in Localised Corrosion, B.F. Brown, J. Kruger, and R.W. Staehle, eds., p. 240, NACE, 1974.

(22) W.H. Hartt, J.S. Tenant, and W.C. Hooper, Corrosion Fatigue Technology, ASTM STP642, pp.5-18, 1978.

(23) R.J. Taunt, and W. Charnock, Mat. Sci. Eng., vol. 35, pp. 219-228, 1978.

(24) R.J. Taunt and W. Charnock,in Influence of Environment on Fatigue, I. Mech. E., London, 1977, p. 43.

(25) J.K. Vennard and R.L. Street, Elementary Fluid Mechanics, John Wiley and Sons, NY, 1976, p. 301.

(26) J.W. Oldfield, and W.H. Sutton, Br. Corros. J., vol. 13(1), pp.13-22, 1978.

(27) J.W. Oldfield and W.H. Sutton, Br. Corros. J., vol. 15(1), pp. 31-34, 1980.

(28) D.A. Vermilyea and C.S. Tedmon, Jr., J. Electrochem. Soc., vol. 117(4), pp. 437-440, 1970.

(29) B.G. Ateya and H.W. Pickering, J. Electrochem. Soc., vol. 122(8), pp.1018-1020, 1975.

(30) T.R. Beck and E.A. Grens II, J. Electrochem. Soc., vol. 116, p.177, 1969.

(31) A. Turnbull, Br. Corr. J., vol. 15(4), pp. 162-171, 1980.

(32) R. Alkire, D. Ernsberger, and T.R. Beck, J. Electrochem. Soc., vol. 125(9), pp. 1382-1388, 1978.

(33) R.C. Alkire and D. Siitari, J. Electrochem. Soc., vol. 129(3), pp. 488-496, 1982.

(34) S.M. Gravano and J.R. Gavele, Corros. Sci., vol. 24(6), pp. 517-534, 1984.

(35) A. Turnbull and J.G.N. Thomas, NPL Report DMA(A)23, 1980.

(36) A. Turnbull and J.G.N. Thomas, J. Electrochem. Soc., vol. 129(7), pp. 1412-1422, 1982.

(37) M.J. Danielson, C.A. Oster, and R.H. Jones, Corrosion Chemistry within Pits, Crevices and Crack", A. Turnbull, ed., HMSO, 1987, p. 213-242.

(38) C.A. Oster and M.J. Danielson, PNL-5821, 1986.

(39) R.R. Schuck and J.L. Swedlow, Localised Corrosion, B.F. Brown, J. Kruger, and R.W. Staehle, eds., pp. 190-207, NACE, 1974.

(40) R.R. Schuck and J.L. Swedlow, Localised Corrosion, B.F. Brown, J. Kruger, and R.W. Staehle, eds., pp. 208-220, NACE, 1974.

(41) K. Hebert and R.C. Alkire, J. Electrochem. Soc., vol. 130(5), pp.1007-1014, 1983.

(42) J.W. Fu and S.K. Chan, Corrosion, vol. 40(10), pp. 540-544, 1984.

(43) U. Bertocci, Embrittlement by the Localized Crack Environment, AIME, pp. 49-58, 1984.

(44) R.A.H. Edwards, PhD Thesis, Dept. of Metallurgy, Delft University of Technology, 1986.

(45) R.C.Alkire, T. Tomasson, and K. Hebert, J. Electrochem. Soc., vol. 132(5), pp.1027-1031, 1985.

(46) P. Zaya, Proceedings of the Int. Congress on Metallic Corrosion, pp. 135-140, 1984.

(47) P.F. Easthope and A Turnbull, Aspects of Fluid Flow of Relevance to Corrosion Fatigue and Stress Corrosion Cracks, NPL Report DMA(A)105, 1985.

(48) R.F. Weiss and B.H. Florsheim,Physics of Fluids, vol. 8(9), pp. 1631, 1965

(49) H.K. Moffat, J. Fluid Mech., vol. 18, p 1, 1964.

(50) O.R. Burggraf, J. Fluid Mech., 24, 1966.

(51) F. Pan and A. Acrivos, J. Fluid Mech., vol.28 (Part 4), pp. 643-655, 1967.

(52) U.B. Mehta and Z. Lavan, J. Appl. Mech., vol. 36, p. 897 , 1969.

(53) R.C. Alkire, D.B. Reiser, and R.L. Sani, J. Electrochem. Soc., vol. 131(12), pp. 2795-2800, 1984.

(54) W.H. Smyrl and J. Newman, J. Electrochem. Soc., vol. 121(8), pp. 1000-1007, 1974.

(55) J. Newman and W.H. Smyrl, Met. Trans., vol. 5, p. 469, 1974.

(56) A. Turnbull, Corros. Sci., vol. 22(9), pp. 877-893,1982.

(57) A. Turnbull, Corrosion Fatigue: Mechanics, Metallurgy, Electrochemistry, and Engineering, ASTM STP 801, T.W. Crooker, and B.N. Leis, eds., pp. 351-365, 1983.

(58) A. Turnbull, NPL Report DMA(A)69, 1983.

(59) A. Turnbull, Mat. Sci. Tech., vol. 1, pp. 700-710, 1985.

(60) D.H. Ferriss and A. Turnbull, NPL Report DMA(A)44, 1982.

(61) A. Turnbull and D.H. Ferriss, Corros. Sci., vol. 26(8), pp. 601-628, 1986.

(62) A. Turnbull and D.H. Ferriss, Corros. Sci., vol. 27(12), pp. 1323-1350, 1987.

(63) A. Turnbull,in Offshore and Coastal Modeling, P.P.G. Dyke, A.O. Moscardini and E.H. Robson, eds., Springer Verlag, p. 353-376,1985.

(64) D.H. Ferriss, NPL Report DNACS 28/80, 1980.

(65) S.M. Sharland and P.W. Tasker, Corros. Sci., vol. 128(6), pp. 603-620, 1988.

(66) S.M. Sharland, Corros. Sci., vol. 128(6), pp. 621-630, 1988.

(67) S.M. Sharland, C.P. Jackson, and A.J. Diver, Corros. Sci., vol. 29(9), pp.1149-1166, 1989.

(68) U. Bertocci, J. Electrochem. Soc., vol. 136(7), pp. 1887-1892, 1989.

(69) R.C.Alkire and S.E. Lott, to be published.

(70) D.D. MacDonald and M. Urquidi-MacDonald, "Modeling of the Electrochemistry of Stress Corrosion Cracks in Sensitized Type 304 SS in Boiling Water Reactors", presented at 4th Int. Symposium on Environmental Degradation of Materials in Nuclear Power Systems - Water Reactors, 6-10 August, 1989, Jekyll Island, GA, USA, D. Cubicotti, chairman.

(71) A. Turnbull, private communication

Chapter 3

MODEL DESCRIPTION AND VERIFICATION

3.1 INTRODUCTION

In order to predict accurately the electrochemistry within cracks and crevices, a complete physical model must be developed including a description of the occluded region and the types of events that occur within this region. A rigorous mathematical model of the physical processes must be established and solved, and, with the use of accurate input data, the mathematical model can be applied to predict the electrochemistry. A detailed summary of the requirements for modeling local electrochemistry in occluded regions is given in Appendix A. In this chapter a complete description of the model that has been developed is provided. The mathematical equations used and the solution technique are explained. Verification of the model against analytic techniques and other numerical solutions developed for more limited systems is also provided.

As explained in Chapter 2, the model presented in this thesis is flexible and rigorous. It was designed not only to model one specific crack or crevice problem, but to be able to model cracks or crevices in any alloy system. The number of species used in the model is limited only by computer power (i.e., memory and speed). As many homogeneous, precipitation, electrode, or radiolysis reactions can be included as is desired. Chemical dissolution of inclusions can also be incorporated. The geometry of the region can be either parallel sided (crevice geometry) or tapered with a blunt tip (crack geometry) as shown in Figure 3-1. Convection induced by movement of the region's walls can be incorporated along with diffusion and ion migration. Thus the

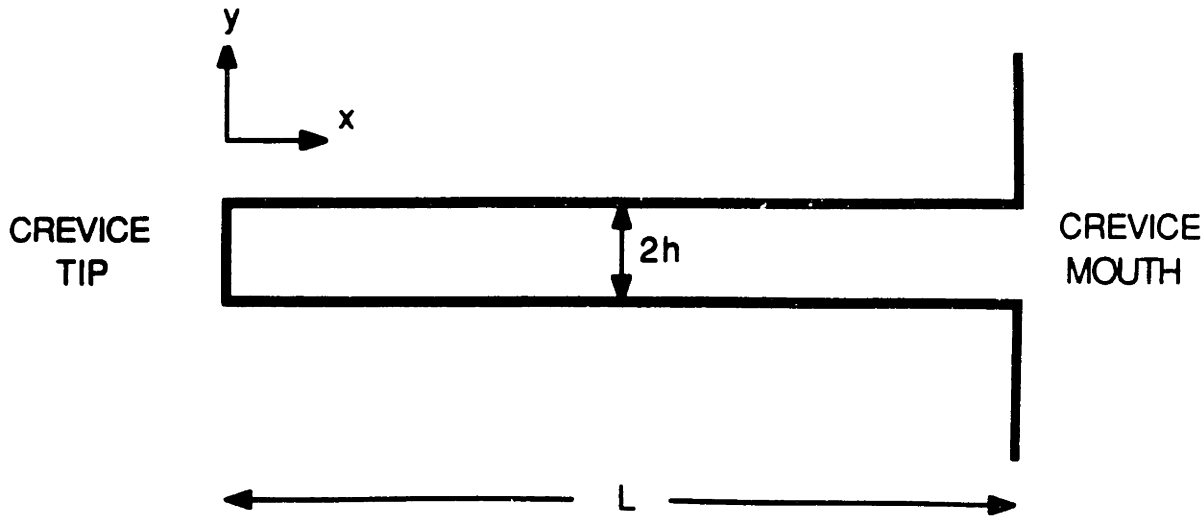

(a) Model crevice.

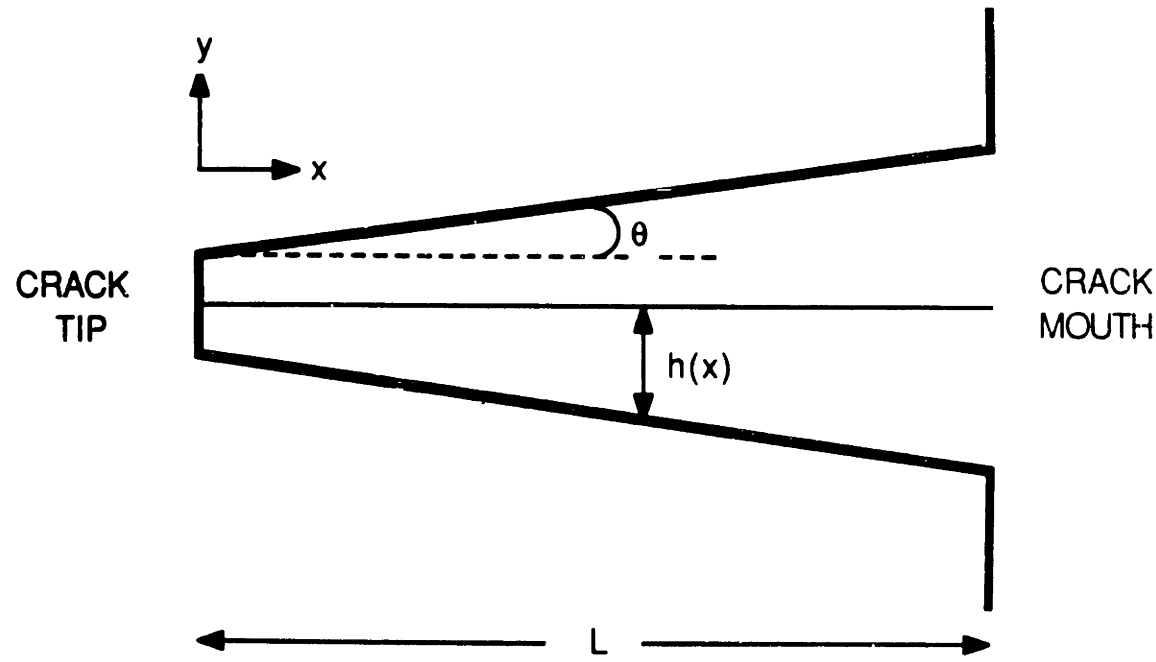

(b) Model crack.

Figure 3-1. Geometry used by model for (a) crevice and (b) crack.

model incorporates most of the necessary factors that could be needed to model stress corrosion cracks, corrosion fatigues cracks, and crevices.

3.2 General Transport Equations

3.2.1 Mass balance

The transport of dissolved species i is controlled by diffusion, ion migration, and convection. These mechanisms of transport can be described by the flux equation, as given by

$$J_i = - D_i \nabla C_i - z_i \mu_i F C_i \nabla \phi + C_i v \qquad (3-1)$$

where J_i = flux of species i (moles/dm^2-sec)

D_i = diffusion coefficient of species i (dm^2/sec)

C_i = concentration of species i (moles/dm^3)

z_i = charge of species i

μ_i = ionic mobility of species i (dm^2-mole/J-sec)

F = Faraday's constant (C/equiv)

ϕ = potential (volts)

v = velocity (dm/sec)

Assuming that the solution of interest is dilute, the activity of species i is approximately equal to its concentration. The diffusion coefficient of species i can be related to its ionic mobility by the Nernst-Einstein relationship:

$$\mu_i = \frac{D_i}{RT} \qquad (3-2)$$

where R = gas constant

T = temperature (K)

Substituting Equation 3-2 into the flux equation given by Equation 3-1 results in the Nernst-Planck equation

$$J_i = - D_i \nabla C_i - \frac{z_i D_i F}{RT} C_i \nabla \phi + C_i v \qquad (3-3)$$

The first term on the right represents diffusion which is the transport of any dissolved species due to a gradient in its concentration. Species will tend to diffuse from regions of high concentrations to regions of low concentration. The second term represents ion migration which is the transport of charged species due to a gradient in potential. This term is only applicable to electrochemical systems. The last term represents convection which is transport induced by flow.

The mass balance or the time rate of change of species i is given by

$$\frac{\partial C_i}{\partial t} = - \nabla \cdot J_i + \sum_j R_{i,j} \qquad (3-4)$$

where R_{ij} = rate of production or consumption of species i by reaction processes (due to homogeneous reactions and radiolysis)

t = time

In one dimension, this equation is given by

$$\frac{\partial C_i}{\partial t} = -\frac{\partial J_i}{\partial x} + \sum_j R_{i,j} \qquad (3-5)$$

Some reactions of importance take place along the walls of the crack or crevice region shown in Figure 3-1. These reactions include electrochemical reactions (both anodic and cathodic), precipitation reactions, and chemical dissolution from the walls. In this case, the system is two dimensional and must be averaged over the y dimension. The resulting equation contains a new type of reaction term and some averaging that accounts for the dilution effect of having tapered walls. This averaging is explained in greater detail in Appendix C. The resulting mass balance equation is given by

$$\frac{\partial C}{\partial t} = -\frac{\partial J_x}{\partial x} + C\frac{\partial v_x}{\partial x} + \frac{\theta D}{h}\frac{\partial C}{\partial x} + \frac{\theta z D F}{hRT} C\frac{\partial \phi}{\partial x} + \sum_j R_j + \sum_j \frac{R_{j,het}}{h} \qquad (3-6)$$

where θ = crack angle (= 0 for crevice)

h = half width of cavity

In this equation, the concentrations represent an average concentration over the crack or crevice width. Substituting the one-dimensional form of Equation 3-3 into this equation and expanding gives

$$\frac{\partial C_i}{\partial t} = D_i \frac{\partial^2 C_i}{\partial x^2} + \frac{z_i D_i F}{RT} \frac{\partial}{\partial x}\left(C_i \frac{\partial \phi}{\partial x}\right) - \frac{\partial}{\partial x}(C_i v) + C_i \frac{\partial v}{\partial x}$$

$$+ \frac{\theta D_i}{h} \frac{\partial C_i}{\partial x} + \frac{\theta z_i D_i F}{hRT} C_i \frac{\partial \phi}{\partial x} + \sum_j R_{i,j} + \sum_j \frac{R_{i,j,het}}{h} \qquad (3-7)$$

for species i.Poisson's equation

$$\frac{\partial^2 \phi}{\partial x^2} = \frac{F}{\varepsilon} \sum_i z_i C_i \qquad (3-8)$$

where ε is the permitivity of the solution, is used to replace the second order derivative in potential. The total current density equation,

$$I = F \sum_i z_i J_i = -F \left[\sum_i z_i D_i \frac{\partial C_i}{\partial x} + \sum_i \frac{F z_i^2 D_i}{RT} C_i \frac{\partial \phi}{\partial x} \right] \qquad (3-9)$$

where I is the current density, is used to replace the first order derivative in potential. The resulting mass balance equation is differenced (as explained in Appendix D) and used to find the concentration of every species as a function of time and position within the cavity. In addition, the total current density equation is used to solve for the potential.

In the following parts of this section, the types of reaction processes incorporated in the model and the resulting rate terms used in Equation 3-7 for each of these reaction processes will be explained in detail.

3.2.2 Homogeneous Chemical Reactions

The general form for a chemical reaction that occurs in solution is :

$$aA + bB + cC + \ldots \underset{k_b}{\overset{k_f}{=}} mM + nN + oO + \ldots \qquad (3\text{-}10)$$

where the capital letters represent dissolved species in solution and the lower case letters preceding a species represent the order of the reaction with respect to that species. The k_f and k_b are the rate constants for the forward and back reactions, respectively. In this model, reactions involving three dissolved products and three dissolved reactants may be considered. The order of the reaction may be up to 9 for each species in the reaction. Thus the typical equation that may be considered looks like :

$$aA + bB + cC \underset{k_b}{\overset{k_f}{=}} dD + eE + fF \qquad (3\text{-}11)$$

where a,b,c,d,e,f may have values between 0 and 9.

The rate of a homogeneous reaction is equal to the product of the concentrations of reacting species times the rate constant for that direction of the reaction . Thus the reaction rate term used in the mass balance equation for species A is given by

$$- k_f C_A^a C_B^b C_C^c + k_b C_D^d C_E^e C_F^f \qquad (3\text{-}12)$$

Since very little rate constant data is available, especially at high temperatures, these rate constants must be chosen. A description of how these rate constants are chosen is presented in Appendix E.

3.2.3 Electrochemical Reactions Along Wall

Both anodic and cathodic reactions occur along the walls of the crack or crevice. Many crack and crevice modelers assume these wall reactions are unimportant. In order for this to be a valid assumption, the production of species by the walls must be insignificant relative to the production from the tip. In other words, the contribution of the current from the wall to the total current density inside the crack must be very small. In a crevice before the breakdown of passivity, the walls and tip are both at the passive current and, therefore, are equally important. Hence the walls will dominate by virtue of their greater area. For a crack, this is more complex because the crack tip is active relative to the walls and, therefore, has a current density that can be several orders of magnitude greater than that of the walls. It might appear that the crack tip would determine the local environment. However, this ignores the fact that the area of the crack tip is small relative to the wall area. Within the crack it is the total current density that is important. In order to calculate the total current density within the crack the wall current density must be integrated over the total length of the crack and added to the tip current density as shown below :

$$I_{total} = I_{tip} + \int_0^l \frac{I_{wall}}{h}\, dx \qquad (3\text{-}13)$$

where I_{total} = total current density

I_{tip} = crack tip current density

I_{wall} = crack wall current density

h = crack half width

If we assume that the crack is parallel sided, as many modelers do, and that the passive current on the walls is independent of potential, the resulting integration over the length of the crack, L, leads to

$$I_{total}(x) = I_{tip} + \frac{I_{wall}\, L}{h} \qquad (3-14)$$

where h is the half width of the crack. The assumption of inert walls can be valid only if

$$I_{tip} >> \frac{I_{wall}\, L}{h} \qquad (3-15)$$

For a 1 cm crack with a width of 10 μm, the **average** crack tip density must be very much greater than 10^3 times I_{wall}. Thus ignoring the electrochemical wall reactions may not be a valid approximation in many cases. In this model, wall electrochemical reactions are incorporated. These reactions may be dependent on the concentration of a species in solution to the p power and exponentially dependent on the potential. For a general electrochemical reaction involving species M_j as shown below (*1*)

$$\sum_j s_j M_j^{z_j} \rightarrow ne^- \qquad (3-16)$$

where s_j = stoichiometric coefficient for species M_j

n = number of electrons transferred

The current density for this reaction can be expressed in the following form (*2*) :

$$I_w = k_o C_j^p \exp\left[-\frac{\alpha_w F (E_m - \phi)}{RT}\right] \qquad (3\text{-}17)$$

where

I_w = current density produced by electrochemical reaction w

k_o = pre-exponential constant for reaction w

C_j = concentration of species j to the p^{th} power

ϕ = potential

αw = transfer coefficient for reaction w

F = Faraday's constant

E_m = electrode potential measured at the mouth of the cavity

R = gas constant

T = temperature in degrees Kelvin

This equation can be related to the flux of species i from the wall using (*1*). The current density is related to the flux by the following expression.

$$J_{i,w} = \frac{s_i I_w}{n_i F} \qquad (3\text{-}18)$$

To be incorporated into the mass balance equation, the expression given Equation 3-17 is substituted into Equation 3-18 and is averaged over the width of the crack or crevice. The resulting exprassion is given by

$$\frac{s_i k_o C_j^p}{n_i F} \exp\left[-\frac{\alpha_w F (E_m - \phi)}{RT}\right] \qquad (3\text{-}19)$$

3.2.4 Solubility Reactions

After the solubility limit of a dissolved species is reached, the species is allowed to precipitate. This precipitation generally occurs along the walls of the crack or crevice. The general form of solubility reaction assumed is

$$M^{2+} + 2\,OH^{-} \xrightarrow{k_s} M(OH)_2 \qquad (3\text{-}20)$$

where k_S is the rate constant for the precipitation reaction. There is no data available for this constant, and therefore, it must be chosen to ensure that the solubility limit is maintained. In the mass balance equation the rate of this reaction is represented by (*2*)

$$\frac{k_s}{h}\left(C_{M^{2+}} C_{OH^-} - K_s\right) \qquad (3\text{-}21)$$

where k_S = rate of precipitation of species M^{2+}

K_S = solubility limit on species M^{2+}

h = half-width of the cavity

3.2.5 Chemical Dissolution

Chemical dissolution of substances is assumed to take place from the walls by a simple reaction such as :

$$A_aB_bC_c = aA + bB + cC \qquad (3\text{-}22)$$

where A, B, C may be charged in solution as long as electroneutrality is maintained. The flux of species A from the wall is given by

$$J_{A,d} = a\, J_d \qquad (3\text{-}23)$$

where $J_{A,d}$ = the flux of species A at the wall due to dissolution reaction

a = the n .mber preceding species A in the dissolution equation

J_d = dissolution rate of $A_aB_bC_c$

The expression used in the mass balance equation for species A is given by

$$\frac{a\, J_d}{h} \qquad (3\text{-}24)$$

where h is the half-width of the cavity.

3.3 SOLUTION OF MATHEMATICAL MODEL

The mathematical model developed involves a series of coupled partial differential equations of the general form

$$\frac{\partial C_i}{\partial t} = D_i \frac{\partial^2 C_i}{\partial x^2} + \frac{z_i D_i F}{RT} \frac{\partial}{\partial x}\left(C_i \frac{\partial \phi}{\partial x}\right) - \frac{\partial}{\partial x}(C_i v) + C_i \frac{\partial v}{\partial x}$$

$$+ \frac{\partial D_i}{h} \frac{\partial C_i}{\partial x} + \frac{\theta z_i D_i F}{hRT} C_i \frac{\partial \phi}{\partial x} + \sum_j R_{i,j} + \sum_j \frac{R_{i,j,het}}{h} \qquad (3\text{-}25)$$

and

$$I = -F\left[\sum_i z_i D_i \frac{\partial C_i}{\partial x} + \sum_i \frac{F z_i^2 D_i}{RT} C_i \frac{\partial \phi}{\partial x}\right] \qquad (3\text{-}26)$$

Each species in solution is modeled using an equation similar to Equation 3-25 and the potential is modeled using Equation 3-30. Thus, for a model system involving n dissolved species, there are n+1 coupled equations. A sample set of governing equations is presented in Appendix F. These equations have been described in detail in the previous section and therefore will not be discussed here. This problem is nonlinear because of the migration and reaction terms. The many reaction terms give rise to a very stiff system of equations. Stiffness can be defined, in this case, as the presence of one or more fast 'decay' type processes. The time constant of this process is short relative to the time constants of the other processes occurring (i.e. diffusion, ion migration, etc) (*3*). (This stiffness will require that an implicit time integration method be used).

In order to more easily solve this system of equations, the numerical method of lines is employed. This converts a system of time dependent partial differential equations into a system of time dependent ordinary differential equations (ODEs) by a spatial discretization procedure (*4*). The right hand side of Equations 3-25 and 3-26 were discretized using finite difference techniques. The details of this discretization are presented in Appendix D. The resulting system of ODEs have the general form

$$A(t,Y)\,\frac{dY}{dT} = A(t,Y)\,\dot{Y} = g(t,y) \qquad (3\text{-}27)$$

where A = a matrix of pre-derivative coefficients

Y = vector of unknowns (i.e.. concentration and potential)

$\dot{Y}$ = time derivative of vector Y

g = vector containing discretized equations

The resulting system of differential/algebraic equations is solved using a package developed for stiff ODEs.

The package that was selected is among a collection of packages called ODEPACK (*3,5-8*). In particular, the package LSODI developed by Hindmarsh and Painter was selected. This selection was made because the package has been applied with great success to the solution of the Navier-Stokes equation in two dimensions. These equations have a similar construction to the equations in the model developed in this thesis (i.e. they are also nonlinear and stiff). The rest of this section will explain the methods employed by LSODI.

The methods employed by LSODI for large stiff systems involve backward differentiation. These are multistep methods which were first implemented by C.W. Gear (*9*). The package used in the model described in this thesis is based on these original packages developed by Gear. These packages solve a stiff system of equations of the simpler general form

$$\dot{Y} = \frac{dY}{dt} = f(t,Y) \qquad (3-28)$$

This system is of size N (i.e., the vector y has a length N). The independent variable, t, need not be time necessarily, but it is in this case. Consider it to be a fixed time step size, Δt, such that

$$t_n = t_{n-1} + \Delta t \qquad (3-29)$$

With this nomenclature it is possible to describe a particular time t_n such that

$$t_n = n \Delta t \qquad (3\text{-}30)$$

In this fashion, it is possible to construct discrete approximations to the unknown value Y at time t_n which will be denoted Y_n. Y_0 is the discrete representation of the initial array Y which is known. $\dot{Y}_n$ is the time derivative of Y_n and is given by $f(t_n, Y_n)$ as described in Equation 3-28.

LSODI uses the particular backward differentiation formula given by

$$Y_n = \sum_{i=1}^{q} \alpha_i Y_{n-i} + \Delta t \, \beta_0 \dot{Y}_n = a_n + \Delta t \, \beta_0 \, f(t_n, Y_n) \qquad (3\text{-}31)$$

In this equation, Y_{n-i} refers to the previous (in time) values of the array Y. The index number q refers to the order of the approximation. This refers to the truncation error that results from the approximation. Thus the value of Y_n is exact within an error that is on the order of $(\Delta t)^{q+1}$, where q has values ranging between 1 and 5. $\dot{Y}_n$ again represents the time derivative of Y_n. α_i and β_0 are coefficients. β_0 is always greater than zero. The result of the summation, a_n, is a constant vector. The expression given by Equation 3-31 represents a fully implicit approximation. Because of the stiffness and nonlinearity of the problem it is usually solved by making a first guess or predicting Y_n and then initiating or correcting this guess to find the true solution. The first guess is denoted $Y_{n(0)}$ and later corrected guesses are denoted $Y_{n(1)}$, etc.

For stiff, nonlinear problems, normal functional iteration, which involves the substitution of the previous guess back into the equation to get the new guess, fails to converge. A modified Newton iteration is used instead. Newton's Method (*10*) assumes that, given a general nonlinear equation of the form $I(x) = 0$, the solution, x, must be

obtained by starting with an initial guess and improving upon it. The initial guess to the solution being x^0 and later guesses being x^1, x^2, etc. Thus, the current approximation is x^k, Newton's Method uses the derivative approximation given by

$$I(x^{k+1}) \approx I(x^k) + I'(x^k)\,(x^{k+1}-x^k) \qquad (3\text{-}32)$$

In this case $I'(x^k)$ represents the Jacobian matrix of the function g. The aim is that $I(x^{k+1}) = 0$, therefore Newton's method uses

$$I'(x^k)\,(x^{k+1}-x^k) = -I(x^k) \qquad (3\text{-}33)$$

and solves for the new corrected approximation x^{k+1}. In this case, the function we are evaluating can be derived from Equation 3-31 and is

$$I(Y_n) = Y_n - a_n - \Delta t\,\beta_0\,f(t_n,Y_n) = 0 \qquad (3\text{-}34)$$

The following equation used for the Newton iteration is given by

$$-P\,[Y_{n(m+1)} - Y_{n(m)}] = Y_{n(m)} - a_n - \Delta t\,\beta_0\,f(t_n,Y_{n(m)}) \qquad (3\text{-}35)$$

where P = a NxN matrix approximating the Jacobian of the algebraic system of equations

m = iteration number

n = time step number

P is given by

$$P \cong I - \Delta t\, \beta_0\, J \qquad (3\text{-}36)$$

In this case I represents an NxN identity matrix and the jacobian matrix, J, is given by

$$J = \frac{\partial f(t_n, Y_{n(m)})}{\partial Y_{n(m)}} \qquad (3\text{-}37)$$

This method differs from the traditional Newton's method in that the jacobian matrix is only evaluated periodically when a new value appears necessary (i.e., when convergence fails). Within LSODI Δt (the time step size) and q (the order of the approximation) are varied to meet local error tolerances.

The problem that must be solved with this model has the general form

$$A(t_n, Y)\, \dot{Y}_n = g(t_n, Y_n) \qquad (3\text{-}38)$$

where A is not necessarily the identity matrix. This equation was described earlier in this section. Another approximation that must be used in the solver instead of Equation 3-31. This obtained by multiplying both sides of Equation 3-31 by $A(t_n, Y_n)$ and replacing $A(t_n, Y_n)Y_n$ by $g(t_n, Y_n)$. The resulting equation can be rearranged to yield the new implicit relation given by

$$S(Y_n) = A(t_n, Y_n)\,[Y_n - a_n] - \Delta t\, \beta_0\, g(t_n, Y_n) = 0 \qquad (3\text{-}39)$$

$S(Y_n)$ in this case is equivalent to $I(Y_n)$ defined in Equation 3-34. The modified Newton iteration is still used, after the introduction of the residual function, $r(t_n, Y_{n(m)})$, as given by

$$r(t_n, Y_{n(m)}) = g(t_n, Y_{n(m)}) - A(t_n, Y_{n(m)})\, s \qquad (3\text{-}40)$$

Here s represents an approximation to $\dot{Y}_n$ and is defined to be

$$s = \frac{(Y_{n(0)} - a_n)}{\Delta t\, \beta_0} \qquad (3\text{-}41)$$

Thus s is the predicted value of $\dot{Y}_n$ that corresponds to the prediction $Y_{n(0)}$. Rearranging Equation 3-40 with the inclusion of Equation 3-41 in substituting into Equation 3-39 results in

$$S(Y_{n(m)}) = A(t_n, Y_{n(m)})\,(Y_{n(m)} - Y_{n(0)}) - \Delta t\ \beta_0\ r(Y_{n(m)}) \qquad (3\text{-}42)$$

The jacobian matrix, P, in this case is given by

$$P = S'(Y_{n(m)}) = A(t_n, Y_{n(m)}) - \Delta t\, \beta_0 \frac{\partial r(t_n, Y_{n(m)})}{\partial Y_{n(m)}} \qquad (3\text{-}43)$$

and the equation used for the Newton iteration is

$$P\,[Y_{n(m+1)} - Y_{n(m)}] = S(Y_{n(m)}) \qquad (3\text{-}44)$$

This is solved for $Y_{n(m+1)}$ which is the next guess. At each time step, an initial guess is made using an implicit Gear's method, in particular, a backward differentiation formula (i.e.. Equation 3-31 times $A(t_n, Y_n)$). The modified Newton's method described above is then applied, in order to account for the stiffness and nonlinearity until the

accurate solution is arrived at. A listing of the program (without the solver LSODI) is provided in Appendix G.

3.4 VERIFICATION OF NUMERICAL MODEL

The verification of the model has taken place as the model has been developed. The initial verifications were established using very simplified cases and analytic solutions. Comparisons of the more complex aspects of the model were made where possible with other published models..

3.4.1 Diffusion

The first verification for the model was a simple one dimensional transient diffusion problem with boundary conditions of the first and second type (i.e. constant concentration and flux boundary conditions). Thus, the problem statement can be given as

$$\frac{\partial C}{\partial t} = D \frac{\partial^2 C}{\partial x^2} \qquad (3-45)$$

with the boundary conditions

$$x = 0, \quad \frac{\partial C}{\partial x} = \frac{J_{tip}}{D} \qquad (3-46)$$

$$x = L, \quad C(L,t) = C_{bulk} \qquad (3-47)$$

where C = concentration

D = diffusion coefficient

t = time

x = distance from tip

J_{tip} = flux at tip

L = length of crack

and an initial condition

$$C(x,0) = C_{bulk} \tag{3-48}$$

The exact solution to this problem can be easily derived and is given by

$$C(x,t) = \frac{J_{tip}}{D}(L-x) + C_{bulk} + \frac{2}{L}\sum e^{-D\beta_m^2 t}\cos \beta_m(x) \left[\left(\frac{K'}{\beta_m} + \frac{K''x}{\beta_m}\right)(-1)^m - \frac{K''}{\beta_m^2}\right] \tag{3-49}$$

where β = positive roots of the equation $\cos \beta_m L = 0$

$$= \frac{(2m+1)\pi}{2L}$$

m = integer

$$K' = C_i - C_{i,bulk} - \frac{J_{tip} L}{D}$$

$$K'' = \frac{J_{tip} L}{D}$$

This exact solution was compared against the solution produced by the numerical model. The conditions for the simulation are given in Table 3-1. Figure 3-2 gives the transient concentration profile at the crack tip and one third of the way into the crack.

Table 3-1. Input Parameters for Diffusion with Linear Source Term Comparison

J_{tip}	5×10^{-7} moles/m^2-sec
C_{bulk}	0.0 M
C_i	0.0 M
L	1×10^{-2} m
D	9.3×10^{-9} m^2/sec

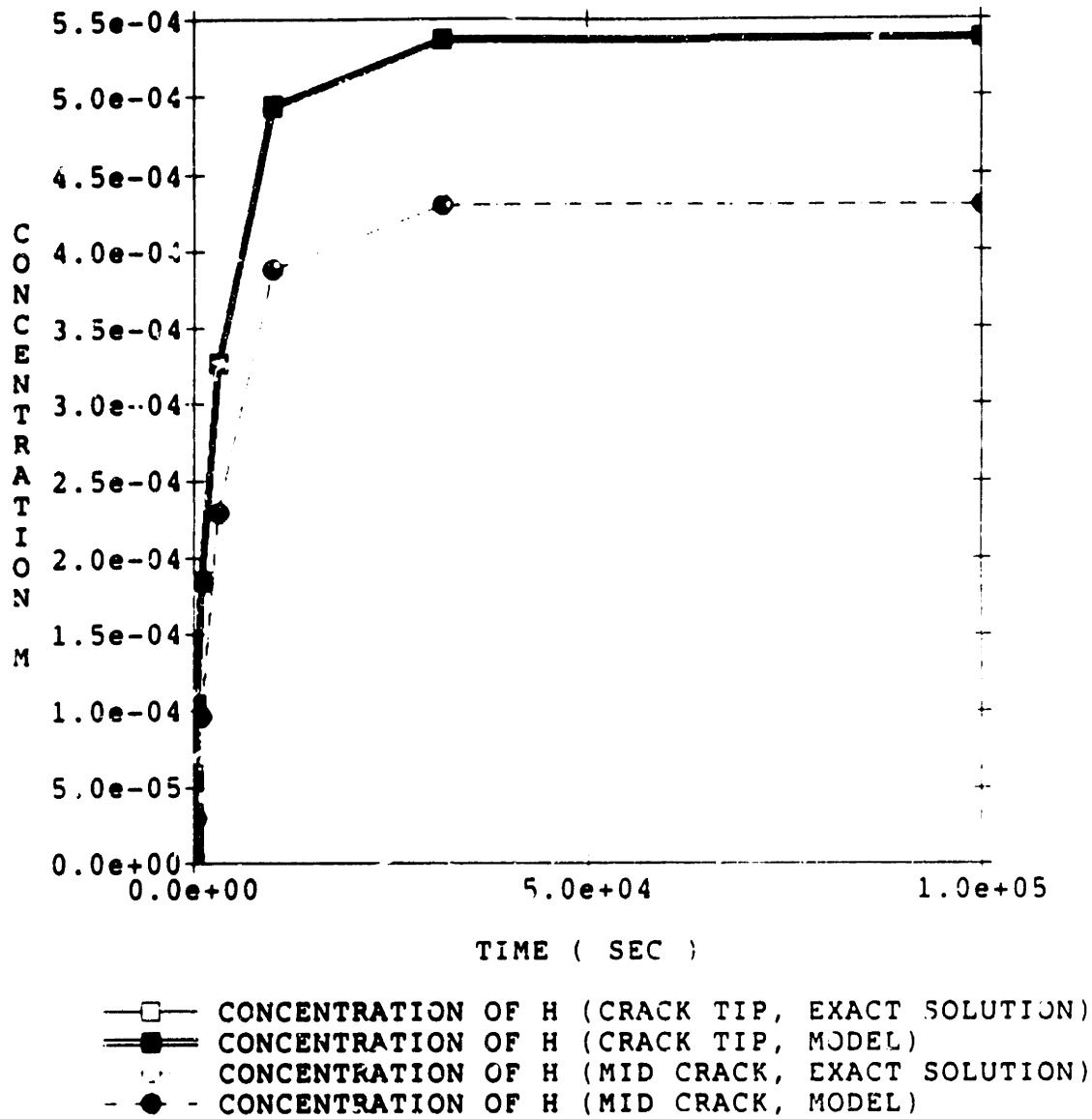

Figure 3-2. Comparison of transient model results with exact solution for diffusion.

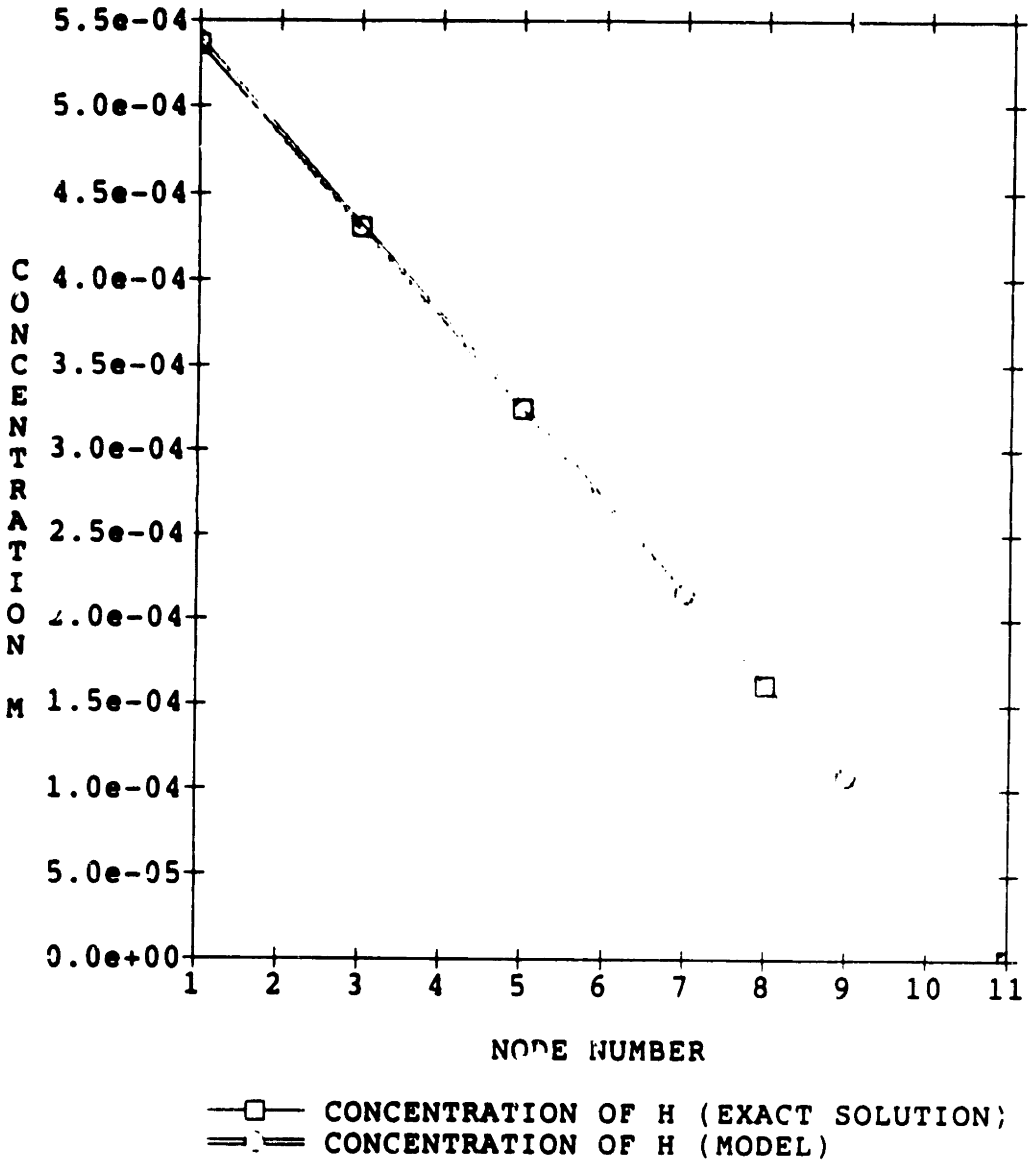

Figure 3-3. Comparison of steady-state model results with exact solution for diffusion.

Figure 3-3 gives the steady state profile within the crack. In both cases the agreement is excellent.

3.4.2 Diffusion and Linear Source Term

In the model there are many homogeneous equilibrium reactions, radiolysis, and the possibility of dissolution reactions that take place. The only way to check this part of the model is by comparison with an analytic solution derived for the diffusion with a linear source term. The equation for this problem is given by

$$\frac{\partial C}{\partial t} = D\frac{\partial^2 C}{\partial x^2} + \gamma C + g \qquad (3\text{-}50)$$

where

C = concentration

D = diffusion coefficient

t = time

x = distance from tip

γ = reaction rate constant

g = source term

The boundary conditions are given by

$$x = 0, \qquad \frac{\partial C}{\partial x} = -\frac{J_{tip}}{D} \qquad (3\text{-}51)$$

$$x = L, \qquad C(L,t) = C_{bulk} \qquad (3\text{-}52)$$

and the initial conditions in the crack are

$$t = 0, \qquad C(x,0) = C_{bulk} \tag{3-53}$$

This problem has an exact solution given by

$$\begin{aligned} C(x,t) = {} & \frac{g}{2D}\left(L^2 - x^2\right) + \frac{J_{tip}}{D}(L - x) + C_{bulk} \\ & + \frac{2}{L}\sum_{m=0}^{\infty} \cos(\beta_m x)\left[\frac{C_{bulk}}{\beta_m}\sin(\beta_m L)e^{(\gamma - D\beta_m)t}\right] \\ & - \frac{2}{L}\sum \cos(\beta_m x)\left[\frac{\left(\frac{C_{bulk}}{\beta_m} + \frac{g}{D\beta_m}\right)\sin(\beta_m L) + \frac{J_{tip}}{D\beta_m^2}}{\left(D\beta_m^2 - \gamma\right)}\right] \\ & + \frac{2}{L}\sum_{m=0}^{\infty} \cos(\beta_m x)\left[D\beta_m^2 e^{(\gamma - D\beta_m)t} - \gamma\right] \end{aligned} \tag{3-54}$$

where β = the positive roots to the equation $\cos \beta_m L = 0$

$$= \frac{(2m+1)\pi}{2L}$$

This exact solution was compared against the solution produced by the model under identical initial and boundary conditions. The conditions and constants for the test case presented are given in Table 3-2. Figure 3-4 gives the concentration profile for the crack tip and halfway down the crack as a function of time. Figure 3-5 shows the comparison of the steady state concentration profile within the crack. In all cases agreement is excellent.

Table 3-2. Input Parameters for Diffusion with Linear Source Term Comparison

J_{tip}	5×10^{-7} moles/m^2-sec
C_{bulk}	0.0 M
C_i	0.0 M
L	1×10^{-2} m
D	4.3×10^{-9} m^2/sec
g	1×10^{-2} moles/sec-m^3
K	1×10^{-7} sec^{-1}

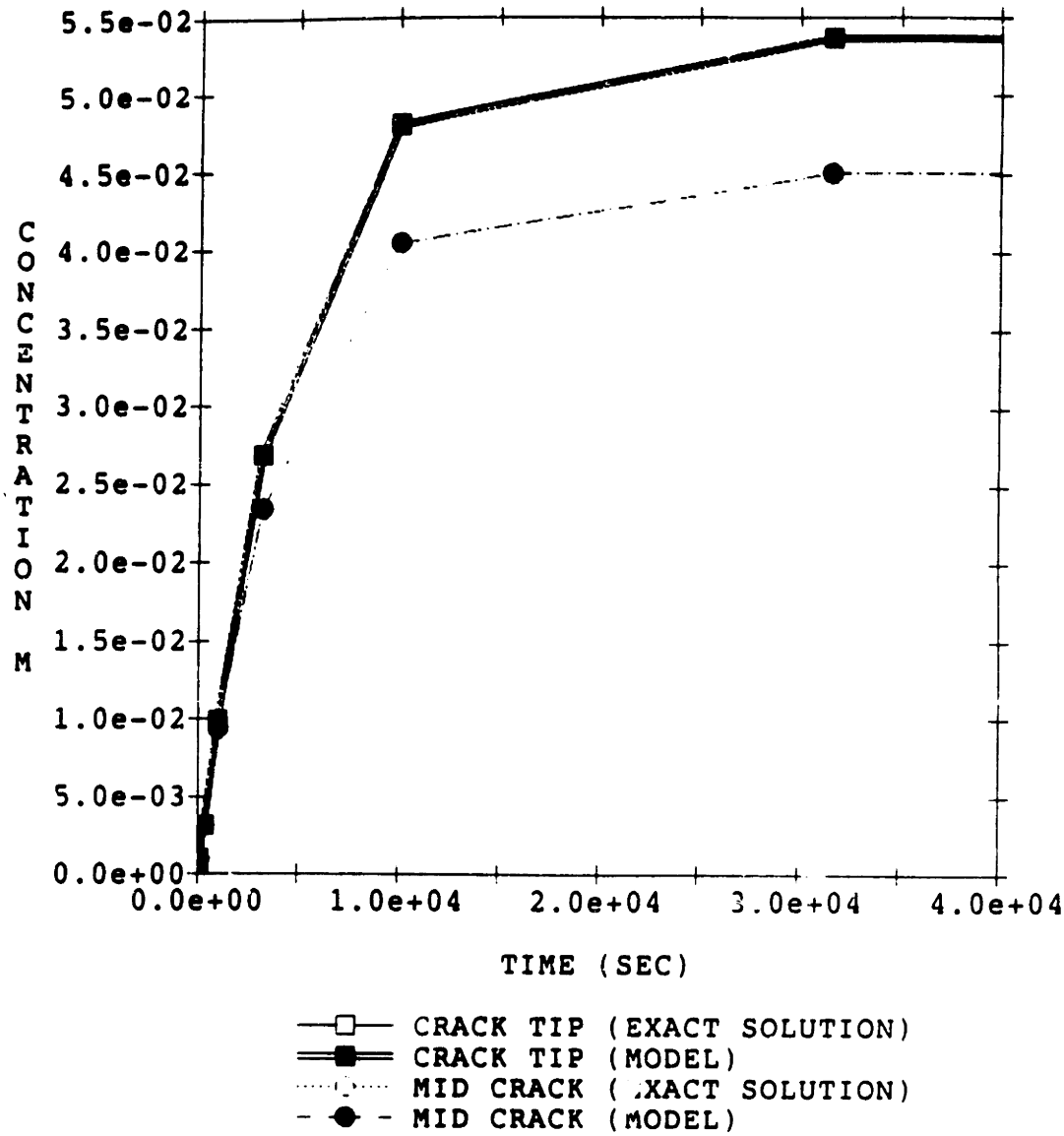

Figure 3-4. Comparison of transient modeling results with exact solution for diffusion with a linear source term (KC+G).

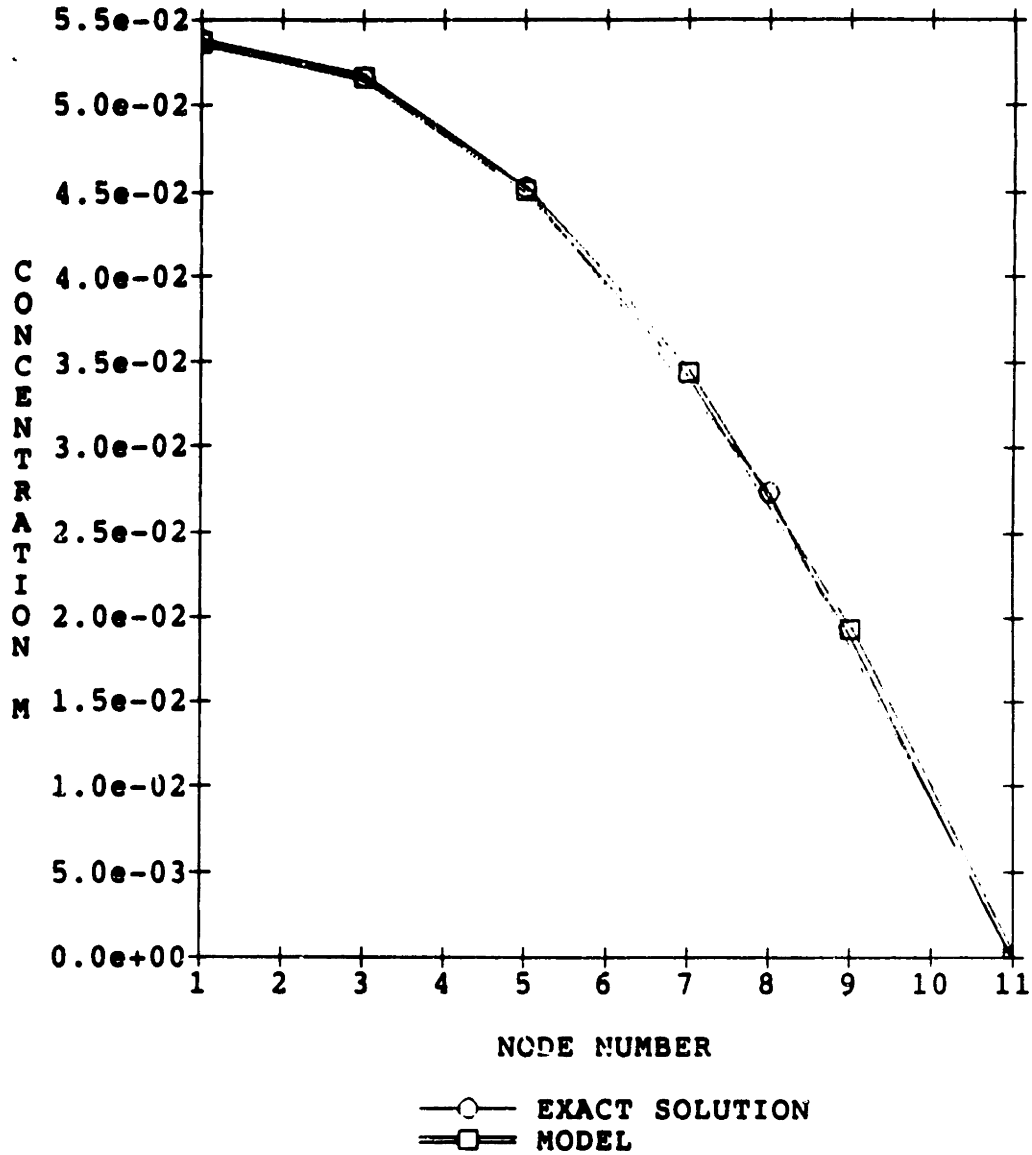

Figure 3-5. Comparison of steady-state modeling results with exact solution for diffusion with a linear source term (KC+G).

3.4.3 Diffusion and Convection With Wall Reactions

In this case, the model is compared with a crack model developed by A. Turnbull (*2*). Mass transfer of oxygen occurs by diffusion and advection (forced convection due to movement of the crack walls) and cathodic consumption of oxygen on the walls of the crack. The crack is assumed to be in a compact tension specimen an the shape of the crack used in the model is assumed to be trapezoidal. Both of these geometries are shown in Figure 3-6. Before showing the comparison of results it is necessary to describe the particulars of the model.

As described in Section 3-1, the fluid velocity at any position, averaged across the width of the crack is given by;

$$\bar{v}(x,t) = - \frac{x}{h} \frac{\partial h}{\partial t} \qquad (3-55)$$

where

$\bar{v}$ = average velocity at position x

h = half width of the crack at position x

x = distance from crack tip

t = time

The half width of the crack is a function of position and time and is given by

$$h(x,t) = h_0(t) + x \tan(\theta(t)) \qquad (3-56)$$

where

$h_0(t)$ = half width at crack tip

$\theta(t)$ = crack angle (Figure 3-1b)

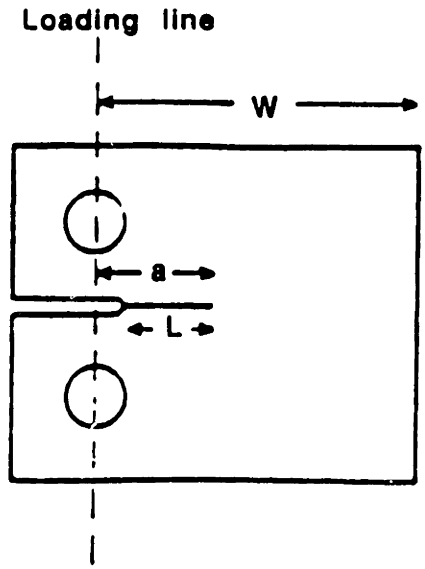

(a) Compact tension speciman.

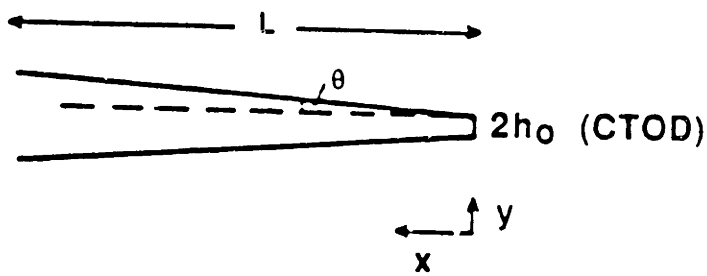

(b) Model Crack

Figure 3.6. Geometry of a) compact tension specimen; and b) model crack (*2*).

The displacement or two times the half width of the crack tip, $2h_0(t)$, is represented by the crack tip opening displacement (CTOD). In this case, the CTOD is evaluated using the Dugdale model of plasticity with the assumption of small scale yielding (*2*). For plane strain conditions, this model for CTOD is expressed by the following for the unloading condition :

$$CTOD(t) = \frac{1}{3}\frac{K_{max}^2}{E''\sigma_y}\left[1 - 0.5\left(1 - \frac{K(t)}{K_{max}}\right)^2\right] \qquad (3\text{-}57)$$

and for the loading condition :

$$CTOD(t) = \frac{1}{3}\frac{K_{max}^2}{E''\sigma_y}\left[1 - 0.5\left(1 - R_D^2\right) + 0.5\left(\frac{K(t)}{K_{max}} - R_D\right)^2\right] \qquad (3\text{-}58)$$

where R_D = minimum load/maximum load

$$E'' = \frac{E'}{\left(1 - \mu^2\right)}$$

E' = Young's Modulus

μ = Poisson's ratio

K = stress intensity factor

K_{max} = maximum stress intensity factor

σ_y = yield strength

In this case, the time dependence of the stress intensity factor is given by

$$K(t) = K_{max} + \delta K \sin(2\pi ft) \qquad (3\text{-}59)$$

where δK = range of stress intensity factor

f = frequency

The displacement at the loading line, $\delta(t)$, for conditions of plane strain is given by

$$\delta(t) = \frac{K(t)\ W\ V_2\left(1 - \mu^2\right)}{\sqrt{a}\ F\ E'} \qquad (3\text{-}60)$$

where W = distance of loading from base of specimen

a = distance of crack tip from loading line

V_2 = function of a/W calculated using the relationship found in reference (*11*)

F = function of a/W

E' = Young's Modulus

F is a function of a/W and for $0.3 \leq a/W \leq 0.7$ is given by (*2*)

$$F\left(\frac{a}{W}\right) = 29.6 - 185.5\left(\frac{a}{W}\right) + 655.7\left(\frac{a}{W}\right)^2 - 1017\left(\frac{a}{W}\right)^3 + 638.9\left(\frac{a}{W}\right)^4 \qquad (3\text{-}61)$$

The crack angle is given by

$$\tan(\theta(t)) = \frac{\delta(t) - CTOD(t)}{2a} \qquad (3\text{-}62)$$

and the width at any value of x is described by

$$w(x,t) = 2\,h(x,t) = CTOD(t) + 2 \times \tan(\vartheta(t)) \qquad (3\text{-}63)$$

Thus, using Equations 3-56 through 3-63 and substituting into Equation 3-55 yields the fluid velocity due to movement of the crack walls as a function of position and time averaged over the width of the crack. This velocity is used in the convective term of the following equation,

$$\frac{\partial C}{\partial t} = D\frac{\partial^2 C}{\partial x^2} - \frac{\partial}{\partial x}(Cv) + C\frac{\partial v}{\partial x} - \frac{I}{4F}C \qquad (3\text{-}64)$$

where

C = concentration of oxygen

D = diffusion coefficient of oxygen

$$I = k' \exp\left[-\frac{\alpha F E}{RT}\right]$$

k' = rate constant for oxygen reduction

α = transfer coefficient

E = electrode potential

F = Faraday's constant

R = gas constant

T = temperature

The the transport of oxygen due to diffusion and convection is incorporated as well as cathodic consumption down the crack. In this equation the last term represents the consumption of oxygen by cathodic reduction as shown below

$$O_2 + 2\,H_2O + 4\,e^- \rightarrow 4\,OH^- \qquad (3\text{-}65)$$

Comparison of the modeling results obtained by Turnbull (*2*) and the model presented in this thesis are shown in Figures 3-7 through 3-9. Table 3-3 gives the basic input parameters used for these figures. Figure 3-7 shows the comparison of the maximum periodic values of normalized oxygen concentration within the model crack for different R values. The agreement is very good. There are some differences at the tip of the crack probably due to some slight difference in application of the boundary condition at this point and the difficulty in identifying the time at maximum concentration is reached in the crack. Figure 3-8 shows the comparison of the maximum periodic values of normalized oxygen concentration profile within the model crack for different i' (i.e. different oxygen consumption rates). The agreement is very good in this case. Figure 3-9 shows a comparison of the transient normalized oxygen concentration at a dimensionless position of .8 from the crack tip. The cyclic nature of the concentration profile is evident is this figure. Agreement between the two models is excellent.

3.4.4 Diffusion, Migration and Electrochemical Reactions at Tip and on Walls

Shuck and Swedlow modeled the electrochemistry within a parallel sided crack using the following governing equation (*12,13*)

$$\frac{\partial C_i}{\partial t} = D_i \frac{\partial^2 C_i}{\partial x^2} + \frac{z_i D_i F}{RT} \frac{\partial}{\partial x}\left(C_i \frac{\partial \phi}{\partial x} \right) + \frac{i_o\, s}{hFn} \qquad (3\text{-}66)$$

Table 3-3. General Input Parameters for Figures 3-7 through 3-9.

D	1.4×10^{-9} m^2/s
σ_y	340 MPa
a/W	0.3
W	6.0×10^{-2} m
L	1.0x10-2 m
k'	4.2×10^{-1} A $mole^{-1}$ m
α	0.5

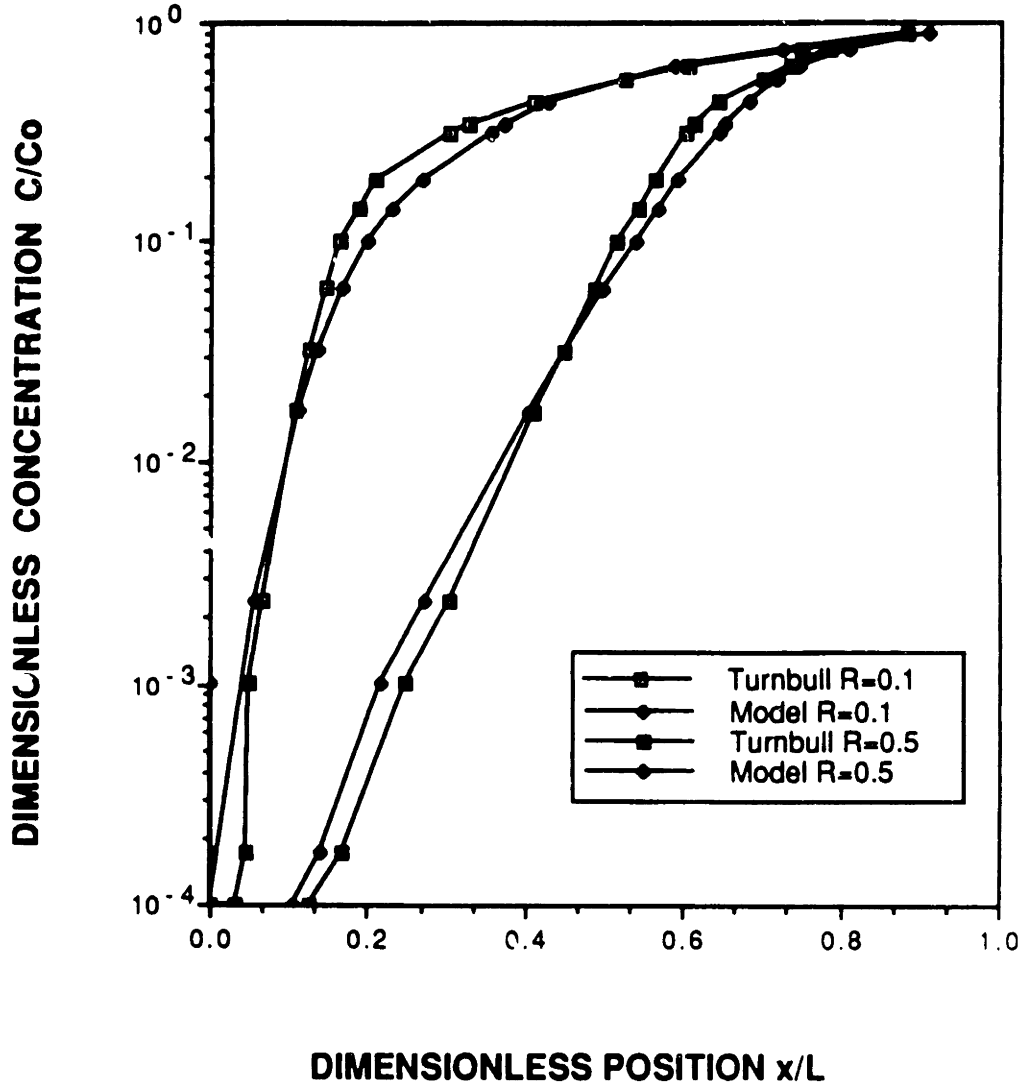

Figure 3-7. Comparison of the maximum periodic value of normalized oxygen concentrations with varying R obtained using model presented in this thesis and modeling results obtained by A. Turnbull (DK = 10 M $Nm^{-3/2}$, f = 0.1 Hz, i' = 50 A $mole^{-1}$ cm) (*2*).

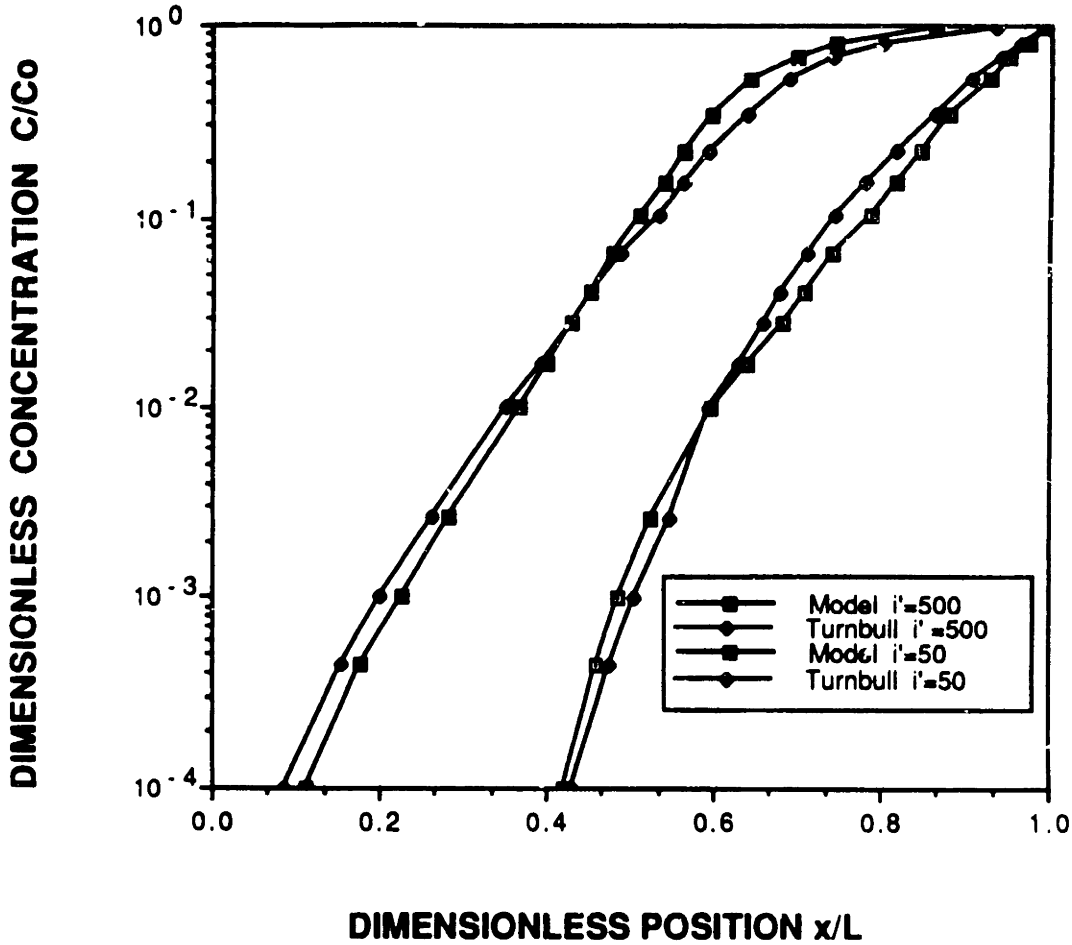

Figure 3-8. Comparison of the maximum periodic value of normalized oxygen concentration for varying i' using model presented in this thesis and modeling results obtained by A. Turnbull (DK = 10MNm$^{-3/2}$, f = 0.1 Hz, R = 0.5, l = 10 mm) (*2*).

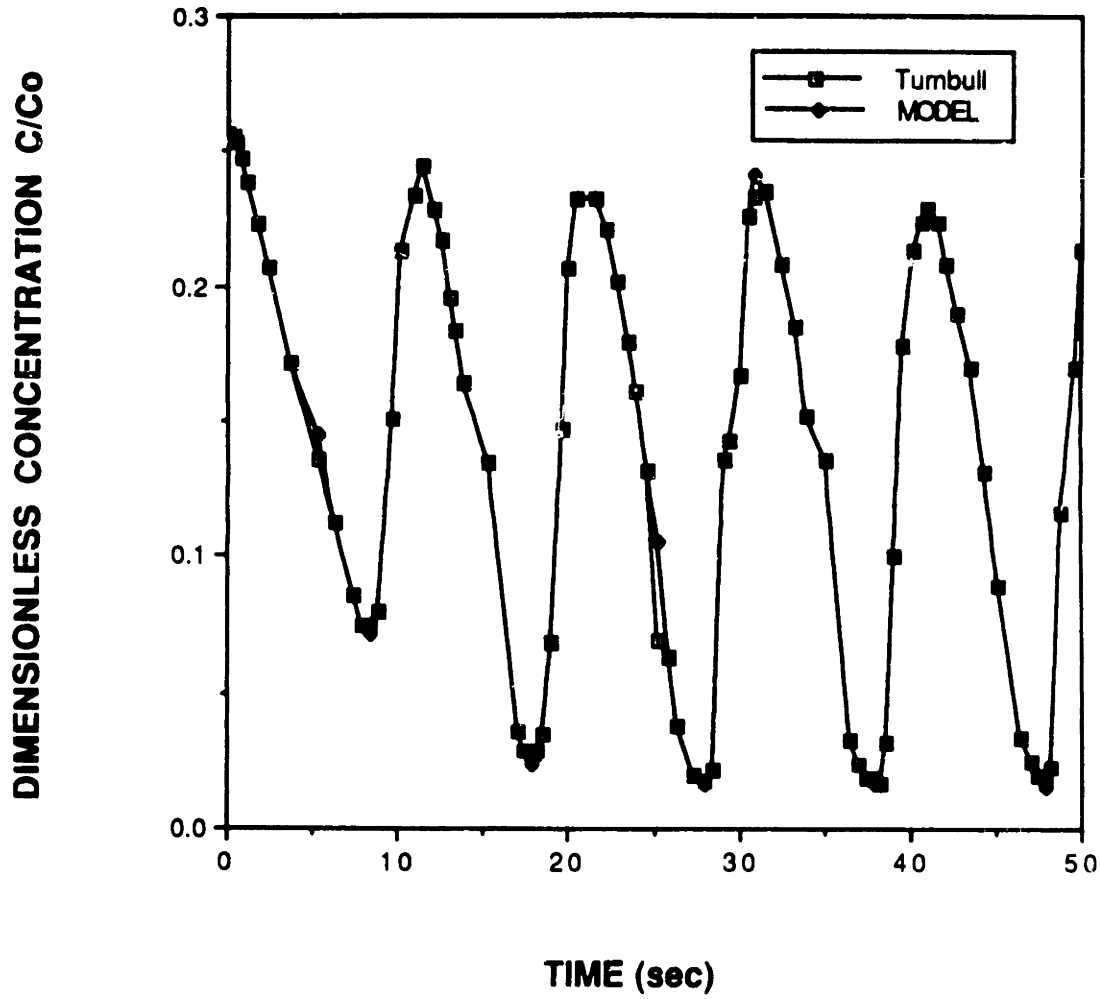

Figure 3-9. Comparison of transient normalized oxygen concentration at x// = 0.8 (2mm from mouth) of model with results obtained by A. Turnbull (DK = 10 $MNm^{-3/2}$, f = 0.1 Hz, R = 0.5, *l* = 10 mm) (*2*).

The transport modes were diffusion and ion migration. There was a constant source of species on the walls and tip of the crack. The method used to average the flux between the walls of the crack is unclear in this model.

The results obtained from this model were compared with results obtained using the model developed in this thesis. Table 3-4 presents conditions and constants used for the simulations. Figure 3-10 presents the transient concentration profiles of the three figures of interest. Figure 3-11 shows the steady state concentration profiles developed. Figure 3-12 presents the initial and steady state potential profile in the crack. In all cases the agreement is good. There are some slight differences in the H^+ profiles and potential profiles which maybe the result of a different method of averaging over the crack width.

Table 3-4. Input Parameters for Figures 3-10 through 3-12

Species	Charge	Diffusion coefficient (m^2/sec)	Initial Concentration (moles/l)
H^+	+ 1	9×10^{-9}	10^{-7}
Na^+	+ 1	1.33×10^{-9}	0.6
Cl^-	- 1	2×10^{-9}	0.6

Equilibrium Reactions	k_f	k_b	K_{eq}
none	-	-	-

Wall/Tip Electrochemical Reactions	sign	no. of e^-	k_o	α	ref. spec.	spec. power
	+		3.1x10-2	0	-	-

Solubility Reactions	k	K_s
none	-	-

Wall/Tip Dissolution Reactions	Flux (dm^2/sec)
none	-

General Data	
Length (dm)	Width (dm)
No. of Nodes	Delta X
Temperature (K) 573	E_m (V)

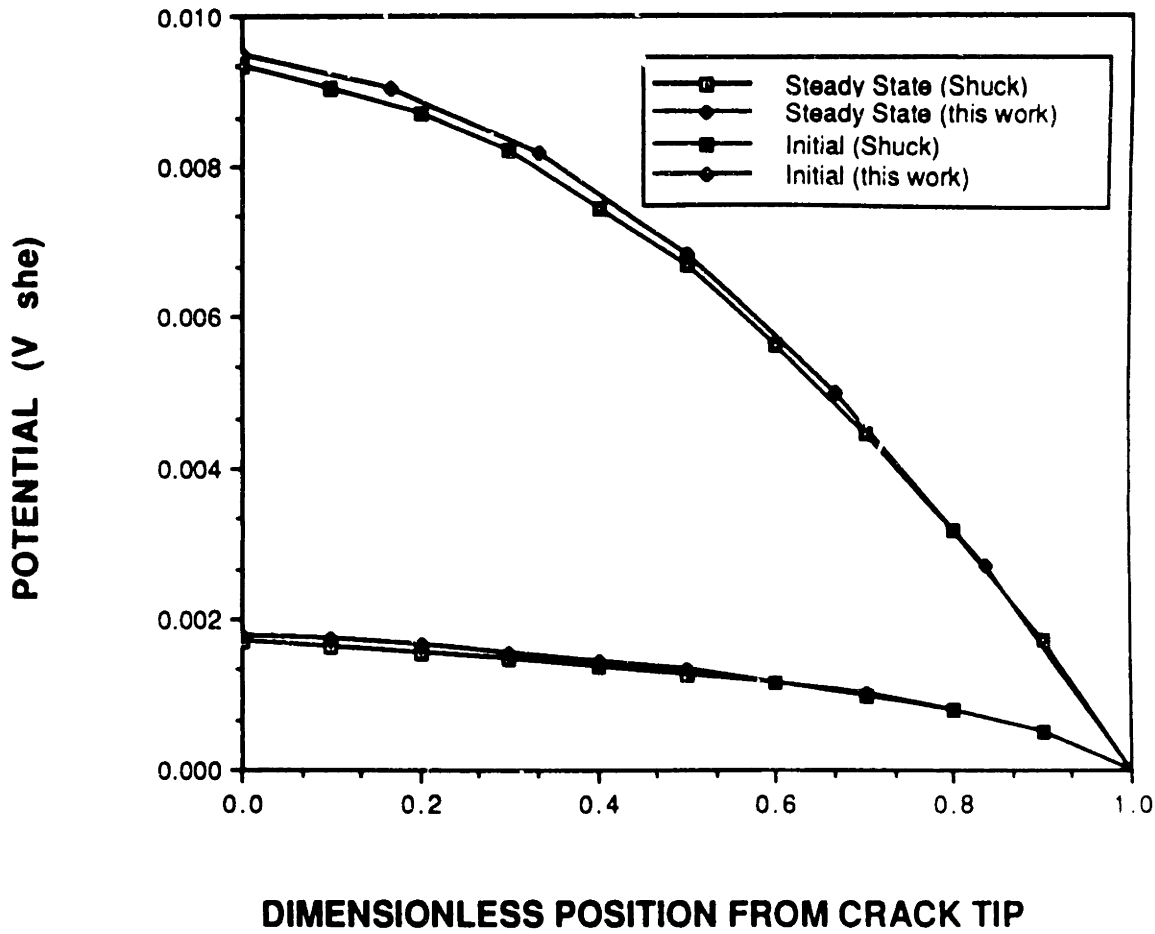

Figure 3-10. Comparison of the transient crevice tip concentrations obtained using model presented in this thesis and results obtained by Shuck and Swedlow (*12,13*).

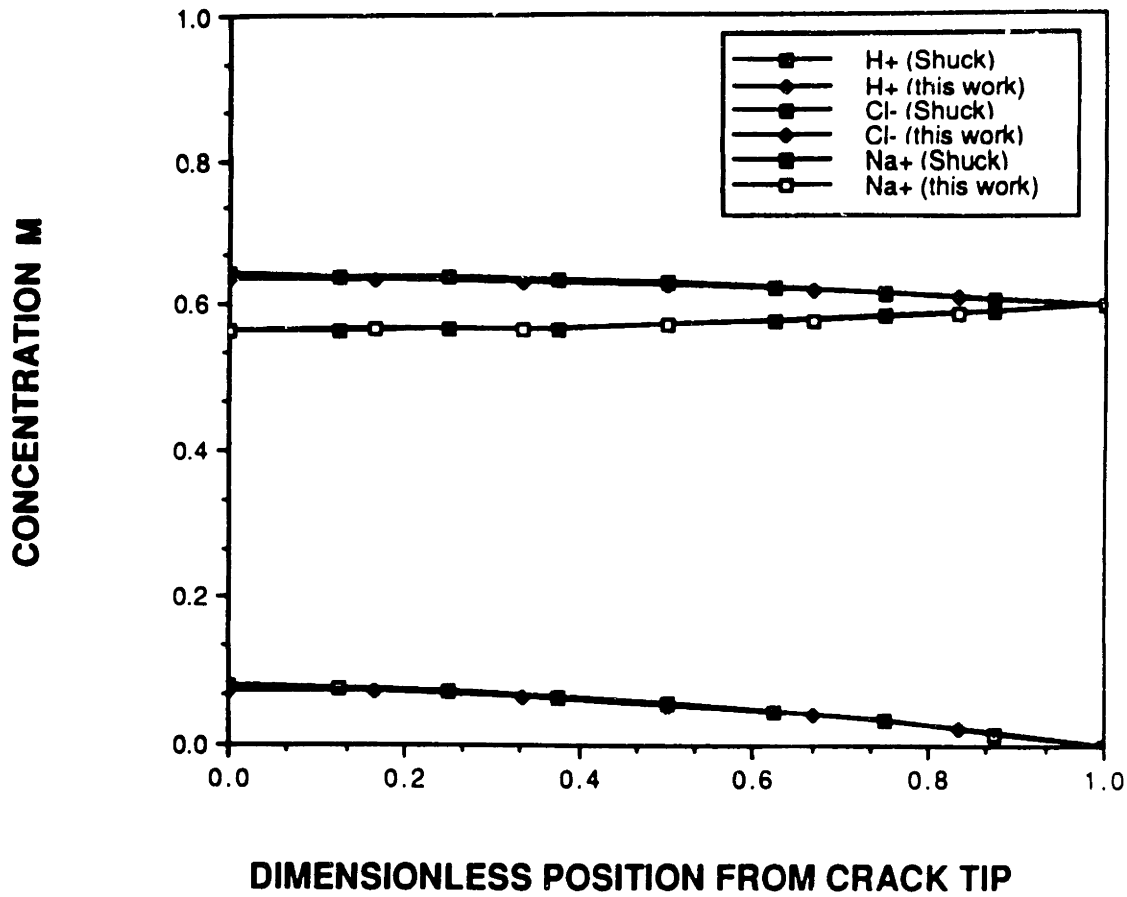

Figure 3-11. Comparison of steady state concentration profile within the crevice obtained using the model presented in this thesis and results obtained by Shuck and Swedlow (*12,13*).

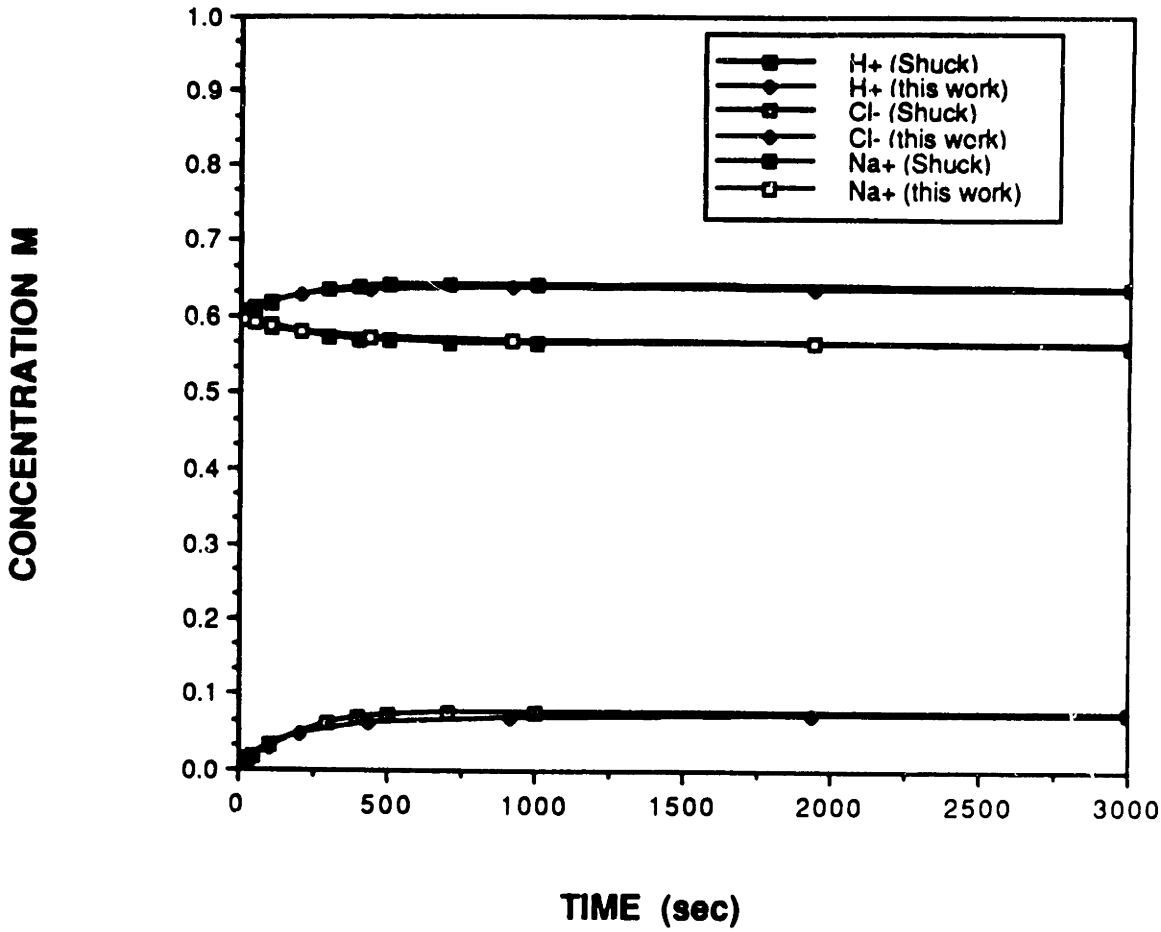

Figure 3-12. Comparison of initial and steady state potential profiles within crevice obtained using the model presented in this thesis and result obtained by Shuck and Swedlow.(*12,13*)

3.5 REFERENCES

(1) J. Newman, Electrochemical Systems, Prentice-Hall, N.J., 1973.

(2) A. Turnbull, Corr. Sci., vol. 22(9), pp. 877-893, 1982.

(3) A.C. Hindmarsh, in Scientific Computing, R. Stepleman et al.,eds., IMACS/North-Holland Publishing Company, 1983, pp. 55-64.

(4) A.M. Loeb and W.E. Schiesser, in Stiff Differential Systems, R.A. Willoughby, ed. Plenum Press, N.Y., 1974, pp. 229-243.

(5) A.C. Hindmarsh, Advances in Computer Methods For Differential Equations (IV), R. Vichnevetsky and R.S. Stepleman, eds., IMACS, 1981, pp. 312-316.

(6) A.C. Hindmarsh, ACM SIGNUM Newsletter, vol. 15(4), pp. 10-11, 1980.

(7) J.F. Painter, Solving the Navier-Stokes Equations with LSODI and the Method of Lines, LLNL Report UCID-19262, 1981.

(8) A.C. Hindmarsh, Linear Multistep Methods for Ordinary Differential Equations : Method, Formulations, Stability, and the Methods of Nordsieck and Gear, LLnl Report TID-4500, UC-32, 1972.

(9) C.W. Gear, Numerical Initial Value Problems in Ordinary Differential Equations, Prentice-Hall, N.J., 1971, pp. 158-166.

(10) G. Strang, Introduction to Applied Mathematics, Wellesley-Cambridge Press, 1986, pp. 373-377.

(11) H. Tada, P. Paris, and G. Irwin, The Stress Analysis of Cracks Handbook, Del Research Corp., 1973.

(12) R.R. Shuck and J.L. Swedlow, Localized Corrosion, B.F. Brown, J. Kruger, and R.W. Staehle, eds., pp. 190-207, NACE, 1974.

(13) R.R. Shuck and J.L. Swedlow, ibid, pp. 208-220.

Chapter 4

MODELLING OF THE ELECTROCHEMISTRY WITHIN CREVICES

4.1 INTRODUCTION

The first application of the model is to the prediction of the electrochemical conditions that develop within a crevice. A crevice can be defined as a narrow region within which mass transport is restricted and little or no convective mixing occurs. Crevices can form at metal/metal or metal/non-metal junctions such as holes, gaskets, lap joints, loose corrosion deposits, marine growths, coupled pipes, threaded joints, bolts, and rivet heads, and are often inherent in the design of structures. The formation of a creviced region produces changes in the local electrochemistry which may be sufficient to cause breakdown of the passive film which may result in EAC. Loss of passivity within a crevice can result in a form of localized attack known as crevice corrosion. Metal or alloys that depend on their passive films for corrosion resistance are particularly susceptible to crevice corrosion. For example, stainless steel, aluminum, and copper based alloys are susceptible to this form of localized attack (*1*). The change in local electrochemistry that occurs in creviced regions even without passivity breakdown can also result in the initiation of stress corrosion cracking in these regions. Both crevice attack and stress corrosion cracking can result in premature failure of the component at the creviced region.

Since there is no convective mixing within a crevice, the concentration of all dissolved species is controlled by their production, consumption, and transport due to diffusion and ion migration in the region. The solution within the crevice quickly becomes deaerated because of the rapid reduction of oxygen on the walls of the crevice coupled with restricted mass transport of oxygen into the crevice region. This difference in oxygen concentration can lead to a difference in potential between the creviced region and the bulk environment. Other changes in local electrochemistry within the crevice that can occur are induced by the dissolution of species from the alloys that make up the crevice, ions that are transported into the crevice from the bulk solution by ion migration, and reactions processes involving these species. The local concentration of these species can increase over a period of time creating a completely different local chemical environment within the crevice. The factors that affect the concentration and potential profiles that develop within the crevice are bulk conductivity, bulk oxygen concentration (which determines the bulk metal potential), passive current (assuming the system is passive), and total cathodic current on the walls of the crevice (the sum of total anodic and total cathodic currents determine the net current in the crevice), and crevice geometry (width and length).

As described above, the formation of crevices is often inherent in the design of the structure or component. In light water reactor systems, creviced regions can occur in steam generators between tubing and tube support plates, at turbine discs in blade root and shroud attachment regions or in the keyway area, and in nozzle safe ends between inlet tube or thermal sleeves and the pressure vessel (*2*). Stress corrosion cracks have initiated in these creviced regions as the result of the local electrochemical environment which develops within these regions (*2*). The initiation of stress corrosion cracking has resulted in premature failure of these components.

The model developed in the present study has been applied to the particular problem of predicting the electrochemistry within a tight crevice exposed to BWR environments in order to evaluate whether the conditions generated within the crevice are sufficient to increase susceptibility to stress corrosion cracking. This possibility of stress corrosion crack initiation will be evaluated using an engineering diagram such as is shown in Figure 4-1. The curve shown in this figure separates regions of stress corrosion cracking susceptibility and immunity as a function of solution conductivity and potential (*3*). If the conditions developed within the crevice fall above the curve when plotted on this figure, it is possible to initiate stress corrosion cracking within the crevice region. The farther above these conditions fall, the more likely it would be to initiate stress corrosion cracking. Conversely, if the electrochemical conditions within the crevice are below the values depicted by this curve, it is unlikely that stress corrosion cracks would initiate. Thus, the objective of this research is to identify the crevice conditions that develop and to place them on this diagram in order to determine the environment or material conditions that might lead to stress corrosion cracking initiation. In this chapter, the results obtained from modeling of crevice electrochemical conditions will be presented and discussed in detail. The implication of these results for a crevice that is present at a BWR recirculation inlet nozzle safe ends will be discussed in Chapter 5.

In order to eventually apply the modeling results obtained to the safe end crevice, it is necessary to use the correct crevice geometry, materials, and environment. A difficulty in modeling the safe end annulus is its length (0.6096 m or 2 feet) and the time necessary to achieve steady state within the crevice. The time necessary to achieve steady state can be calculated approximately as follows

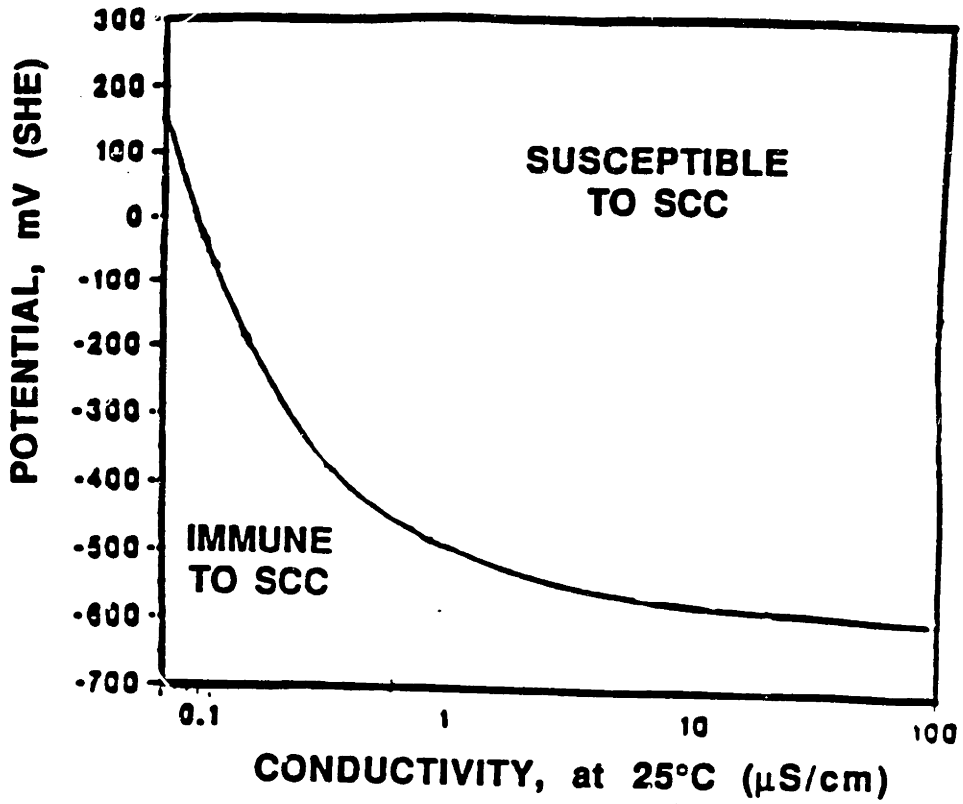

Figure 4-1. Stress corrosion cracking susceptibility curve for lightly sensitized stainless steel (*3*).

$$t_{steady\ state} \approx \frac{(length)^2}{diffusion\ \ coefficient} = \frac{L^2}{D} \qquad (4-1)$$

With $D_{metal\ ion} \approx 1.3 \times 10^{-8}\ m^2/s$, the time to steady state is approximately 1 year. This combination of length and time to steady state is a computational problem because of the large number of nodes (large array sizes) and time steps (long run times) necessary for accurate predictions. To overcome this computational difficulty some previously developed understanding of crevice problems involving dimensionless analysis will be employed (*4,5*).

Since a crevice may be a passive system (until the passive layer breaks down), it should be dominated by the reactions occurring on the walls because the area of the walls is much greater than that of the tip. Thus, the crevice geometry should scale as $(length)^2/(crevice\ half\ width)$ or L^2/h when using the parameters dimensionless time [$\tau = Dt/L^2$] and dimensionless length [$X = x/L$] . As long as the scaling parameter, L^2/h, is constant the time evolution and steady state profiles for concentration and potential within the crevice should be identical when plotted vs dimensionless time and length respectively. Thus, in principle, the long safe end annulus can be simulated by a shorter but narrower crevice saving much computational time. Verification of this L^2/h scaling is presented in the next section.

The crevice used in the modeling is a one dimensional parallel sided, stagnant region composed of Inconel® 600 on one side and type 304 stainless steel on the other. It is similar to the BWR recirculation inlet safe-end crevice. A schematic of the model crevice is shown in Figure 4-2. In this figure, the safe end piece is assumed to be located at the crevice tip. The passive current of Inconel® 600 was used since it is twenty times greater than the passive current of type 304 stainless steel. The passive current was divided by two since only one wall of the crevice is Inconel® 600.

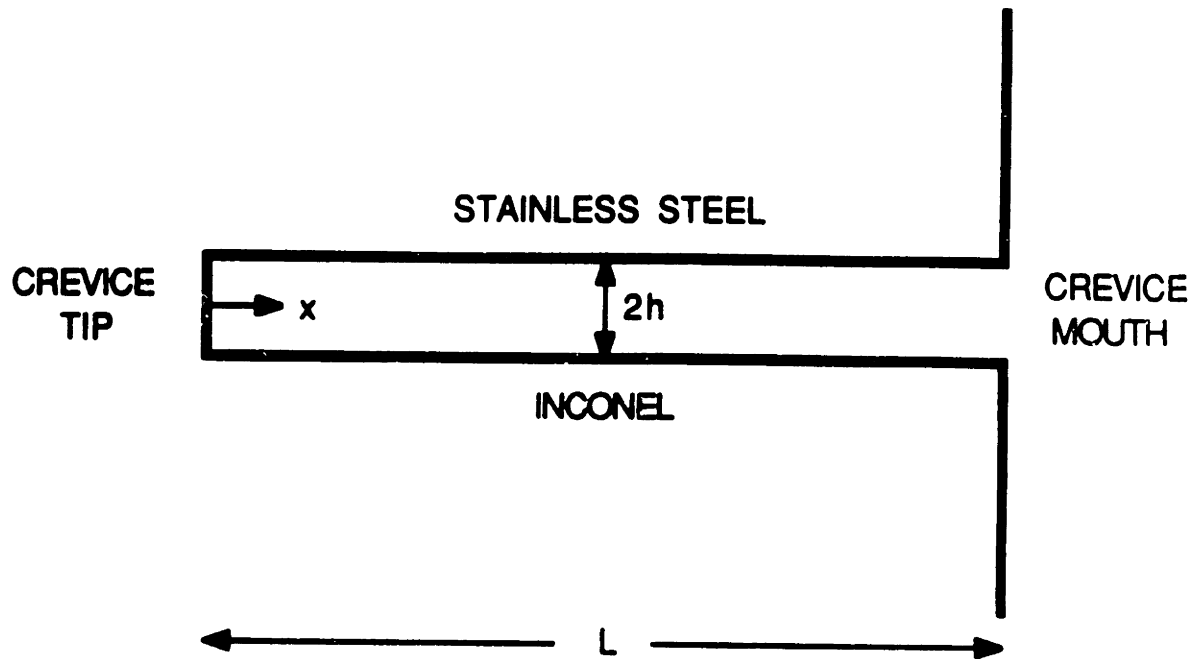

Figure 4-2. Schematic of crevice used in model. The walls of the crevice are made of stainless steel and Inconel.

Unless otherwise stated, the external bulk concentration used was that of normal BWR water chemistry as described in Table 4-1. The upper limits on normal conductivity and oxygen concentration were used. The temperature assumed for the modelling was 300 °C.

Table 4-1 Normal BWR Water Electrochemistry (*2*)

Conductivity (at 25 °C)	< 0.3 μS/cm
Dissolved Oxygen	< 200 ppb
Potential	~0 V

In order to develop a scientific understanding of the importance of different variables on the electrochemistry developed within a crevice as well as to apply the model to the specific problem of a BWR crevice, the model has been applied in a logical, step by step fashion. The first objective was to establish the minimum level of complexity that must be included in order to model a crevice accurately. In this context the initial factors evaluated are described below :

- Establishment of the validity of the L^2/h scaling parameter.
- Evaluation of the conditions developed within the crevice when both solubility and internal cathodic reduction reactions are ignored.
- Evaluation of the effect of cathodic reduction reactions on crevice electrochemistry.

These preliminary studies are described in detail in Sections 4.2.1-4.2.3 and summarized in Section 4.2.4. After the completion of these primary objectives, the model was applied more specifically to modelling the local electrochemistry within a BWR crevice. The factors that were considered and evaluated in relation to their influence on crevice chemistry are described below

- Assessment of the importance of solubility limits on local electrochemistry
- The role of more soluble alloying elements and impurities.
- The effect of excursions in bulk conductivity.
- The significance of hydrogen water chemistry.
- The importance of crevice geometry on crevice chemistry.

These more realistic calculations are described in Sections 4.2.5-4.2.8. In addition, in view of the uncertainty in the necessary input data (i.e., kinetics of cathodic reduction reactions), the sensitivity of the conclusions to the values of kinetic parameters chosen has also been considered.

4.2 RESULTS OF CREVICE MODELING

4.2.1 Verification of L^2/h Scaling Parameter

As discussed in the previous section of this chapter, scaling of a crevice is possible, in principle, provided that the L^2/h scaling parameter remains constant. The steady-state concentration profiles should be identical provided the results are plotted

using the dimensionless position parameter, X=x/L. Similarly, the transient profiles of concentration should be the same if plotted using the dimensionless time parameter, $\tau = Dt/L^2$. Verification of this prediction has been demonstrated by running a full length annulus case with a length of 0.6096 m (2 feet) and with a half width of 6.35×10^{-3} m and then comparing the results to a those obtained from crevice with a length of 0.1 dm and a half width of 1.709×10^{-3} m. The scaling parameter L^2/h in both the long wide crevice and the short narrow crevice was 58.5 m. Except for crevice geometry, the modelling conditions were identical for the long and short crevice. Since nickel is the major component of Inconel® Alloy 600 (see Table 4-2), it was assumed that only nickel was dissolving from the walls and tip of the crevice. Inclusion of the other major alloying elements has no major effect since their reaction and transport characteristics are similar. The passive current for Inconel® 600 at this temperature in BWR water is 7.58×10^{-2} A/m^2 (*6*). Nickel ions were also allowed to hydrolyze, but no solubility limits were applied. A bulk solution of NaCl was assumed which was equivalent to approximately 0.55 μS/cm at 25°C. Reduction reactions within the crevice were neglected. The initial conditions and constants for the long and short crevice are listed in Tables 4-3 and 4-4, respectively.

The time dependent results are compared in Figure 4-3a and b for the Ni^{2+} and Cl^- concentrations and for potential. A comparison of the steady state Ni^{2+} and Cl^- concentration and potential profiles in the crevice are shown in Figure 4-4 a and b. There is very good agreement in all cases. Thus, the rest of the cases were run using shorter, narrower crevices to speed up computational time. The figures depicting the results in this section will have concentrations and/or potential plotted as a function of dimensionless units. For time the dimensionless unit is given by

Table 4-2.. Nominal Composition of Inconel® Alloy 600 and 304 Stainless Steel.

(wt%)

	Ni	Fe	C	Mn	S	Cr	Si	Cu	P
Alloy 600	bal	6-10	0.15	1.0	0.015	14-18	0.5	0.5	-
304 SS	8-10.5	bal	0.08	2.00	0.03	18-20	1.00	-	0.045

Table 4-3. Input Parameters for Long Crevice

Species	Charge	Diffusion coefficient (dm^2/sec)	Initial Concentration (moles/l)
H	+ 1	1.76×10^{-5}	2.23×10^{-6}
OH	- 1	9.8×10^{-6}	2.23×10^{-6}
Na	+ 1	2.5×10^{-6}	4.4×10^{-6}
Cl	- 1	3.8×10^{-6}	4.4×10^{-6}
Ni	+ 2	1.3×10^{-6}	0
NiOH	+ 1	1.3×10^{-6}	0

Equilibrium Reactions	k_f	k_b	K_{eq}
$H^+ + OH^- = H_2O$	1×10^{12}	5	2×10^{11}
$Ni^{2+} + H_2O = NiOH^+ + H^+$	6×10^{3}	1×10^{9}	6×10^{-6}

Wall/Tip Electrochemical Reactions	sign	no. of e^-	k_o	α	ref. spec.	spec. power
$Ni \rightarrow Ni^{2+} + 2e^-$	+ 1	2	7.56×10^{-4}	0	-	-

Solubility Reactions	k	K_s
none	-	-

Wall/Tip Dissolution Reactions	Flux (dm^2/sec)
none	-

General Data			
Length (dm)	6.096	Width (dm)	0.127
No. of Nodes	51	Delta X	0.139
Temperature (K)	573	E_m (V)	0

Table 4-4. Input Parameters for Short Crevice.

Species	Charge	Diffusion coefficient (dm^2/sec)	Initial Concentration (moles/l)
H	+ 1	1.76×10^{-5}	2.23×10^{-6}
OH	- 1	9.8×10^{-6}	2.23×10^{-6}
Na	+ 1	2.5×10^{-6}	4.4×10^{-6}
Cl	- 1	3.8×10^{-6}	4.4×10^{-6}
Ni	+ 2	1.3×10^{-6}	0
NiOH	+ 1	1.3×10^{-6}	0

Equilibrium Reactions	k_f	k_b	K_{eq}
$H^+ + OH^- = H_2O$	1×10^{12}	5	2×10^{11}
$Ni^{2+} + H_2O = NiOH^+ + H^+$	6×10^{3}	1×10^{9}	6×10^{-6}

Wall/Tip Electrochemical Reactions	sign	no. of e^-	k_o	α	ref. spec.	spec. power
$Ni \rightarrow Ni^{2+} + 2e^-$	+ 1	2	7.56×10^{-4}	0	-	-

Solubility Reactions	k	K_s
none	-	-

Wall/Tip Dissolution Reactions	Flux (dm^2/sec)
none	-

General Data			
Length (dm)	0.1	Width (dm)	1.709×10^{-5}
No. of Nodes	21	Delta X	0.005
Temperature (K)	573	E_m (V)	0

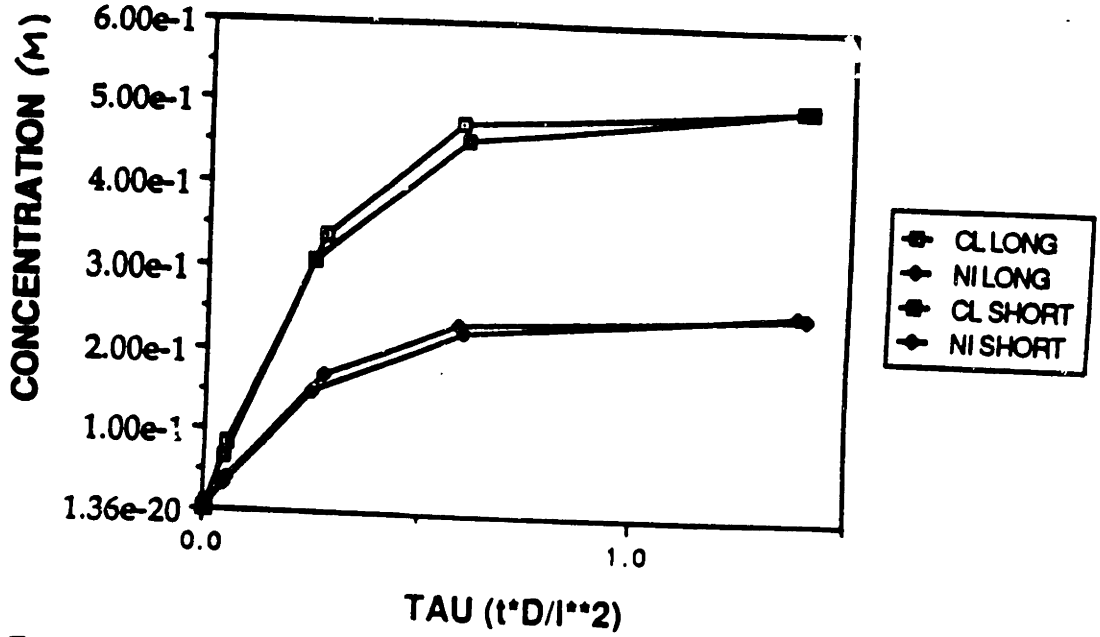

a) Transient crevice tip concentration profiles of Cl^- and Ni^{2+} in long and short crevices. Plotted versus dimensionless time.

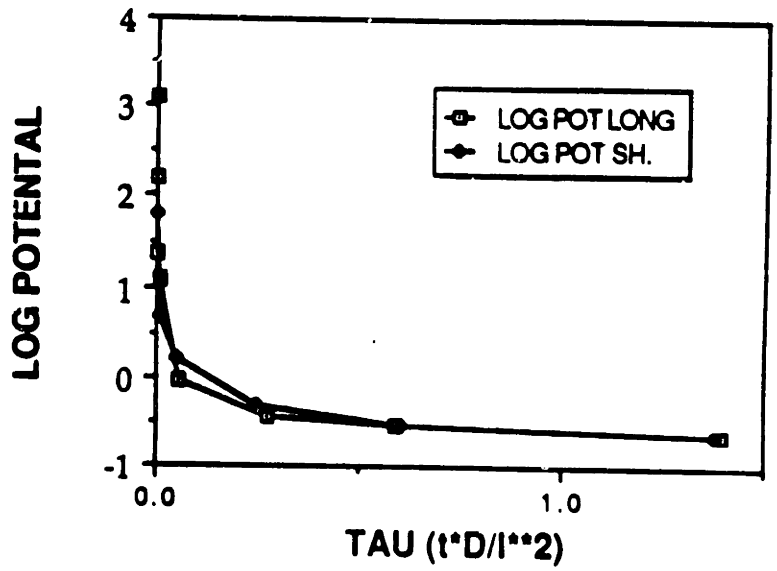

b) Transient crevice tip potential profiles for long and short crevice. Plotted versus dimensionless time.

Figure 4-3. Validation of L^2/h scaling parameter by comparison of transient crevice tip a) concentration, and b) potential profiles.

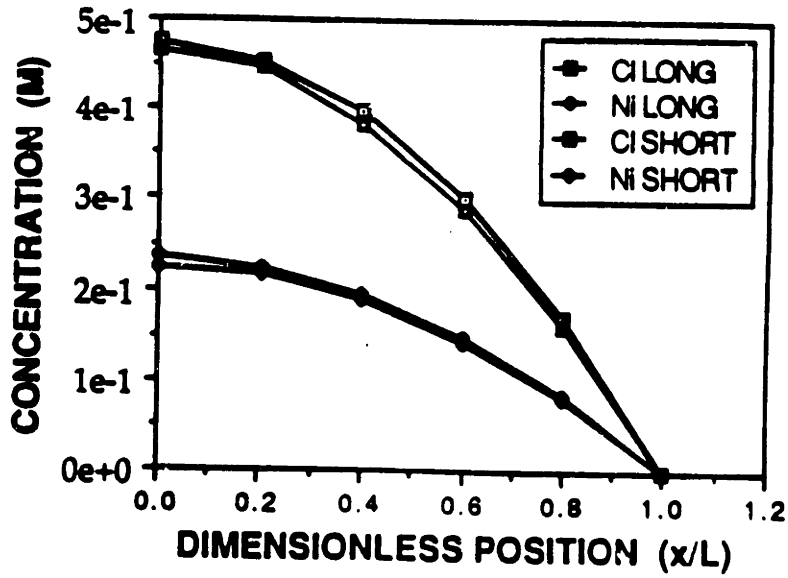

a) Steady-state concentration profiles of Cl^- and Ni^{2+} along long and short crevices. Plotted versus dimensionless position from crevice tip.

Figure 4-4. Validation of L^2/h scaling parameter by comparison of steady-state a) concentration, and b) potential profiles along crevice.

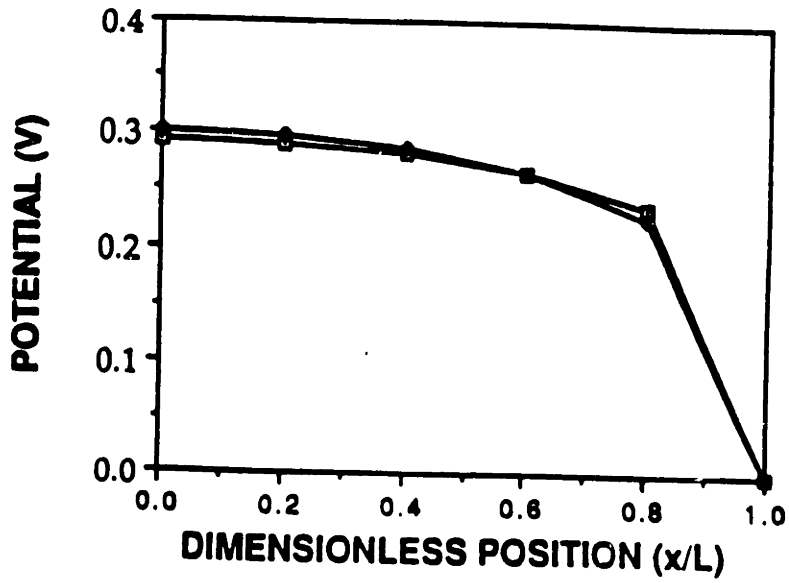

b) Steady-state potential profile along long and short crevice. Plotted versus dimensionless position from crevice tip.

$$\text{dimensionless time} = \frac{\text{(time) (diffusion coefficient)}}{\text{(crevice length)}^2} = \frac{t\,D}{L^2} \qquad (4-2)$$

and for dimensionless distance :

$$\text{dimensionless distance} = \frac{\text{distance from crevice tip}}{\text{crevice length}} = \frac{x}{L} \qquad (4-3)$$

4.2.2 Electrochemistry Developed Within Crevice Without Solubility Limits and Cathodic Reactions

In this section, the conditions developed within the crevice will be evaluated without restraint on the solubility of dissolved species and neglecting any cathodic reactions that may be occurring within the crevice. Figure 4-5 depicts the transient crevice tip concentration and potential profiles that develop. The initial conditions and constants used in this case are shown in Table 4-5. As is apparent in this figure, the initial crevice tip potential is -1400 V. Potentials expected within crevices should be limited by the corrosion potential in oxygen free media because the effect of a large potential drop is simply to decouple the crevice for the external surface. Thus, the predicted initial value of -1400 V is meaningless and arises because no cathodic reactions have been considered. The H^+ ion concentration initially dips, since the positive ions are initially being forced out by ion migration due to the large potential gradient. As the potential drop in the crevice decreases and the ionic concentration increases, ion migration becomes less important and the H^+ concentration increases (pH decreases). The metal ion concentrations (Ni^{2+} and $NiOH^+$) jump very quickly from 0

Table 4-5. Input Parameters for Figure 4-5.

Species	Charge	Diffusion coefficient (dm^2/sec)	Initial Concentration (moles/l)
H	+ 1	1.76×10^{-5}	2.23×10^{-6}
OH	- 1	9.8×10^{-6}	2.23×10^{-6}
Na	+ 1	2.5×10^{-6}	1.968×10^{-6}
Cl	- 1	3.8×10^{-6}	1.968×10^{-6}
Ni	+ 2	1.3×10^{-6}	0
NiOH	+ 1	1.3×10^{-6}	0

Equilibrium Reactions	k_f	k_b	K_{eq}
$H^+ + OH^- = H_2O$	1×10^{12}	5	2×10^{11}
$Ni^{2+} + H_2O = NiOH^+ + H^+$	6×10^{3}	1×10^{9}	6×10^{-6}

Wall/Tip Electrochemical Reactions	sign	no. of e^-	k_o	α	ref. spec.	spec. power
$Ni \rightarrow Ni^{2+} + 2e^-$	+ 1	2	7.56×10^{-4}	0	-	-

Solubility Reactions	k	K_s
none	-	-

Wall/Tip Dissolution Reactions	Flux (dm^2/sec)
none	-

General Data			
Length (dm)	0.01	Width (dm)	1.71×10^{-7}
No. of Nodes	31	Delta X	3.33×10^{-4}
Temperature (K)	573	E_m (V)	0

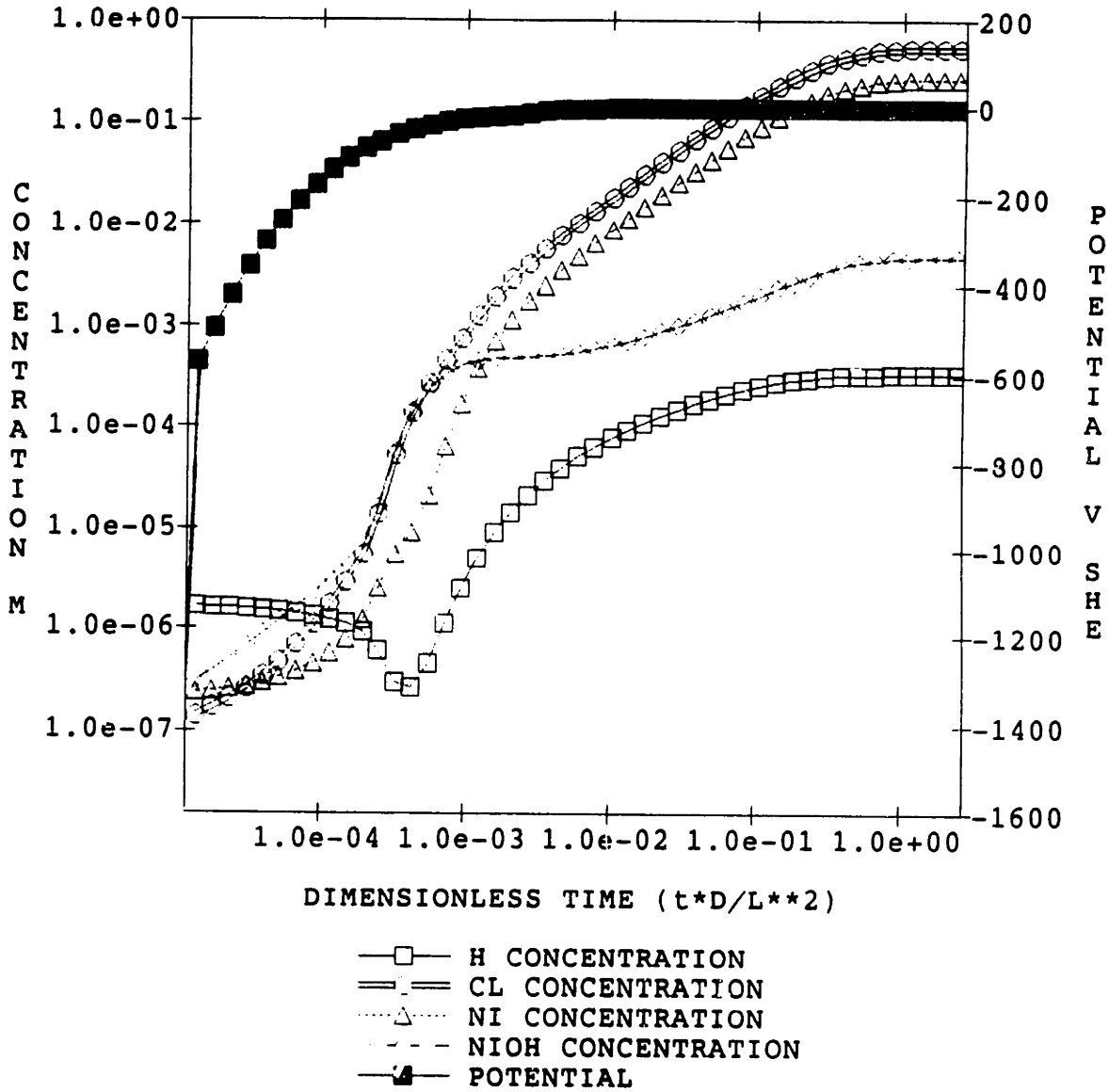

Figure 4-5. Transient crevice tip concentration and potential profiles for nickel dissolution without solubility limits or cathodic reactions.

M to approximately $2x10^{-7}$ M (not seen in Figure 4-5 because of the time scale), then rise more gradually. Initially, the $NiOH^+$ concentration is greater than the Ni^{2+} concentration because the H^+ concentration is very low. This pushes the nickel hydrolysis equilibrium reaction

$$Ni^{2+} + H_2O = NiOH^+ + H^+ \qquad (4-4)$$

to the right. Later in time, as acidification occurs (pH decreases). the reaction shifts towards the left and the Ni^{2+} increases, exceeding the $NiOH^+$concentration, as expected.

As the system approaches steady state, the crevice tip potential achieves a more realistic value of -0.2 V. Figure 4-6 shows the steady state profile developed within the crevice. The dissolved nickel species reach a steady state concentration of 0.2 M for Ni^{2+} and $6.0x10^{-3}$ M for $NiOH^+$. This is at least an order of magnitude above the solubility limit for dissolved nickel at this temperature and pH (*7-12*). This is obviously unrealistic. Nevertheless, it demonstrates that significant polarization can occur with the production of soluble cations.

Another indication of the lack of feasibility of the assumptions of no solubility limit and no cathodic reactions is the insensitivity of crevice electrochemistry to bulk conductivity as shown in Figures 4-7 and 4-8. These figures show the steady state H^+, Cl^-, Ni^{2+} concentration and potential profiles for a range of conductivity increasing from 0.3 µS/cm to approximately 300 µS/cm (at 25 °C). Table 4-6 gives the conditions for these modelling runs. There is no noticeable difference between the steady state profiles for all conductivities, even close to the crevice mouth. Thus, there is no sensitivity of crevice conditions to bulk conductivity. Sensitivity to conductivity is expected because of the enhanced cracking rates experienced in plants that undergo

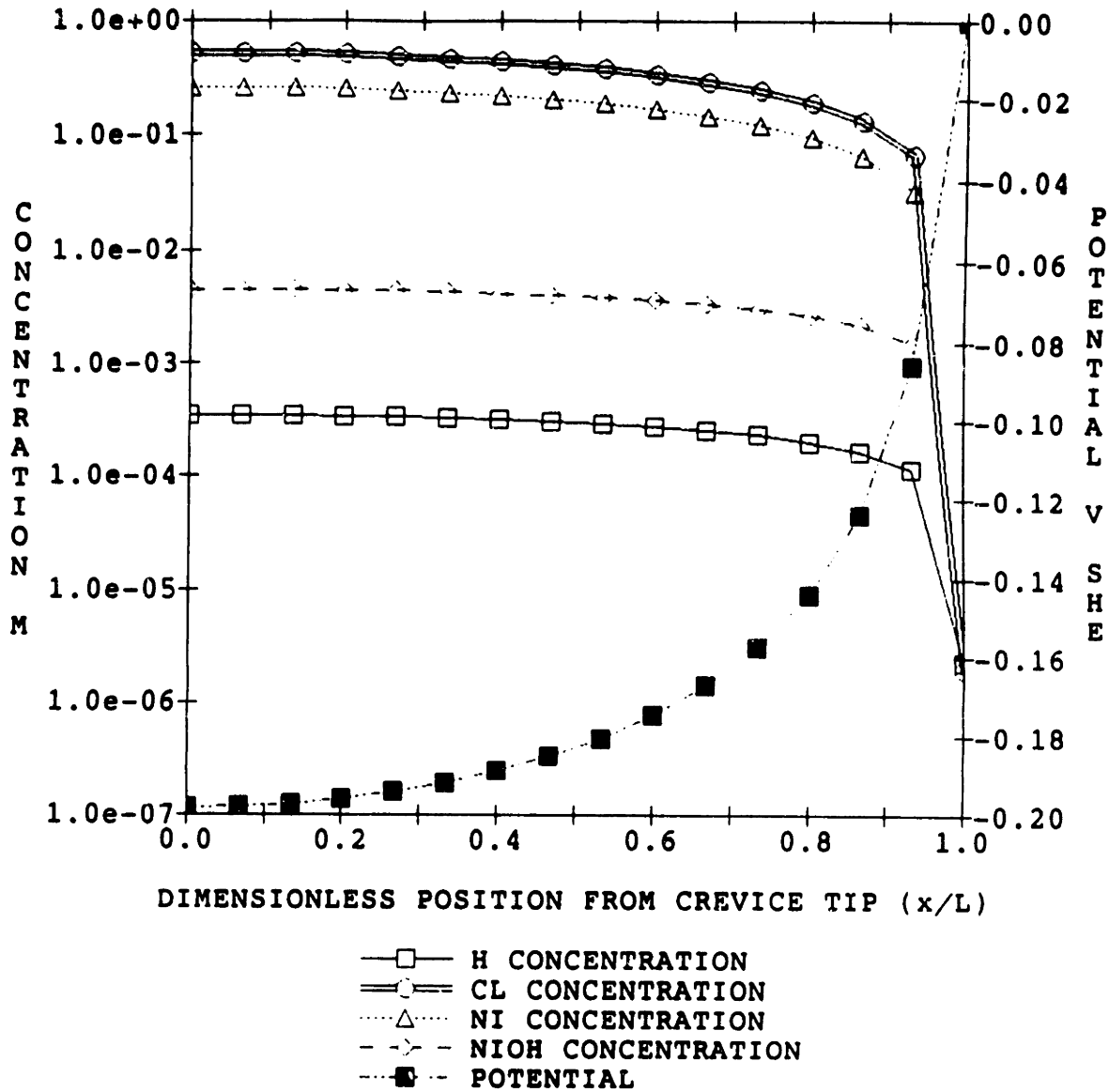

Figure 4-6. Steady-state concentration and potential profile within the crevice for nickel dissolution without solubility limits or cathodic reactions.

Table 4-6. Input Parameters for Figures 4-7 and 4-8.

Species	Charge	Diffusion coefficient (dm^2/sec)	Initial Concentration (moles/l)
H	+ 1	1.76×10^{-5}	2.23×10^{-6}
OH	- 1	9.8×10^{-6}	2.23×10^{-6}
Na	+ 1	2.5×10^{-6}	(1) 1.968×10^{-6}
			(2) 1×10^{-5}
			(3) 1×10^{-4}
			(4) 1×10^{-3}
Cl	- 1	3.8×10^{-6}	(1) 1.968×10^{-6}
			(2) 1×10^{-5}
			(3) 1×10^{-4}
			(4) 1×10^{-3}
Ni	+ 2	1.3×10^{-6}	0
NiOH	+ 1	1.3×10^{-6}	0

Equilibrium Reactions	k_f	k_b	K_{eq}
$H^+ + OH^- = H_2O$	1×10^{12}	5	2×10^{11}
$Ni^{2+} + H_2O = NiOH^+ + H^+$	6×10^{3}	1×10^{9}	6×10^{-6}

Wall/Tip Electrochemical Reactions	sign	no. of e^-	k_o	α	ref. spec.	spec. power
$Ni \rightarrow Ni^{2+} + 2e^-$	+ 1	2	7.56×10^{-4}	0	-	-

Solubility Reactions	k	K_s
none	-	-

Wall/Tip Dissolution Reactions	Flux (dm^2/sec)
none	-

General Data			
Length (dm)	0.01	Width (dm)	1.71×10^{-7}
No. of Nodes	31	Delta X	3.33×10^{-4}
Temperature (K)	573	E_m (V)	0

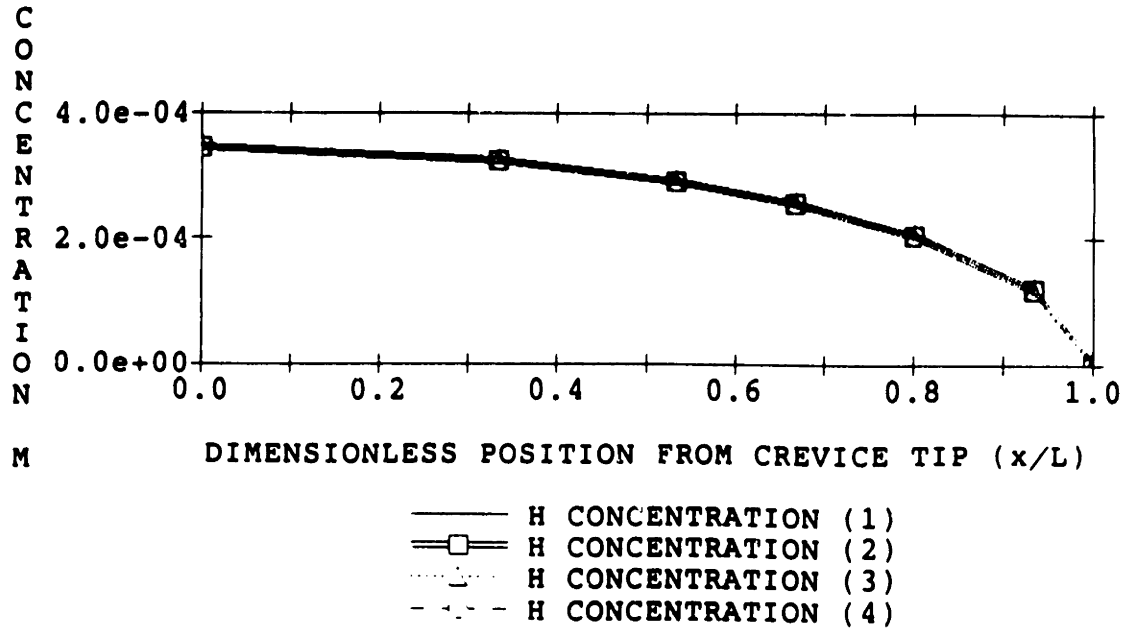

a) Steady-state H^+ concentration profiles.

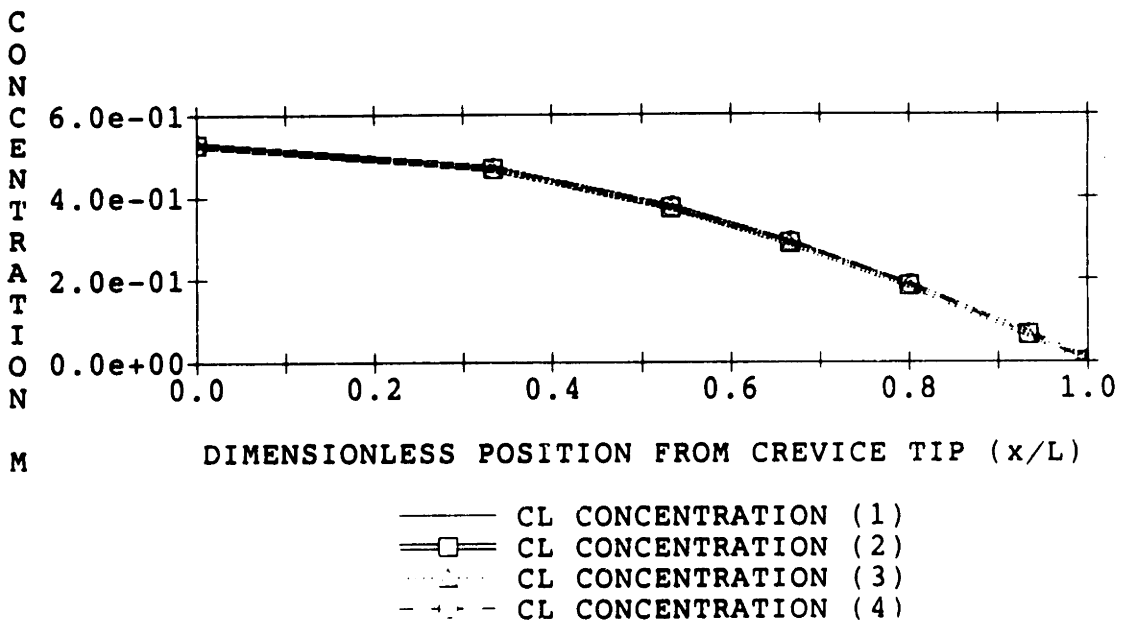

b) Steady-state Cl^- concentration profiles.

Figure 4-7. The steady-state H^+ and Cl^- concentration profiles within the crevice as a function of bulk conductivity. Bulk NaCl concentration is (1) 1.968 x 10^{-6} M, (2) 1 x 10^{-5} M (3) 1 x 10^{-4} M, (4) 1 x 10^{-3} M. There is no difference in the profiles that develop.

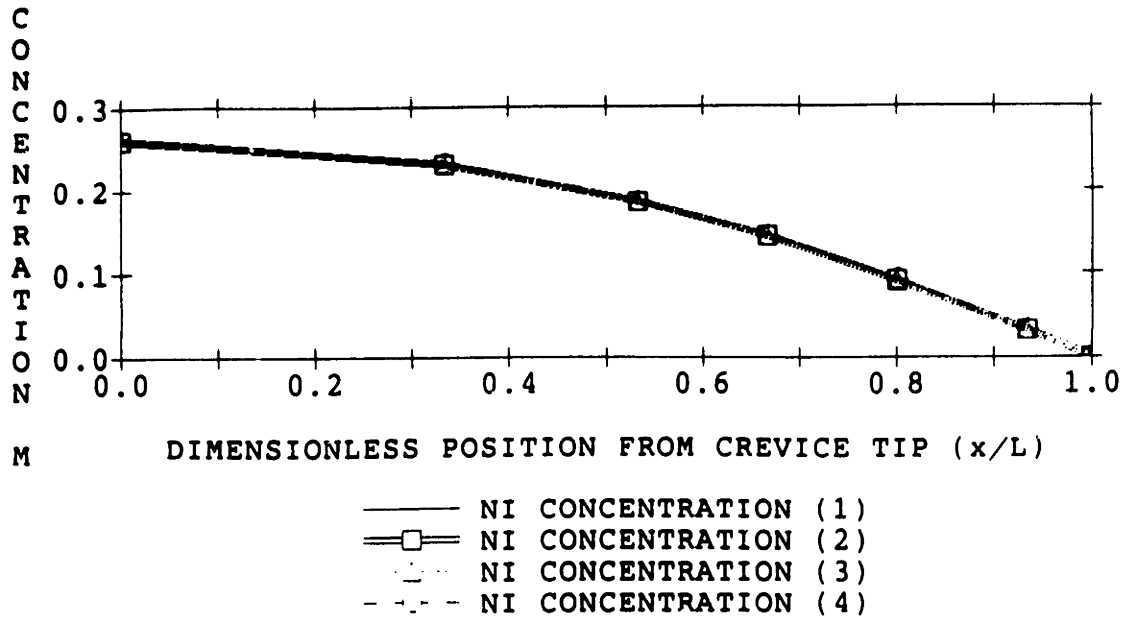

a) Steady-state Ni^{2+} concentration profiles.

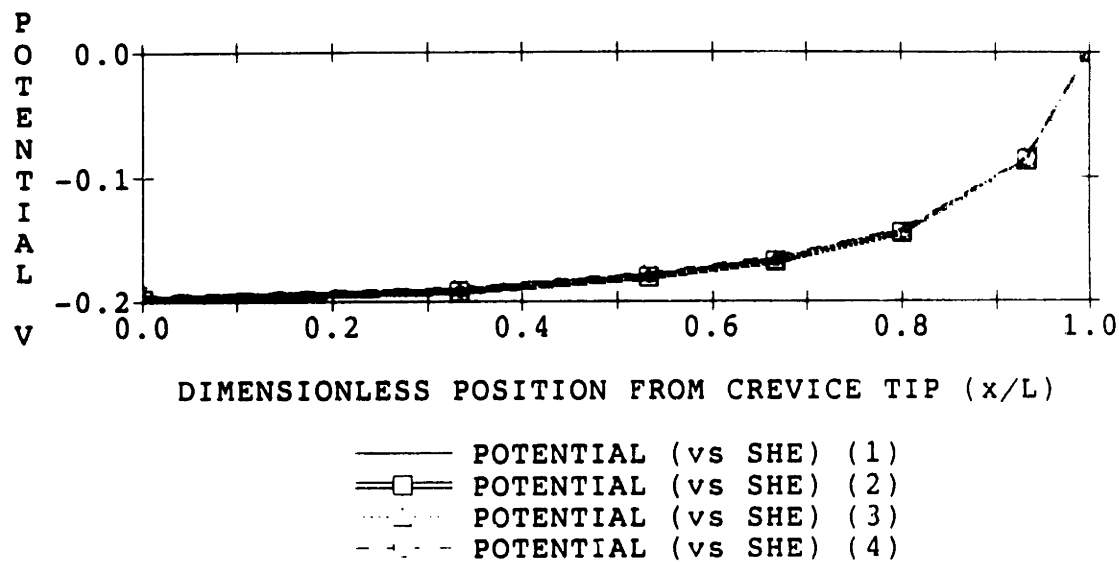

b) Steady-state potential profile.

Figure 4-8. The steady-state Ni^{2+} concentration and potential profiles within the crevice as a function of bulk conductivity. Bulk NaCl concentration is (1) 1.968 x 10^{-6} M, (2) 1 x 10^{-5} M, (3) 1 x 10^{-4}M, (4) 1 x 10^{-3}M of here is no difference in the profiles that develop.

significant excursions in bulk conductivity (*2,13,14*). This lack of sensitivity is probably due to high concentrations achieved within the crevice (0.2 M) which results from the assumption of no solubility limit on dissolved nickel concentration. The cation production rate determines the chemistry developed within the crevice rather than the bulk chemistry. This could have significance at lower temperatures where metal ion solubilities are much higher. Under these conditions it is predicted that the internal conditions within crevices and cracks may be relatively insensitive to initial and bulk concentrations unless the bulk concentration of salt is high.

Neglecting the solubility limits on metal ions and cathodic reactions results in an unrealistic time dependent and steady state concentration and potential profile development within the crevice. Because of the discrepancies in initial potential, concentrations of metal ions and their hydroxides, and the lack of crevice chemistry sensitivity to solution conductivity that result from assuming no solubility limits and ignoring cathodic reactions, it is obvious that these assumptions are inherently incorrect. Solubility limits and cathodic reactions **must** be incorporated into the modeling of high temperature local electrochemistry and the effect of these factors on crevice electrochemistry is demonstrated in the next two sections.

4.2.3 Effect of Internal Cathodic Reactions Without Solubility Limits

The cathodic reactions that have been considered are the reduction of water , hydrogen ions and oxygen as listed below

$$H_2O + e^- \rightarrow OH^- + H$$

$$H^+ + e^- \rightarrow H \qquad (4-5)$$

$$O_2 + 2\,H_2O + 4\,e^- \rightarrow 4\,OH^-$$

The kinetics, of these reactions are extremely important not only in the development of the potential profiles, but also the development of the pH profiles within the crevice. The kinetics of these reduction processes are exponentially dependent on the potential as described in Section 3.2.3. This potential dependence fixes the minimum potential that can be developed within the crevice since the sum of the anodic current densities must equal the sum of the cathodic current densities at every point within the crevice when solution conductivity is very low and no polarization can occur. Thus, in the case of crevice modelling, the cathodic reactions (balanced by the anodic current) fix the initial potential to the corrosion potential of the alloy in deaerated neutral water. The cathodic reactions either consume H^+ ions or produce OH^- ions. The production of excess OH^- ions is equivalent to consuming H^+ ions because of their interaction in the water equilibrium described below

$$H^+ + OH^- = H_2O \qquad (4-6)$$

The production of OH^- drives the reaction to the right, consuming H^+ ions. Thus, cathodic reactions have the net effect of consuming H^+ ions and, therefore, tend to increase the pH.

The kinetics of electrochemical reactions can be obtained from polarization scans using electrodes of the approximate material (in this case Inconel® Alloy 600) and solutions composed of the appropriate solutes (dilute Cl^-, SO_4^{2-} solutions) and at the

appropriate temperature (approximately 300°C). Unfortunately, the data available are extremely limited and inconsistent. No systematic studies have been conducted to analyze the kinetics of these various cathodic reactions on different alloys at temperature in dilute solutions. What little data exist were often obtained using solutions of high concentration and with oxygen concentrations that were not well defined or insufficiently low. Also, most of these scans were conducted using fast scan rates. The resulting current densities do not reflect steady state values at each potential and are therefore may be unreliable from the viewpoint of quantitative modeling. Nonetheless, these data are used where available, and appropriate. The kinetic parameters obtained are somewhat modified so that they correspond to values that accurately predict the corrosion potential of Inconel®Alloy 600 in pure, deaerated water, which is a well established value (*15*).

The only data for water reduction on Inconel® alloy 600 were obtained by Bogaert et al. (*16*). Analysis of the polarization scans yields the following kinetic parameters for water reduction kinetics:

$$\alpha_{H_2O} = 0.6$$
$$k_{0,H_2O} = 1.5 \times 10^{-6} \qquad (4-7)$$

where α is the transfer coefficient and k_0 is the pre-exponential rate constant for the electrode reaction (as described in Section 3.2.3). Thus, the water reduction chemistry current density is given by

$$i_{H_2O} = k_{0,H_2O} \exp\left[- \frac{\alpha_{H_2O} F (E_m - \phi)}{R T} \right] \qquad (4-8)$$

There are no cathodic polarization scans available from which H^+ ion reduction kinetics can be deduced. In order to include this important reduction reaction we must apply knowledge developed at room temperature. It has been shown at room temperature in neutral pH solutions that the kinetics of H^+ ion reduction is first order and equal to that of water reduction (*17*). Thus, remembering that neutral pH at 300 °C is equal to 5.6 ($[H^+] = 2.239 \times 10^{-6}$ M) and assuming the same potential dependence as for water reduction, the kinetic parameters for H^+ ion reduction are :

$$\alpha_{H^+} = 0.6$$
$$k_{0,H^+} = 1.5 \times 10^{-6} \qquad (4-9)$$

and the H^+ reduction current density is given by

$$i_{H^+} = k_{0,H^+} C_{H^+} \exp\left[- \frac{\alpha_{H^+} F (E_m - \phi)}{R T} \right] \qquad (4-10)$$

Assuming that the passive current is independent of potential, these cathodic current densities can be intersected with the passive current density to obtain the corrosion potential. The total anodic current density equals the total cathodic current density, as shown below

$$i_{passive} = i_{H_2O} + i_{H^+}$$
$$i_{passive} = \left(k_{0,H_2O} + k_{0,H^+} C_{H^+}\right) \exp\left[- \frac{\alpha F (E_m - \phi)}{R T} \right] \qquad (4-10)$$

This equation can be used to solve for the corrosion potential which is given by

$$E_{corrosion} = E_m - \phi \qquad (4\text{-}11)$$

Setting the external metal potential, E_m, to zero, the passive current density to 7.56×10^{-4} A/dm^2, using the known H^+ concentration of 2.239×10^{-6} M, and the values of α and k_0 as defined above, the resulting corrosion potential is approximately -450 mV. However, experimental evidence indicates that the corrosion potential for Inconel®600 in deaerated water should be -750 mV (*15*). These data are well characterized and probably reliable. The discrepancy is possibly the result of some residual dissolved oxygen in the experiments, reported by Bogaerts et al. (*16*), who quotes values of 10-20 ppb oxygen. Because of this inconsistency, another set of water and hydrogen reduction kinetics are adopted which results in the correct corrosion potential. The values of α are assumed to be the same for these reactions but the values of k_0 are changed, resulting in a slower set of reduction kinetics parameters. Both sets are presented in the table below for comparison.

Table 4-7. Summary of Reduction Kinetic Parameters for Crevice Problem

		Fast kinetics	Slow Kinetics
H_2O reduction :	α	0.6	0.6
	k_0	1.5×10^{-6}	4.55×10^{-8}
H^+ reduction :	α	0.6	0.6
	k_0	0.671	2.03×10^{-2}

Because of the inaccuracy of the data used, both fast kinetic parameters and slow kinetic parameters will often be used in the modeling presented in the following sections for comparison. It should be noted that the slow reduction kinetic parameters (shown in the second column of Table 4-7) are probably more realistic since there is solid evidence supporting the lower corrosion potential and because the fast kinetics where derived from polarization scans conducted at fast scan rates and in conditions where the oxygen concentration was not necessarily insignificant.

The kinetics of oxygen reduction under activation control are also unknown in high temperature water. However, some information exists which indicates that the oxygen reduction current density has the form

$$i_{O_2} = k_{0,O_2} C_{O_2} \exp\left[- \frac{\alpha_{O_2} F (E_m - \phi)}{R T} \right] \qquad (4-12)$$

Assuming that α has the same value as at room temperature (i.e, $\alpha = 0.5$), k_0 can be calculated using the known bulk potential and oxygen concentration in BWR water. As above, the total anodic current density equals the total cathodic current density

$$i_{passive} = i_{H_2O} + i_{H^+} + i_{O_2}$$

$$i_{passive} = (k_{0,H_2O} + k_{0,H^+} C_{H^+}) \exp\left[- \frac{\alpha F (E_m - \phi)}{R T} \right] + k_{0,O_2} C_{O_2} \exp\left[- \frac{\alpha_{O_2} F (E_m - \phi)}{R T} \right] \qquad (4-13)$$

In the bulk solution $E_m = 0.0$ V and $\phi = 0.0$ V, therefore

Table 4-8. Input Parameters for Figure 4-9.

Species	Charge	Diffusion coefficient (dm^2/sec)	Initial Concentration (moles/l)
H	+ 1	1.76×10^{-5}	2.23×10^{-6}
OH	- 1	9.8×10^{-6}	2.23×10^{-6}
Na	+ 1	2.5×10^{-6}	1.968×10^{-6}
SO_4	- 2	2.0×10^{-6}	1.968×10^{-6}
Cu	+ 2	1.3×10^{-6}	0
O_2	0	1.89×10^{-6}	?????

Equilibrium Reactions	k_f	k_b	K_{eq}
$H^+ + OH^- = H_2O$	1×10^{12}	5	2×10^{11}

Wall/Tip Electrochemical Reactions	sign	no. of e^-	k_o	α	ref. spec.	spec. power
$Ni + H_2O \rightarrow 2H^+ + 2e^- + NiO$	+ 1	2	7.48×10^{-4}	0	-	-
$H_2O + e^- \rightarrow H + OH^-$	- 1	1	1.5×10^{-6}	0.6	-	-
$H^+ + e^- \rightarrow H$	- 1	1	0.671	0.6	H^+	1
$Cu \rightarrow Cu^{2+} + 2e^-$	+ 1	2	7.56×10^{-6}	0	-	-
$4\ e^- + O_2 + 2\ H_2O \rightarrow 4\ OH^-$	- 1	4	1.71×10^{2}	0.5	O_2	1

Solubility Reactions	k	K_s
none	-	-

Wall/Tip Dissolution Reactions	Flux (dm^2/sec)
none	-

General Data			
Length (dm)	0.01	Width (dm)	1.71×10^{-7}
No. of Nodes	31	Delta X	3.33×10^{-4}
Temperature (K)	573	E_m (V)	0

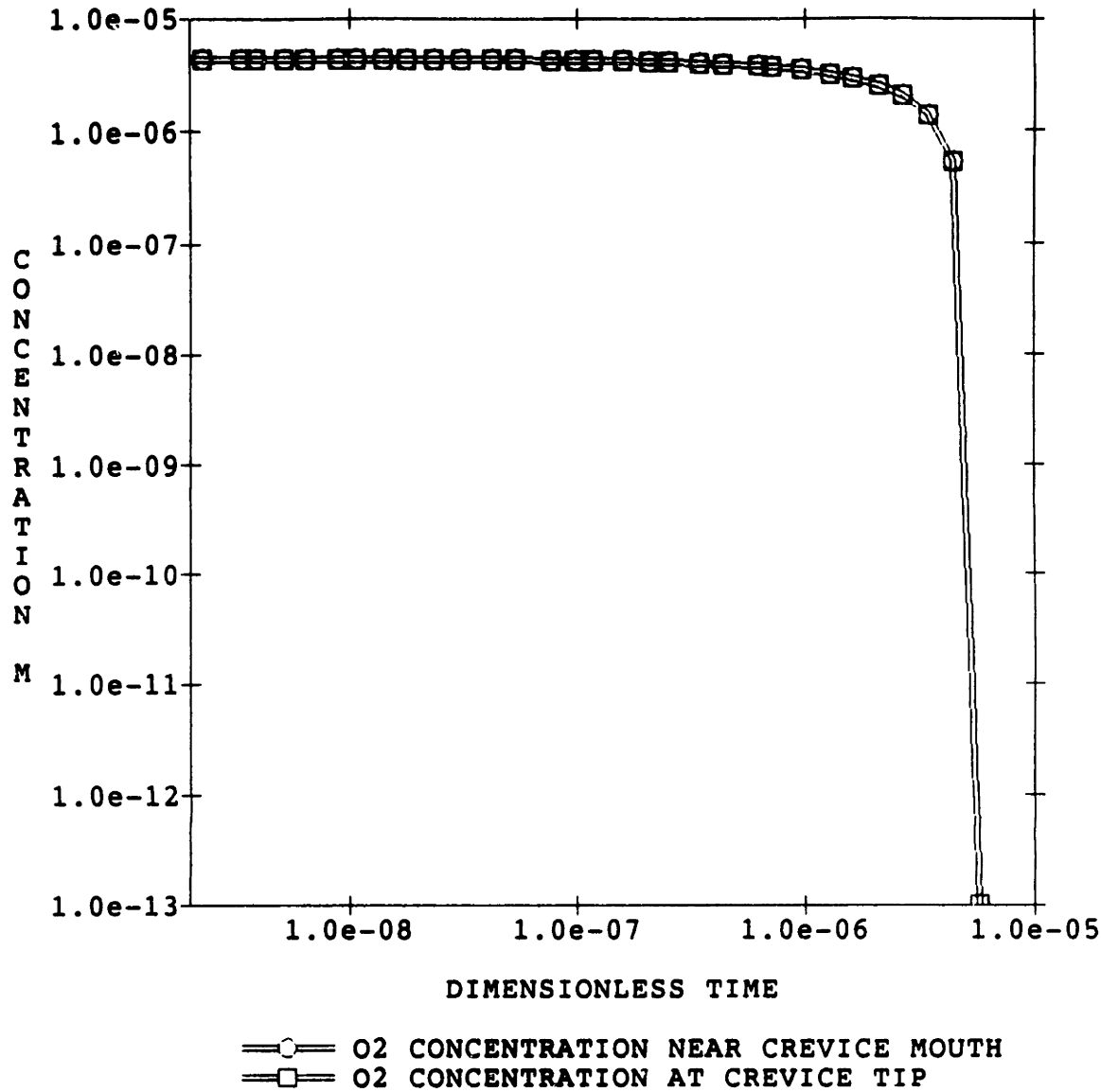

Figure 4-9. Oxygen depletion at the crevice tip and near the crevice mouth.

$$i_{passive} = k_{0,H_2O} + k_{0,H^+} C_{H^+} + k_{0,O_2} C_{O_2} \qquad (4-14)$$

Assuming approximately 200 ppb O_2 (4.4×10^{-6} M) and knowing the values of k_0 from Table 4-7, the k_0 for oxygen reduction can be calculated. For fast H^+ and H_2O reduction kinetics the calculated k_0 = 171.1 A/(dm^2 M) and for slow H^+ and H_2O reduction kinetics the calculated k_0 = 171.8 A/(dm^2 M). The calculated oxygen reduction k_0 value for the fast and slow kinetics are very similar and, therefore, should result in similar behavior when applied in the model.

Figure 4-9 shows the depletion of oxygen at the crevice tip and near the crevice mouth using conditions described in Table 4-8. As can be seen, oxygen is rapidly consumed within the crevice. In the two foot long safe end crevice, the oxygen is depleted in approximately two minutes. Since oxygen is not produced within the crevice (radiolysis, which produces oxygen, decays exponentially with length and is therefore unimportant within most of the crevice), oxygen is consumed faster than it can be transported into the crevice and the solution rapidly becomes deaerated. In all crevice modelling presented in this chapter, oxygen reduction is ignored within the crevice but it is recognized that radiolytic processes can be important in shorter crevices or cracks and thus is being considered for future work.

Figures 4-10 and 4-11 show a comparison of the transient pH and potential profiles at the crevice tip with and without cathodic reactions. The initial conditions and constants for this modelling without and with cathodic reactions are presented in Tables 4-5 and 4-9, respectively. Allowing cathodic reactions within the crevice limits the initial potential to the corrosion potential in oxygen free solution (-450 mV for fast reduction kinetics and -750 mV for slow reduction kinetics). Without cathodic reactions to limit the initial potential a huge unrealistic potential of **-1400 V** develops

Table 4-9. Input Parameters for Transient Potential and pH Data Incorporating Cathodic Reduction Depicted in Figures 4-10 and 4-11.

Species	Charge	Diffusion coefficient (dm^2/sec)	Initial Concentration (moles/l)
H	+ 1	1.76×10^{-5}	2.23×10^{-6}
OH	- 1	9.8×10^{-6}	2.23×10^{-6}
Na	+ 1	2.5×10^{-6}	1.968×10^{-6}
Cl	- 1	3.8×10^{-6}	1.968×10^{-6}
Ni	+ 2	1.3×10^{-6}	0
NiOH	+ 1	1.3×10^{-6}	0

Equilibrium Reactions	k_f	k_b	K_{eq}
$H^+ + OH^- = H_2O$	1×10^{12}	5	2×10^{11}
$Ni^{2+} + H_2O = NiOH^+ + H^+$	6×10^3	1×10^9	6×10^{-6}

Wall Tip Electrochemical Reactions	sign	no. of e^-	k_o	α	ref. spec.	spec. power
$Ni \rightarrow Ni^{2+} + 2e^-$	+ 1	2	7.56×10^{-4}	0	-	-
$H_2O + e^- \rightarrow H + OH^-$	- 1	1	1.5×10^{-6}	0.6	-	-
$H^+ + e^- \rightarrow H$	- 1	1	0.671	0.6	H	1

Solubility Reactions	k	K_s
none	-	-

Wall/Tip Dissolution Reactions	Flux (dm^2/sec)
none	-

General Data			
Length (dm)	0.01	Width (dm)	1.71×10^{-7}
No. of Nodes	31	Delta X	3.33×10^{-4}
Temperature (K)	573	E_m (V)	0

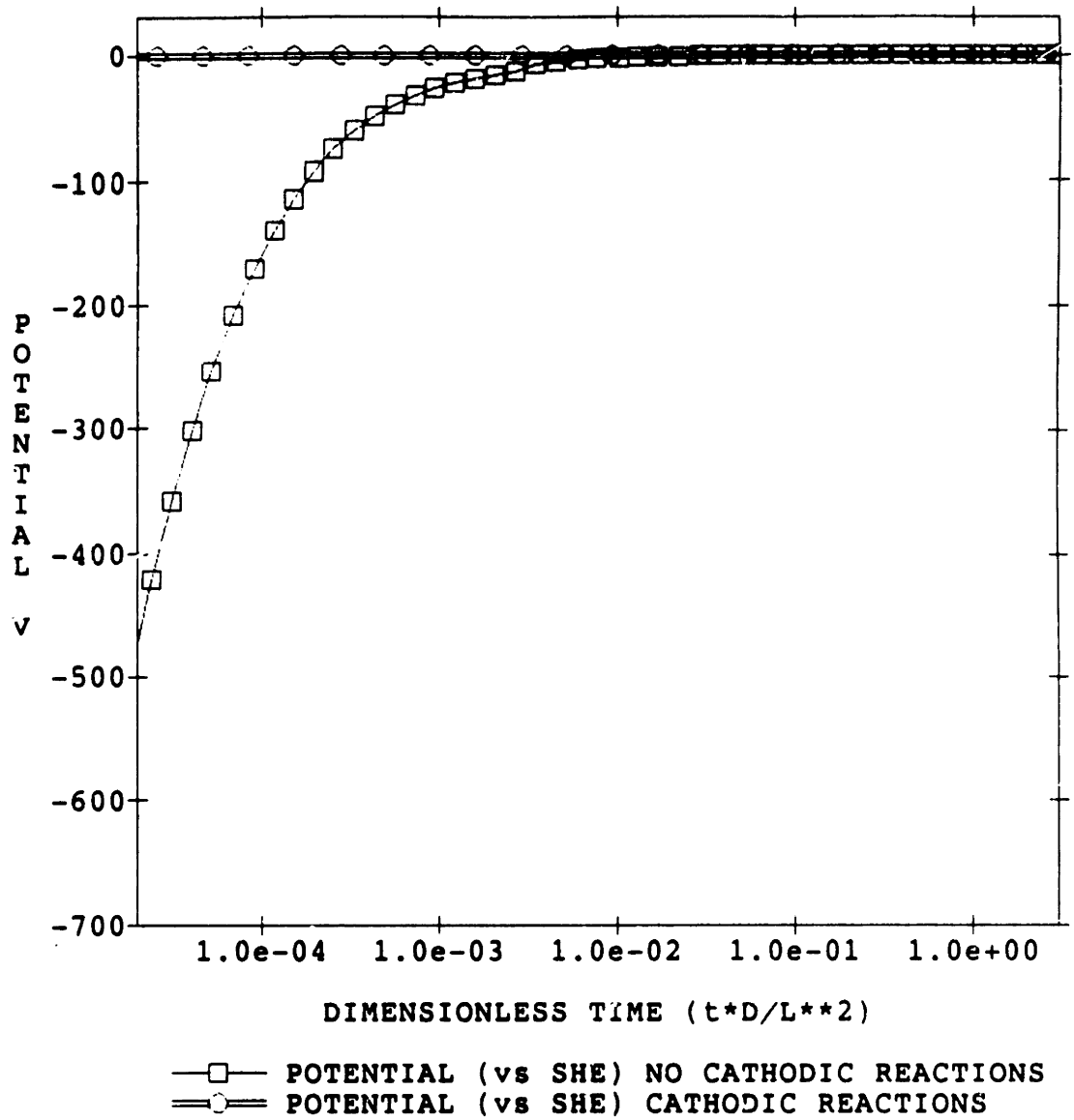

Figure 4-10. Comparison of transient potential profile at crevice tip with and without internal cathodic reactions.

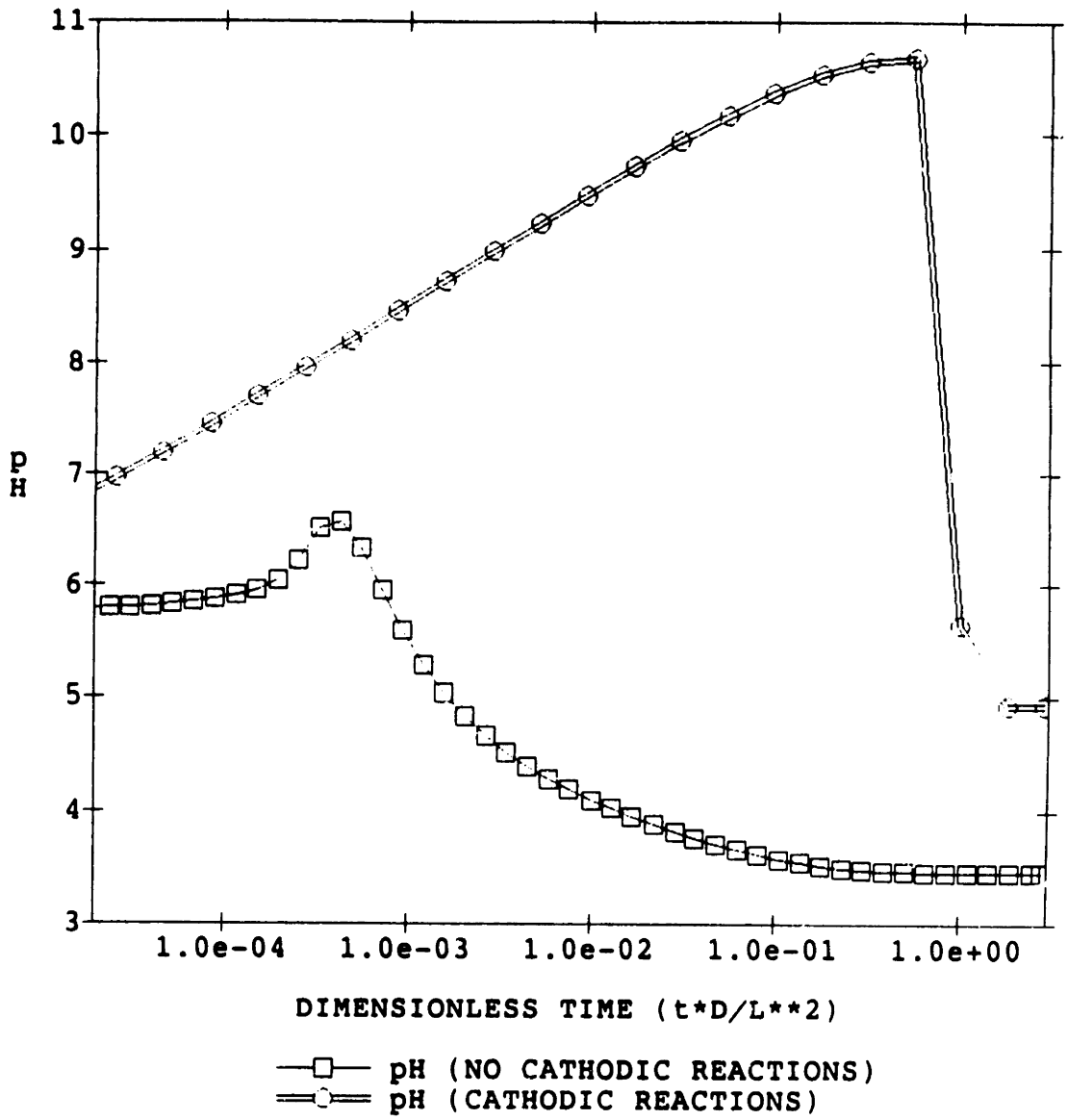

Figure 4-11. Comparison of transient pH profiles at crevice tip with and without internal cathodic reactions.

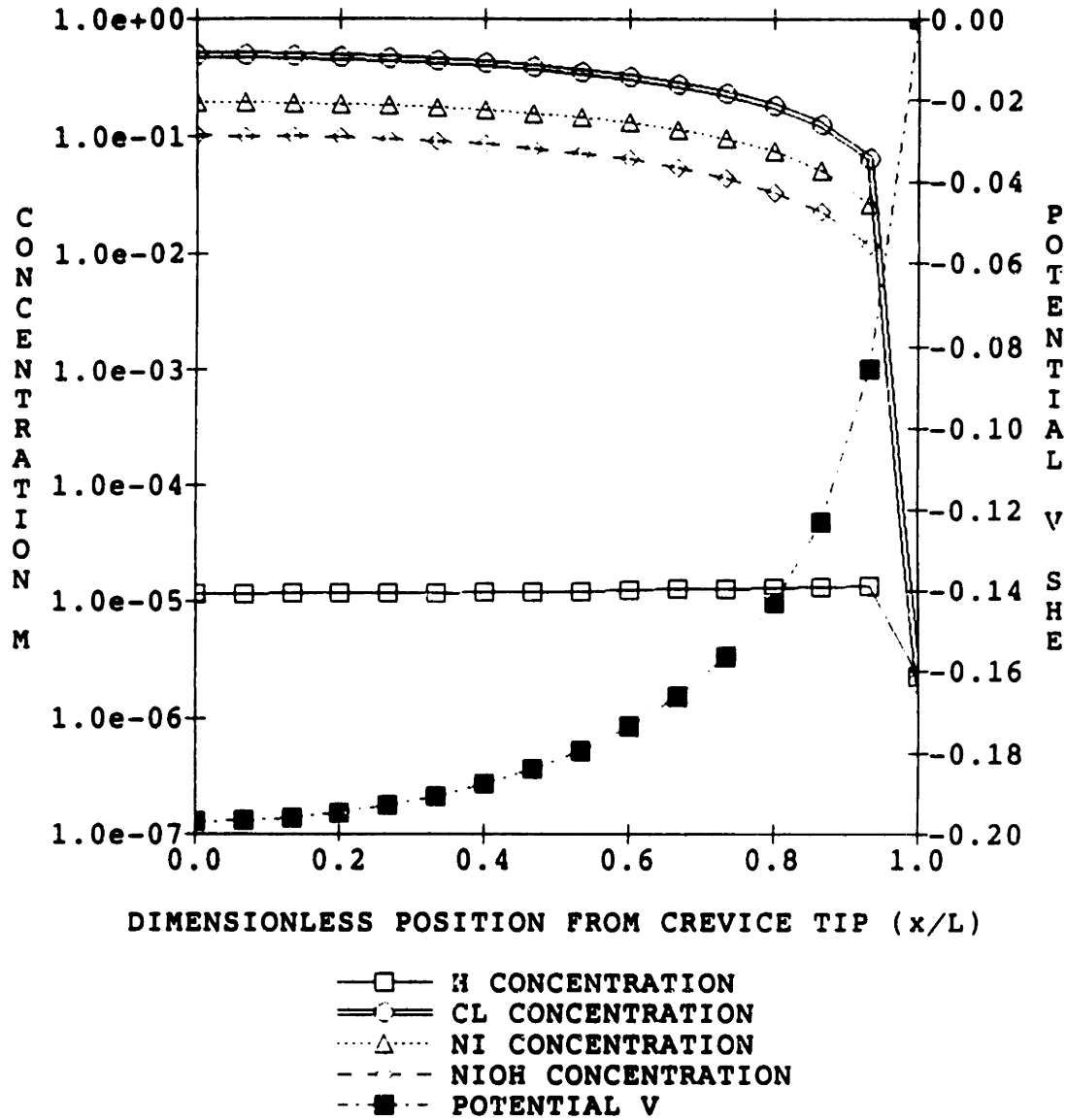

Figure 4-12. Steady-state concentration and potential profiles within crevice with cathodic reactions and no solubility limits.

as described in Section 4.2.2. The potential eventually rises to approximately the same value as that without reduction reactions because of the increase in conductivity associated with the limited cation solubility. The large increase in conductivity from metal ion dissolution enables significant polarization to occur and therefore there is an increase in potential. The pH initially increases (H^+ concentration decreases) with time because cathodic reactions are consuming H^+ or producing OH^-, as previously described. The cathodic reactions consume H^+ more effectively than the passive current can produce H^+ since Ni^{2+} hydrolysis to $NiOH^+$ is incomplete. However, once the Ni^{2+} concentration is sufficiently high polarization occurs and excess H^+ ions are produced. Acidification results, but not to the same extent as achieved **without** cathodic reactions because of the consumption of H^+ by reduction reaction as described above.

The steady state concentration profiles are shown in Figure 4-12. By comparing this figure with Figure 4-6, it can be seen that allowing cathodic reactions affects only the steady state pH and $NiOH^+$ profiles. As discussed above , the pH reached within the crevice with cathodic reactions is not as low as without these reactions because cathodic reactions have the net effect of H^+ consumption. The $NiOH^+$ concentration is affected through the equilibrium reaction

$$Ni^{2+} + H_2O = NiOH^+ + H^+ \qquad (4-15)$$

Decreasing the H^+ concentration results in an increased $NiOH^+$ concentration. The steady state potential profile remains unchanged since it is governed by the increase in conductivity which results from the increase in cation concentration (there is no limit placed on Ni^{2+} solubility) and the resulting polarization.

Allowing cathodic reactions within the crevice has reduced the **initial** potential drop in the crevice from **1400 V** to **450 mV**. The pH that develops within the crevice

is also higher because cathodic reactions have the net effect of consuming H^+ ions. Therefore cathodic reactions cannot be ignored within a crevice exposed to BWR environments. However, the Ni^{2+} and $NiOH^+$ concentrations are still much too high in relation to the cation solubility (this discussed in Section 4.4.5). The application of solubility limits on metal ion concentration is essential and will be discussed in Section 4.2.5.

4.2.4. Description of Minimum Conditions Necessary to Model Crevice

The previous sections have described modeling results that were obtained expressly to determine the processes that must be applied in the model in order for the model to predict realistic transient and steady state electrochemical conditions within a crevice. From this work, it is apparent that cathodic reactions must be included within the crevice in order to develop realistic potential and pH profiles. Without the application of cathodic reactions, the initial potential is at least three orders of magnitude larger than it should be, the pH transient profile is vary different, and the resulting steady state pH is 1.5 units lower. Thus, the incorporation of cathodic reactions occuring within the crevice is imperative. Also, solubility limits must be placed on nickel species in order to prevent unrealistic metal ion concentrations that would otherwise develop. Higher unrealistic metal ion concentrations result in higher conductivities that may lead to more polarization. Hence, solubility limits must be included in the evaluation of high temperature local electrochemistry. In the following result sections, the model is applied more directly to the specific problem of evaluating

the electrochemistry that develops within a BWR crevice. In all the following modelling, both cathodic reactions and solubility limits on Ni^{2+} are incorporated.

4.2.5 Effect of Solubility Limits

In this section, the solubility limit on dissolved Ni^{2+} ions is applied as described in Section 3.2.4. As previously discussed, the behavior of the major alloying elements (Fe, Cr, Ni) has been modeled using nickel. Thus the passive current for Alloy 600 is attributed to the dissolution of nickel. The question arises as to the validity of this approach with the incorporation of solubility limits. Since the solubility limits of Fe^{2+} and Cr^{3+} are equivalent to or lower than that of nickel (all are low), the behavior of the model with nickel dissolution should be representative. The value of the Ni^{2+} solubility limit (*7-12*) used is given by

$$[Ni^{2+}][OH^-]^2 = 2.25 \times 10^{-20} \qquad (4-16)$$

Figures 4-13 and 4-14 show the transient concentration and potential profiles for the crevice tip for fast and slow reduction kinetics, respectively. Tables 4-10 and 4-11 present initial conditions and constants for these two cases, respectively. Initially, the concentration of dissolved nickel species, Ni^{2+} and $NiOH^+$, is limited to very low values (virtually zero) and the H^+ ion concentration decreases. This decrease in H^+ concentration or increase in pH occurs because the cathodic reactions have the net effect of consuming H^+ ions. Because of the decrease in H^+ concentration, the water reduction

Table 4-10. Input Parameters for Figure 4-13 (fast reduction kinetics)

Species	Charge	Diffusion coefficient (dm^2/sec)	Initial Concentration (moles/l)
H	+ 1	1.76×10^{-5}	2.23×10^{-6}
OH	- 1	9.8×10^{-6}	2.23×10^{-6}
Na	+ 1	2.5×10^{-6}	1.968×10^{-6} (3.158×10^{-5})
Cl	- 1	3.8×10^{-6}	1.968×10^{-6}
Ni	+ 2	1.3×10^{-6}	0
NiOH	+ 1	1.3×10^{-6}	0
HSO_4	- 1	2.0×10^{-6}	0 (2.961×10^{-5})

Equilibrium Reactions	k_f	k_b	K_{eq}
$H^+ + OH^- = H_2O$	1×10^{12}	5	2×10^{11}
$Ni^{2+} + H_2O = NiOH^+ + H^+$	6×10^{3}	1×10^{9}	6×10^{-6}

Wall/Tip Electrochemical Reactions	sign	no. of e^-	k_o	α	ref. spec.	spec. power
$Ni \rightarrow Ni^{2+} + 2e^-$	+ 1	2	7.56×10^{-4}	0	-	-
$H_2O + e^- \rightarrow H + OH^-$	- 1	1	1.50×10^{-6}	0.6	-	-
$H^+ + e^- \rightarrow H$	- 1	1	0.671	0.6	H^+	1

Solubility Reactions	k	K_s
$Ni^{2+} + 2OH^- \rightarrow Ni(OH)_2$	1×10^{14}	2.25×10^{-20}

Wall/Tip Dissolution Reactions	Flux (dm^2/sec)
none	-

General Data			
Length (dm)	0.01	Width (dm)	1.71×10^{-7}
No. of Nodes	31	Delta X	3.33×10^{-4}
Temperature (K)	573	E_m (V)	0

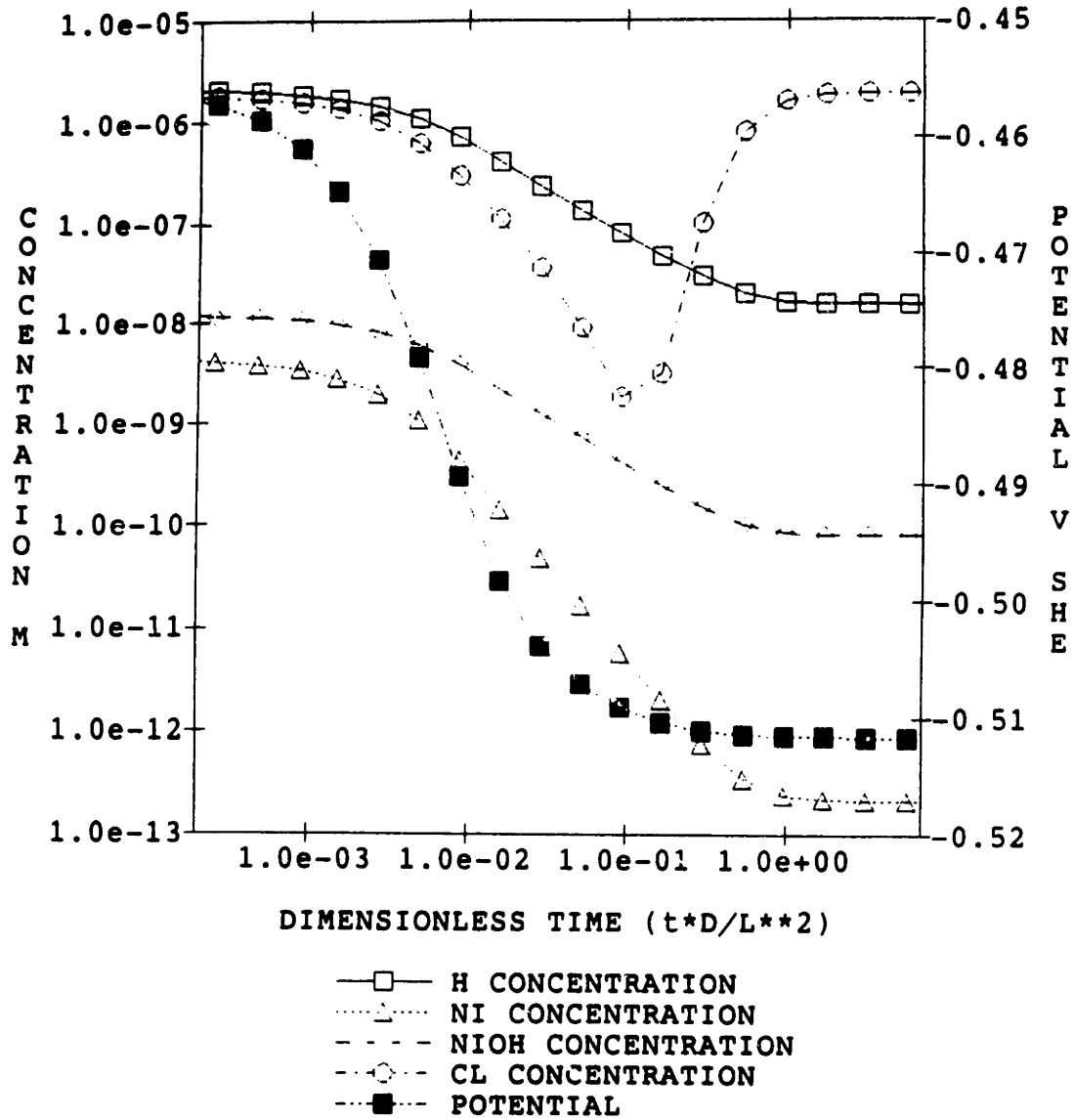

Figure 4-13. Transient concentration and potential profiles at crevice tip using fast reduction kinetics and incorporating a solubility limit on Ni^{2+}.

Table 4-11. Input Parameters for Figure 4-14 (slow reduction kinetics)

Species	Charge	Diffusion coefficient (dm^2/sec)	Initial Concentration (moles/l)
H	+ 1	1.76×10^{-5}	2.23×10^{-6}
OH	- 1	9.8×10^{-6}	2.23×10^{-6}
Na	+ 1	2.5×10^{-6}	2.51×10^{-6}
Ni	+ 2	1.3×10^{-6}	0
NiOH	+ 1	1.3×10^{-6}	0
HSO_4	- 1	2.0×10^{-6}	2.51×10^{-6} (2.961×10^{-5})

Equilibrium Reactions	k_f	k_b	K_{eq}
$H^+ + OH^- = H_2O$	1×10^{12}	5	2×10^{11}
$Ni^{2+} + H_2O = NiOH^+ + H^+$	6×10^{3}	1×10^{9}	6×10^{-6}

Wall/Tip Electrochemical Reactions	sign	no. of e^-	k_o	α	ref. spec.	spec. power
$Ni \rightarrow Ni^{2+} + 2e^-$	+ 1	2	7.56×10^{-4}	0	-	-
$H_2O + e^- \rightarrow H + OH^-$	- 1	1	4.55×10^{-8}	0.6	-	-
$H^+ + e^- \rightarrow H$	- 1	1	2.03×10^{-2}	0.6	H^+	1

Solubility Reactions	k	K_s
$Ni^{2+} + 2\ OH^- \rightarrow Ni(OH)_2$	1×10^{14}	2.25×10^{-20}

Wall/Tip Dissolution Reactions	Flux (dm^2/sec)
none	-

General Data			
Length (dm)	0.01	Width (dm)	1.71×10^{-7}
No. of Nodes	31	Delta X	3.33×10^{-4}
Temperature (K)	573	Em (V)	0

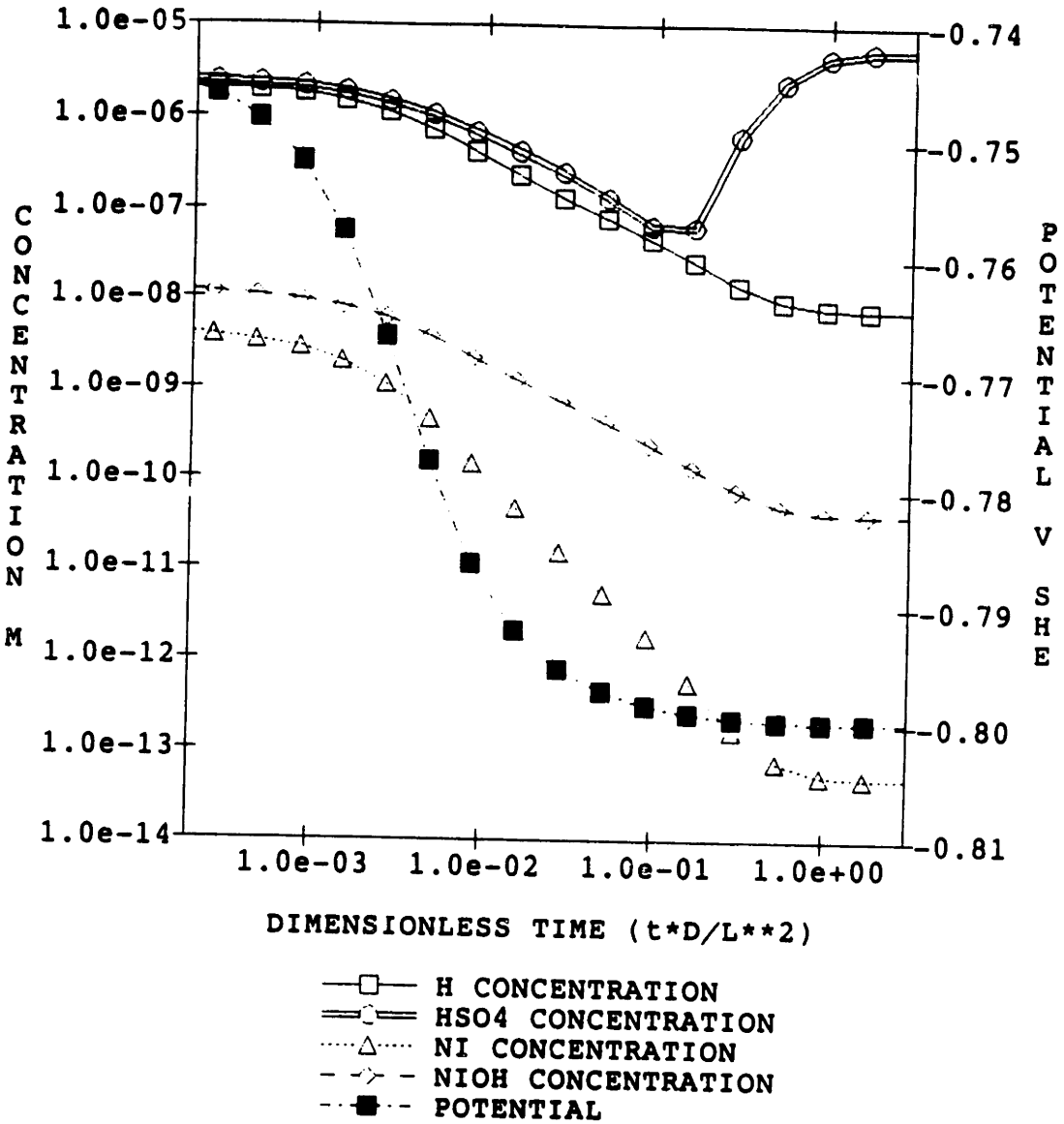

Figure 4-14. Transient concentration and potential profiles at crevice tip using slow reduction kinetics and incorporating a solubility limit on Ni^{2+}.

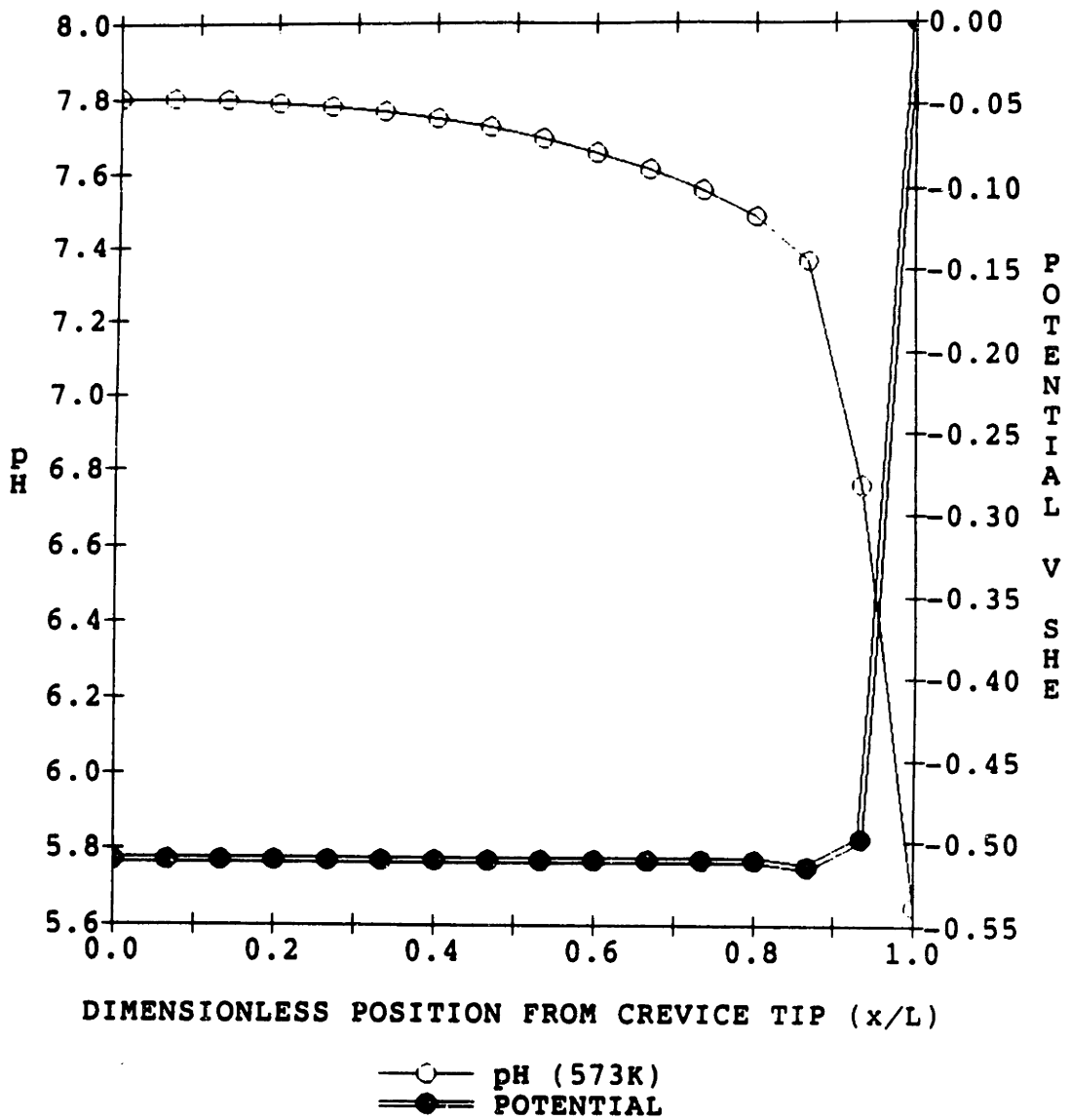

Figure 4-15. Steady-state pH and potential profile within crevice (fast reduction kinetics and solubility limit on Ni^{2+}).

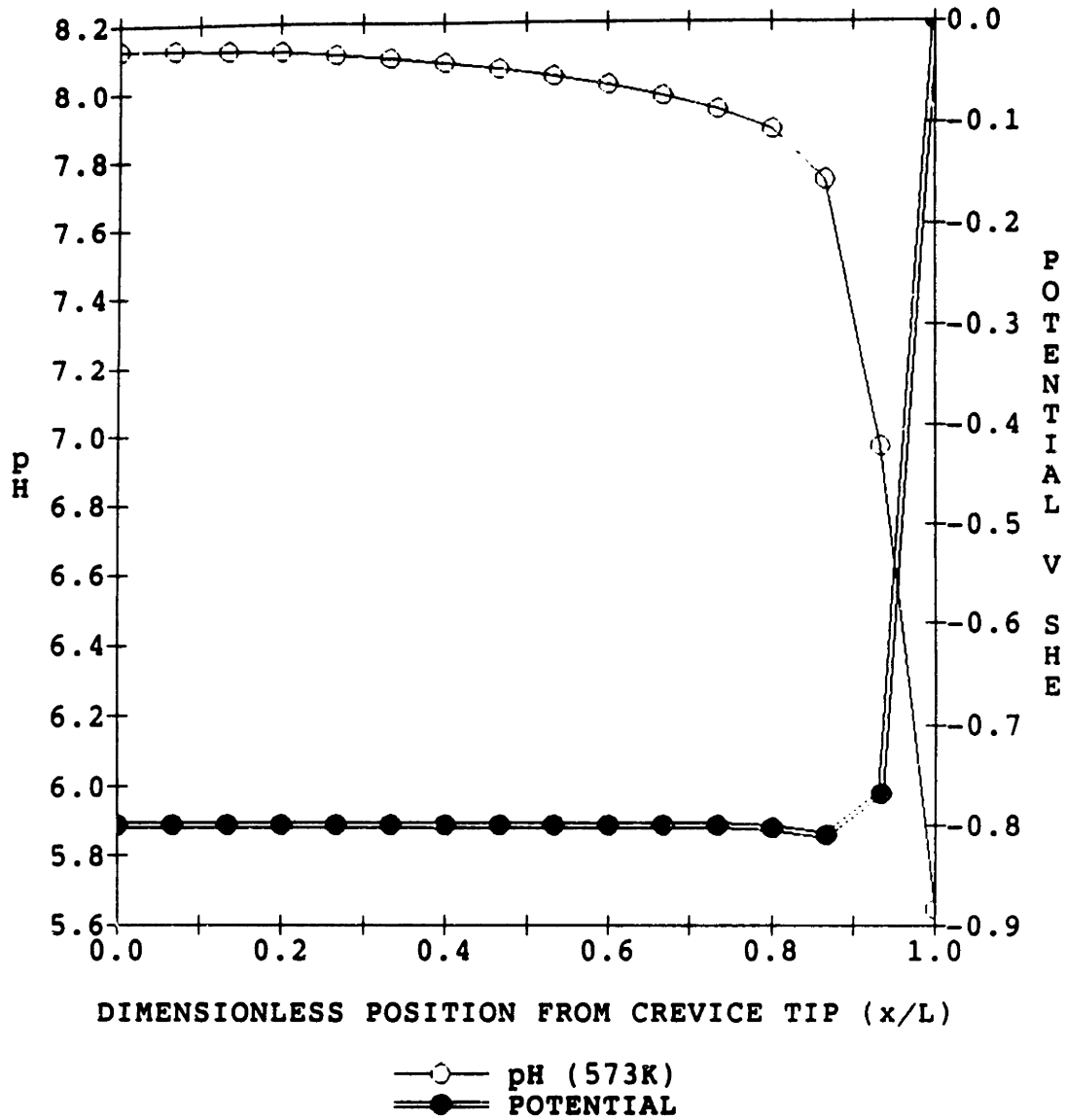

Figure 4-16. Steady-state pH and potential profile within crevice (slow reduction kinetics and solubility limit on Ni^{2+}).

sreaction dominates the cathodic reactions and the potential drops to a new corrosion potential, -512mV for fast reduction kinetics and -800 mV for slow reduction kinetics.

Thus, the addition of solubility limits restricts the concentration of dissolved nickel species, as expected. The pH increases because Ni^{2+} hydrolysis is incomplete and the potential field causes H^+ to migrate out. Because of the increase in pH, the metal ion concentration is fixed at very low values: $2.0x10^{-13}$ M for Ni^{2+} and $2.0x10^{-10}$ M for $NiOH^+$. Since the conductivity of the solution does not significantly increase as it did in the previous case (with no solubility limit), there is no polarization within the crevice. Figures 4-15 and 4-16 present the steady state pH and potential profiles for fast and low reduction kinetics, respectively. The potential remains at the corrosion potential relative to the local environment. Without polarization, there is no acidification and the pH remains above neutral within the crevice. The internal crevice surface becomes **isolated** from the bulk.

Thus, the application of solubility limits drastically changes the steady state and transient concentration and potential profiles within the crevice. The electrochemistry that develops within the crevice is one of low potential (the corrosion potential of the alloy), low conductivity, and basic pH. It is very unlikely that stress corrosion cracking would initiate under these conditions (see Figure 4-1) (*3*). In order for a sufficiently aggressive crevice electrochemistry (i.e.. high potential, low pH, High conductivity) to develop with normal BWR water as the bulk solution, some more soluble species must be introduced into the crevice region or the conductivity within the crevice must increase in some other way. There are two possible sources for such soluble species or increased conductivity:

(1). the dissolution of more soluble species from the alloys making up the crevice,

(2). an excursion in the conductivity of the bulk solution at the crevice mouth.

The dissolution of more soluble species will be discussed in Section 4.2.6 and excursions in bulk conductivity will be discussed in Section 4.2.7.

4.2.6 Dissolution of Soluble or Partially Soluble Species

Table 4-2 shows the composition of Inconel®Alloy 600 and stainless steel 304. These alloys are made up primarily of three elements (nickel, iron, and chromium), numerous minor alloying elements and impurities. The primary alloying elements are very insoluble in high temperature, neutral (pH 5.6) water (*7-12*). There is little solubility data on the remaining elements present in the alloys. The little information that does exist suggests that manganese is partially soluble and sulfur is very soluble in high temperature water (*12*). The effect of dissolution of these two soluble species on the electrochemistry within the crevice region will be evaluated in this section.

Manganese

As shown in Table 4-2, manganese is present in the alloys of interest at about 1 weight percent. Since the atomic percent of manganese is approximately equal to its weight percent (i.e., 1%), it is assumed that 1 % of the passive current is due to the dissolution of manganese. This implies that each element anodically dissolves at a rate

proportional to its concentration in the alloy (atomic percent) and that no preferential dissolution occurs. Thus, the current densities for nickel and manganese are

$$i_{Ni} = 7.4844 \times 10^{-4} \quad A/dm^2$$
$$i_{Mn} = 7.56 \times 10^{-6} \quad A/dm^2 \qquad (4-17)$$

Since the solubility of Ni^{2+} is four orders of magnitude less than that of Mn^{2+} and because the number of species that can be incorporated in the model using the present computer is limited, it is assumed that nickel dissolves to form NiO as shown below

$$Ni + H_2O = NiO + 2H^+ + 2e^- \qquad (4-18)$$

to form H^+ ions instead of Ni^{2+}. This assumption has been validated using the model.

The first case modeled was the dissolution of manganese without limiting its solubility and using fast reduction kinetics. The results, shown in Figure 4-17, were obtained using the initial conditions and constants presented in Table 4-12. The Mn^{2+} and $MnOH^+$ ion concentrations increase, drawing in the Cl^- ions and thus increasing the solution conductivity. The increased conductivity allows polarization to occur raising the potential. Some slight acidification also occurs as a result of this polarization. The steady state electrochemistry that is developed within the crevice is shown in Figure 4-18. The Mn^{2+} concentration reached a value of approximately 2.0×10^{-3} M. The solution is more conductive and slightly acidic, and the potential in the crevice is high.

However, application of a solubility limit to as given by the following reaction

$$[Mn^{2+}][OH^-]^2 = 2.3 \times 10^{-16} \qquad (4-19)$$

Table 4-12. Input Parameters for Figures 4-17 and 4-18 (Mn dissolution, no solubility limit on Mn^{2+})

Species	Charge	Diffusion coefficient (dm^2/sec)	Initial Concentration (moles/l)
H	+1	1.76×10^{-5}	2.23×10^{-6}
OH	-1	9.8×10^{-6}	2.23×10^{-6}
Na	+1	2.5×10^{-6}	1.968×10^{-6}
Cl	-1	3.8×10^{-6}	1.968×10^{-6}
Mn	+2	1.3×10^{-6}	0
MnOH	+1	1.3×10^{-6}	0

Equilibrium Reactions	k_f	k_b	K_{eq}
$H^+ + OH^- = H_2O$	1×10^{12}	5	2×10^{11}
$Mn^{2+} + H_2O = MnOH^+ + H^+$	1.7×10^{3}	10^9	1.7×10^{-6}

Wall/Tip Electrochemical Reactions	sign	no. of e^-	k_o	α	ref. spec.	spec. power
$Ni + H_2O \rightarrow 2H^+ + 2e^- + NiO$	+1	2	7.48×10^{-4}	0	-	-
$H_2O + e^- \rightarrow H + OH^-$	-1	1	1.5×10^{-6}	0.6	-	-
$H^+ + e^- \rightarrow H$	-1	1	0.671	0.6	H^+	1
$Mn \rightarrow Mn^{2+} + 2e^-$	+1	2	7.56×10^{-6}	0	-	-

Solubility Reactions	k	K_s
none	-	-

Wall/Tip Dissolution Reactions	Flux (dm^2/sec)
none	-

General Data			
Length (dm)	0.01	Width (dm)	1.71×10^{-7}
No. of Nodes	31	Delta X	3.33×10^{-4}
Temperature (K)	573	E_m (V)	0

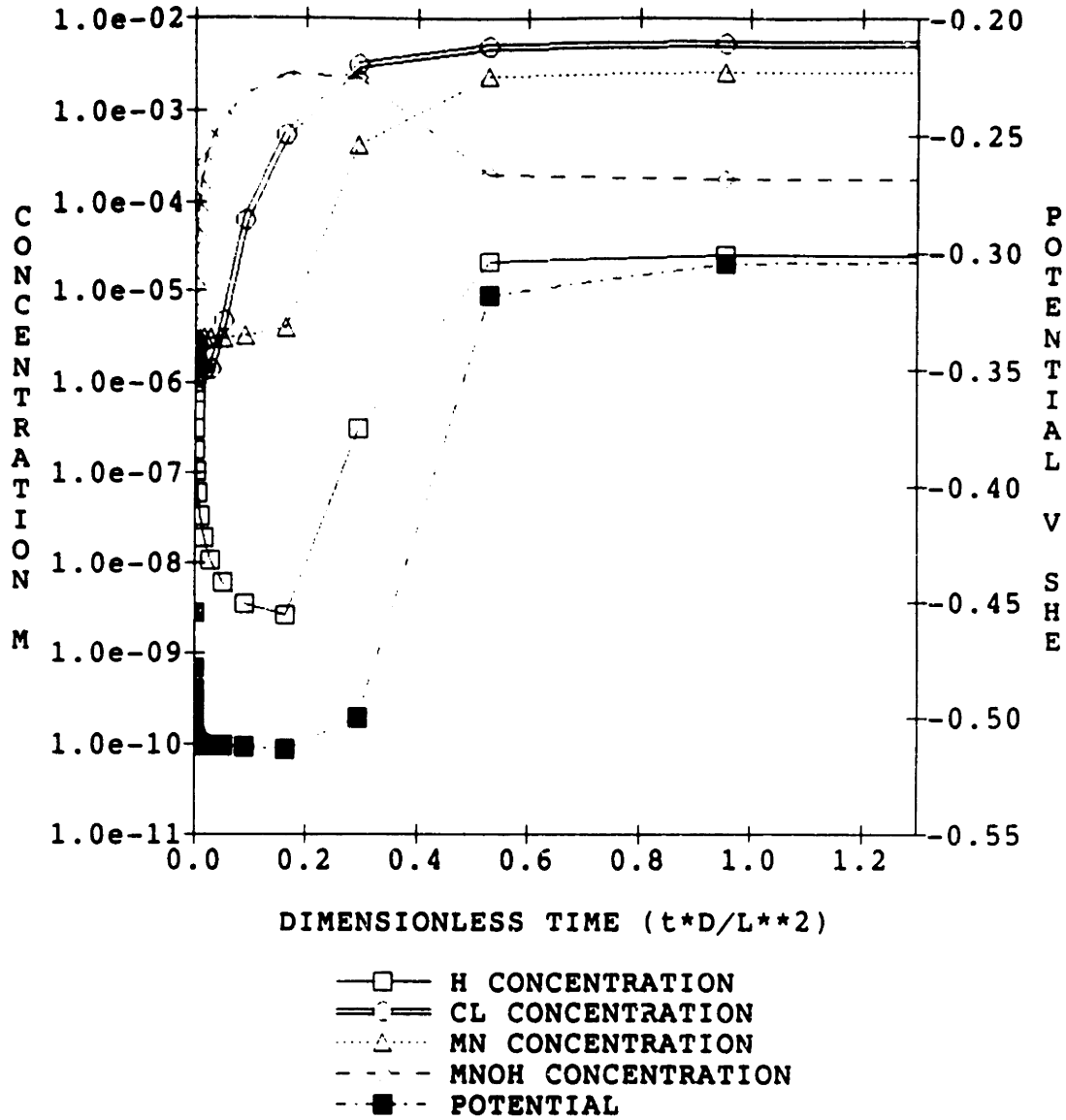

Figure 4-17. Transient concentration and potential profiles at crevice tip when Mn dissolves from the metal at 1% of the passive current and Mn^{2+} has not solubility limit (fast reduction kinetics).

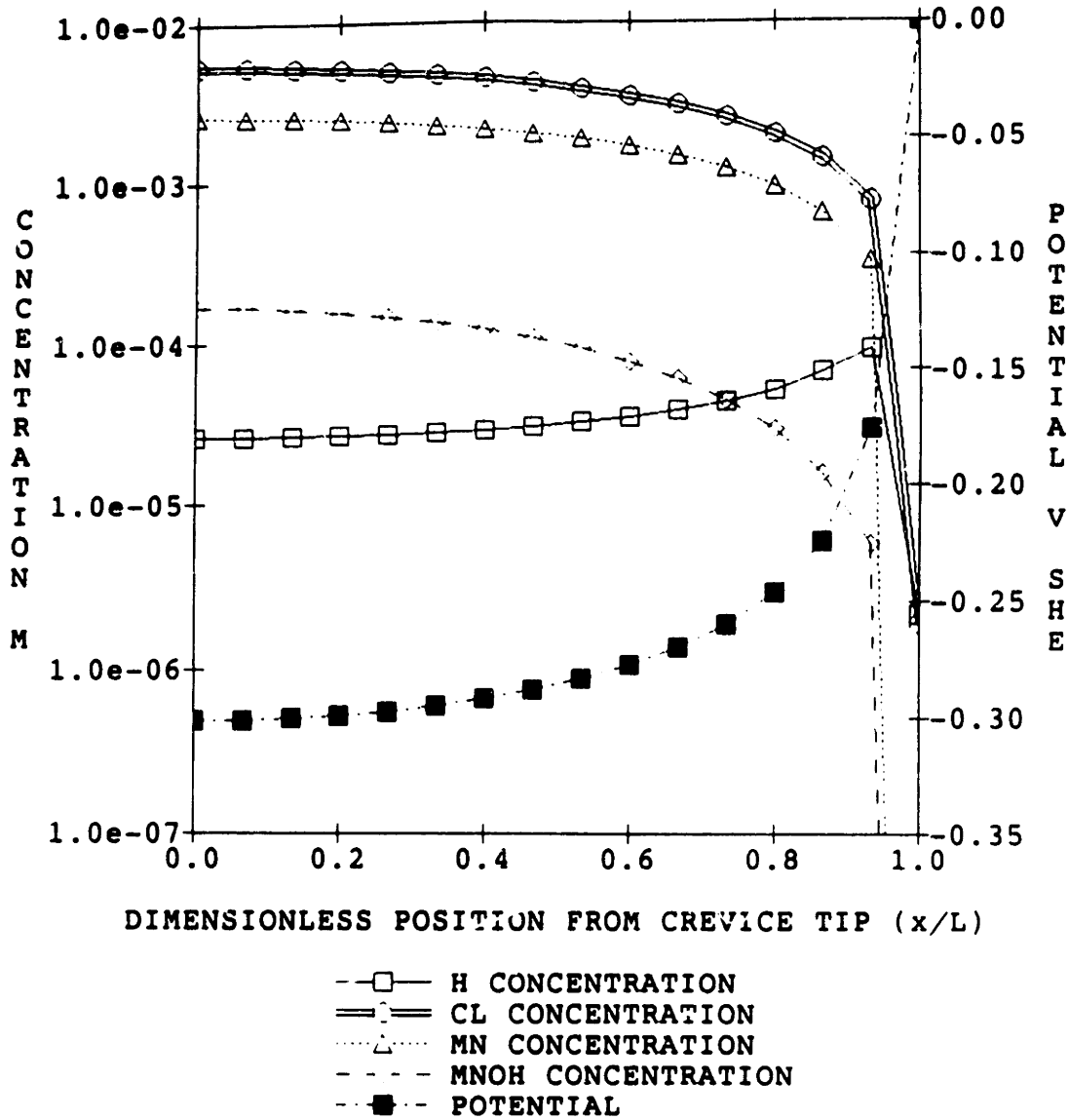

Figure 4-18 Steady-state concentration and potential profiles within the crevice when Mn dissolves from the metal at 1% of the passive current and Mn^{2+} has no solubility limit (fast reduction kinetics).

Table 4-13. Input Parameters for Figure 4-19 (Mn dissolution with solubility limit on Mn^{2+}, fast reduction kinetics)

Species	Charge	Diffusion coefficient (dm^2/sec)	Initial Concentration (moles/l)
H	+ 1	1.76×10^{-5}	2.23×10^{-6}
OH	- 1	9.8×10^{-6}	2.23×10^{-6}
Na	+ 1	2.5×10^{-6}	1.968×10^{-6}
Cl	- 1	3.8×10^{-6}	1.968×10^{-6}
Mn	+ 2	1.3×10^{-6}	0
MnOH	+ 1	1.3×10^{-6}	0

Equilibrium Reactions	k_f	k_b	K_{eq}
$H^+ + OH^- = H_2O$	1×10^{12}	5	2×10^{11}
$Mn^{2+} + H_2O = MnOH^+ + H^+$	1.7×10^{3}	10^9	1.7×10^{-6}

Wall/Tip Electrochemical Reactions	sign	no. of e^-	k_o	α	ref. spec.	spec. power
$Ni + H_2O \rightarrow 2\,H^+ + 2e^- + NiO$	+ 1	2	7.48×10^{-4}	0	-	-
$H_2O + e^- \rightarrow H + OH^-$	- 1	1	1.5×10^{-6}	0.6	-	-
$H^+ + e^- \rightarrow H$	- 1	1	0.671	0.6	H^+	1
$Mn \rightarrow Mn^{2+} + 2e^-$	+ 1	2	7.56×10^{-6}	0	-	-

Solubility Reactions	k	K_s
$Mn^{2+} + 2\,OH^- = Mn(OH)_2$	1×10^{8}	2.3×10^{-16}

Wall/Tip Dissolution Reactions	Flux (dm^2/sec)
none	-

General Data			
Length (dm)	0.01	Width (dm)	1.71×10^{-7}
No. of Nodes	31	Delta X	3.33×10^{-4}
Temperature (K)	573	E_m (V)	0

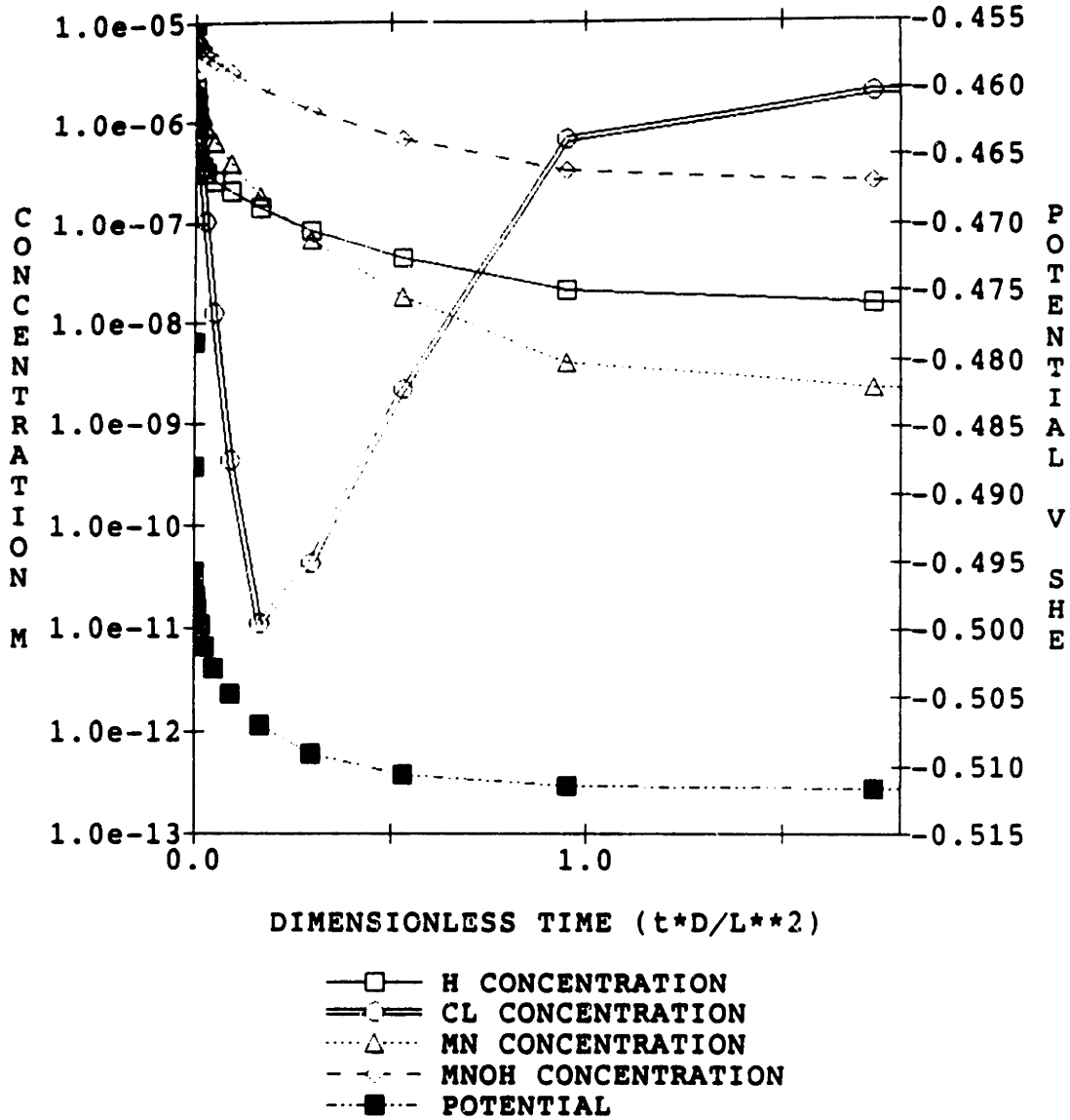

Figure 4-19. Transient concentration and potential profile at crevice tip when Mn dissolves at 1% of the passive current and Mn^{2+} is limited in solubility (fast reduction kinetics).

gives very different results (*12*). Figure 4-19 shows the transient concentration and potential profiles that develop at the crevice tip using the conditions and constants presented in Table 4-13. As explained previously, the solution goes basic as the result of H^+ consumption by cathodic reactions. Since the solubility of Mn^{2+} ions is directly proportional to the H^+ concentration squared, the solubility of Mn^{2+} becomes very low as the H^+ concentration decreases. Thus, after an initial increase (cannot be seen in Figure 4-19 because of the x-axis scale), the Mn^{2+} concentration decreases as the H^+ concentration decreases. Since the Mn^{2+} concentration does not significantly increase, the conductivity within the crevice does not increase. This continuing low conductivity within the crevice does not allow polarization to occur. Thus the initial increase in pH fixes the solution electrochemistry to one of low potential (at the corrosion potential), low conductivity, and high pH similar to that for Ni dissolution. Comparison of Figures 4-17 and 4-19 and the steady state pH and potential profiles for each case as shown in Figure 4-20 demonstrates again the importance of applying solubility limits on all metal ions at this temperature even when the metal ions are being produced at such a low rate.

The same model case was run with slow reduction kinetics. Figure 4-21 shows the transient concentration and potential profile at the crevice tip using the initial conditions and constants shown in Table 4-14. By comparison with Figure 4-19, it is apparent that the trends are the same. The increase in pH (decrease in H^+ concentration) fixes the Mn^{2+} concentration thus fixing the conductivity. A direct comparison of the steady state pH and potential profiles developed for the different reduction kinetic parameters is shown in Figure 4-22. The faster kinetics result in a higher pH because more H^+ ions are consumed or more OH^- produced. The corrosion

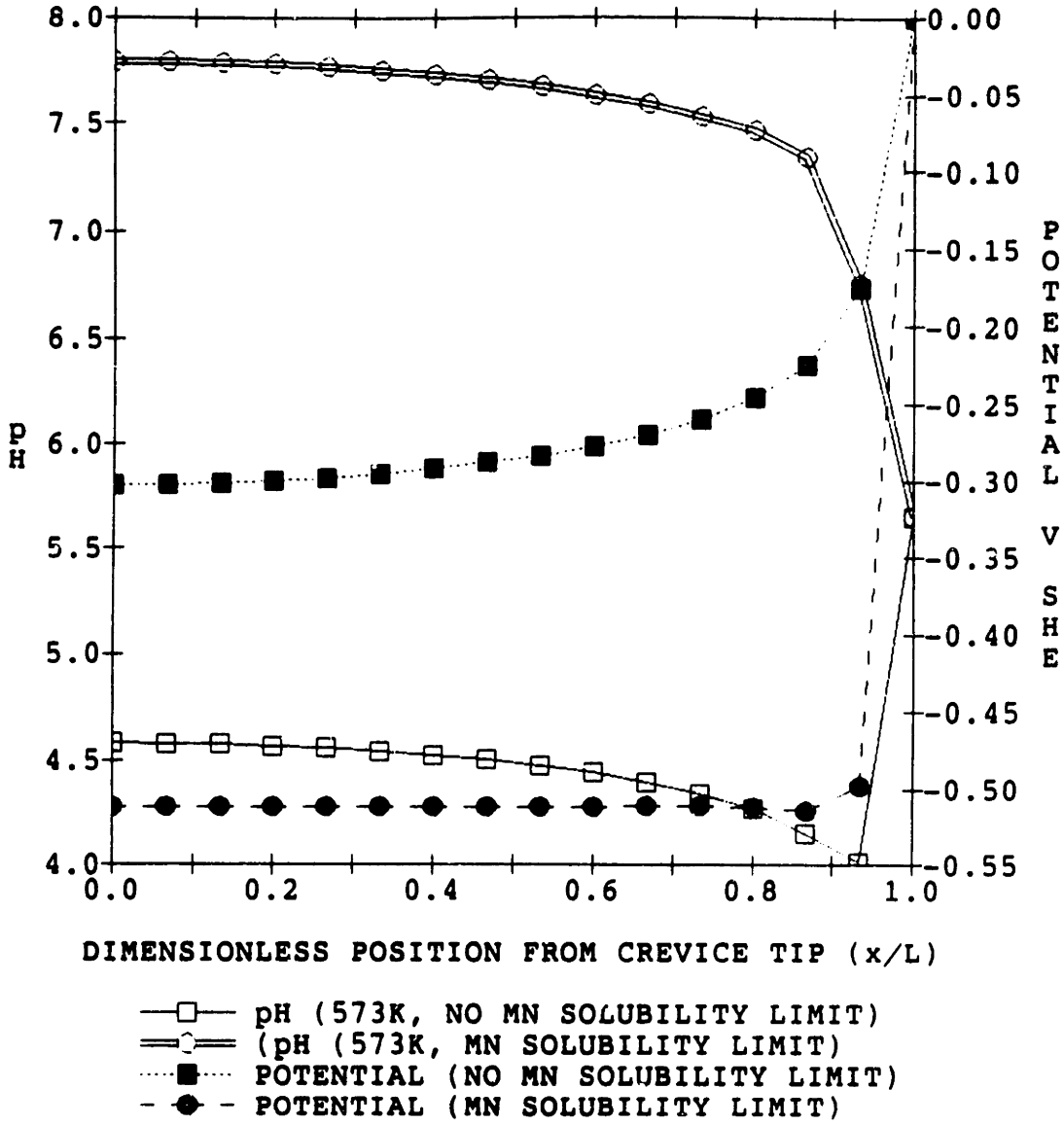

Figure 4-20. Comparison of steady-state pH and potential profiles developed with Mn dissolution with and without Mn^{2+} solubility limit (fast reduction kinetics).

Table 4-14. Input Parameters for Figure 4-21 (Mn dissolution, Mn^{2+} solubility limit, slow reduction kinetics)

Species	Charge	Diffusion coefficient (dm^2/sec)	Initial Concentration (moles/l)
H	+1	1.76×10^{-5}	2.23×10^{-6}
OH	-1	9.8×10^{-6}	2.23×10^{-6}
Na	+1	2.5×10^{-6}	1.968×10^{-6}
Cl	-1	3.8×10^{-6}	1.968×10^{-6}
Mn	+2	1.3×10^{-6}	0
MnOH	+1	1.3×10^{-6}	0

Equilibrium Reactions	k_f	k_b	K_{eq}
$H^+ + OH^- = H_2O$	1×10^{12}	5	2×10^{11}
$Mn^{2+} + H_2O = MnOH^+ + H^+$	1.7×10^{3}	10^9	1.7×10^{-6}

Wall/Tip Electrochemical Reactions	sign	no. of e^-	k_o	α	ref. spec.	spec. power
$Ni + H_2O \rightarrow 2H^+ + 2e^- + NiO$	+1	2	7.48×10^{-4}	0	-	-
$H_2O + e^- \rightarrow H + OH^-$	-1	1	4.55×10^{-8}	0.6	-	-
$H^+ + e^- \rightarrow H$	-1	1	2.03×10^{-2}	0.6	H^+	1
$Mn \rightarrow Mn^{2+} + 2e^-$	+1	2	7.56×10^{-6}	0	-	-

Solubility Reactions	k	K_s
$Mn^{2+} + 2\,OH^- = Mn(OH)_2$	1×10^{8}	2.3×10^{-16}

Wall/Tip Dissolution Reactions	Flux (dm^2/sec)
none	-

General Data			
Length (dm)	0.01	Width (dm)	1.71×10^{-7}
No. of Nodes	31	Delta X	3.33×10^{-4}
Temperature (K)	573	E_m (V)	0

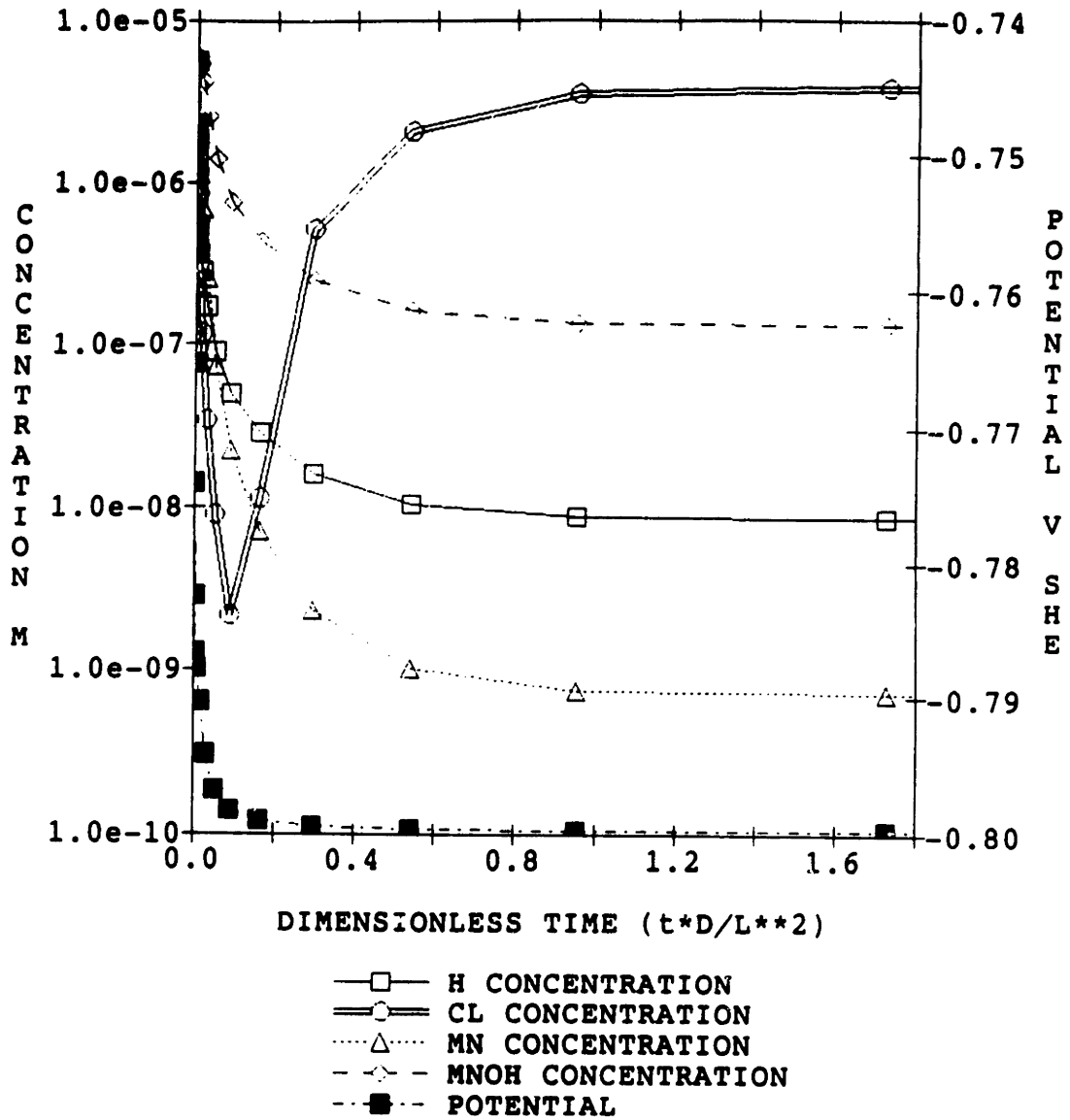

Figure 4-21. Transient concentration and potential profiles at the crevice tip when Mn dissolves at 1% of the passive current, Mn^{2+} is limited in solubility, and slow reduction kinetics are applied.

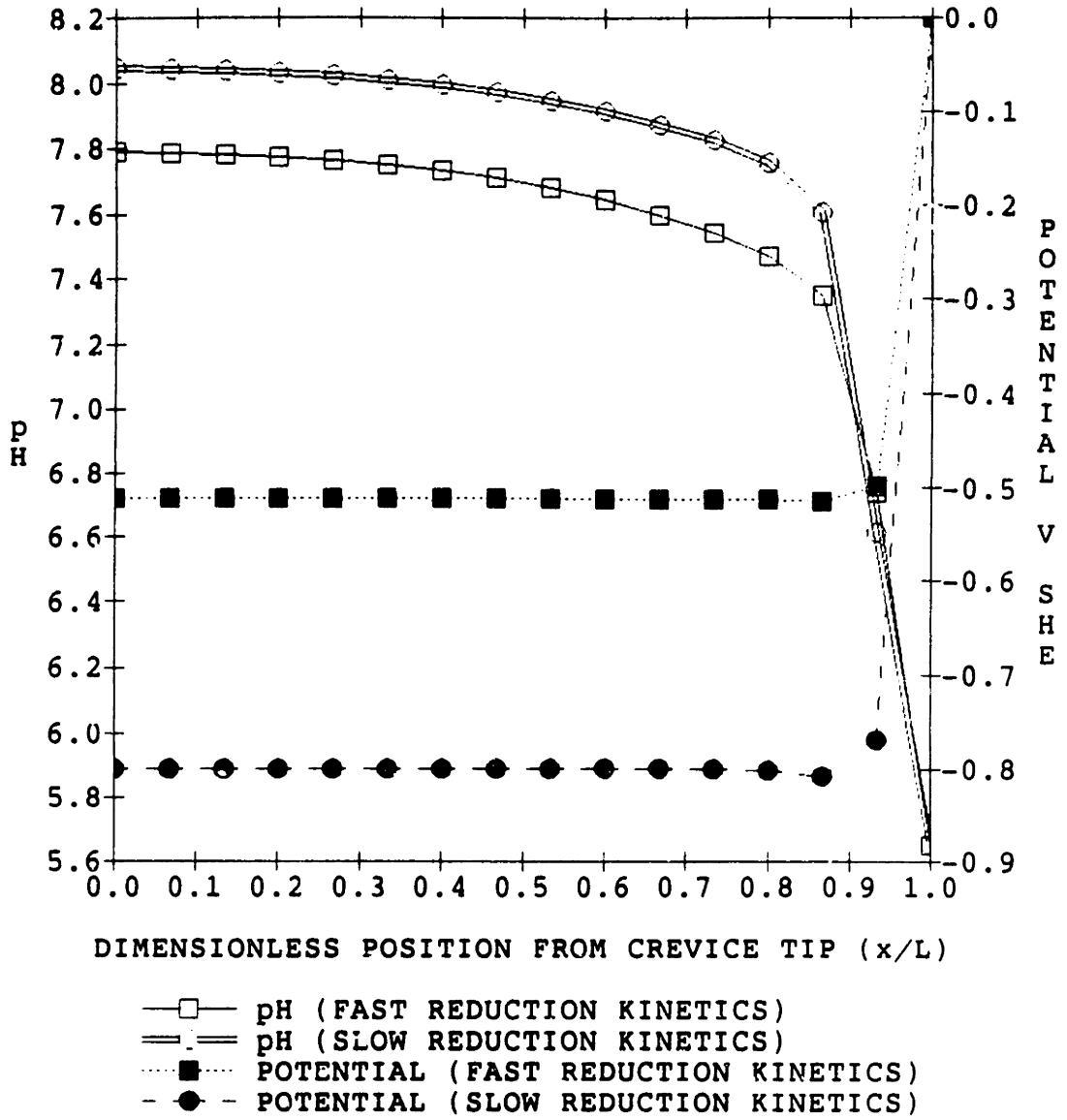

Figure 4-22. Comparison of fast and slow reduction kinetics for Mn dissolution with Mn^{2+} solubility limit.

potential is reached in both cases, but the value of the corrosion potential is dependent on these kinetic parameters. The corrosion potential (after H^+ concentration is decreased) for the fast kinetics is -512 mV and for the slower kinetics it is -800 mV, as previously described.

In conclusion, the electrochemical conditions that develop within the crevice (high pH, low potential, low conductivity) from the dissolution of the potentially more soluble manganese are not sufficient to promote stress corrosion cracking in the crevice (*3*). If the charged species produced has a much higher or no solubility limit then it may be possible to initiate and propagate stress corrosion cracking. If the species has some solubility limit then its influence may be limited by the initial increase in pH. Further data are necessary in order to evaluate the relative solubilities of the other metallic minor alloying elements so that their effects can be evaluated.

Sulfur

Sulfur is present, in the stainless steels alloys of interest and in Inconel® Alloy 600, in small amounts as shown in Table 4-2. In steels, non metallic materials, such as sulfur, enter the alloy during the deoxidation process when the alloy is being made. It is present in the alloy primarily as a metallic sulfide inclusion, in particular, manganese sulfide (MnS). Manganese sulfide dissolves chemically from the alloy to give manganese species (Mn^{2+} or MnO) and a dissolved sulfur species (S^{2-}, HS^-, or H_2S) (*18,19*). This chemical dissolution process may play a role in stress corrosion cracking (*20*). At this pH, temperature, and potential (5.6, 300 °C, and the corrosion potential,

respectively), the dissolution process results in H_2S (*18,19*). The net reaction can be represented by either

$$MnS + 2H^+ = Mn^{2+} + H_2S \qquad (4\text{-}20)$$

or

$$MnS + H_2O = MnO + H_2S \qquad (4\text{-}21)$$

Use of either of these equations results in similar conditions being generated in the crevice. In the modelling presented in this section, the second reaction is used to account for MnS chemical dissolution. The data for this dissolution process are very limited and are available only for low alloy steel. Even for this case, the reported dissolution rates span three orders of magnitude (*21*). In order to account for this variability, the modeling has been carried out using three different dissolution rates.

The electrochemistry of sulfur species is very complex and has not been studied experimentally in high temperature water. Figure 4-23 shows a calculated E-pH

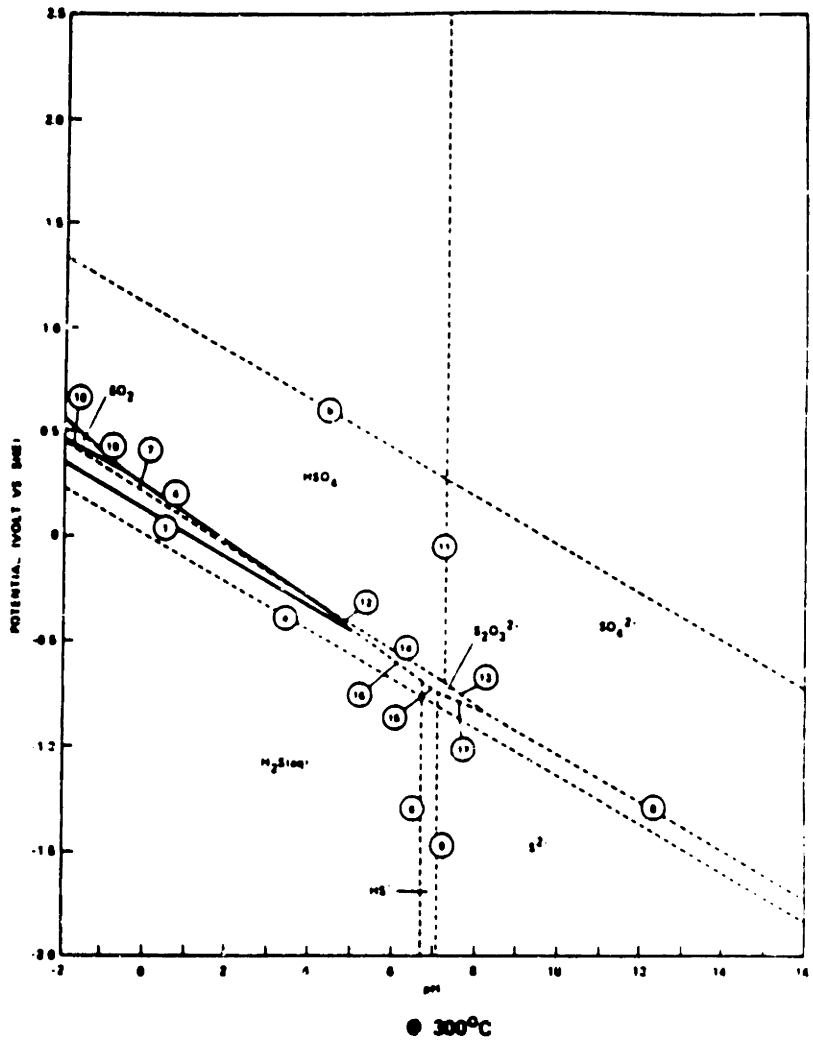

Figure 4-23. Calculated high temperature E/pH diagram.

diagram for sulfur species in 300°C water (*22*). The important species (for occluded regions in high temperature BWR water) shown on the diagram include H_2S, HS^-,S^{2-}, $S_2O_3^{2-}$, and HSO_4^-. In the calculation of this table the reduction of H_2S has been ignored. Indeed even at room temperature this reduction processes has, in general, been ignored in the formation of E-pH diagrams. Nonetheless, it is well established that at ambient temperatures direct reduction of H_2S can be significant (*23,24*). Thus, the reduction of H_2S is incorporated into the model, as given by

$$H_2S + e^- \rightarrow HS^- + H \qquad (4\text{-}22)$$

This reaction has interesting implications when coupled with the chemical equilibrium between H_2S and HS^-

$$H_2S = HS^- + H^+ \qquad (4\text{-}23)$$

It becomes apparent that HS^- could be considered a 'catalyst' for H^+ reduction. H_2S is reduced to produce HS^- and HS^- combines with H^+, returning it to reform H_2S. The pH would therefore increase. This pseudo-catalytic effect would be pH dependent and would only be self-sustaining provided a source of H^+ is maintained. Indeed, it may be possible to explain, in part, the enhanced hydrogen production at metal surfaces and hydrogen diffusion into metals seen in the presence of H_2S (for example see reference 28) by this reduction/equilibrium induced catalytic behavior (*25*).

The kinetics of this reaction are unknown at high temperature so it is necessary to extrapolate knowledge obtained at room temperature. At room temperature the kinetics of H_2S reduction is comparable to or faster than H^+ ion reduction (*27*).

Therefore, the same reduction kinetic parameters will be chosen (i.e.. α_{H2S} = 0.6 and $k_{0,H2S} = 2.03 \times 10^{-2}$). The resulting H_2S reduction current density would be given by

$$i_{H_2S} = k_{0,H_2S} C_{H_2S} \exp\left[- \frac{\alpha_{H_2S} F (E_m - \phi)}{R T} \right] \qquad (4-24)$$

In view of the uncertainty of the data, faster H_2S reduction kinetics (i.e.. $k_{0,H2S} = 2.03 \times 10^{-1}$) will also be evaluated.

Figures 4-24, 4-25, and 4-26, show the transient concentration and potential profiles at the crevice tip for the three H_2S dissolution rates described above assuming the **slow**, more realistic reduction kinetic parameters. The initial conditions and constants for these figures are given in Table 4-13 In Figure 4-24, the rate of MnS dissolution is large (flux of H_2S is 10^{-10} moles/(dm^2sec)) and the concentration of H_2S and HS^- increases to a high value (>10^{-3} M). It becomes necessary at this point to define two types of increase in potential which will be labelled polarization and net polarization. Polarization will be defined as an increase in potential relative to the initial potential (at time equal to zero). Net polarization will be defined as an increase in potential (at time t) above the **local** corrosion potential (i.e.. potential at which total anodic current equals the total cathodic current at each point) in the crevice at that time. The need for such a definition arises because the local environment changes. This change in the local environment can change the rate of electrochemical processes occuring in the crevice. In this case with fast dissolution of MnS and slow reduction kinetics, the resulting steady state potential (-166mV) is polarized relative to the initial potential (-750mV) but no net polarization occurs. The corrosion potential in 5×10^{-3} M H_2S solution is -0.166mV. Since MnS is considered to dissolves chemically, not electrochemically, the production of H_2S in solution results in an extra source of

Table 4-15. Input Parameters for Figures 4-24 through 4-26 (MnS dissolution, H_2S reduction, slow reduction kinetics).

Species	Charge	Diffusion coefficient (dm^2/sec)	Initial Concentration (moles/l)
H	+ 1	1.76×10^{-5}	2.23×10^{-6}
OH	- 1	9.8×10^{-6}	2.23×10^{-6}
Na	+ 1	2.5×10^{-6}	1.968×10^{-6}
Cl	- 1	3.8×10^{-6}	1.968×10^{-6}
H_2S	0	2.0×10^{-6}	0
HS	- 1	2.0×10^{-6}	0

Equilibrium Reactions	k_f	k_b	K_{eq}
$H^+ + OH^- = H_2O$	1×10^{12}	5	2×10^{11}
$H_2S = H^+ + HS^-$	1.8×10^{3}	1×10^{10}	1.8×10^{-7}

Wall/Tip Electrochemical Reactions	sign	no. of e^-	k_o	α	ref. spec.	spec. power
$Ni + H_2O \rightarrow NiO + 2H^+ + 2e^-$	+ 1	2	7.56×10^{-4}	0	-	-
$H_2O + e^- \rightarrow H + OH^-$	- 1	1	4.55×10^{-8}	0.6	-	-
$H^+ + e^- \rightarrow H$	- 1	1	2.03×10^{-2}	0.6	H^+	1
$H_2S + e^- \rightarrow HS^- + H$	- 1	1	2.03×10^{-2}	0.6	H_2S	1

Solubility Reactions	k	K_s
none	-	-

Wall/Tip Dissolution Reactions	Flux (dm^2/sec)
$MnS + H_2O \rightarrow MnO + H_2S$	1×10^{-10} (Fig. 24) 1×10^{-11} (Fig. 25) 1×10^{-12} (Fig. 26)

General Data			
Length (dm)	0.01	Width (dm)	1.71×10^{-7}
No. of Nodes	31	Delta X	3.33×10^{-4}
Temperature (K)	573	E_m (V)	0

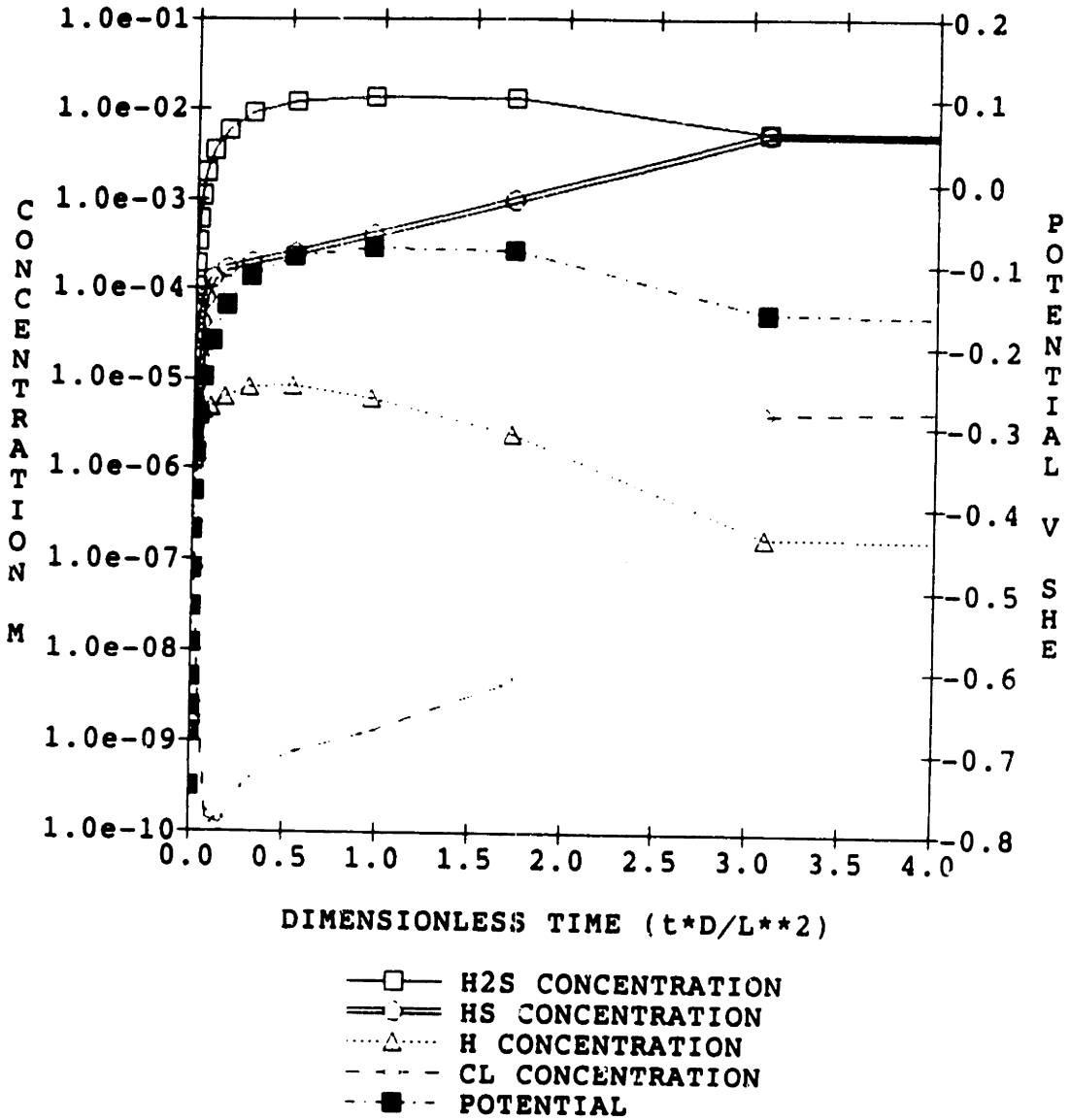

Figure 4-24. Transient concentration and potential profiles at the crevice tip with MnS dissolution (H_2S flux = 10^{-10} moles/dm^2_{sec}) and slow reduction kinetics.

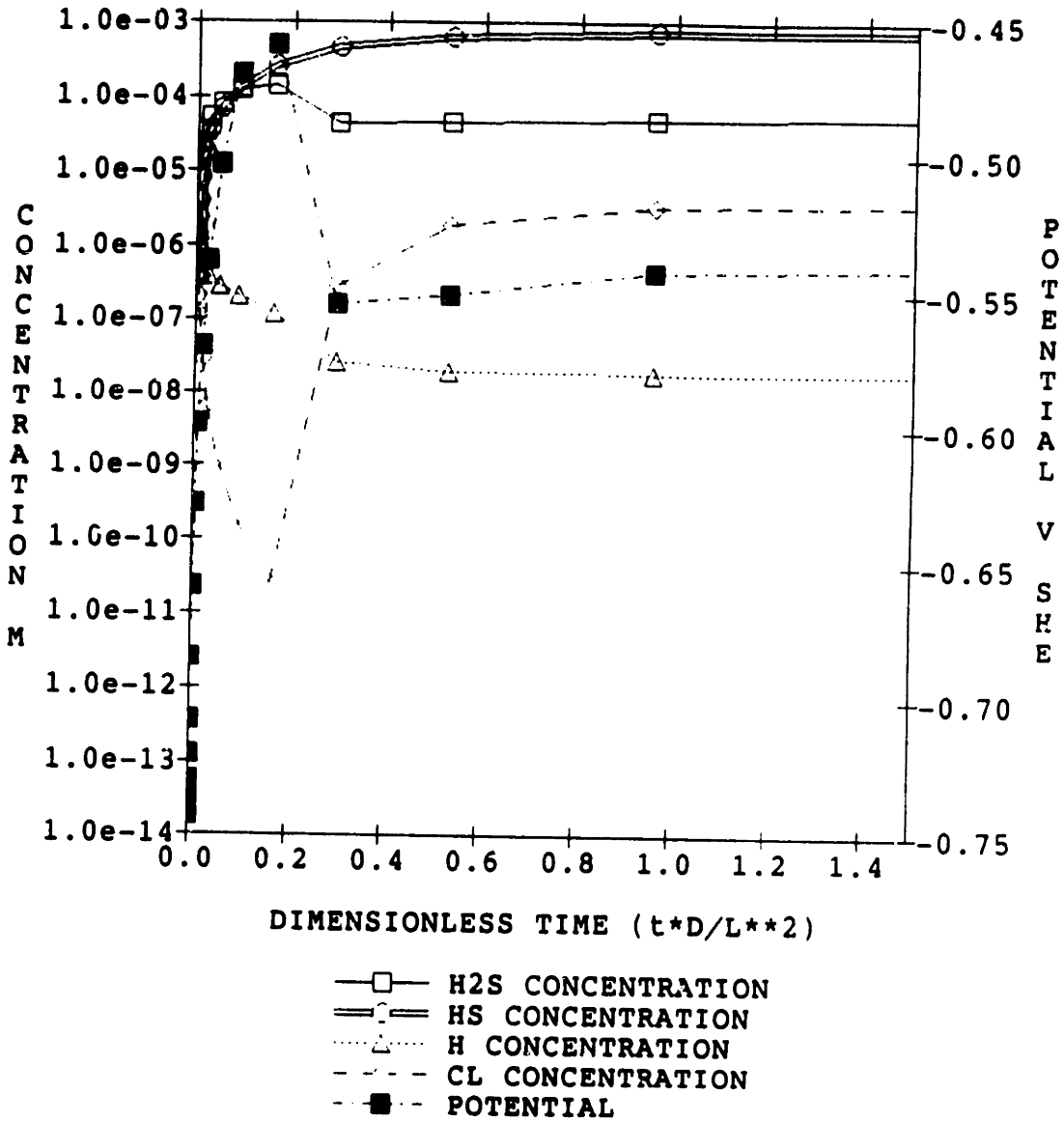

Figure 4-25. Transient concentration and potential profiles at the crevice tip with MnS dissolution (H_2S flux = 10^{-11} $^{moles}/_{cm^2 sec}$) and slow reduction kinetics.

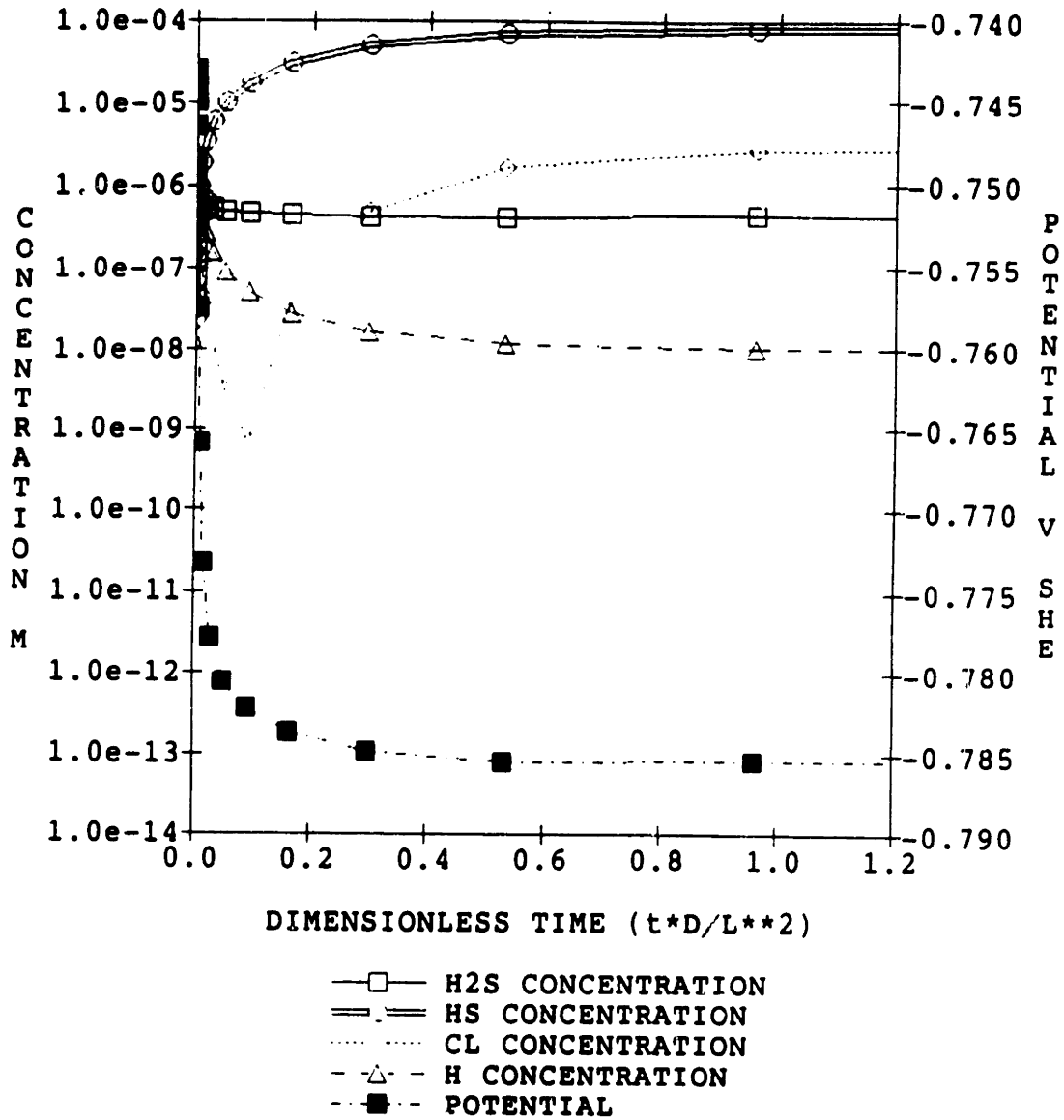

Figure 4-26. Transient concentration and potential profiles at the crevice tip with MnS dissolution (H_2S flux = 10^{-12} $^{moles}/_{dm^2 sec}$) and slow reduction kinetics.

cathodic reactant. This stimulation of the cathodic process raises the potential. This is further demonstrated by the fact that the potential curve closely follows the H_2S concentration curve in Figure 4-24.

For the medium MnS dissolution rate (flux of H_2S is 10^{-11} moles/(dm^2sec)), a smaller transient concentration and potential profile develops, as shown in Figure 4-25. There is an increase in the H_2S and HS^- concentrations. The values do not get as high, which is expected since the dissolution rate is lower. Again, the potential rises because of the cathodic stimulation of H_2S. However, the lower H_2S production rate results in a smaller degree of polarization. Since the local corrosion potential is -540 mV (in $5x10^{-5}$ M H_2S) no net polarization exists.

The transient concentration and potential profiles at the crevice tip for slow MnS dissolution (flux of H_2S is 10^{-12} moles/(dm^2sec)) are shown in Figure 4-26. The H_2S and HS^- concentrations increase in a similar manner as before, but the concentrations reached are even lower because of the lower MnS dissolution rate. The potential in this case does not rise at all. It decreases to approximately -785 mV (the corrosion potential in the local environment). Indeed, comparing this figure to Figure 4-22 shows how little effect MnS dissolution at this low rate has on the local pH and potential at the crevice tip.

A comparison of the steady state potential profiles in the crevice for these three dissolution rates is shown in Figure 4-27. This figure shows another interesting effect of the stimulus of the H_2S reduction reaction. The slope of the potential changes sign in the crevice. Close to the crevice mouth, between 0.9 and 1 in the dimensionless position, the slope of the potential curve is positive. As we move into the crevice, the slope of the curve is negative. Since the reduction of H_2S is dependent on its concentration, and the concentration of H_2S is greater at the crevice tip compared to the

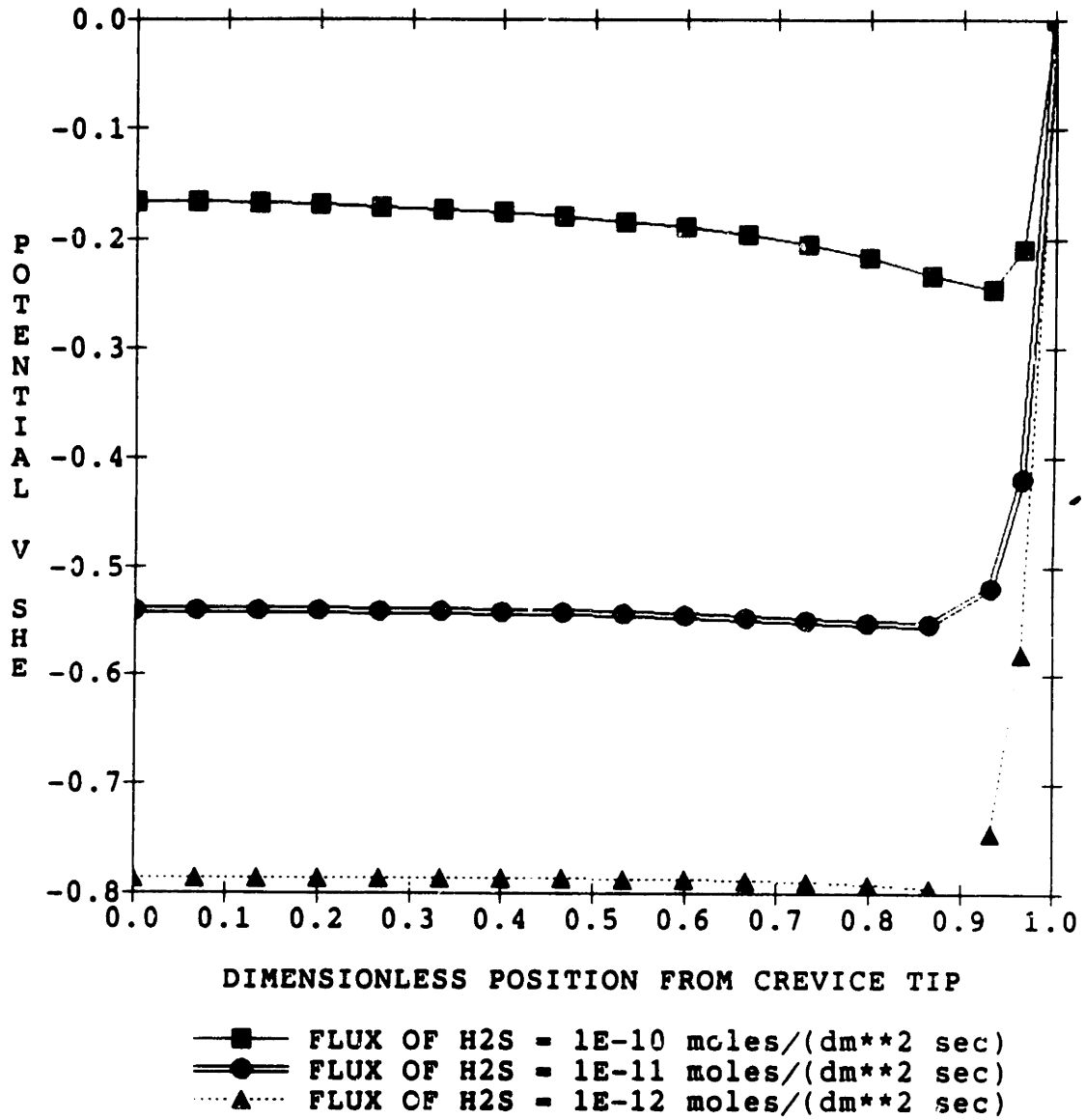

Figure 4-27. Steady-state potential profiles within crevice for each of the MnS dissolution rates (or H_2S fluxes).

mouth, the cathodic reaction stimulation is greater at the tip than the mouth. This raises the potential at the tip more than at the mouth. This effect is most obvious in the top curve of Figure 4-27 for the fastest MnS dissolution rate, as one might expect.

Increasing the kinetics of H_2S reduction by changing k_0 from 2.03×10^{-2} to 2.03×10^{-1} causes significant upward shifts in the potential profiles to develop within the crevice. This dramatic effect is shown in Figure 4-28 for H_2S flux = 10^{-10} moles/dm^2-sec. The initial conditions and constants for faster H_2S reduction kinetics are given in Table 4-16. The potential develcped within the crevice is significantly higher with fast H_2S reduction kinetics. Again there is no net polarization within the crevice. There is also some change in the H_2S concentration profile within the crevice as shown in Figure 4-29. As one might expect, the H_2S concentration is lower for faster reduction kinetics.

If the fast reduction kinetics is used for all cathodic reactions, including H_2S reduction (as described in Section 4.2.3), the effect is dramatic for all dissolution rates. Figure 4-30 shows the steady state potential profiles that develop within the crevice for the three dissolution rates of interest using the initial conditions described in Table 4-17. Comparing this figure with Figure 4-27 shows the effect of fast and slow cathodic reduction kinetics respectively. The steady state potentials for all three dissolution rates shift upward with faster reduction kinetics. The potential for the fastest dissolution rate even goes positive. The change in sign of the potential gradient becomes more significant. Even at the lowest dissolution rate the change in slope is obvious and dramatic. Indeed, it is fortunate that these kinetics are probably unrealistic, because such an drastic increase in potential would probably result in cracking.

In all cases run involving MnS dissolution, once the MnS inclusions are consumed and H_2S is no longer being produced, the electrochemical conditions within the

Table 4-16. Input Parameters for Fast H_2S Reduction

Species	Charge	Diffusion coefficient (dm^2/sec)	Initial Concentration (moles/l)
H	+ 1	1.76×10^{-5}	2.23×10^{-6}
OH	- 1	9.8×10^{-6}	2.23×10^{-6}
Na	+ 1	2.5×10^{-6}	1.968×10^{-6}
Cl	- 1	3.8×10^{-6}	1.968×10^{-6}
H_2S	0	2.0×10^{-6}	0
HS	- 1	2.0×10^{-6}	0

Equilibrium Reactions	k_f	k_b	K_{eq}
$H^+ + OH^- = H_2O$	1×10^{12}	5	2×10^{11}
$H_2S = H^+ + HS^-$	1.8×10^{3}	1×10^{10}	1.8×10^{-7}

Wall/Tip Electrochemical Reactions	sign	no. of e^-	k_o	α	ref. spec.	spec. power
$Ni + H_2O \rightarrow NiO + 2H^+ + 2e^-$	+ 1	2	7.56×10^{-4}	0	-	-
$H_2O + e^- \rightarrow H + OH^-$	- 1	1	4.55×10^{-8}	0.6	-	-
$H^+ + e^- \rightarrow H$	- 1	1	2.03×10^{-2}	0.6	H^+	1
$H_2S + e^- \rightarrow HS^- + H$	- 1	1	2.03×10^{-1}	0.6	H_2S	1

Solubility Reactions	k	K_s
none	-	-

Wall/Tip Dissolution Reactions	Flux (dm^2/sec)
$MnS + H_2O \rightarrow MnO + H_2S$	1×10^{-10}

General Data			
Length (dm)	0.01	Width (dm)	1.71×10^{-7}
No. of Nodes	31	Delta X	3.33×10^{-4}
Temperature (K)	573	E_m (V)	0

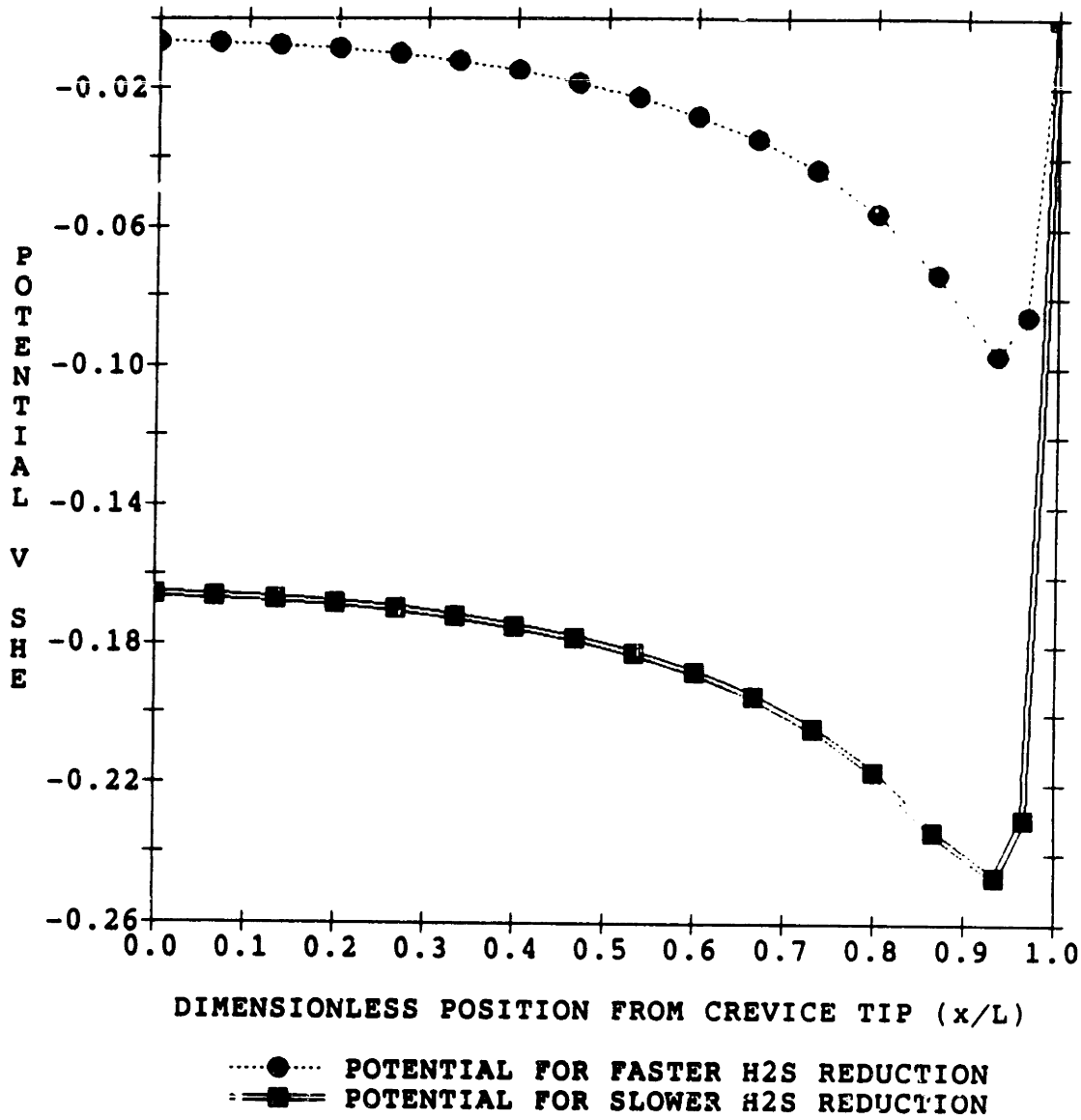

Figure 4-28. Comparison of steady-state potential profiles developed within the crevice with fast and slow H_2S reduction kinetics (H_2S flux = 10^{-10} moles/dm^2sec).

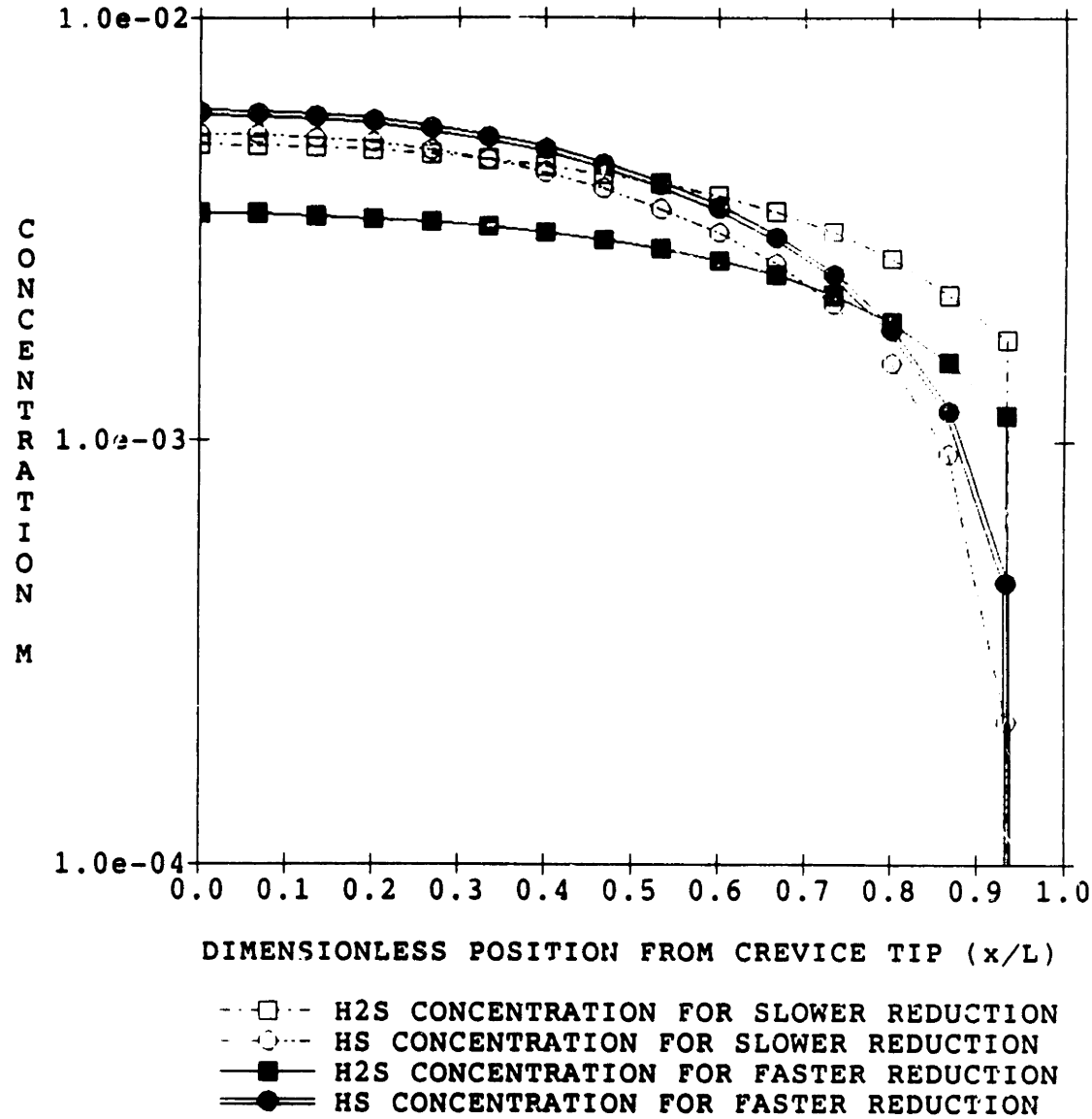

Figure 4-29. Comparison of steady-state H_2S and HS^- concentration profiles within the crevice with fast and slow H_2S reduction kinetics (H_2S flux = 10^{-10} moles/$_{dm^2 sec}$).

Table 4-17. Input Parameters for Figure 4-30 (MnS dissolution, H_2S reduction, fast reduction kinetics)

Species	Charge	Diffusion coefficient (dm^2/sec)	Initial Concentration (moles/l)
H	+ 1	1.76×10^{-5}	2.23×10^{-6}
OH	- 1	9.8×10^{-6}	2.23×10^{-6}
Na	+ 1	2.5×10^{-6}	1.968×10^{-6}
Cl	- 1	3.8×10^{-6}	1.968×10^{-6}
H_2S	0	2.0×10^{-6}	0
HS	- 1	2.0×10^{-6}	0

Equilibrium Reactions	k_f	k_b	K_{eq}
$H^+ + OH^- = H_2O$	1×10^{12}	5	2×10^{11}
$H_2S = H^+ + HS^-$	1.8×10^{3}	1×10^{10}	1.8×10^{-7}

Wall/Tip Electrochemical Reactions	sign	no. of e^-	k_o	α	ref. spec.	spec. power
$Ni + H_2O \rightarrow NiO + 2H^+ + 2e^-$	+ 1	2	7.56×10^{-4}	0	-	-
$H_2O + e^- \rightarrow H + OH^-$	- 1	1	1.5×10^{-6}	0.6	-	-
$H^+ + e^- \rightarrow H$	- 1	1	0.671	0.6	H^+	1
$H_2S + e^- \rightarrow HS^- + H$	- 1	1	0.671	0.6	H_2S	1

Solubility Reactions	k	K_s
none	-	-

Wall/Tip Dissolution Reactions	Flux (dm^2/sec)
$MnS + H_2O \rightarrow MnO + H_2S$	a. 1×10^{-10} b. 1×10^{-11} c. 1×10^{-12}

General Data			
Length (dm)	0.01	Width (dm)	1.71×10^{-7}
No. of Nodes	31	Delta X	3.33×10^{-4}
Temperature (K)	573	Em (V)	0

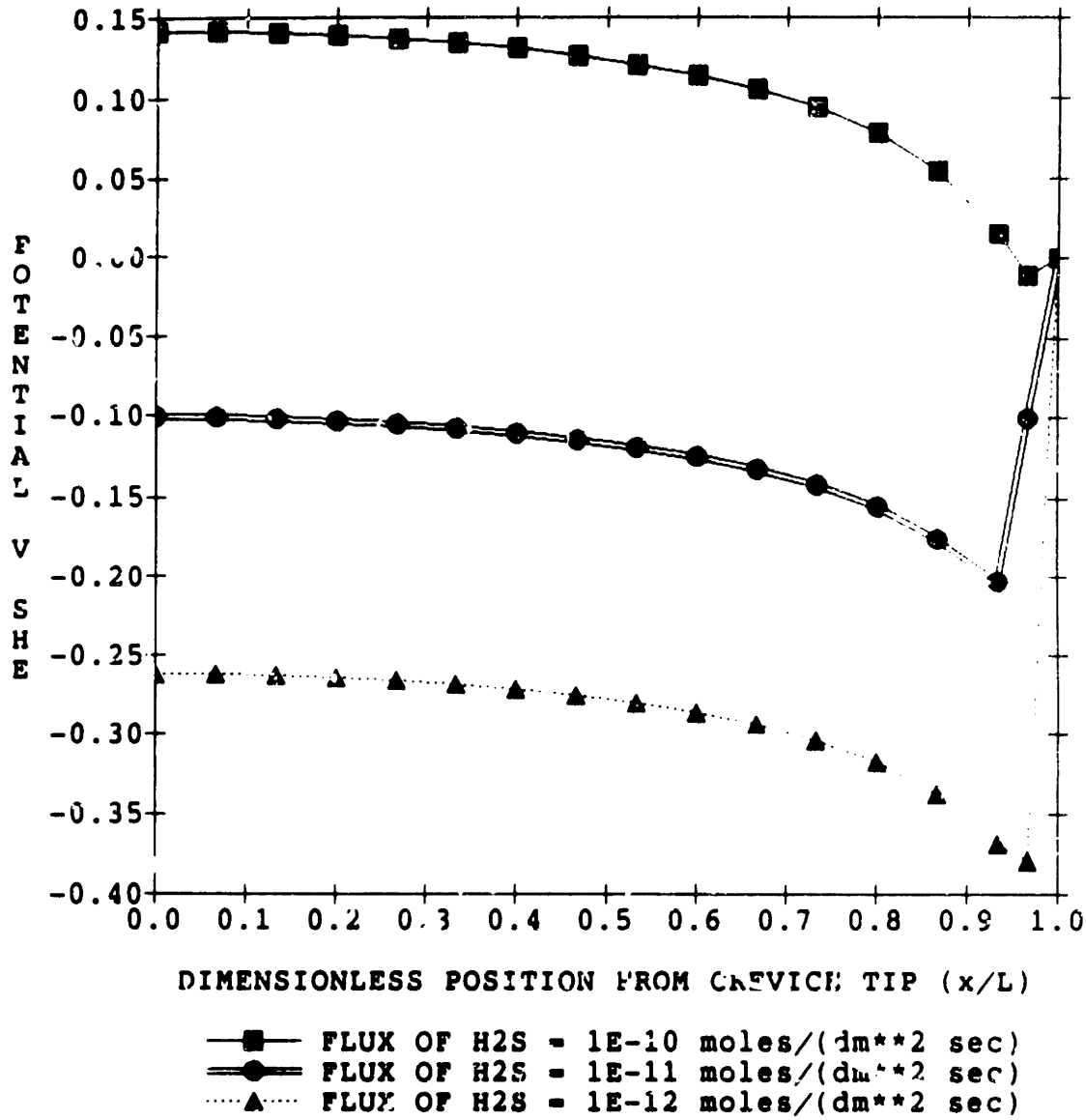

Figure 4-30. Steady-state potential profiles within the crevice when MnS dissolves with H_2S reduction and fast reduction kinetics.

crevice return to the benign conditions that were described in Section 4.2.5 and shown in Figure 4-16. The pH in the solution becomes basic, there is no H_2S or HS^- present, and the potential returns to the corrosion potential for deaerated basic solutions (-512 mV for fast reduction kinetics and -800 mV for slow reduction kinetics). Thus, the electrochemistry generated by MnS dissolution is **reversible** to high pH, low potential conditions.

Therefore, the presence of MnS inclusions is only important for certain limited circumstances. One case when MnS inclusion could be important is when the crevice is initially submerged. It is possible to create conditions within the crevice that could initiate stress corrosion cracking shortly after submersion. If cracks are not initiated during the initial period of time they will not initiate unless stimulated by some other process such as excursions (which will be discussed in the next section). Another time that the presence of MnS inclusions may be of importance is when precracked specimens are used in mechanical testing. These specimens are cracked in air possibly exposing MnS inclusions. Once submerged for testing, these inclusions will dissolve from the crack planes in the precrack region producing H_2S. Production of H_2S may raise the potential at the crack tip which may increase the crack propagation rate. Eventually, this transient increased crack propagation rate would decrease with time as the MnS inclusions in the precrack region dissolve away and the true propagation rate would be reached. Though recognized as a feasible factor in crack growth rates, the scatter in results from variations in MnS distribution makes it difficult to observe such effects (*26*).

4.2.7 Excursions in Bulk Conductivity

In a BWR, excursions in bulk conductivity can be attributed to two different types of intrusions. One type is the intrusion of seawater through the condenser. If the demineralizer capacity is exceeded, there will be an increase in the bulk chloride ion concentration. Such an intrusion occurred at the Millstone plant in 1972 resulting in Cl^- concentrations exceeding 50 ppm, conductivities greater than 100 μS/cm and a pH of approximately 3.5 in the bulk solution (*13*). This was obviously a severe, but rare, excursion in bulk conductivity. Another type of intrusion is of demineralizer resins from the reactor vessel clean up loop. The resins release bisulfate ions (HSO_4^-) generally in the form of dilute sulfuric acid. Such an excursion occurred at the Duane Arnold plant in 1975 resulting in conductivities of greater than 50 μS/cm (*13*). In both cases the bulk electrochemistry was well within the stress corrosion cracking susceptibility region shown in Figure 4-1. These excursions were extreme cases. Nevertheless, excursions due to resin intrusions are to some extent unavoidable in nuclear power plants. Most excursions result in a conductivity increase and an increase in concentration of some aggressive anion.

In the modelling conducted, excursions of both sodium bisulfate ($NaHSO_4$) and sulfuric acid (H_2SO_4) were considered. There was no difference in the results using either sodium sulfate or sulfuric acid since the bulk environment contains dissolved oxygen and oxygen reduction dominates the cathodic processes. In this section, the results for sulfuric acid excursions of one and two orders of magnitude increase in bulk conductivity will be presented. It is important to note that the bisulfate ion is considered an inert conducting ionic species, like chloride (Cl^-), in this case. This is

not completely accurate since it is possible and, indeed, likely that HSO_4^- will be reduced within the crevice according to the following reaction

$$HSO_4^- + 9\,H^+ + 8\,e^- \rightarrow H_2S + 4\,H_2O \qquad (4\text{-}25)$$

Since the kinetics of this reaction are completely unknown, there is no way to realistically evaluate the effect of this reduction reaction. Once H_2S is formed it can be reduced to form HS^- as discussed in Section 4.2.6. If the potential or pH increase (possibly due to HSO_4^- or H_2S reduction) H_2S may be oxidized back to HSO_4^-. This reaction

$$H_2S + 4\,H_2O \rightarrow HSO_4^- + 9\,H^+ + 8\,e^- \qquad (4\text{-}25)$$

would then certainly increase the pH. It is likely that the resulting conditions would be some equilibrium between HSO_4^- and H_2S dependent on the specific conditions in the crevice. Again it would be extremely difficult to realistically evaluate the effect of these electrochemical reactions since the kinetics of HSO_4^- reduction and H_2S oxidation are completely unknown.

The first excursion that will be discussed involves an increase in the bulk conductivity by increasing HSO_4^- concentration at the mouth of the crevice to 2.96×10^{-5} M. This intrusion of bisulfate is assumed to be of the form H_2SO_4 therefore there is also an increase in the H^+ concentration at the mouth. The other species in solution are present in concentrations on the order of 10^{-6} M or less. Two situations are considered. The first case is that of just nickel dissolution. Nickel is

assumed to dissolve from the walls and tip of the crevice to form Ni^{2+} at a rate equal to the passive current. The dissolution reaction for this case is given by

$$Ni \rightarrow Ni^{2+} + 2\,e^- \qquad (4\text{-}26)$$

The second case assumes that nickel and manganese dissolve from the alloy. The other alloying elements, such as Fe or Cr, are not incorporated in the model since their ions have solubilities close to or below that of Ni^{2+}. In this case manganese is assumed to dissolve to form Mn^{2+} at a rate proportional to 1% of the passive current (as explained in Section 4.2.6). Nickel is assumed to form NiO and H^+ at a rate of 99% of the passive current. The dissolution reactions for this case are given by

$$\begin{aligned} Mn &\rightarrow Mn^{2+} + 2\,e^- \\ Ni + H_2O &\rightarrow NiO + 2\,H^+ + 2\,e^- \end{aligned} \qquad (4\text{-}27)$$

Figures 4-31 and 4-32 give transient crevice tip concentration, pH and potential profiles that develop for nickel dissolution using initial conditions given in Table 4-18. Figures 4-33 and 4-34 show those that develop when manganese dissolution is also included using the initial conditions given in Table 4-19. In both cases the excursion starts at a dimensionless time of 0.0 from initially steady state crevice conditions. This small increase in bulk ion concentrations or conductivity is sufficient to cause drastic changes within the crevice.

For both the Ni^{2+}, and, Ni^{2+} with Mn^{2+} dissolution cases there is a rapid acidification to a pH of approximately 8 to 8.5. The bisulfate concentration at the crevice tip reaches 8.0×10^{-3} M. The metal ion concentration for both cases is

Table 4-18. Input Parameters for Figure 4-31 and 4-32 (Excursion in bulk conductivity, slow reduction kinetics)

Species	Charge	Diffusion coefficient (dm^2/sec)	Initial Concentration (moles/l)
H	+ 1	1.76×10^{-5}	2.23×10^{-6}
OH	- 1	9.8×10^{-6}	2.23×10^{-6}
Na	+ 1	2.5×10^{-6}	2.51×10^{-6} (2.961×10^{-5})
Ni	+ 2	1.3×10^{-6}	0
NiOH	+ 1	1.3×10^{-6}	0
HSO_4	- 1	2.0×10^{-6}	2.51×10^{-6} (2.961×10^{-5})

Equilibrium Reactions	k_f	k_b	K_{eq}
$H^+ + OH^- = H_2O$	1×10^{12}	5	2×10^{11}
$Ni^{2+} + H_2O = NiOH^+ + H^+$	6×10^{3}	1×10^{9}	6×10^{-6}

Wall/Tip Electrochemical Reactions	sign	no. of e^-	k_o	α	ref. spec.	spec. power
$Ni \rightarrow Ni^{2+} + 2e^-$	+ 1	2	7.56×10^{-4}	0	-	-
$H_2O + e^- \rightarrow H + OH^-$	- 1	1	4.55×10^{-8}	0.6	-	-
$H^+ + e^- \rightarrow H$	- 1	1	2.03×10^{-2}	0.6	H^+	1

Solubility Reactions	k	K_s
$Ni^{2+} + 2\ OH^- \rightarrow Ni(OH)_2$	1×10^{14}	2.25×10^{-20}

Wall/Tip Dissolution Reactions	Flux (dm^2/sec)
none	-

General Data			
Length (dm)	0.01	Width (dm)	1.71×10^{-7}
No. of Nodes	31	Delta X	3.33×10^{-4}
Temperature (K)	573	Em (V)	0

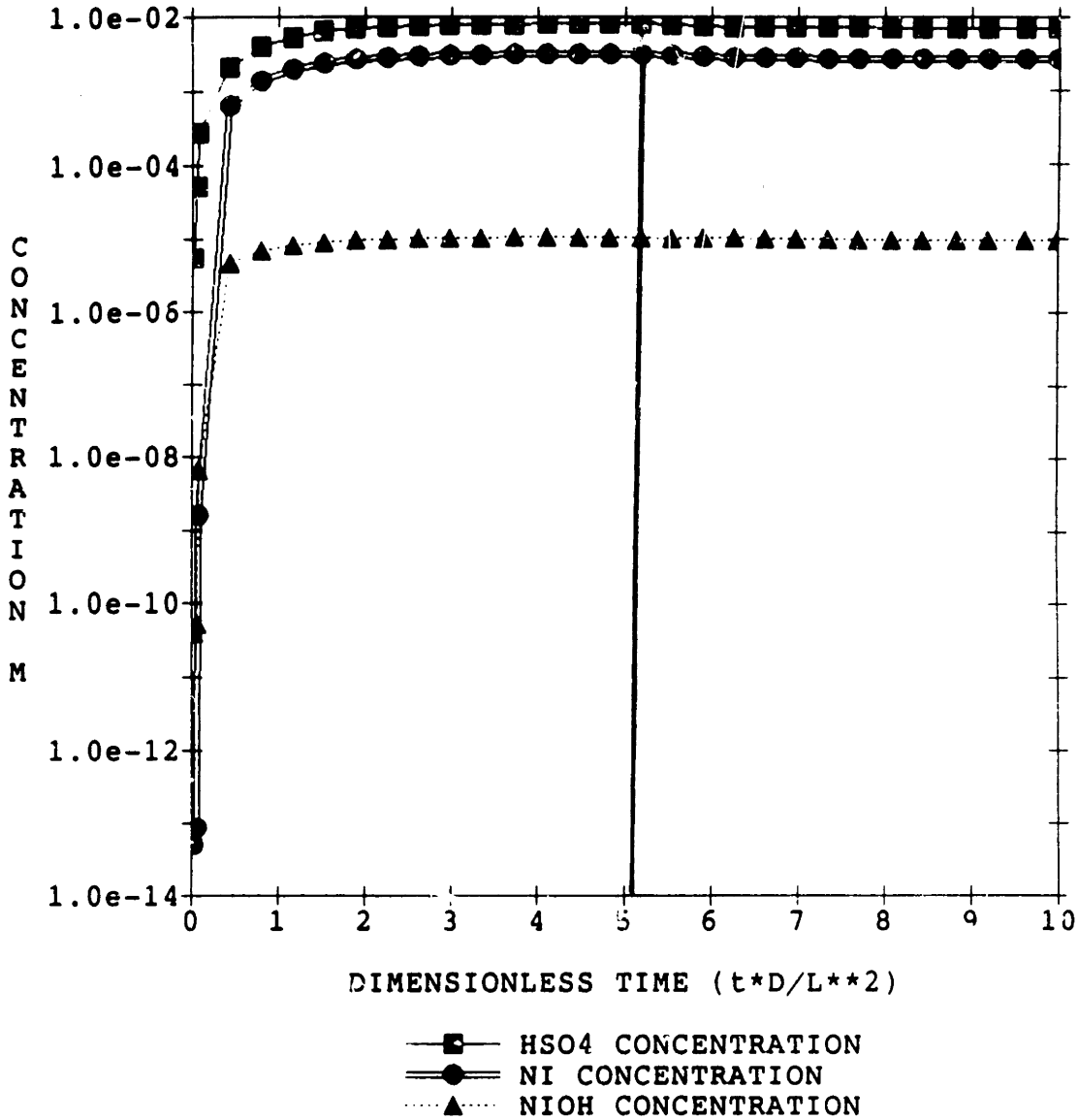

Figure 4-31. Transient HSO_4^{2-}, Ni^{2+} and $NiOH^+$ concentration profiles during and after an excursion in bulk conductivity (Nickel dissolution). Excursion starts at dimensionless time 0 and ends at dimensionless time 5.4. Slow reduction kinetics were used. The conditions are irreversible within the crevice.

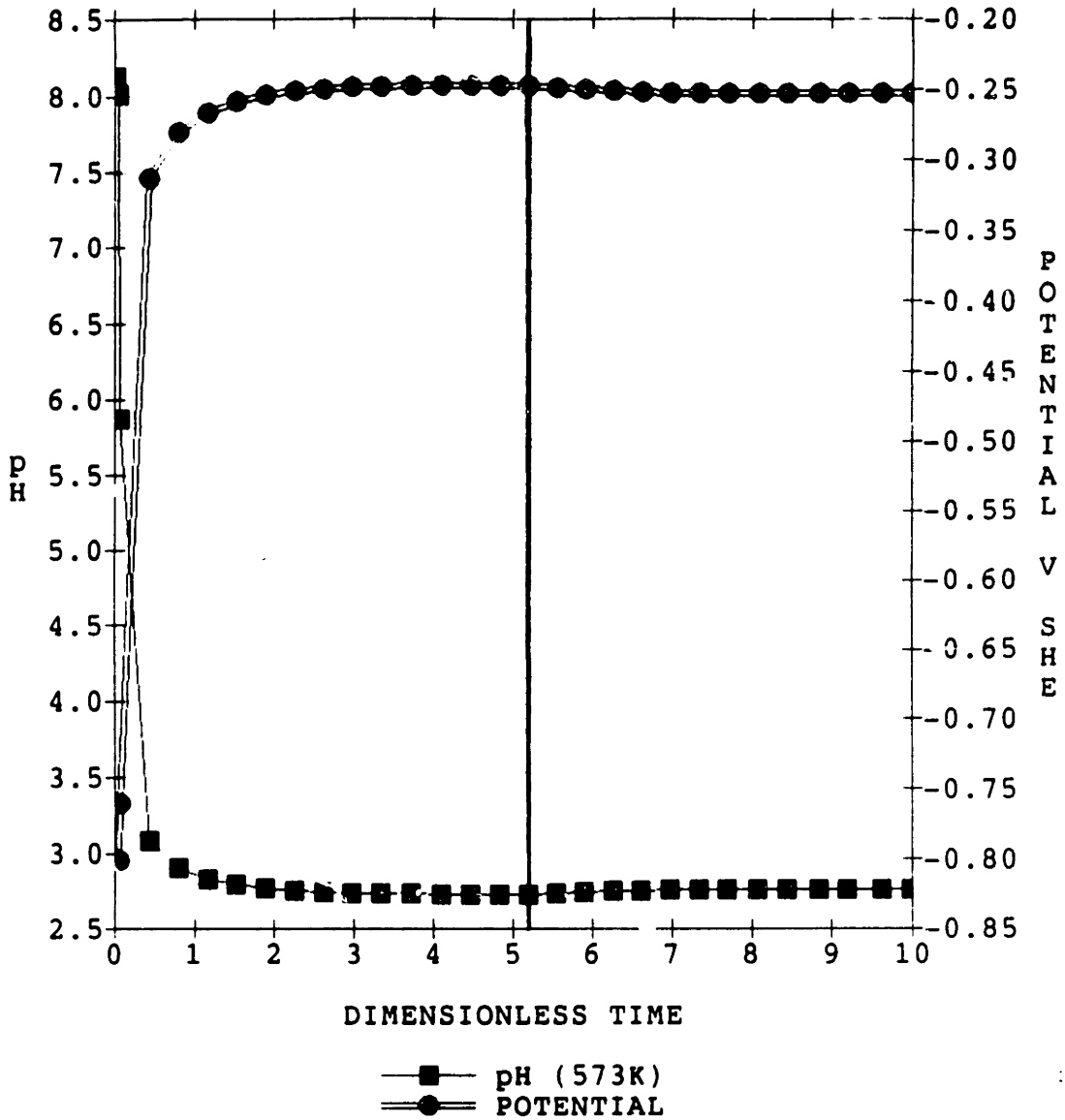

Figure 4-32. Transient pH and potential profiles during and often an excursion. The same conditions hold as in figure 4-31 (Nickel dissolution).

Table 4-19. Input Parameters for Figures 4-33 and 4-34 (excursion in bulk conductivity, Mn dissolution, slow reduction kinetics)

Species	Charge	Diffusion coefficient (dm^2/sec)	Initial Concentration (moles/l)
H	+ 1	1.76×10^{-5}	2.23×10^{-6}
OH	- 1	9.8×10^{-6}	2.23×10^{-6}
Na	+ 1	2.5×10^{-6}	2.51×10^{-6} (2.961×10^{-5})
Mn	+ 2	1.3×10^{-6}	0
MnOH	+ 1	1.3×10^{-6}	0
HSO_4	- 1	2.0×10^{-6}	2.51×10^{-6} (2.961×10^{-5})

Equilibrium Reactions	k_f	k_b	K_{eq}
$H^+ + OH^- = H_2O$	1×10^{12}	5	2×10^{11}
$Mn^{2+} + H_2O = MnOH^+ + H^+$	6.0×10^{3}	1×10^{9}	6.0×10^{-6}

Wall/Tip Electrochemical Reactions	sign	no. of e^-	k_o	α	ref. spec.	spec. power
$Mn \rightarrow Mn^{2+} + 2e^-$	+ 1	2	7.56×10^{-5}	-	-	-
$Ni + H_2O \rightarrow NiO + 2H^+ + 2e^-$	+ 1	2	7.48×10^{-3}	-	-	-
$H_2O + e^- \rightarrow H + OH^-$	- 1	1	4.55×10^{-8}	0.6	-	-
$H^+ + e^- \rightarrow H$	- 1	1	2.03×10^{-2}	0.6	H^+	1

Solubility Reactions	k	K_s
$Mn^{2+} + 2\ OH^- \rightarrow Mn(OH)_2$	1×10^{8}	2.30×10^{-16}

Wall/Tip Dissolution Reactions	Flux (dm^2/sec)
none	-

General Data			
Length (dm)	0.01	Width (dm)	1.71×10^{-7}
No. of Nodes	31	Delta X	3.33×10^{-4}
Temperature (K)	573	E_m (V)	0

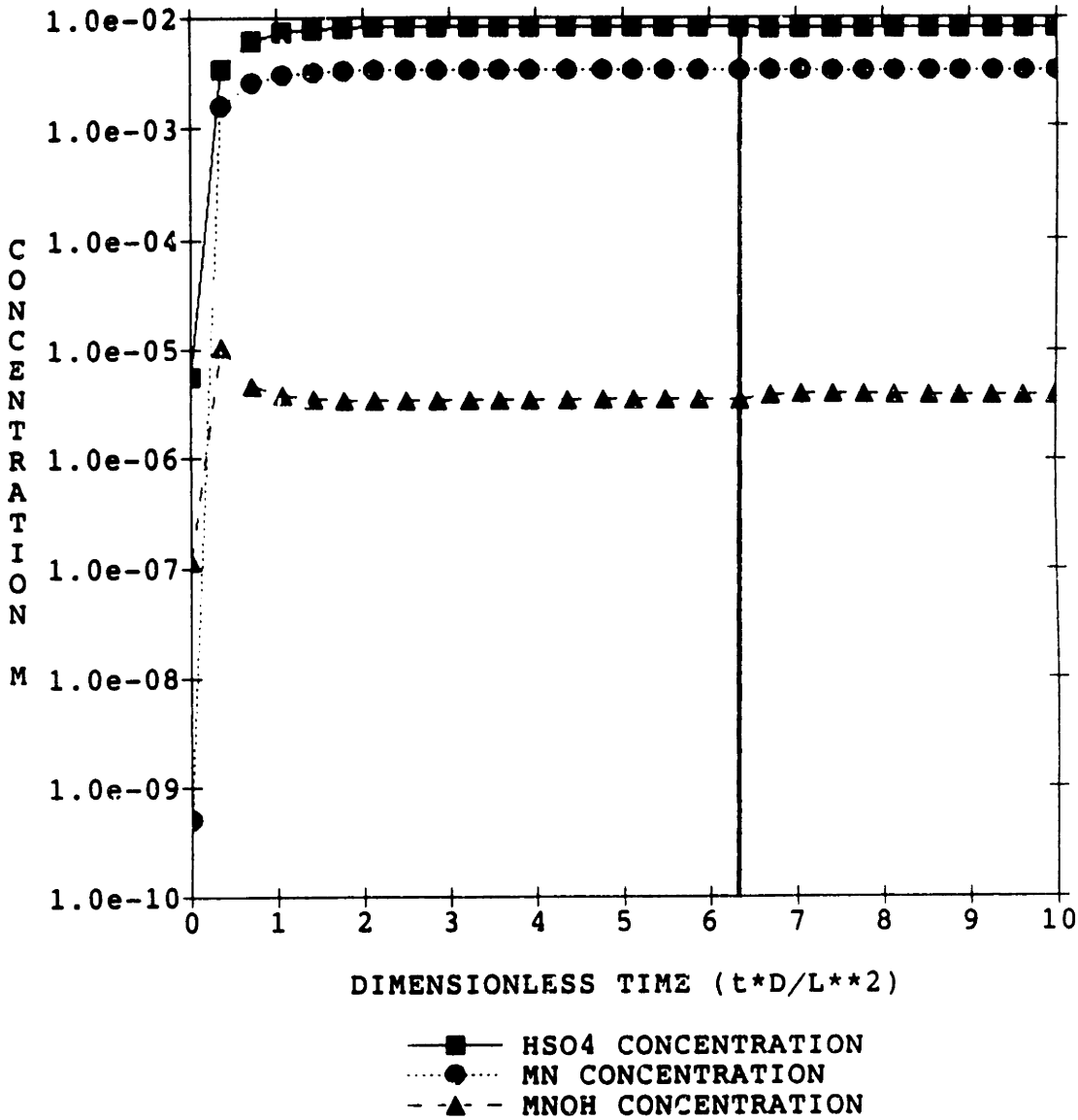

Figure 4-33. Transient HSO_4^-, Na^{2+} and $MnOH^+$ concentration profiles during and after an excursion in bulk conductivity (Nickel and manganese dissolution). Excursion starts at dimensionless time 0 and ends at dimensionless time 6.3. Slow reduction kinetics were used. Again, the conditions were irreversible within the crevice.

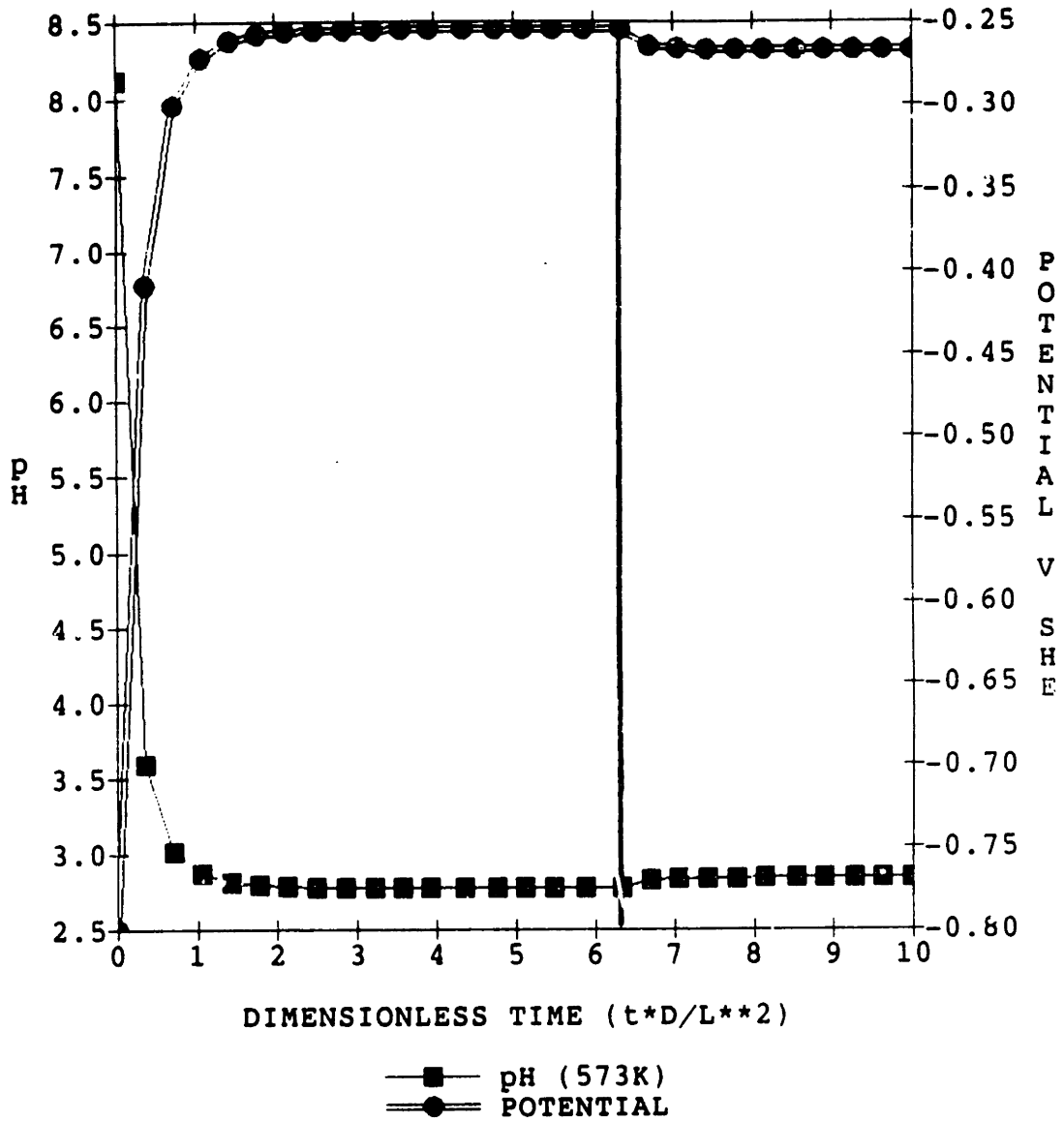

Figure 4-34. Transient pH and potential profiles during and after an excursion in bulk conductivity. This excursion was the same as that in Figure 4-33 (Nickel and Manganese dissolution)

approximately $3x10^{-3}$ M. A high value of dissolved metal species is reached because the solution becomes very acidic. The potential rises dramatically to a value of -247 mV for Ni^{2+} dissolution and -255 mV for Mn^{2+} dissolution. In both cases these potentials are above the corrosion potentials relative to the local environment; therefore, net polarization does occur. The resulting electrochemistry which rapidly develops in the crevice is highly conducting,low pH, and high potential which is readily capable of initiating and propagating stress corrosion cracking (see Figure 4-1).

After the excursion is over and the bulk electrochemistry is returned to its normal 'ideal' conditions (at a dimensionless time of approximately 5.3 for nickel dissolution and 6.2 for manganese dissolution) there is a small increase in the pH and a slight decrease in the potential. The conditions do not revert to those shown in Figure 4-19 of the previous section. Thus the excursion was **irreversible** for both the $Ni^{2+}$and Ni^{2+} with Mn^{2+} dissolution cases. The implications of this non-reversibility are important and will be discussed later in this section.

An increase in the magnitude of the excursion was considered. The bulk conductivity was raised by two orders of magnitude. The concentration of bisulfate was increased to approximately $3x10^{-4}$ M in the bulk with a corresponding increase in H^+ concentration. Additionally Mn^{2+} dissolution was considered. The initial conditions and constants are given in Table 4-20. A comparison of the pH's and potentials during and after the excursion for this and the previous excursion is presented in Figure 4-35. During the higher excursion the pH is more acidic and the potential is higher (-188 mV). Thus, the conditions developed during a larger excursion are, more severe than during a smaller excursion which is expected. After the excursion is over, at a dimensionless time of 6.0 on Figure 4-36, and the bulk concentrations for all the species are returned to their normal ideal values, the conditions drop close to those

Table 4-20. Input Parameters for Figure 4-35.

Species	Charge	Diffusion coefficient (dm^2/sec)	Initial Concentration (moles/l)
H	+ 1	1.76×10^{-5}	2.23×10^{-6}
OH	- 1	9.8×10^{-6}	2.23×10^{-6}
Na	+ 1	2.5×10^{-6}	2.51×10^{-6} (3.0×10^{-4})
Mn	+ 2	1.3×10^{-6}	0
MnOH	+ 1	1.3×10^{-6}	0
HSO_4	- 1	2.0×10^{-6}	2.51×10^{-6} (3.0×10^{-4})

Equilibrium Reactions	k_f	k_b	K_{eq}
$H^+ + OH^- = H_2O$	1×10^{12}	5	2×10^{11}
$Mn^{2+} + H_2O = MnOH^+ + H^+$	6.0×10^3	1×10^9	6.0×10^{-6}

Wall/Tip Electrochemical Reactions	sign	no. of e^-	k_o	α	ref. spec.	spec. power
$Mn \rightarrow Mn^{2+} + 2e^-$	+ 1	2	7.56×10^{-5}	-	-	-
$Ni + H_2O \rightarrow NiO + 2H^+ + 2e^-$	+ 1	2	7.48×10^{-3}	-	-	-
$H_2O + e^- \rightarrow H + OH^-$	- 1	1	4.55×10^{-8}	0.6	-	-
$H^+ + e^- \rightarrow H$	- 1	1	2.03×10^{-2}	0.6	H^+	1

Solubility Reactions	k	K_s
$Mn^{2+} + 2\ OH^- \rightarrow Mn(OH)_2$	1×10^8	2.30×10^{-16}

Wall/Tip Dissolution Reactions	Flux (dm^2/sec)
none	-

General Data			
Length (dm)	0.01	Width (dm)	1.71×10^{-7}
No. of Nodes	31	Delta X	3.33×10^{-4}
Temperature (K)	573	E_m (V)	0

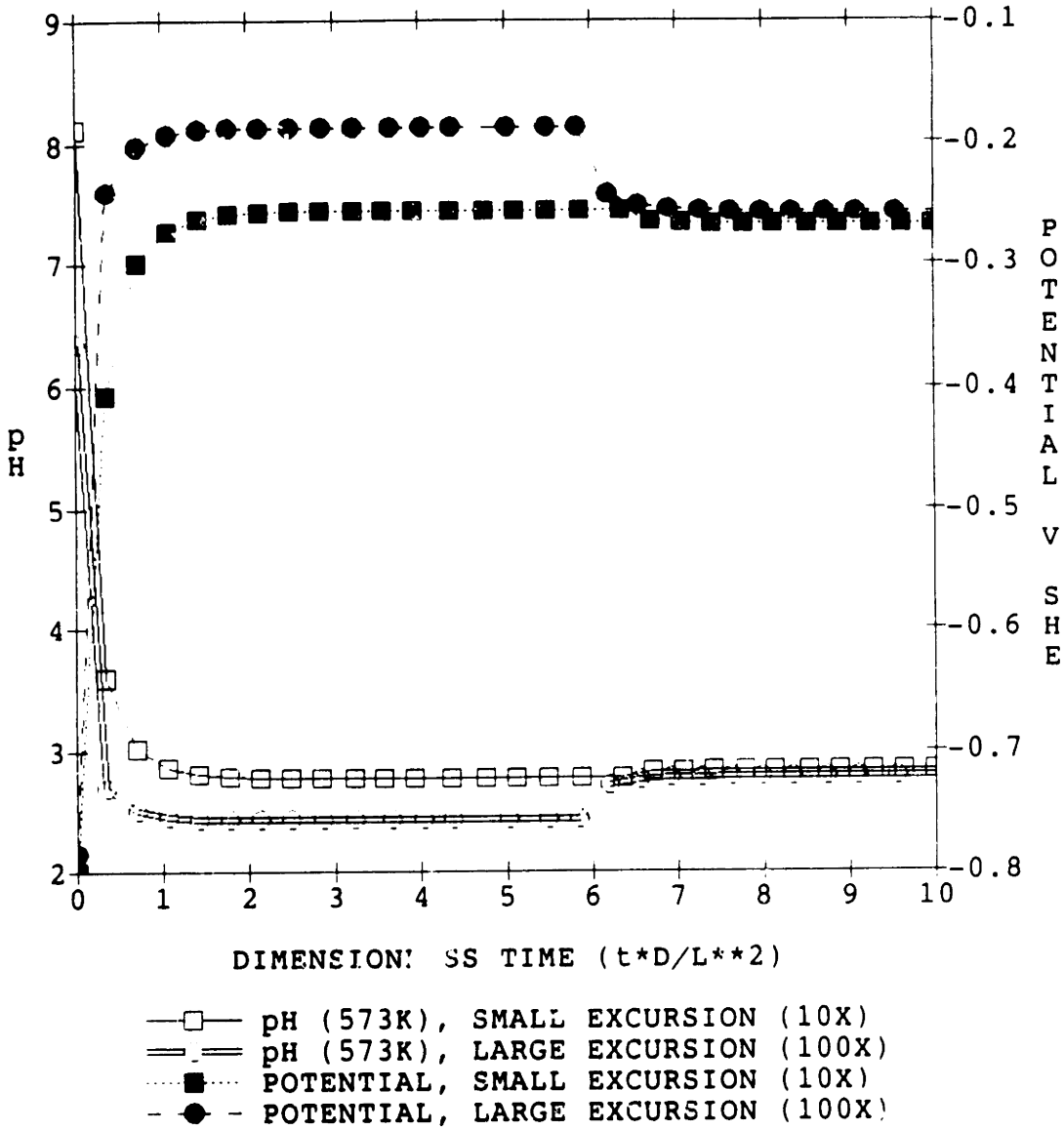

Figure 4-35. Comparison of the pH and potential developed during and after excursions of different orders of magnitude in bulk conductivity.

experienced after the previous smaller excursion case. Thus the conditions developed after an excursion are independent of excursion size but are not reversible to original steady state conditions.

Since the hydrogen ion concentration that develops within the crevice after an excursion is high, it is important to evaluate the effect of our choice of the H^+ reduction kinetic parameter k_0 (in this case $k_0 = 2.03 \times 10^{-2}$ for slow reduction kinetics) relative to water reduction kinetics. The kinetic parameter was increased ($k_0 = 2.03 \times 10^{-1}$) and decreased ($k_0 = 2.03 \times 10^{-3}$) an order of magnitude in order to evaluate the effects. Note, the increased H^+ kinetics used in this case were approximately a factor of 3 or less than the fast reduction kinetics described in Table 4-21. Figures 4-36 and 4-37 show the transient and steady state pH and potential profiles developed in the crevice during and after an order of magnitude excursion in bulk conductivity. These model experiments were conducted using the initial conditions and constants presented in Table 4-21. The effect of H^+ reduction kinetics on the potential profile during the excursion is not extreme. Faster H^+ reduction kinetics result in a lower potential within the crevice but the differences are not large. For every decade increase in k_0, a 30 mV decrease in potential develops at the crevice tip because of a decrease in conductivity (more H^+ was consumed).

There was also a significant change in the pH developed at the crevice tip during the excursion. A factor of ten decrease in k_0 resulted in a factor of 12.7 increase in the H^+ concentration. Thus, as expected, the slower the kinetics of H^+ reduction the higher the resulting H^+ concentration and the lower the pH. Since the H^+ concentration is higher, the amount of metal ion that can go into solution is greater and the conductivity is higher. The high conductivity that develops causes net polarization to occur relative to the local corrosion potential. Thus, the rise in potential discussed above is due partly

Table 4-21. Input Parameters for Figure 4-36.

Species	Charge	Diffusion coefficient (dm^2/sec)	Initial Concentration (moles/l)
H	+ 1	1.76×10^{-5}	2.23×10^{-6}
OH	- 1	9.8×10^{-6}	2.23×10^{-6}
Na	+ 1	2.5×10^{-6}	2.51×10^{-6} (2.961×10^{-5})
Ni	+ 2	1.3×10^{-6}	0
Mn	+ 2	1.3×10^{-6}	0
NiOH	+ 1	1.3×10^{-6}	0
MnOH	+ 1	1.3×10^{-6}	0
HSO_4	- 1	2.0×10^{-6}	2.51×10^{-6} (2.961×10^{-5})

Equilibrium Reactions	k_f	k_b	K_{eq}
$H^+ + OH^- = H_2O$	1×10^{12}	5	2×10^{11}
$Mn^{2+} + H_2O = MnOH^+ + H^+$	6.0x10^3	1×10^9	6.0×10^{-6}

Wall/Tip Electrochemical Reactions	sign	no. of e^-	k_o	α	ref. spec.	spec. power
$Mn \rightarrow Mn^{2+} + 2e^-$	+ 1	2	7.56×10^{-5}	-	-	-
$Ni + H_2O \rightarrow NiO + 2H^+ + 2e^-$	+ 1	2	7.48×10^{-3}	-	-	-
$H_2O + e^- \rightarrow H + OH^-$	- 1	1	4.55x1C 8	0.6	-	-
$H^+ + e^- \rightarrow H$	- 1	1	a.	0.6	H^+	1
			2.03×10^{-2} b.			
			2.03×10^{-1} c.			
			2.03×10^{-3}			

Solubility Reactions	k	K_s
$Mn^{2+} + 2\ OH^- \rightarrow Mn(OH)_2$	1×10^8	2.30×10^{-16}
$Ni^{2+} + 2\ OH^- \rightarrow Ni(OH)_2$	1×10^{14}	2.25×10^{-20}

Wall/Tip Dissolution Reactions	Flux (dm^2/sec)
none	-

General Data			
Length (dm)	0.01	Width (dm)	1.71×10^{-7}
No. of Nodes	31	Delta X	3.33×10^{-4}
Temperature (K)	573	E_m (V)	0

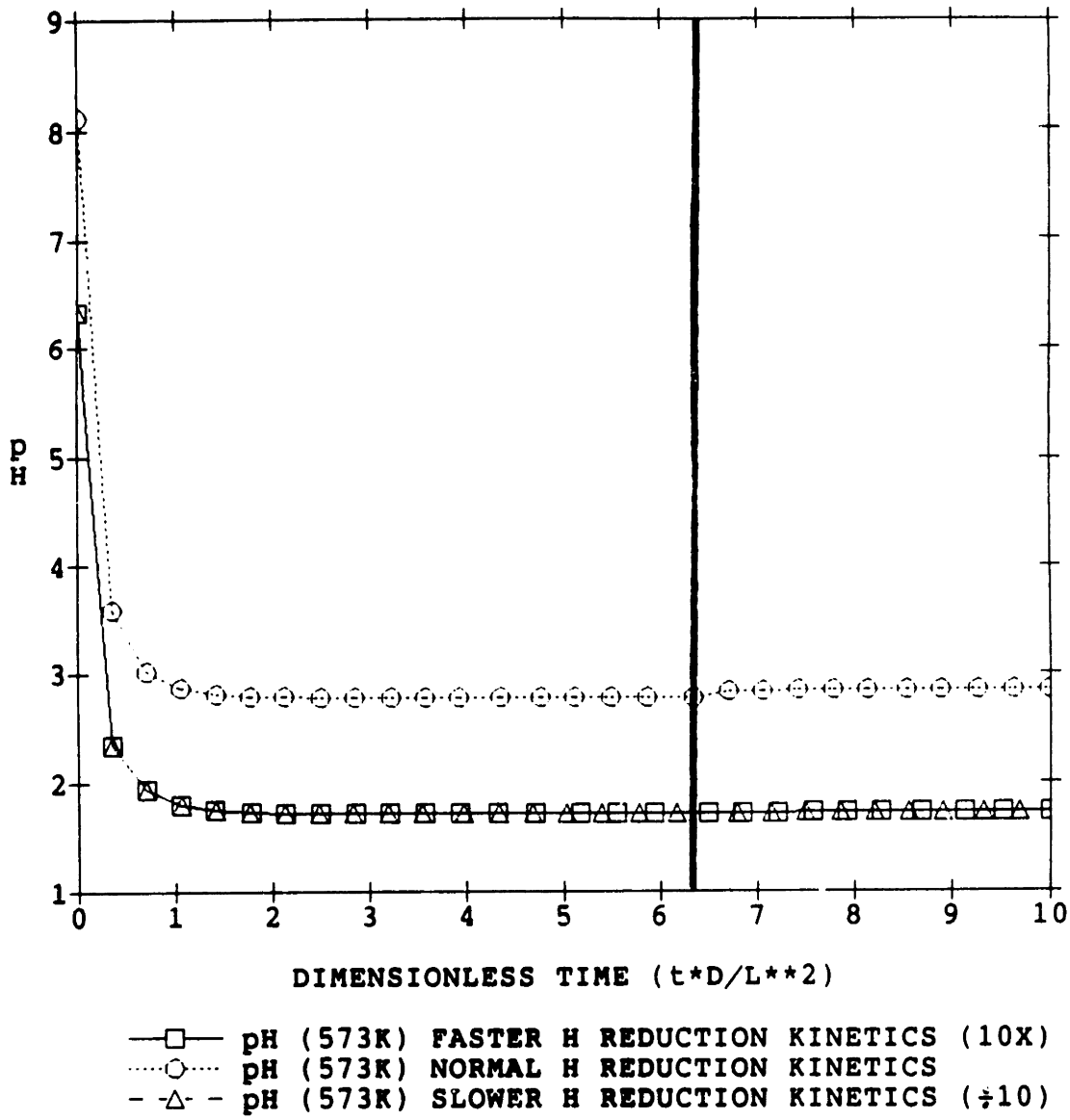

Figure 4-36. Effect of H^+ reduction kinetics on the transient pH profile developed within the crevice during and after an excursion.

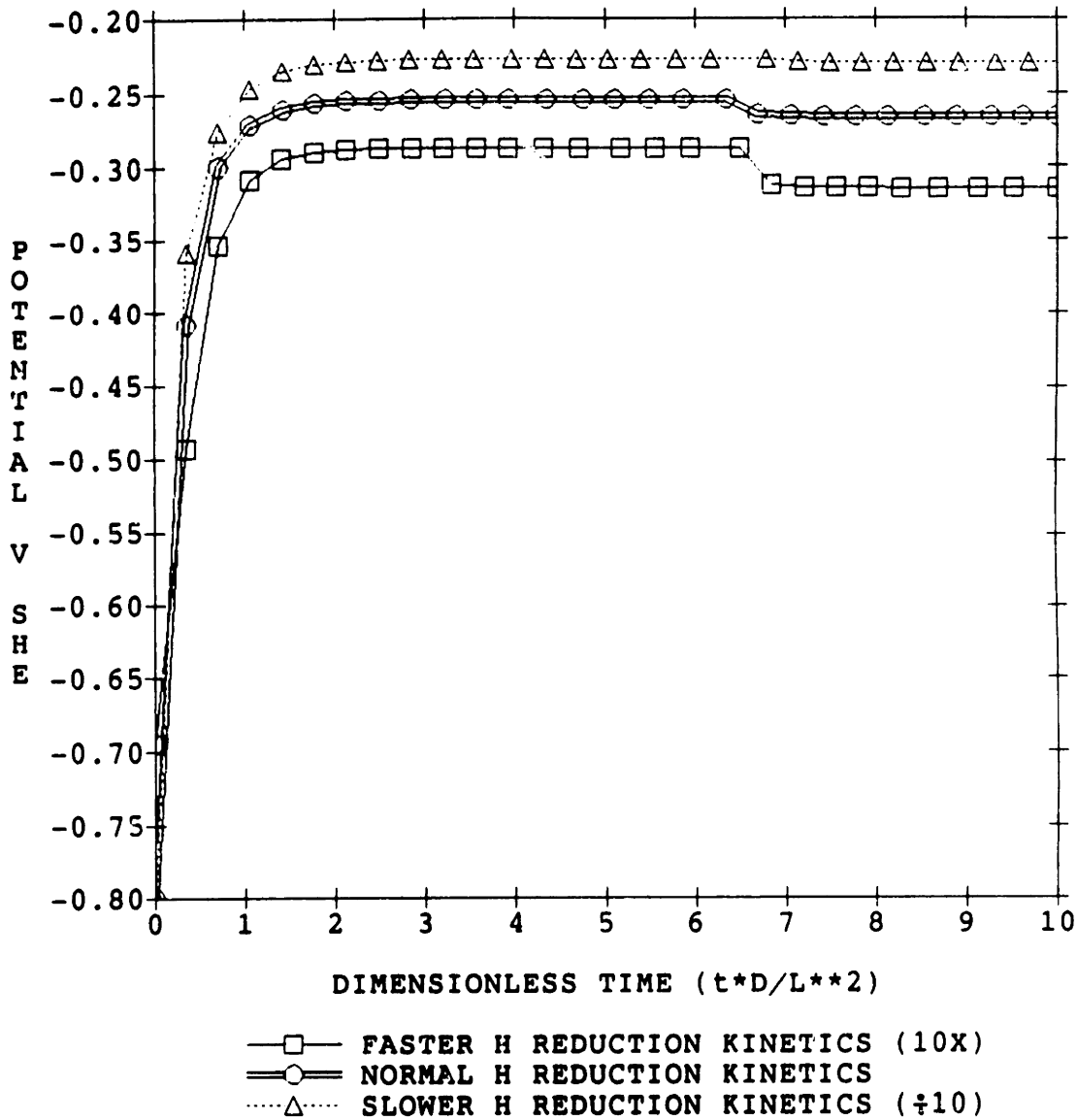

Figure 4-37. Effect of H^+ reduction kinetics on the transient potential profile developed within the crevice during and after an excursion.

to an increase in the H^+ ion concentration and therefore an increase in the corrosion potential, and partly to net polarization. The amount of polarization that occurs is dependent on the kinetics of H^+ reduction. For the lowest value of k_0, slowest kinetics, there is 17 mV of net polarization at the crevice tip. In the other two cases the amount of polarization is less, 1 mV for the medium k_0 and 0.8 mV for the largest k_0.

After the excursion is over, at a dimensionless time of about 6.5, the resulting local electrochemistry developed for the different H^+ reduction kinetics is also different. The highest value of k_0 results in a more reversible pH and potential, but it is still not completely reversible. The potential drops from -287 mV to - 314 mV and the pH rises from 3.95 to 4.09. In contrast, the return to normal bulk concentrations of HSO_4^- and H^+ does not significantly change the pH and potential for slow H^+ reduction kinetics (small k_0). It is important to note that in each case, the amount of polarization during and after an excursion does not significantly change. Indeed, the **net** polarization may be the cause of the irreversibility of the electrochemical conditions developed in the crevice. The polarization induces a net cation production rate which is sufficient to maintain the conductive electrochemistry and potential distribution within the crevice. The potential field holds the bisulfate ions inside the crevice (due to ion migration), balancing diffusion even after their bulk concentration is reduced.

The effect of applying fast reduction kinetics to all reduction reactions, as described in Section 4.2.3, demonstrates strongly the important effect of cathodic reaction kinetics. It is important to note that these fast kinetics are probably unrealistic (as described in Section 4.2.3). They are included here only for completeness. Figures 4-38 and 4-39 show the transient concentration and potential *profiles developed at the crevice tip during and after two different excursions in bulk* conductivity. The excursions differ by one order of magnitude. Thus in Figure 4-38,

Table 4-22. Input Parameters for Figure 4-38 (fast reduction kinetics)

Species	Charge	Diffusion coefficient (dm^2/sec)	Initial Concentration (moles/l)
H	+ 1	1.76×10^{-5}	2.23×10^{-6}
OH	- 1	9.8×10^{-6}	2.23×10^{-6}
Na	+ 1	2.5×10^{-6}	1.968×10^{-6} (3.158×10^{-5})
Cl	- 1	3.8×10^{-6}	1.968×10^{-6}
Ni	+ 2	1.3×10^{-6}	0
NiOH	+ 1	1.3×10^{-6}	0
HSO_4	- 1	2.0×10^{-6}	0 (2.961×10^{-5})

Equilibrium Reactions	k_f	k_b	K_{eq}
$H^+ + OH^- = H_2O$	1×10^{12}	5	2×10^{11}
$Ni^{2+} + H_2O = NiOH^+ + H^+$	6×10^{3}	1×10^{9}	6×10^{-6}

Wall/Tip Electrochemical Reactions	sign	no. of e^-	k_o	α	ref. spec.	spec. power
$Ni \rightarrow Ni^{2+} + 2e^-$	+ 1	2	7.56×10^{-4}	0	-	-
$H_2O + e^- \rightarrow H + OH^-$	- 1	1	1.50×10^{-6}	0.6	-	-
$H^+ + e^- \rightarrow H$	- 1	1	0.671	0.6	H^+	1

Solubility Reactions	k	K_s
$Ni^{2+} + 2OH^- \rightarrow Ni(OH)_2$	1×10^{14}	2.25×10^{-20}

Wall/Tip Dissolution Reactions	Flux (dm^2/sec)
none	-

General Data			
Length (dm)	0.01	Width (dm)	1.71×10^{-7}
No. of Nodes	31	Delta X	3.33×10^{-4}
Temperature (K)	573	E_m (V)	0

Table 4-23. Input Parameters for Figure 4-39 (fast reduction kinetics).

Species	Charge	Diffusion coefficient (dm^2/sec)	Initial Concentration (moles/l)
H	+ 1	1.76×10^{-5}	2.23×10^{-6}
OH	- 1	9.8×10^{-6}	2.23×10^{-6}
Na	+ 1	2.5×10^{-6}	1.968×10^{-6} (3.023×10^{-4})
Cl	- 1	3.8×10^{-6}	1.968×10^{-6}
Ni	+ 2	1.3×10^{-6}	0
NiOH	+ 1	1.3×10^{-6}	0
HSO_4	- 1	2.0×10^{-6}	0 (3.004×10^{-4})

Equilibrium Reactions	k_f	k_b	K_{eq}
$H^+ + OH^- = H_2O$	1×10^{12}	5	2×10^{11}
$Ni^{2+} + H_2O = NiOH^+ + H^+$	6×10^{3}	1×10^{9}	6×10^{-6}

Wall/Tip Electrochemical Reactions	sign	no. of e^-	k_o	α	ref. spec.	spec. power
$Ni \rightarrow Ni^{2+} + 2e^-$	+ 1	2	7.56×10^{-4}	0	-	-
$H_2O + e^- \rightarrow H + OH^-$	- 1	1	1.50×10^{-6}	0.6	-	-
$H^+ + e^- \rightarrow H$	- 1	1	0.671	0.6	H^+	1

Solubility Reactions	k	K_s
$Ni^{2+} + 2OH^- \rightarrow Ni(OH)_2$	1×10^{14}	2.25×10^{-20}

Wall/Tip Dissolution Reactions	Flux (dm^2/sec)
none	-

General Data			
Length (dm)	0.01	Width (dm)	1.71×10^{-7}
No. of Nodes	31	Delta X	3.33×10^{-4}
Temperature (K)	573	Em (V)	0

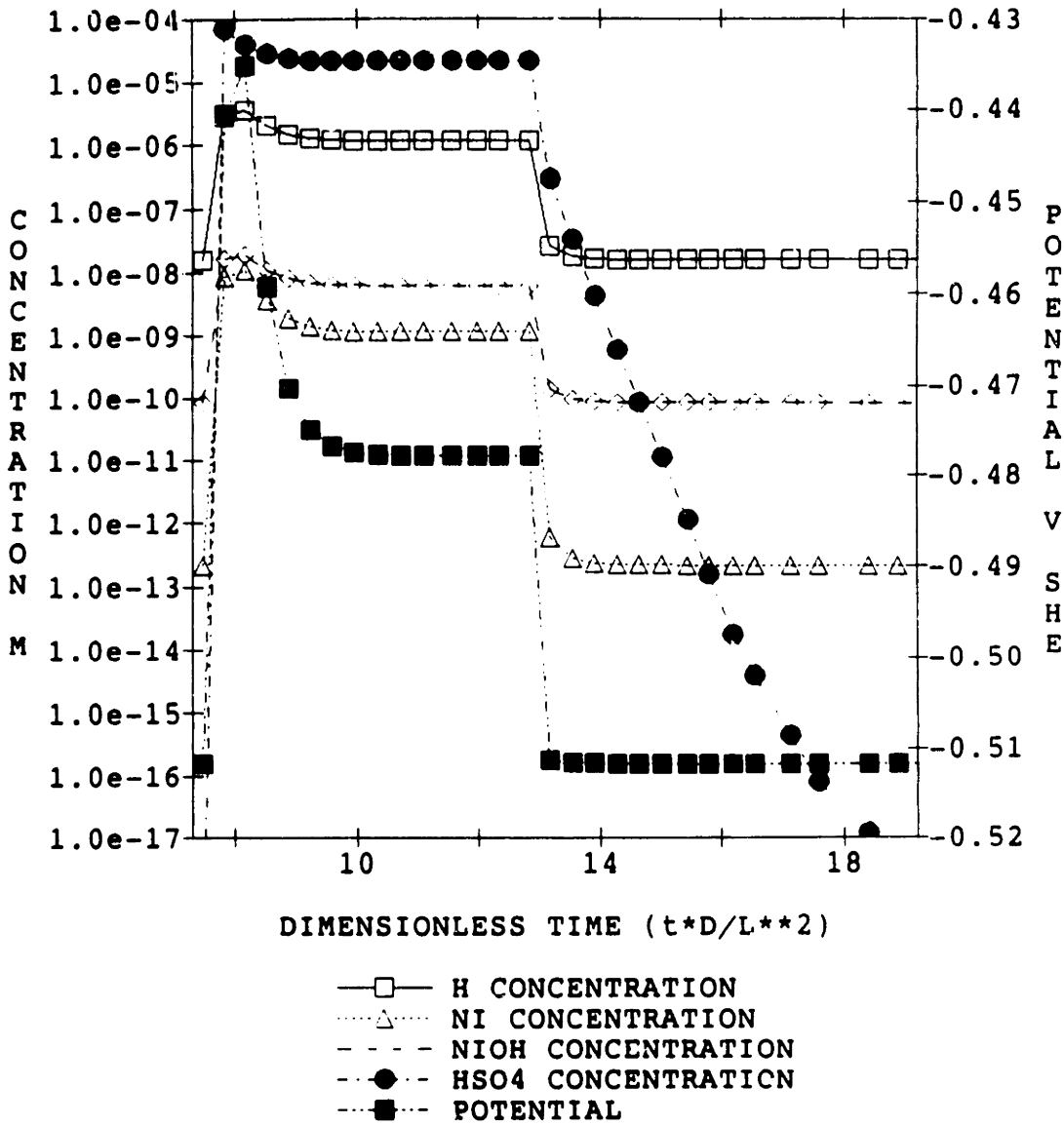

Figure 4-38 Transient concentration and potential profiles developed at the crevice tip during and after an excursion to 3μs/cm in bulk conductivity. Fast reduction kinetics were used.

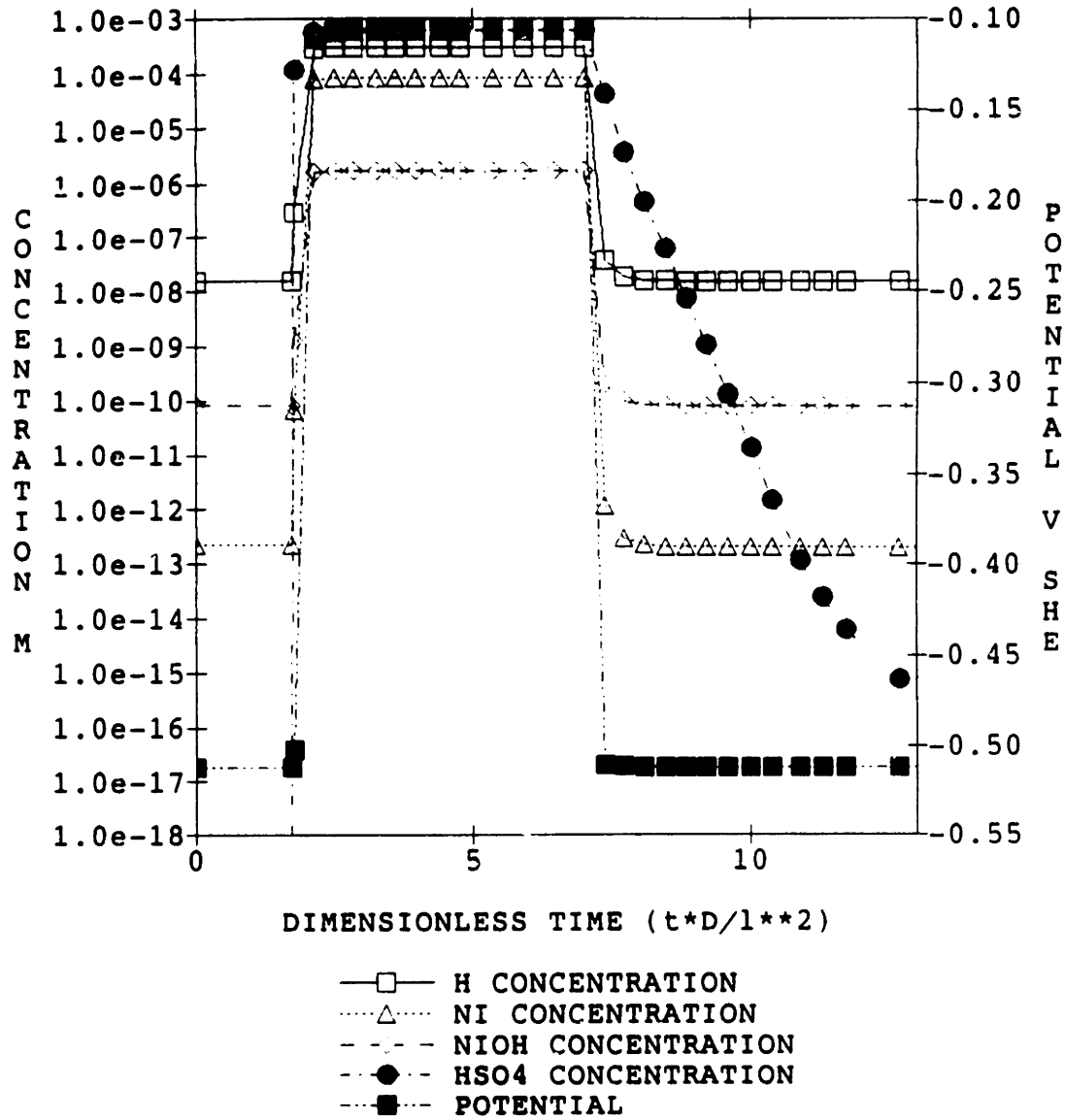

Figure 4-39 Transient concentration and potential profiles developed at the crevice tip during and after an excursion to 30μs/cm in bulk conductivity. Fast reduction kinetics were used.

the conductivity changes from 0.3 μS/cm to 3 μS/cm and in Figure 4-39 the conductivity changes to 30 μS/cm. In both cases only Ni^{2+} dissolution is allowed to occur. The initial conditions for these figure are shown in Tables 4-22 and 4-23 respectively. In this figure the excursion occurs at a dimensionless time of 7.5. The H^+ concentration at the crevice tip does not drastically increase as in the previous case shown in Figure 4-36 . Since there is no significant acidification, the metal ion concentration cannot increase. This limits the increase in conductivity that is possible. Without an increase in conductivity there is no polarization in the crevice. The lack of polarization becomes obvious after the excursion ends at dimensionless time. The conditions within the crevice revert to their original values after the bulk conductivity excursion has ended. When Mn^{2+} is allowed to dissolve at 1% of the passive current, the conditions developed in the crevice are only partially reversible for these fast reduction kinetics. Thus, reduction kinetics are important in determining reversibility after excursions in bulk conductivity.

The net effect of excursions in bulk conductivity with more realistic slow reduction kinetics is an increase in conductivity, a decrease in pH (acidification), and an increase in potential with polarization within the crevice. These changes in electrochemistry are irreversible. Even increases in the H^+ reduction kinetics result in conditions which are largely irreversible. These electrochemical conditions that develop in the crevice (i.e., high potential, low pH, and high conductivity) during and irreversibly after an excursion could cause initiation and propagation of stress corrosion cracking (see Figure 4-1).

Irreversibility after a bulk conductivity excursion demonstrates that the electrochemical conditions that develop within the crevice are dependent on its past history. The implications of this finding become more obvious when one examines two of the steady state conditions that are reached during this model excursion: first, just before the excursion begins and ,second, after an excursion is over. Before an excursion

in bulk conductivity, when the bulk conductivity is 0.3 μS/cm, the pH in the crevice is high (i.e., basic) and the potential is low (at the corrosion potential for that local environment). After the excursion is over and the bulk conductivity is returned to 0.3 μS/cm, the steady state electrochemical condition that develop within the crevice are one of low pH (acidic) and high potential (with polarization from the corrosion potential). Thus for the **same boundary conditions** there exists two steady state solutions; the solution chemistry predicted within the crevice depends on the history experienced by the crevice.

The existence of multiple steady state solutions has significant consequences for modelers using steady state analysis because their work must either assume that the boundary conditions for the crack, crevice, or pit remain constant over the time of interest, or that the history experienced by the crack, crevice, or pit does not effect the steady state results (i.e.., that multiple steady states do not exist). The first assumption may be valid under very controlled conditions, such as laboratory experiments, but are unlikely to exist in practical cases. The assumption that the history experienced by the region of interest does not effect the steady state results must be carefully considered before application. In the case described in this section, this assumption is invalid. Steady state analysis could not be applied to this case because there would be nc way for account for the occurrence of such transients. Thus, the existence of multiple steady state solutions must be ruled out before steady state modelling can be applied to any situation.

4.2.8 Hydrogen Water Chemistry

Hydrogen water chemistry is being considered and applied in many BWR plants in an effort to control intergranular stress corrosion cracking by decreasing the dissolved

oxygen concentration. In general, radiolysis of water produces dissolved oxygen (100-300 ppb) and dissolved hydrogen (12-38 ppb) (*6*). This level of oxygen is sufficient to facilitate stress corrosion cracking of many structural materials in BWR's. By adding hydrogen (hence hydrogen water chemistry) to the feedwater, the dissolved oxygen concentration is reduced in the reactor coolant water. This reduces the oxidizing capability of the water and the bulk reactor coolant potential, thereby improving the stress corrosion cracking performance of the alloys in this environment. In this section, the application of hydrogen water chemistry to the model crevice is described in order to evaluate its effect on stress corrosion cracking initiation within the crevice.

The bulk conditions used are described in Table 4-24 . These data are typical of a plant at 90% power (*6*). Comparing this table to Table 4-1, it is apparent that the conductivity is the same as for regular water chemistry. The dissolved oxygen concentration is lowered thus decreasing the potential.

Table 4-24 Hydrogen Water Chemistry (*6*)

Conductivity (at 25 °C)	< 0.3 μS/cm
Dissolved Oxygen	< 100 ppb
Potential	-230 mV

Application of hydrogen water chemistry significantly changes the condition that develop within the crevice before, during and after an excursion. Figures 4-40 and 4-41 show a comparison of the steady state pH profiles developed with or without hydrogen water chemistry for $Ni^{2+}$and Ni^{2+} with Mn^{2+} formation using the initial conditions shown in Tables 4-25 and 4-26, respectively. In all the figures in this section, HWC and NWC represent hydrogen water chemistry and normal water chemistry, respectively. The steady state pH that develops the crevice is not as basic as

Table 4-25. Input Parameters for Figure 4-40.

Species	Charge	Diffusion coefficient (dm^2/sec)	Initial Concentration (moles/l)
H	+ 1	1.76×10^{-5}	2.23×10^{-6}
OH	- 1	9.8×10^{-6}	2.23×10^{-6}
Na	+ 1	2.5×10^{-6}	2.51×10^{-6}
HSO_4	- 1	2.0×10^{-6}	2.51×10^{-6} (2.961×10^{-5})
Mn	+ 2	1.3×10^{-6}	0
MnOH	+ 1	1.3×10^{-6}	0

Equilibrium Reactions	k_f	k_b	K_{eq}
$H^+ + OH^- = H_2O$	1×10^{12}	5	2×10^{11}
$Mn^{2+} + H_2O = MnOH^+ + H^+$	1.7×10^{3}	10^{9}	1.7×10^{-6}

Wall/Tip Electrochemical Reactions	sign	no. of e^-	k_o	α	ref. spec.	spec. power
$Ni + H_2O \rightarrow 2\,H^+ + 2e^- + NiO$	+ 1	2	7.48×10^{-4}	0	-	-
$H_2O + e^- \rightarrow H + OH^-$	- 1	1	4.5×10^{-8}	0.6	-	-
$H^+ + e^- \rightarrow H$	- 1	1	2.03×10^{-2}	0.6	H^+	1
$Mn \rightarrow Mn^{2+} + 2e^-$	+ 1	2	7.56×10^{-5}	-	-	-

Solubility Reactions	k	K_S
$Mn^{2+} + 2\,OH^- = Mn(OH)_2$	1×10^{8}	2.3×10^{-16}

Wall/Tip Dissolution Reactions	Flux (dm^2/sec)
none	-

General Data			
Length (dm)	0.01	Width (dm)	1.71×10^{-7}
No. of Nodes	31	Delta X	3.33×10^{-4}
Temperature (K)	573	E_m (V)	-0.230

Table 4-26. Input Parameters for Figure 4-41.

Species	Charge	Diffusion coefficient (dm^2/sec)	Initial Concentration (moles/l)
H	+ 1	1.76×10^{-5}	2.23×10^{-6}
OH	- 1	9.8×10^{-6}	2.23×10^{-6}
Na	+ 1	2.5×10^{-6}	2.51×10^{-6} (2.961×10^{-5})
Ni	+ 2	1.3×10^{-6}	0
NiOH	+ 1	1.3×10^{-6}	0
HSO_4	- 1	2.0×10^{-6}	2.51×10^{-6} (2.961×10^{-5})

Equilibrium Reactions	k_f	k_b	K_{eq}
$H^+ + OH^- = H_2O$	1×10^{12}	5	2×10^{11}
$Ni^{2+} + H_2O = NiOH^+ + H^+$	6×10^{3}	1×10^{9}	6×10^{-6}

Wall/Tip Electrochemical Reactions	sign	no. of e^-	k_o	α	ref. spec.	spec. power
$Ni \rightarrow Ni^{2+} + 2e^-$	+ 1	2	7.56×10^{-4}	0	-	-
$H_2O + e^- \rightarrow H + OH^-$	- 1	1	4.55×10^{-8}	0.6	-	-
$H^+ + e^- \rightarrow H$	- 1	1	2.03×10^{-2}	0.6	H^+	1

Solubility Reactions	k	K_s
$Ni^{2+} + 2\ OH^- \rightarrow Ni(OH)_2$	1×10^{14}	2.25×10^{-20}

Wall/Tip Dissolution Reactions	Flux (dm^2/sec)
none	-

General Data			
Length (dm)	0.01	Width (dm)	1.71×10^{-7}
No. of Nodes	31	Delta X	3.33×10^{-4}
Temperature (K)	573	E_m (V)	0

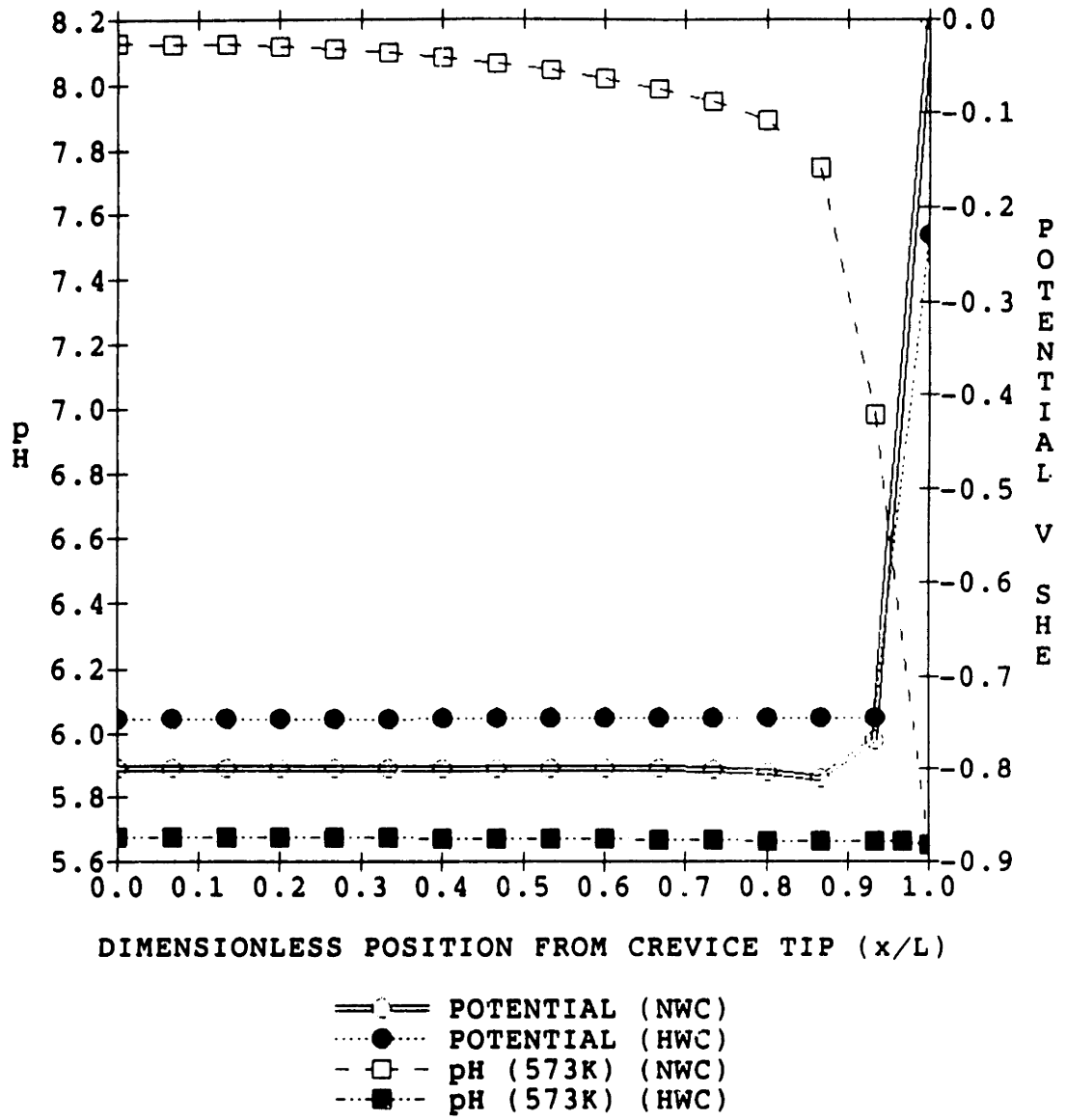

Figure 4-40 A comparison of steady-state pH and potential profiles (before excursion)with normal water chemistry (NWC) and hydrogen water chemistry (HWC) (Nickel dissolution)

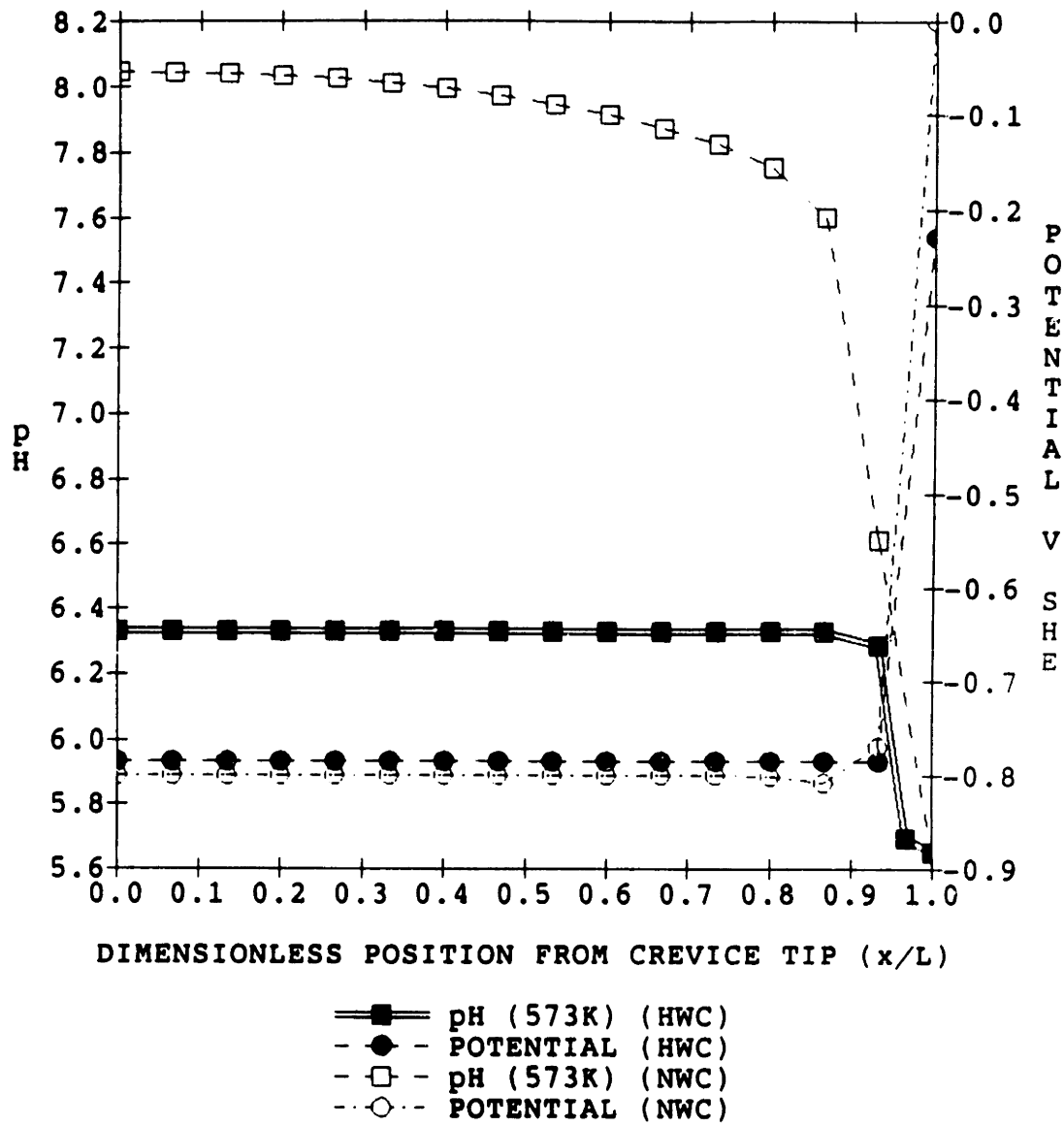

Figure 4-41 A comparison of steady-state pH and potential profiles (before excursion) with normal water chemistry (NWC) and hydrogen water chemistry (HWC) (Nickel and manganese dissolution)

with normal water chemistry. Indeed, for nickel dissolution alone the pH is virtually that of the bulk solution, approximately 5.7. When 1% of the passive current is assumed to be attributed to manganese dissolution, the pH rises to a value of 6.33. At these pH's the metal ion concentration is very low and no polarization occurs. The potential in both cases drops to the corrosion potential for the alloy relative to the local chemical environment in the crevice. This is different for manganese dissolution with hydrogen water chemistry than with normal water chemistry because the pH does not get as high and, thus, hydrogen reduction is still significant and affects the corrosion potential.

During and after an order of magnitude excursion in bulk conductivity with hydrogen water chemistry the results were considerably different from those for normal water chemistry. Figures 4-42, 4-43, and 4-44 show the steady state and crevice tip transient pH and potential for profiles that develop using the initial conditions described in Table 4-27. Simple Ni^{2+} dissolution and Ni^{2+} with Mn^{2+} dissolution are compared in these figures. Comparing Figure 4-44 with Figures 4-32 and 4-34 one can immediately see the differences. With hydrogen water chemistry the conditions developed within the crevice during an excursion are partially reversible and there is a significant difference between simple Ni^{2+} dissolution and Ni^{2+} with Mn^{2+}. In normal BWR water chemistry the results for Ni and Mn are virtually identical. But for hydrogen water chemistry, during the excursion from dimensionless time of 0 to about 7, in Figure 4-43, the pH drops more significantly for Ni dissolution case than for the Mn dissolution case, representing much more acidification (steady state pH is 3.87 for the Ni case and 5.77 for the Mn case). The potential rises more for the case of nickel dissolution only (-460 mV for nickel only and -569 mV for manganese). In the previous section, it was suggested that <u>net</u> polarization was the cause of, or at least indicative of, irreversibility of the crevice electrochemistry after an excursion. In this case, there is only a slight amount of <u>net</u> polarization in the nickel dissolution case

Table 4-27. Input Parameters for Figures 4-42 through 4-44.

Species	Charge	Diffusion coefficient (dm^2/sec)	Initial Concentration (moles/l)
H	+ 1	1.76×10^{-5}	2.23×10^{-6}
OH	- 1	9.8×10^{-6}	2.23×10^{-6}
Na	+ 1	2.5×10^{-6}	2.51×10^{-6}
a. Ni	+ 2	1.3×10^{-6}	0
a. NiOH	+ 1	1.3×10^{-6}	0
b. Mn	+ 2	1.3×10^{-6}	0
b. MnOH	+ 1	1.3×10^{-6}	0
HSO_4	- 1	2.0×10^{-6}	2.51×10^{-6} (2.961×10^{-5})

Equilibrium Reactions	k_f	k_b	K_{eq}
$H^+ + OH^- = H_2O$	1×10^{12}	5	2×10^{11}
a. $Ni^{2+} + H_2O = NiOH^+ + H^+$	6×10^{3}	1×10^{9}	6×10^{-6}
b. $Mn^{2+} + H_2O = MnOH^+ + H^+$	1.7×10^{3}	1×10^{9}	1.7×10^{-6}

Wall/Tip Electrochemical Reactions	sign	no. of e^-	k_o	α	ref. spec.	spec. power
a. $Ni \rightarrow Ni^{2+} + 2e^-$	+ 1	2	7.56×10^{-4}	0	-	-
$H_2O + e^- \rightarrow H + OH^-$	- 1	1	4.55×10^{-8}	0.6	-	-
$H^+ + e^- \rightarrow H$	- 1	1	2.03×10^{-2}	0.6	H^+	1
b. $Ni^{2+} + H_2O \rightarrow NiO + 2H^+ + 2e^-$	+ 1	2	7.48×10^{-4}	-	-	-
b. $Mn \rightarrow Mn^{2+} + 2e^-$	+ 1	2	7.56×10^{-5}	-	-	-

Solubility Reactions	k	K_s
a. $Ni^{2+} + 2\,OH^- \rightarrow Ni(OH)_2$	1×10^{14}	2.25×10^{-20}
b. $Mn^{2+} + 2\,OH^- \rightarrow Mn(OH)_2$	1×10^{8}	2.30×10^{-16}

Wall/Tip Dissolution Reactions	Flux (dm^2/sec)
none	-

General Data			
Length (dm)	0.01	Width (dm)	1.71×10^{-7}
No. of Nodes	31	Delta X	3.33×10^{-4}
Temperature (K)	573	E_m (V)	-0.230

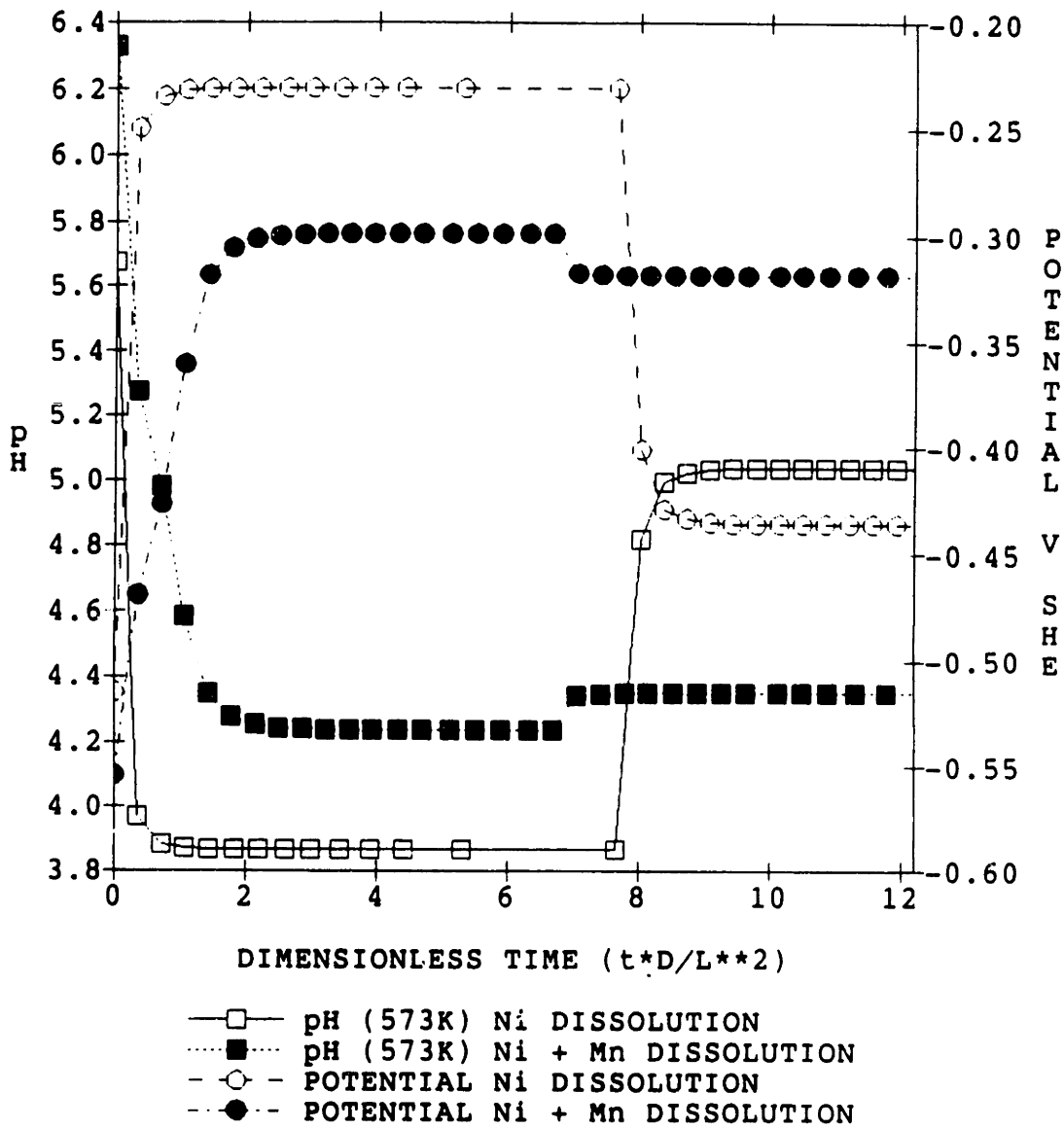

Figure 4-42 Comparison of transient pH and potential profile at the crevice tip during and after an excursion in bulk conductivity for simple Ni dissolution and Ni with Mn dissolution. Hydrogen water chemistry was applied.

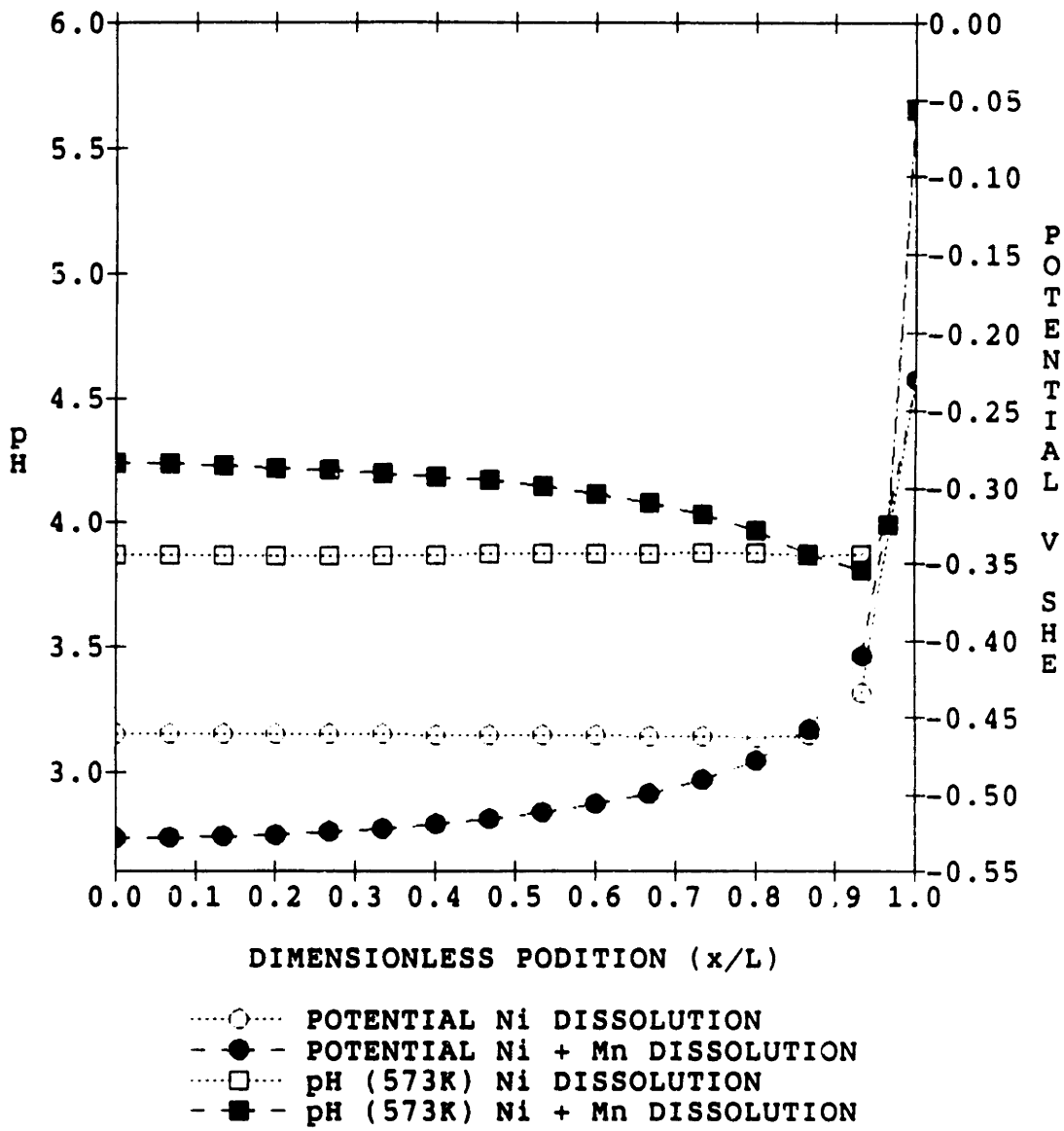

Figure 4-43. Comparison of the steady-state pH and potential profiles developed during an excursion of simple Ni dissolution and Ni with Mn dissolution. Hydrogen water chemistry was applied.

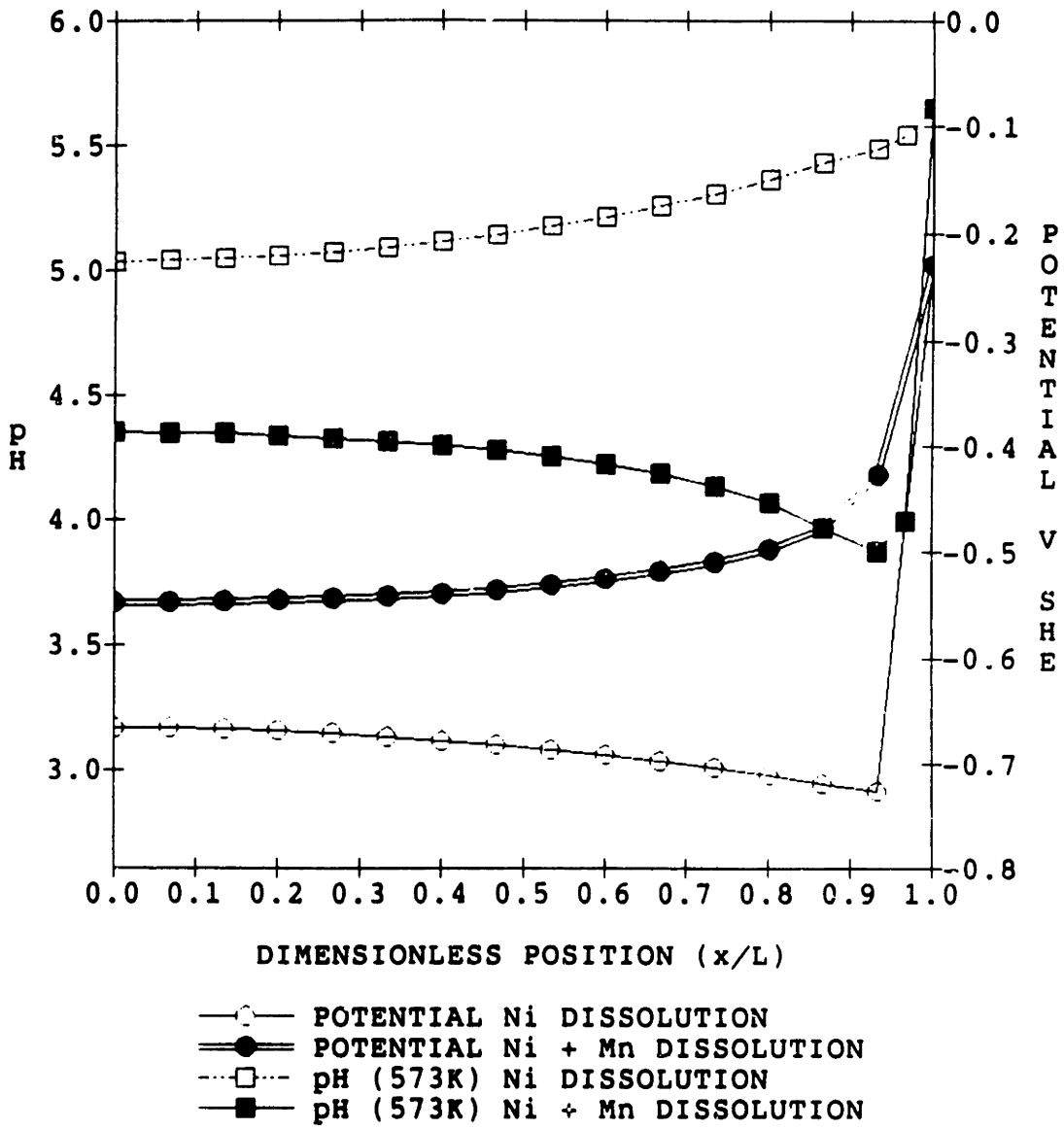

Figure 4-44. A comparison of the steady-state pH and potential profiles developed, after an excursion in bulk conductivity, of simple Ni dissolution and Ni with Mn dissolution. Hydrogen water chemistry was applied.

(1.52×10^{-2} mV) which is negligible and somewhat more net polarization in the manganese case, approximately 0.82 mV, which is also very small.

The amount of polarization is reflected in the reversibility of the local electrochemistry after the excursion is over (between 7 and 7.5 on the dimensionless ime scale). When only nickel dissolution is considered, the local electrochemistry is almost completely reversible. The original pH and potential before the excursion were 5.7 and -745 mV respectively. After the excursion is over the pH and potential return to values of 5.0 and -666 mV respectively, almost complete reversibility. For the case including manganese dissolution, the pH and potential at the crevice tip before the excursion were 6.3 and -784 mV. After the excursion has ended and a new steady state is reached the pH and potential are given by 4.4 and -549 mV, respectively and, thus, the situation is not completely reversible. It is interesting to note that the amount of net polarization at the crevice tip after the excursion is over and steady state is reached are almost identical to that achieved during the excursion (0.81 mV versus 0.82 mV, respectively). When nickel dissolution is considered there is very little net polarization within the crevice and almost complete reversibility after the excursion. In comparison, when manganese dissolution is incorporated there is more net polarization and less reversibility. The trend proposed in the previous section is consistent. But the magnitude of net polarization in these cases seems insignificant and, therefore, it is possible that net polarization alone does not explain irreversibility after bulk conductivity excursions.

The conditions that develop within the crevice using hydrogen water chemistry before, during, and after excursions are significantly different than those that develop in normal BWR water chemistry. The pH does not decrease as much (less acidification) and the potential does not rise as much. There is also less net polarization within the crevice and, therefore, the situation is somewhat more reversible. Thus, because of the higher pH and lower potential, that are maintained, the use of hydrogen water chemistry does

reduce the probability of stress corrosion cracking susceptibility. The system is not immune but somewhat less susceptible.

4.3 COMPARISON OF MODELLING RESULTS WITH EXPERIMENTAL DATA

Ideally, one would like to compare the crevice results presented in this chapter to a range of experimental crevice data. Unfortunately, this type of work is difficult and consequently very little has been conducted in evaluating high temperature aqueous crevice electrochemistry. Only two groups of researchers have tried to experimentally determine the high temperature electrochemistry within occluded regions : Gabetta, et al. (*27*) and Taylor et al. (*28-34*).

Gabetta et al. (*27*) measured the potential inside a growing corrosion fatigue crack in A533B pressure vessel steel exposed to low conductivity (1 μS/cm) water at 288 °C. Standard compact tension specimens were used with varying notch depth. All specimens were precracked to a 5 mm crack length. The corrosion potential was measured at three positions representing the external corrosion potential, the internal (within crack) central corrosion potential, and the internal side value of corrosion potential. The internal corrosion potentials were measured by probes placed in holes drilled on crack plane and on crack path, respectively. Unfortunately, direct comparison with the crevice data presented earlier in this chapter are not advisable since this data is for a crack not a crevice and it shows a large effect of stress ratio.

The data do show a significant difference in potential measured within the crevice (at the surface) and the external potential. For aerated bulk conditions, the potential within the crevice is **higher** than the external potential. One must question the experimenter's interpretation of these results as being due to the transport of dissolved

oxygen into the crevice. Other modelling work (Turnbull) has shown that oxygen is quickly consumed very close to the crack mouth. Therefore, oxygen would not have an opportunity to be transported into the crack.. Other possible explanations for the data include leakage of oxygen into the system at the seals of the Teflon probes used to measure potential, diffusion of oxygen through the Teflon of the probe and then into the crevice, or the chemical dissolution of manganese sulfide inclusions to form H_2S. This H_2S can be reduced, as discussed in Section 4.2.6, which would raise the potential. The H_2S mechanism cannot be proven in this case because there is no information on heat of A533B steel used or even if all the specimens came from the same heat. Since the MnS inclusion size, distribution, and type vary from heat to heat, it is difficult to evaluate how much H_2S could be formed in each case.

Taylor et al. have been working on the experimental modelling of high temperature crevice electrochemistry for the past ten years using a variety of methods (*28-34*). All of the work has involved a long narrow bore tube made of the alloy of interest (either Inconel® Alloy 600 or type 304 stainless steel). The tube was bent into a U shape and closed at one end (either welded or with the electrode). The tube was typically filled with a highly conducting solution (0.1-0.2 M concentration) of Na_2SO_4 or NaCl which was occasionally acidified to a pH of ~1.5 (at room temperature) using H_2SO_4 or HCl, respectively. The tube was attached to an autoclave and the open end was exposed, generally, to aerated pure water at 290 °C for 5-7 days. Three different types of experiments have been conducted over the ten year period using similar tube design. Each experiment was capable of measuring different things. The steady state concentration and pH profile within the crevice, the transient pH and potential at the crevice tip, or the current distribution within the crevice. A description of the results obtained in each type of experiment is presented later in the section. Before describing the experiments and data in detail, a discussion of the choice of crevice solution will be

presented since the implications of this choice will be referred to frequently in the rest of this section.

The choice of high conductivity 0.1-0.2 M sulfate or chloride solutions as the initial crevice solution has not been explained in any of Taylor's work. The objective may have been to assume the final crevice chemistry following an excursion and to determine the change with time. Since it has been known for some period of time that such concentrations can not develop within actual crevices (*35*), this choice is peculiar to say the least. It is only possible to generate these conditions if all metallic ions produced are completely soluble (Section 4.2.2 and 4.2.3). At high temperatures the solution must be extremelt acidic for metal ions to have significant solubility (*7-12*). In Taylor's only experiments involving high purity water the pH went basic, therefore, the metal ion concentration would be very low (*28*). No description of the conditions necessary to generate the internal conditions has been given. Also, fixing the chemistry uniformly within the crevice initially is unrealistic since the concentration and potential gradients developed within the crevice will greatly affect the electrochemical and transport properties of the system, as can be seen by examining Equations 3-1 and 3-7.

Another question that must be raised is the stability of the passive film in these solutions. It is possible that breakdown of the passive film could occur and may account for some of the peculiar results. Coupling the above problems with the possible existence of multiple steady states dependent on crevice history (described in Section 4.2.7), it is difficult to apply these experimental results directly to the practical problem of crevices in nuclear power plants. It is hoped that future experiments will include filling the crevice tube with pure water and changing the bulk solution to various concentrations and solute species appropriate to excursions in order to develop understanding of such crevices in nuclear power plants. Nonetheless, this experimental work will be evaluated in the rest of the section. Where possible, comparisons will be

drawn or possible alternate explanations of the experimental work will be presented based on the understanding derived from the modelling work presented in this chapter.

The first method used to measure steady state concentrations of dissolved species and pH incorporated freezing the solution, cutting the tube into sections, and testing. All these tests, except one, were carried out in 0.1 M solutions. The experiment was terminated by shutting off the heating mantle and cooling to 100 °C. The model crevice tubes were removed and immersed in liquid nitrogen. The frozen tube was cut into 3 cm sections each containing 30 μL solution. The solution from each section was removed and the pH and metal concentrations were determined at room temperature. The results obtained by this method were generally invalid because changing temperature from 286°C to 25°C drastically changed the equilibrium constants and solubility limits. Later experimental work by Taylor (*32*) showed that these results were, indeed, not valid, especially those involving sulfate species. The one set of data which has some validity is shown in Figure 4-45. In this test, the tube was filled with deaerated water and exposed to bulk aerated water. As predicted by the model described in this thesis, the solution in the crevice becomes basic (see Figures 4-16 and 4-20).

The second type of experiment attempted in situ (at temperature) measurements of pH and potential at the opposite ends of the bent tube. This allowed for the transient behavior of pH and potential to be determined. Since the pH electrode was located at the end of the tube exposed to the bulk solution (close to the mouth of the crevice), one must question exactly what pH was being measured; certainly not the pH at the crevice tip. Again, the tubes were filled with 0.1-0.2 M solution of Na_2SO_4 and NaCl. This

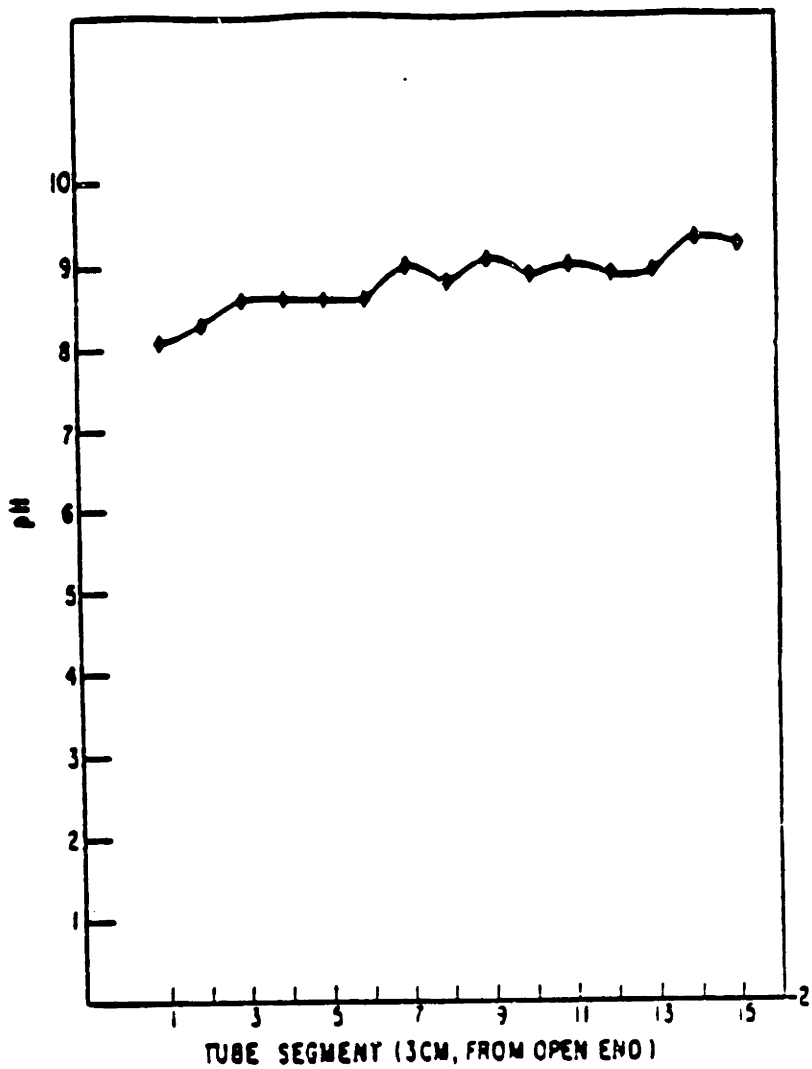

Figure 4-45. pH of solution in segments from tube filled with deaerated water and exposed to aerated water at 288 C for 1 week. (D. Taylor, G.E.)

invalidates direct comparison of the experimental results with the modelling results. Nevertheless, the knowledge developed by the modelling presented in the chapter can be applied to help understand the results obtained. The pH and potential are measured at different times. After a short period of time acidification takes place, due to polarization, and the potential rises. After two days, the pH begins to rise (eventually becoming close to neutral) but the potential remains high. This high potential is usually associated with acidic polarized conditions.

Taylor's explanation of these results involve the reversibility of the hydrogen electrode. He argues that the dissolved hydrogen concentration is high enough that reversible conditions are reached and dissolved hydrogen is oxidized to produce H^+ ions as shown below :

$$H \rightarrow H^+ + e^- \qquad (4\text{-}28)$$

This proposed mechanism does not explain the high potential since the addition of another anodic reaction (with the passive current) would increase the total anodic current within the crevice and thus lower the potential. Taylor does suggest that another cathodic reaction may be involved but no specific reactions were put forth (4.5.5). One possibility is HSO_4^- and subsequently H_2S reduction. H_2S is the most likely form of sulfur at the initial pH, temperature and potential. As previously discussed in Section 4.2.6, HSO_4^- can be reduced to give H_2S by the following reaction

$$HSO_4^- + 9\,H^+ + 8\,e^- \rightarrow H_2S + 4\,H_2O \qquad (4\text{-}29)$$

The H_2S can then be reduced

$$H_2S + e^- \longrightarrow HS^- + H \qquad (4\text{-}30)$$

HS^- will revert back to H_2S in acidic environments

$$H_2S = HS^- + H^+ \qquad (4\text{-}31)$$

consuming H^+ ions and allowing further H_2S reduction. As shown in Section 4.2.6, this process raises the potential and brings the pH close to neutral. This process would proceed until HS^- became the favored form based on the equilibrium constant and pH or the potential was high enough to oxidize H_2S by

$$H_2S + 4\,H_2O \rightarrow HSO_4^- + 9\,H^+ + 8\,e^- \qquad (4\text{-}32)$$

producing HSO_4^-. Eventually, some steady state will be reached between the above equilibrium and electrochemical reactions. This could explain the rise in pH at such a high potential.

The third type of crevice experiment performed by Taylor was a segmented tube experiment. The tubes were cut into sections and insulated from each other using zirconia spacers. The tubes were assembled using polytetrafluoroethylene (PTFE) sleeves. The sections were electrically connected with wire of the same alloy and the tubes were bent into a U shape. The tubes were again filled with conducting 0.1-0.2 M Na_2SO_4 or NaCl solutions. Again, because of the high concentration of solution initially put into the tubes, the results cannot be compared to the model nor can they be practically applied. Localized anodic and cathodic zones develop within the experimental crevice which Taylor argues separates H^+ reduction and H_2 oxidation regions. This is speculation and such local currents may be associated with breakdown of the passive film or variations in H_2S concentration. The model does not account for localized breakdown.

In summary, comparison of the modelling results presented earlier in this chapter with experimental data is extremely limited. In one case, comparison is

difficult because the experiments were conducted using corrosion fatigue cracks. In the other case, the choice of initial crevice concentration make comparison with modelling results impossible in all but one test. Where comparison is possible, model and experiment exhibit the same trends. The understanding developed through the modelling can be used to provide plausible explanations for the experimental crevice work examined.

4.4 SUMMARY

Quantitative predictions depend on the reliability of our knowledge base. Indeed, the quality of the results obtained from the model depends on the quality of the input data. Because of the lack of availability and poor quality of the required input data (electrochemical reaction kinetic parameters, solubility limits, etc.) the results obtained can only be considered as indicating broad trends. Nevertheless, an understanding of high temperature crevice electrochemistry has been developed and will be summarized in this section

Cathodic reactions occuring on the internal surfaces of the crevice and solubility limits on the partially soluble Ni^{2+} produced within the crevice must be applied in the model. The inclusion of cathodic reactions results in realistic potential and pH development within the crevice. Solubility limits prevent the unrealistic accumulation of metal ions which would artificially increase the conductivity of the solution within the crevice and cause polarization. Thus in order to accurately predict the electrochemical conditions that develop within a crevice, both cathodic reactions and solubility limits must be used.

The engineering implications of the results that have been presented in this chapter (using both cathodic reactions and a solubility limit on Ni^{2+}) are summarized

in Figure 4-46. This is the potential/conductivity curve, indicating the region of stress corrosion cracking susceptibility and immunity, presented in Figure 4-1. On this figure the potential conductivity fields, obtained from the modeling presented in this chapter, are plotted. It must be noted that this curve should be considered qualitative since it was generated for lightly sensitized 304 stainless steel and not alloy 600. Also, since the conductivity in the figure is measured at 25°C, there is some uncertainty in extrapolating the modeling results from 25°C to 300°C.

The first two boxes in Figure 4-46 are presented for reference. They represent the conductivity and potential regimes of the bulk BWR solutions with normal water chemistry and hydrogen water chemistry, respectively. As represented in this figure by box 1, normal water chemistry puts the bulk solution into the stress corrosion cracking regime, especially if the conductivity is sufficiently high. Hydrogen water chemistry (box 2) greatly improves the conditions within the bulk, lowering the cracking susceptibility. As in the previous case, keeping a low conductivity is extremely important in reducing the chances of crack initiation and propagation.

If one considers simple Ni^{2+} dissolution or Ni^{2+} with Mn^{2+} dissolution and the application of solubility limits on these metal ions in solutions, the conditions that develop within the crevice are very different from the bulk conditions. These conditions are shown in Figure 4-46 by box 3. The electrochemistry within the crevice is

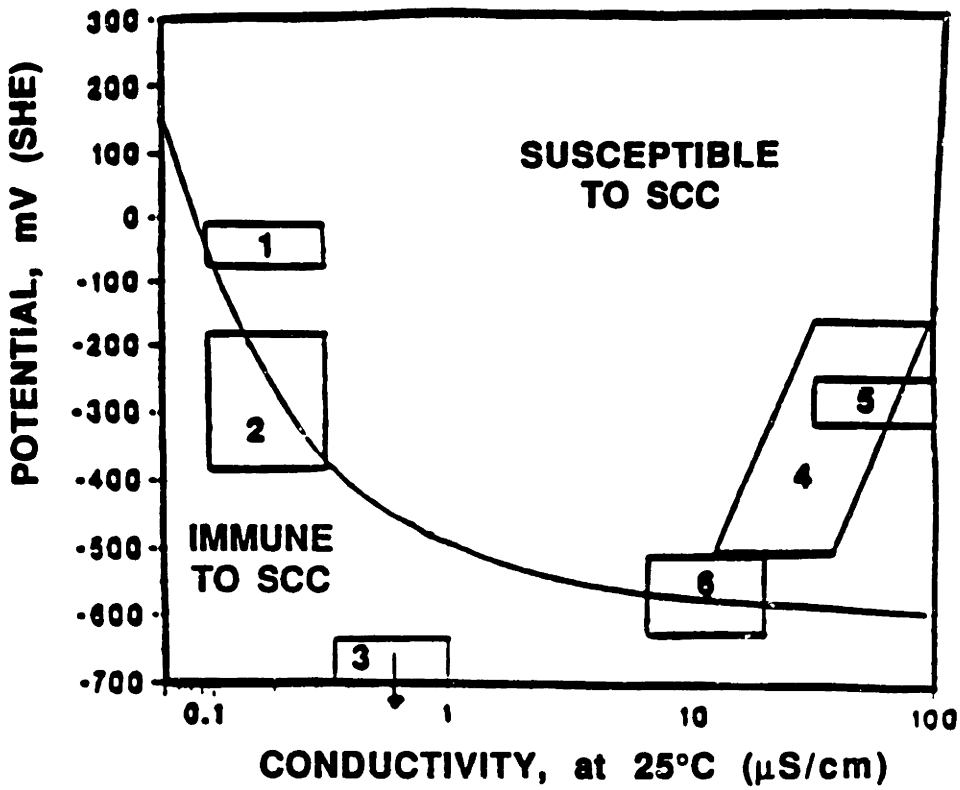

Figure 4-46. Typical stress corrosion cracking susceptibility curve with bulk and crevice regions of electrochemistry defined: (*3*) (1) conditions in bulk solution with normal water chemistry; (2) conditions in bulk solution with hydrogen water chemistry; (3) conditions developed at crevice tip by dissolution of Ni^{2+} or Ni^{2+} with Mn^{2+}; (4) potential/conductivity conditions developed as the result of MnS dissolutions; (5) conditions developed in crevice after an excursion in bulk conductivity in normal water chemistry; and (6) conditions developed in crevice after an excursion in bulk conductivity in hydrogen water chemistry.

characterized by high pH, slightly elevated conductivity and very low potential. The potential achieved within the crevice is the corrosion potential for the local crevice environment. No polarization occurs. Thus, the crevice should be immune to stress corrosion cracking. If some soluble metal ion was produced within the crevice these conditions would alter and the conditions developed within the crevice would put it in the stress corrosion cracking susceptibility range.

The chemical dissolution of MnS inclusions to form H_2S has been found to play an important role in the development of local electrochemical conditions within occluded regions. The formation of H_2S by chemical dissolution can, in principle, stimulate the cathodic processes through the reduction of H_2S to form HS^-. This results in an increase in potential within the crevice without lowering the pH. This is shown by box 4 in Figure 4-46. For the higher MnS dissolution rates, the crevice conditions developed make the region susceptible to stress corrosion cracking. The polarization that occurs is **not net** polarization. This means that the local anodic and cathodic processes are equal. After the MnS inclusions are consumed and the production of H_2S ceases, the crevice chemistry returns to the benign conditions discussed above (i.e., high pH and low potential). This stimulation of the cathodic processes may explain some experimental crevice measurements.

Excursions in bulk conductivity drastically change the electrochemistry within the crevice. The potential increases, the pH decreases, and the conductivity of the local crevice solution increases. In this case, the **net** polarization **does** occur. After the excursion was over, the bulk conductivity was returned to its original value. The electrochemical changes that had developed within the crevice during the excursion did not revert to the benign conditions expected given the low conductivity boundary condition. Thus, the conditions of high potential, low pH, and high conductivity are maintained within the crevice. This is depicted by box 5 in Figure 4-46. These conditions within the crevice are well within the stress corrosion cracking region. This

irreversibility was sensitive to the reduction kinetics chosen, but was completely irreversible for realistic reduction kinetics. There was no significant difference between simple Ni^{2+} dissolution and Ni^{2+} with Mn^{2+} dissolution. Once the crevice becomes net polarized it does not revert to its original conditions. This result has obvious importance in operating BWR reactors but is also important to modeling. Such a system cannot be modeled using a steady state model, since the local electrochemistry is history dependent.

Lowering of the bulk oxygen concentration through the addition of hydrogen (i.e., applying hydrogen water chemistry) reduces the severity of conditions developed within the crevice during and after an excursion (box 6 in Figure 4-46). In the realistic case of Ni^{2+} with Mn^{2+} dissolution, the electrochemical conditions developed within the crevice during an excursion are partially reversible. The resulting electrochemistry puts the crevice on the borderline between stress corrosion cracking susceptibility and immunity. Thus, the crevice exposed to hydrogen water chemistry is less likely to initiate stress corrosion cracking.

This chapter has evaluated the electrochemical conditions that develop within a crevice exposed to typical BWR environments has been evaluated. By varying the material and bulk conditions realistically, the effect of the parameters has been evaluated and the bulk conditions necessary to induce stress corrosion cracking within the crevice ave been estimated. By changing certain input parameters, the sensitivity of the results to these input parameters was examined and the need for accurate and reliable input data was clearly demonstrated. Nonetheless, an understanding for high temperature electrochemistry within occluded regions was developed and conclusions can be drawn about cracking in such regions from this information.

The implications of these conclusions for laboratory cracking experiments and BWR safe end crevice cracking are explored in the next chapter.

4.5 REFERENCES

(1) M.G. Fontana and N.D. Greene, Corrosion Engineering, McGraw-Hill, NY, 1978.

(2) J.T. Adrian Roberts, Structural Materials in Nuclear Power Plants, Plenum Press, New York, 1981, p. 243.

(3) W.J. Shack, et. al., Environmentally Assisted Cracking in Light Water Reactors : Annual Report October 1983-September 1984, NUREG/CR-4287, ANL-85-33, June 1985.

(4) A. Turnbull, J.G.N. Thomas, J. Electrochem. Soc., vol. 129, p. 1412, 1982.

(5) A. Turnbull, J.G.N. Thomas, NPL Report DMA(A)23, 1980.

(6) B.M. Gordon,C.W. Jewett,A.E. Pickett,M.E. Indig,P.L. Andresen,L.W. Niedrach, Hydrogen Water Chemistry for BWRs, EPRI NP 39595, July 1985.

(7) P.R. Tremaine and J.C. LeBlanc, J. Chem. Thermodynamics, vol. 12, p. 521, 1980.

(8) P.R. Tremaine and J.C. LeBlanc, J. Solution Chem., vol. 9, p. 415, 1980.

(9) D.D. MacDonald, Corrosion Science, vol. 16, p. 461, 1976.

(10) D.D. MacDonald and P. Butler, Corrosion Science, vol. 13, p. 259, 1973.

(11) P.R. Tremaine, R. Von Massow, and G.R. Shierman, Thermochimica Acta, vol. 19, p. 287, 1977.

(12) D.D. MacDonald, T.E. Rummery, and M. Tomlinson, IAEA-SM-190/19, p.123.

(13) R.M. van Kuijk, ,Light Water Reactor Structural Integrity, Stahlkopf,K.E., and L.E. Steele,ed,Elsevier Applied Science Publishers, London and New York, 1984, pp. 79-94.

(14) Investigations and Evaluation of Stress-Corrosion Cracking in Piping of Light Water Reactor Plants, NUREG-0531, Feb. 1979, Pipe Crack Study Group.

(15) R.A. Page, Corrosion, vol. 39, p. 409, 1983.

(16) W.F. Bogaerts and C. Bettendorf, Electrochemistry and Corrosion in High Temperature Water, EPRI NP-4705, July 1986.

(17) L.I. Krishtalik, Soviet Electrochem., vol. 3, p. 203, 1967.

(18) F.P. Ford, Proceedings of the Second International Atomic Energy Agency Specialists 'Meeting on Subcritical Crack Growth, Sendai, Japan, May 15-17, 1985, p. 3.

(19) H. Hänninen,H. Illi, K. Torrönen, and M. Vuili, ibid., p. 179.

(20) J.H. Bulloch, Environmental Degradation of Materials in Nuclear Power Systems - Water Reactors, G.J. Thews and J.R. Weeks, eds., AMS pp. 261-268, 1988.

(21) J.D. Atkinson and J.E. Forrest, unpublished data.

(22) C.M. Chen, K.Aral, G.J. Thews, Computer- Calculated Potential-pH Diagrams to 300 °C. Volume 2 : Handbook of Diagrams, EPRI, NP-3137,vol. 2, 1983.

(23) P.W. Bolmer, Corrosion, vol. 121, p. 69, 1965.

(24) G.I. Ogundele and W.E. White, Corrosion, vol. 421, p. 398, 1986.

(25) R.N. Iyer, H.W. Pickering, and M. Zamanzaden, Scripta Met., vol. 22, p. 911, 1988.

(26) J.D. Atkinson, private communication, October , 1989.

(27) Giovanni Gabetta and E. Caretta, Corrosion Chemistry within Pits, Crevices, and Cracks, ed. A.Turnbull, HMSO Books, London,1987, p. 287.

(28) D.F. Taylor, Corrosion, vol. 35, p. 550, 1979.

(29) D.F. Taylor and M. Silverman, Corrosion, vol. 30, p. 447, 1980.

(30) D. F. Taylor and C. Caramihas, High Temperature Materials Chemistry, ed., D.D. Cubiciotti and D.L. Hildebrand, The Electrochemical Society Softbound Series, Pennington, N.J., 1982.

(31) D.F. Taylor and C.A. Caramihas, J. Electrochem. Soc., vol. 129, p. 2458, 1982.

(32) D.F. Taylor and C.A. Caramihas, Embrittlement by the Localized Crack Environment, ed., R.P. Ganloff, p. 105, The Metallurgical Socirty of Aime, Warrendale, PA , 1984.

(33) D.F. Taylor and C. A. Caramihas-Foust, J. Electrochem. Soc., vol. 132, p. 1811, 1985.

(34) D.F. Taylor and C.C. Foust, Corrosion, vol. 44, p. 204 , 1988.

(35) P.L. Andresen, Mechanisms and Modelling of Water Chemistry Effects in Inconels and Stainless, Low Alloy and Carbon Steel in High Temperature Water, Corrosion 89, Paper #566, April 17-29, 1989, New Orleans, LA.

Chapter 5

IMPLICATIONS OF CREVICE MODELING FOR BWR RECIRCULATION INLET SAFE END CRACKING

5.1 INTRODUCTION

Since 1969, cracks have been found in BWR feedwater, core spray and recirculation nozzle safe ends initiating from the creviced region in the United States (*1,2,3*). Similar safe end cracking has also been experienced in Japanese and German nuclear reactors (*4*). It is believed that this cracking is induced by the crevice chemistry generated in the nozzle safe-end annulus. In this chapter, the understanding and insight developed in Chapter 4 will be used to determine the material and/or operating conditions that could be inducing stress corrosion cracking of the safe-end annulus.

The safe-end crevice of particular interest is that formed in the recirculation inlet nozzle. This safe-end crevice will be described in detail and the limitations of applying modeling results to this safe-end are discussed. Then the implications of the crevice modeling results for laboratory experiments seeking to simulate safe-end cracking will be considered. Finally, the relevance of this to in-reactor safe-end performance will be evaluated.

5.2 DESCRIPTION OF BWR NOZZLE SAFE ENDS

The location of some nozzle safe-ends on a BWR pressure vessel is shown in Figure 5-1. A typical safe end is an Inconel® alloy 600 or stainless steel (type 304, 316, or 316NG) transition piece used to facilitate the welding of the stainless steel piping to the carbon steel pressure vessel nozzles (*1*). The composition of these alloys is given in Table 5-1. A cross sectional schematic of a typical recirculation inlet safe end annulus or crevice is shown in Figure 5-2. The crevice region shown is 0.6096m (2 ft) long with a width that varies from 5.08×10^{-3} m to 1.27×10^{-2} m (0.2 in. to 0.5 in.). In addition, supporting pads block 16% to 90% of the circumferential opening at the crevice mouth. The amount of blockage varies from plant to plant. Flow past the crevice opening at the mouth, in the BWR core region, is typically between 0.6 and 1.2 m/s during normal operating conditions. This crevice is typically formed by two different alloys, namely type 304 stainless steel and Inconel® 600.

Stress corrosion cracking initiates near the weld between the safe end and the inlet pipe in the chromium depleted heat affected zone of the safe end (see Figure 5-2) (*3*). The crack typically propagates from this region into the weld material. It is not necessary that the material be sensitized (i.e. , have a chromium content of less than 12% in the heat affected zone) for this type of cracking to occur (*3,4*). Indeed, there is evidence that even low carbon steels, which are not susceptible to sensitization, will experience cracking in these regions (*4,5*). In some plants the cracking problem is so severe that all the safe ends of certain systems (i.e., recirculation system) have had to be replaced.

There are three complicating factors which must be considered when applying the modeling results to the BWR inlet safe end annulus or crevice : width of the crevice, flow past the mouth of the crevice, and crevice closure due to support pads. The width of the

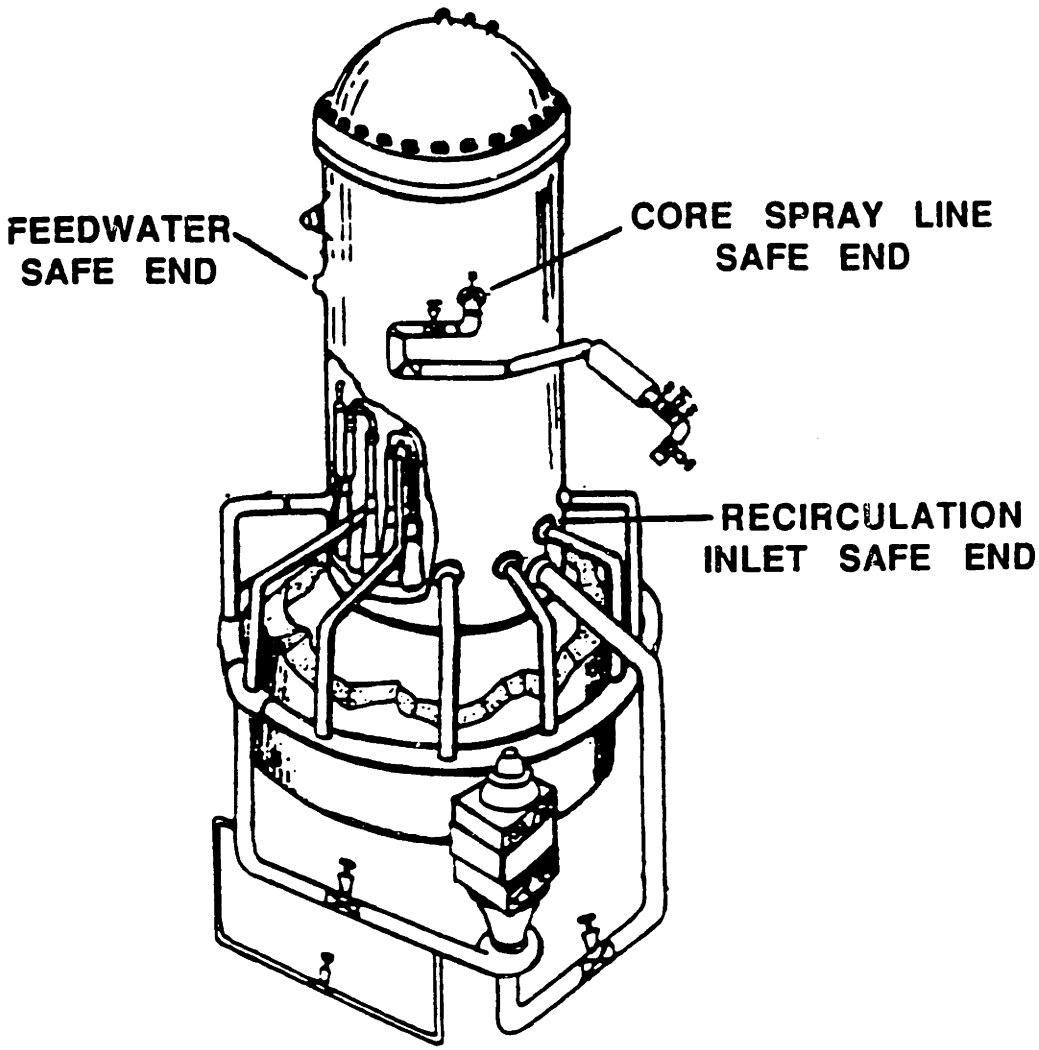

Figure 5-1. Location of safe-end on BWR pressure vessel.

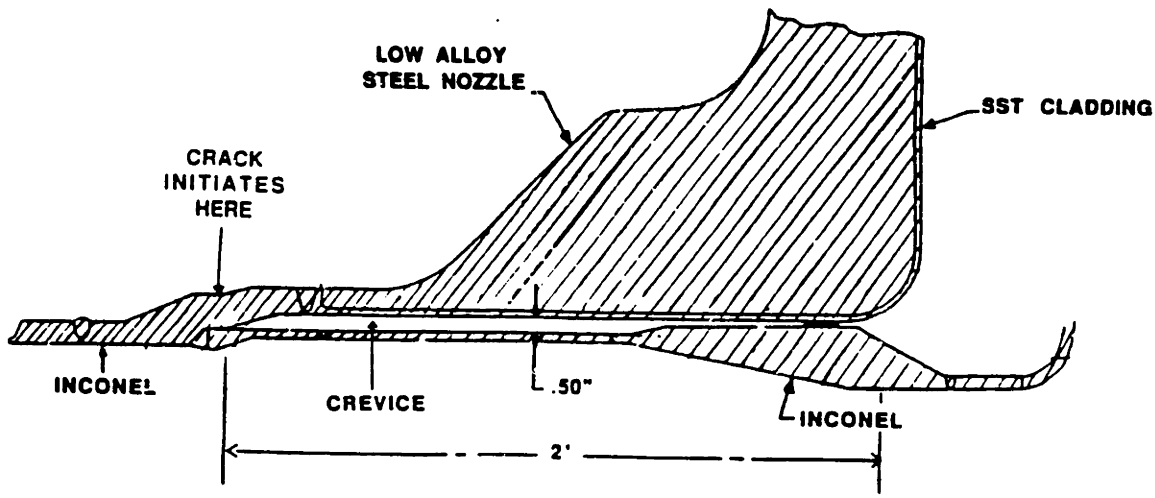

Figure 5-2. Schematic of typical BWR recirculation inlet nozzle crevice.

crevice, 6.25×10^{-3} m (0.5"), is large. This width poses a question about the validity of the averaging techniques employed when incorporating electrochemical wall reactions, solubility reactions, and chemical dissolution reactions. Averaging over the width of the crevice assumes that any concentration gradients between the walls of the crevice are small. This may not be exactly true in this case. To model this accurately, the crevice would have to be modelled in two dimensions. Nevertheless, the one-dimensional model will provide understanding of the local electrochemistry and the effect of material choice and operating parameters on the local electrochemistry.

Flow past the opening of the annulus may induce two-dimensional convective motion inside the annulus (*6,7,8*) . Induced flow in the annulus area may result in mixing within the crevice region thus reducing the effective transport length and changing the dimensionality of the problem from one dimension to two dimensions. No existing model can analyze the effect of diffusion, ion migration, and complex reaction processes in two dimensions as well as this possible induced convective flow. In-reactor experience shows that crud does build up within the safe end region crevice region. This implies that mixing within the crevice is not vigorous, certainly at long times. Even if there is some mixing, crud would build up gradually, reducing the effectiveness of this mixing.

The third complicating factor is the presence of the supporting pads at the end of the annulus. These pads may have a large effect on the transport processes occurring inside the annulus depending on the extent of annulus closure. The potential field lines will be concentrated near the pad resulting in an increase potential gradient. This will affect the transport of ions due to ion migration in the pad regions. Also, the convective motion induced by flow past the mouth of the crevice may be considerably dampened, resulting in a decrease in mixing and an increase in the effective transport length.

Experimental work has been carried out at MIT to try and simulate the flow induced in a typical BWR recirculation inlet nozzle crevice by flow past the mouth of

this crevice (*8*). The work has been carried out using a scaled down plastic model of the crevice region. This plastic model was modified to simulate the closure of the crevice region by supporting pads. Dye was injected at the tip of this model and the amount of time necessary for most of the dye to be swept out of the crevice induced convection was monitored. These experiments showed that crevice should be flushing rapidly. These results conflict somewhat with in-reactor experience of crud buildup within the safe-end crevice region. It is possible that the crevice initially flushes freely, but that after some time crud builds up in this region and gradually reduces the extent of flushing. The numerical model in this thesis has been applied to the limiting case of a stagnant safe-end crevice.

5.3 IMPLICATIONS OF CREVICE MODELING RESULTS FOR INCONEL® ALLOY 600 LABORATORY CRACKING EXPERIMENTS

Much of the Inconel®Alloy 600 safe-end cracking experimental work has been carried out by R. Page and A. McMinn (*9-12*). The experiments were carried out in creviced and uncreviced conditions. The creviced conditions were obtained by wrapping the slow strain rate test specimens with a layer of graphite cloth and an outer layer of nickel foil. These creviced specimens were exposed for 168 hours (7 days) in the autoclave prior to initiation or straining in order to allow crevice chemistry to develop. In most cases the bulk environment was low conductivity water with varying amount of dissolved oxygen : 200 ppb or 8 ppm O_2 for uncreviced specimens and 16 ppm O_2 for creviced specimens. The results show that alloy 600 is immune to SCC under normal conditions but cracks when creviced or when excursions in bulk conductivity occur.

Unfortunately, the exact dimensions of the crevice in the experiments are not known and, therefore it is impossible to verify the scaling parameter of the experiment. The experiment should be scaled by L^2/h in order to produce conditions similar to those found in the real safe-end crevice. Also, the composition of the nickel foil and the graphite cloth are not known. Any soluble impurities present would be important in analyzing the results. The modeling results presented in Chapter 4 indicate that polarization, acidification, or an increase in conductivity would not occur unless some completely soluble or reducible species, such as MnS, dissolved from the alloy or an excursion occurred. Since, in these experiments, the crevices slow strain rate specimens were exposed to high purity water the cracking may have been induced by dissolution of some soluble or reducible species from the alloy. The dissolution of MnS may explain the results though there is no way to be sure. If this is the case then the results from these short term laboratory tests may not reflect long term plant conditions for which the MnS would have dissolved.

The dissolution of MnS may have implications in other experimental work. Specimens used in environmentally enhanced cracking testing are often precracked in air exposing fresh metal surface in a tight crack. Once these specimens are placed in their test environment, any MnS inclusions present may dissolve providing an extra cathodic source thus possibly raising the potential into the cracking regime. This would result in an initially high crack propagation rate which would decay after the MnS exposed on the crack surfaces dissolved. As discussed in Chapter 4, there is such variability in specimen to specimen cracking because of the sensitivity of cracking behavior to MnS distribution that definitive conclusions are not possible. It may be wise to expose specimens to the environment of interest for a period of time depending on size and distribution of MnS particles before any load is applied in order to get accurate crack propagation information.

5.4 IMPLICATIONS OF MODELLING RESULTS FOR BWR RECIRCULATION INLET SAFE ENDS

The results presented in Chapter 4 are directly applicable to the BWR recirculation inlet safe-end crevice since the L^2/h for the model crevice and the BWR safe-end are identical. As described in chapter 4, the crevice is predicted to be self protecting under normal operating conditions. The pH should be high and the potential should be low (at the local corrosion potential). Only two of the effects evaluated produced conditions which were sufficient to initiate and propagate stress corrosion cracks within the crevice. The effects were :

(1) The chemical dissolution of manganese sulfide (MnS) inclusions to produce H2S.

(2) Excursions in bulk conductivity.

The importance of these two phenomena in the development of local electrochemical conditions in a BWR recirculation inlet nozzle crevice will be evaluated in this section.

The dissolution of MnS inclusions to form H_2S results in a rise in potential induced by the cathodic stimulus of H_2S. This process is limited by the amount of MnS available on the walls and at the tip of the crevice. Once these inclusions are consumed, the conditions within the crevice revert to the high pH, low potential conditions described in the previous paragraph. If cracks do not initiate during the period of time while MnS inclusions are dissolving, it is unlikely that they would initiate unless some other factor induces change within the crevice. Additionally, the driving force for propagation is removed as the inclusions are consumed.

Excursions in bulk conductivity produces electrochemical changes within the model crevice. These electrochemical changes include acidification, increase in conductivity, and a rise in potential. The most significant aspect of this change in local conditions within the crevice is that these are not reversible once the excursion in bulk conductivity is over. Thus, once the crevice is polarized it remains polarized. The probability that this polarization could develop in an operating BWR is low if the EPRI "BWR Water Chemistry Guidelines" are followed (*2*). The EPRI guidelines are not binding, but are considered good operating practice for BWR's. If these guidelines are followed, the duration of an excursion is strictly limited to a time span shorter than that needed to develop polarization. If no polarization occurs, then the conditions within the crevice should remain benign.

Thus, according to the modeling results presented in this thesis, the conditions within the BWR crevice should remain protective (high pH and low potential). The only other possible sources for changes in crevice electrochemistry are the dissolution of soluble species from the metal or a decrease in temperature (as would occur during an outage). The dissolution of soluble species, even if present in extremely small amounts in the metal, may be sufficient to cause polarization and initiate cracking within the crevice. Since very little solubility data is available, this possibility can not be thoroughly evaluated. A decrease in temperature would increase the solubility of metal ions, thus increasing the conductivity of the solution within the crevice. This buildup of ions would not depend on transport from the bulk in this case. The rate of production of cations in the crevice may be sufficient to increase the conductivity within the time-scale of the plant outage. An increase in conductivity could result in polarization within the crevice, and stress corrosion cracks could initiate. Also, once this chemistry was developed, it might not convert to the high pH, low potential conditions as the temperature is raised. The temperature excursion may be irreversible. In order to accurately assess this phenomena, cracking susceptibility must be established for such a

scenario. Care must be taken that the experimental model is designed to have the same L^2/h value as the in-reactor crevice. An experiment should be carried out in which a system experiences low temperatures characteristic of an outage, and then experiences temperatures characteristic of normal operation. The reversibility or irreversibility of polarization induced by a temperature outage can then be established. After susceptibility is determined, it will then be possible to ascertain whether cracking is induced by chemistry changes created by restricted mass transport within the crevice, or whether it is induced by residual stress, cold working, etc. In addition, solubilities of all alloying elements and impurities must be evaluated to ascertain whether any of these species are sufficiently soluble to cause polarization, and subsequent cracking, within the crevice.

5.5 REFERENCES

(1) J.T. Adrian Roberts, Structural Materials in Nuclear Power Plants, Plenum Press, New York, 1981, p.243.

(2) BWR Water Chemistry Guidelines, EPRI NP-3589-SR-LD, BWR Owner's Group Water Chemistry Guidelines Committee, April 1985.

(3) R.M. van Kuijk, Light Water Reactor Structural Integrity, Stahlkopf,K.E., and L.E. Steele, ed, Elsevier Applied Science Publishers, London and New York, 1984, pp. 79-94.

(4) Investigations and Evaluation of Stress-Corrosion Cracking in Piping of Light Water Reactor Plants, NUREG-0531, Feb. 1979, Pipe Crack Study Group.

(5) R.H. Koppe, E.A.J. Olson, D.W. LeShay, Nuclear Unit Operating Experience : 1983 - 1984 Update, EPRI NP-4368, January, 1986.

(6) R.C. Alkire, D.B. Reiser, and R.L.Sani, J. Electrochem. Soc., vol. 131, 12, 1984, pp. 2795-2800.

(7) F.Pan, and A. Acrivos, J. Fluid Mech.,vol..28, part 4, 1967, pp. 643-655.

(8) P.F. Easthope, and A. Turnbull, Aspects of Fluid Flow of Relevance to Corrosion Fatigue and Stress Corrosion Cracks, NPL Report DMA(A)105, July 1985.

(9) R.A. Page, Corrosion, vol. 39, p. 409, 1983.

(10) R.A. Page, Corrosion, vol. 41,p. 339, 1985.

(11) R.A. Page and A. McMinn, Met. Trans. A.,vol. 17A, p. 877, 1986.

(12) A. McMinn and R.A. Page, Corrosion, vol. 44, p. 239, 1988.

Chapter 6

GENERAL DISCUSSION

6.1 DISCUSSION

The goal of this research has been to develop a model to predict the local electrochemistry in cracks and crevices. This goal has been achieved but in applying the model the primary emphasis has been in defining the electrochemistry in crevices. This is of immediate practical concern to BWR's in so far as it impinges on cracking susceptibility. In the process, a significant step forward in the understanding of the electrochemistry of cavities in high temperature waters has been achieved. Much of the understanding developed can be applied directly to cracking phenomena because in most cases the electrochemical conditions developed within cracks are dominated by processes occurring at the walls. This is because the surface area of the walls is so much greater than that of the tip. In general, tip processes can only dominate in situations where the time-averaged current density is many orders of magnitude greater than that of the walls. An exception is when species are produced uniquely at the tip that are not produced on the walls (e.g. the dissolution of MnS to produce a dissolved sulfur species). Thus, in this chapter the most important features illuminated by this modeling work will be briefly highlighted and applied more generally to an understanding of cracking behavior.

It is obvious from this work that the electrochemistry which develops in occluded regions is a complicated function of the many processes (transport and

homogeneous and heterogeneous reactions) occurring within these regions. It has been the inclusion of these important processes that has resulted in a more complete understanding of the electrochemical conditions developed within these regions. Many important features of high temperature local electrochemistry have been brought to light and have been discussed in previous chapters of this thesis. Some of these features are "technical" in so far as they indicate requirements for successful modeling e.g. the interrelation between diffusion and migration, the role of cathodic reactions internally, and the importance of solubility. However, in conceptual understanding, the most dramatic of the features exposed by the modeling involve the possible role of manganese sulfide inclusion dissolution not only in supplying sulfur species to the crack tip region but also in raising the potential by supplying an additional source of cathodic reactant The other most dramatic feature is the irreversibility of electrochemical conditions within occluded regions which can develop under appropriate conditions once polarization occurs. Apart from the practical engineering consequences, the latter raises questions concerning the application of steady state modeling to this environment since predictions depend on the history of the system and are not uniquely defined by the steady-state boundary conditions. It is important to point out that in the model crevice polarization did not occur unless some solubles species was introduced into the crevice region thereby increasing the local conductivity. This could occur as a consequence of dissolution of species from the metal or due to transport of species from the bulk into the crevice during an excursion. In the absence of soluble species, the crevice was isolated from the bulk and protected. In part, this was due to the fact that the model crevice was geometrically very restricted (i.e.. it had a large L^2/h) conditions appropriate to practical crevice situations in-plant. Nevertheless, it may be possible to polarize

cracks, particularly short cracks, even in low conductivity water. This possibility will be evaluated fully when the model is applied directly to cracks.

In order to discuss the importance of these and other features in relation to local crack electrochemistry, the prevalent understanding of electrochemical aspects cracking in Inconel, stainless steel and low alloy pressure vessel steel will be discussed and re-assessed in the context of the modeling results presented in this thesis.

6.1.1 Inconels and Stainless Steels

In the case of cracking in Inconels and stainless steels in high temperature water no clear distinction can be made as to the detailed mechanism at this point although there is little argument that cracking precedes due to anodic processes. The quantitative crack growth rate model developed by Ford and Andresen (*1-3*) has been used to characterize both inconels and stainless steels. This work has been the vanguard of predictive modeling in nuclear applications and can be seen as the representation of postulated views about localized electrochemistry and high temperature cracking behavior. Hence, in order to evaluate the current understanding of the electrochemistry within cracks in these materials, it is appropriate to review the assumptions and approximations used in the Andresen/Ford model and compare and contrast with the understanding developed by the rigorous modeling presented in this thesis.

The model developed is based primarily on the film rupture/slip dissolution mechanism of crack advance though the film induced cleavage process, as proposed by Sieradzki and Newman (*4*), has been incorporated into later versions. The precise mechanism is not critical to this discussion. The crack growth model is dependent on

three basic parameters : (1) the crack tip strain rate, (2) time to rupture of the oxide film, and (3) the repassivation kinetics of the bare metal surface exposed by film rupture. These factors are incorporated into the crack growth model in the form (for simplicity film induced cleavage is not considered)

$$\dot{a} = f(n)(\dot{\varepsilon}_{ct})^n \qquad (6-1)$$

ε_{ct} is the crack tip strain rate; n represents the decay constant associated with the transient oxidation current given by

$$I = I_0 \left(\frac{t}{t_o}\right)^n \qquad (6-2)$$

where I_0 is the bare surface current density and t_0 is the time this bare surface current density is maintained before oxide nucleation and growth occurs reducing the current density.

The parameter n depends on the local potential and anion concentration, as shown in Figures 6-1 and 6-2, and even on the type of anion. Generally, when applying this crack growth model, the material, stresses (can be measured or calculated), and the bulk environment are known. The important unknown factors are the local environment and potential at the crack tip. Hence it is necessary to develop a relationship between the known bulk environment and the crack tip environment.

In recent work, Andresen has developed a method of evaluating this parameter n through quantitative calculations of crack chemistry (*1,2*). Crack growth rates calculated using this model have had good agreement with experimental work. For reasons indicated below, this agreement is perhaps surprising. Since application of

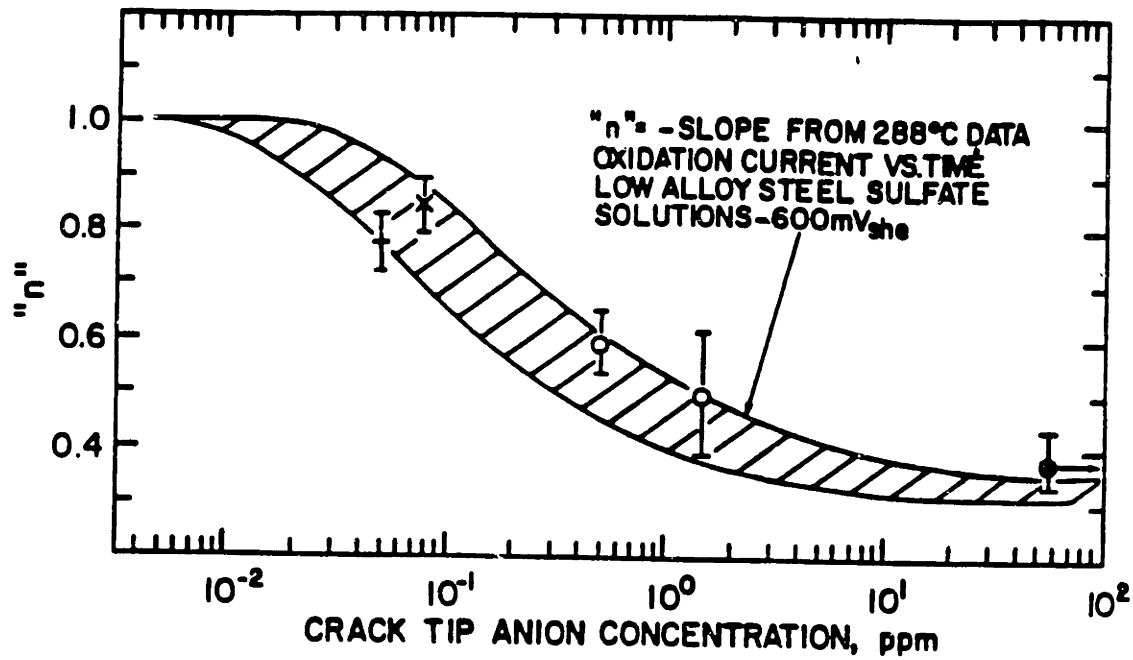

Figure 6-1. Variation of parameter "n" with crack tip anion concentration for mid and low alloy steels in various solutions of sulfate, borate, molybdate and chloride at 288°C (*3*).

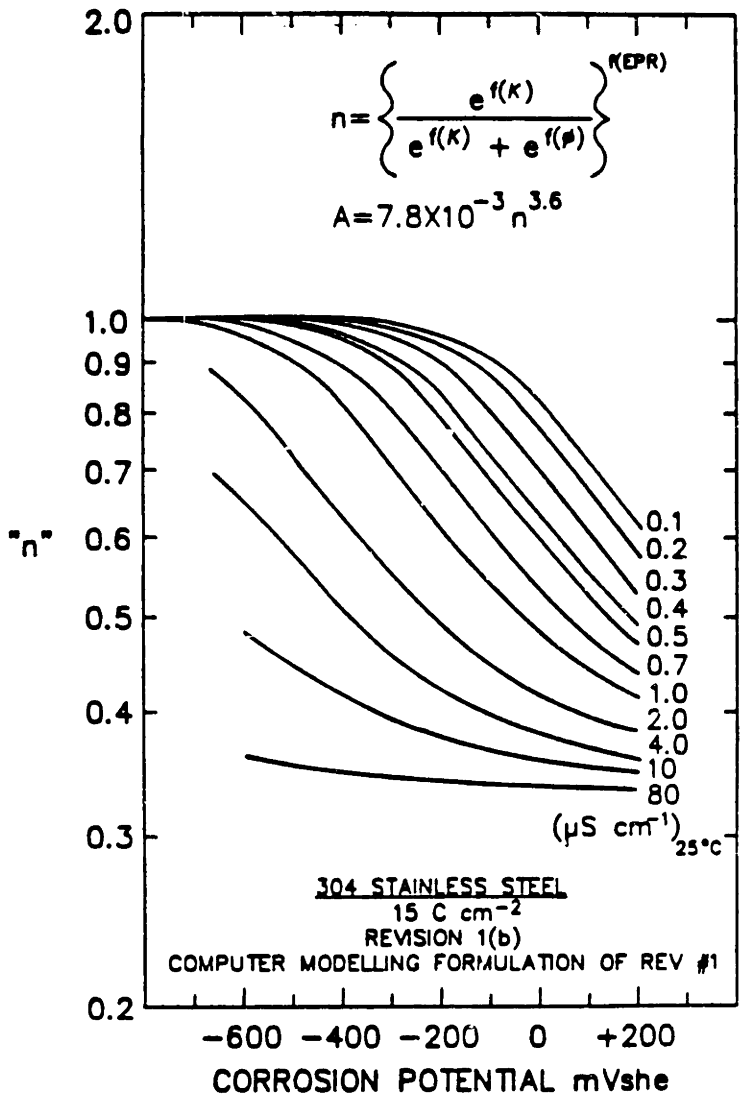

Figure 6-2. Variation of parameter "n" with corrosion potential and bulk solution conductivity for sensitized (EPR = 15Ccm^{-2}) Type 304 Stainless Steel in water at 288°C (*3*).

the model will be extended to predicting crack growth rates for situations for which there is little or no data for comparison (i.e.. irradiation conditions, fluid velocity, etc.), It is important to examine the assumptions made in quantitatively predicting crack chemistry and potential and the parameter n using the understanding developed in this model.

In the absence of a mathematical model such as described herein, experiments were employed to quantify the electrochemical conditions that developed within a crack (*1-3*). These experiments are carried out at **room temperature** using a Teflon® 1T compact tension specimen with a crack slot machined into the specimen at the bottom of the notch. The chemistry was measured within the crack slot using twenty chloride ion sensitive probes. Two types of experiments were carried out. Either the crack plane was flooded with KCl solution or a flux of hydrogen ions was generated at the "crack" tip. In both cases the transport of chloride ions and the steady state concentrations developed in the region were monitored. There are major criticisms of this experimental approach. The assumption that room temperature experiments using Teflon® could simulate a crack in a metallic material at high temperatures is certainly questionable. The temperature change results in differences in equilibrium constant and transport properties. A Teflon® specimen, even with an active hydrogen ion producing tip is unrealistic for two important reasons. The first reason is that the walls of the crack slot are inert. In real cracks, the passive current on the walls will often dominate the chemistry within the crack as described in the first paragraph of this chapter. The second reason is that Teflon® has slip, which is important to the flow characteristics, whereas metals do not have slip, so the simulation of convective transport is also unrealistic.

This experimental work led to a relationship between the bulk concentration of anions and the crack tip anion concentration given by

$$C_{ct} \approx C_{ext}(10)^{\frac{\Delta\phi}{0.4}} \qquad (6-3)$$

To use such an experimental set-up to evaluate local electrochemistry, it was critical to establish the uniqueness of this relationship for the range of bulk concentrations, H^+ fluxes at the crack tip, and sources on the walls. This was not done and hence, even without any theoretical considerations, the experiments must be considered to be fundamentally inadequate. Furthermore, the theoretical analysis herein indicates that there is no basis for the relationship. The potential drop in the above equation is the potential difference between the crack mouth and the crack tip. Since the value is unknown, a value must be assumed in the Andresen model. The value used is the corrosion potential of stainless steel in deaerated pure water (i.e., ≈ -0.55 V (SHE)). This is a fixed value and does not change. By assuming that the potential within the crack is at the corrosion potential, it is assumed that no polarization occurs within the crack. Andresen assumes that changes in potential are small because the change in pH is assumed to be no larger than 3 units. The results presented in this thesis show that very significant polarization will occur with such a change in pH. Also ignored in this approach is the importance of changes in the bulk conductivity which may effect the degree of polarization in the crack. Based on Equation 6-2, the crack tip anion concentration is limited to approximately 100 times that of the bulk. The results presented in this thesis show that it may be possible to generate higher concentrations in occluded regions.

In Andresen's model, the concentrations generated in the crack are considered to have no bearing on the local potential. The potential is assumed and then the concentration of ions is calculated. This separation is based on the assumption that the corrosion potential within the crack is dependent on the availability of species which

do not alter the local conductivity of the solution in the crack (i.e.. oxygen). This completely ignores the reduction of hydrogen ions and the strong effect of hydrogen ions on the conductivity of the solution due to their very high mobility. Once net polarization occurs (i.e.. the local anodic processes are greater than the cathodic processes), acidification will result and, since the kinetics of hydrogen ion reduction are dependent on its concentration, this will be a major contributing factor in controlling the potential in the crack.

The fact that the predicted crack growth rates from Andresen's model appear to compare well with experimental crack growth rated is **not** proof that all the component parts of the model and the assumptions made are correct. There is considerable scatter in the experimental data used to access the model and the sensitivity to the uncertainties in each component of the model is unclear. While the model may compare with crack growth data, perhaps fortuitously, the model is inherently flawed in its assumptions and may provide misleading perspectives on the important factors determining local electrochemistry. Nonetheless, this model should be recognized as the first attempt to incorporate crack tip electrochemistry into a model to predict crack growth rates in high temperature waters. It is a future objective to link the model described in this thesis to to the crack growth model as a basis for more effective prediction

6.1.2 Low Alloy Steels

Cracking in low alloy pressure vessel steels has been studied for some time. Though the basic mechanism is unclear, the results of these studies indicate that three parameters acting either separately or in conjunction control the cracking of this material : (1) the water flow rate, (2) water chemistry, and (3) the steel sulfur

content (*4*). Trends in data and the complexity of the interactions of these parameters can be understood in terms of their effect on controlling the concentration of sulfur species in solution within the crack (*5*). The flow rate would affect the concentration of species by inducing convective motion within the crack and sweeping out any accumulation of species. The bulk water chemistry could play an important role by providing sulfate ions (from resin intrusions) which could accumulate in the crack due to ion migration. The sulfur content probably plays the most important role because it is a "constant" source for these aggravating sulfur species at the crack tip. The sulfur in the steel is present in the form of sulfide inclusions, particularly manganese sulfide. These inclusions are soluble and dissolve from the steel to form H_2S (*1-8*). H_2S and HS^- are the stable form of sulfur in deaerated media. The size, distribution and type of manganese sulfide inclusion plays an important role in the cracking behavior in so far as they influence the effective flux (*6-8*). Ccmbrade et al. have attempted to incorporate these factors in a simple diffusion based model to obtain a rough estimate of the crack tip sulfur concentrations. This model ignores homogeneous reactions and H_2S reduction and the results obtained will have to be confirmed in future application of the present model. It is suggested that the sulfur species could affect the crack propagation rate in three ways (*5*) :

(1) The dissolution rate of the alloy increases in the presence of sulfur species.

(2) The fracture properties of the film could be altered by the presence of precipitate sulfides on the surface.

(3) The cathodic processes could increase because of delayed crack tip

repassivation.

Thus, the more sulfur present, the more these processes and properties would be affected.

In the modeling work presented in this thesis, the effect of the dissolution of manganese sulfide dissolution on the electrochemistry developed within the model crevice was studied. In this modeling approach, manganese sulfide dissolved chemically to yield H_2S. The reduction of H_2S (a well documented reaction at room temperature) and the equilibrium between H_2S and HS^- was also considered. The reduction of H_2S has not been previously considered as a process occurring in cracks in high temperature water. Through this modeling it was discovered that the production of H_2S by chemical dissolution would yield an extra cathodic source, thus stimulating the cathodic current. This resulted in an increase in potential inside the crack. This increase in potential and extra cathodic source could be another potential reason for cracking in this material and should be considered in future experimental and modeling work.

6.2 APPLICATION OF MODEL TO CRACK ELECTROCHEMISTRY PREDICTION

The framework for modeling the electrochemistry within cracks is already available. There are two important differences in modeling cracks as opposed to crevices. The first difference is the geometry. A crack is modeled with a trapezoidal geometry whereas the crevice is parallel sided. This difference in geometry causes some dilution effects as the crack opens from the tip to the mouth and must be

accounted for in the transport equations as shown in Equation 3-7. This effect is incorporated into the model.

The second difference is the crack tip. In the crevice the crack tip has the same properties as the crack walls. Anodic reactions occurred at the passive current density and the kinetics of cathodic processes are assumed identical. In a crack, the tip region is more active than the walls because of the effect of localized straining or film rupture. While in the case of stainless steel and Inconel this may not have the dominant effect on the electrochemistry, it is important to account for it correctly until this can be demonstrated for the systems of interest. It is certainly critical for low alloy steels. In the model the crack tip is blunt and has a crack opening that is defined by fracture mechanics (as described in chapter 3). This opening may be significantly larger than the **active** area of the tip. It is necessary before applying the model presented in this thesis to a cracking problem, to evaluate the averaged properties of the crack tip so that these averaged properties may be used in the model. This averaging will be done over the area of the crack tip and may also be done in time to account for both the fracture of the passive film and repassivation kinetics. Later, it may be necessary to incorporate this time dependence of rupture and repassivation into the model.

The modeling of the crack tip in the case of low alloy steel is straight forward. The crack tip region is important as a source of H_2S. Indeed, it may be possible to ignore the production of metal species at the tip since the exposure and dissolution of manganese sulfide inclusions is the dominant effect. Crack advance exposes new manganese sulfide inclusions that dissolve away at some rate until either the inclusion is depleted or new metal surface is exposed by crack advance. Knowing the size and distribution of these inclusions, the dissolution rate of manganese sulfide, and the crack propagation rate will enable averaging of the flux of H_2S over the crack tip area

(CTOD). It may be possible, eventually, to account for any time fluctuations in concentration of H_2S production and concentration within the crack due to the depletion of manganese sulfide inclusions or the exposure of new inclusions by the advance of the crack.

In the case of cracking in stainless steels and inconels, the definition of the crack tip model is not so clear. One must define the area exposed by the intersection of the oxide film at the tip by slip planes. This is the area over which the bare metal current density acts. This current density must be time averaged over the time for film rupture to account for repassivation. The rest of the crack tip region has an oxide film on the surface and the appropriate current density must be used for this region. Thus one would arrive at an averaged current density for the crack tip as shown

$$i_{\text{average crack tip}} = \left(i_{\text{averaged over time between rupture events}}\right)\left(\frac{\text{AREA EXPOSED}}{\text{TOTAL AREA OF CRACK TIP}}\right) + \left(i_{\text{oxide covered surface}}\right)\left(\frac{\text{AREA NOT EXPOSED}}{\text{TOTAL AREA OF CRACK TIP}}\right) \quad (6-4)$$

In the case of sensitized materials, there is a region at the crack tip (i.e., near the grain boundary) which has very different properties. The area of this region must be defined and the current from this region must be incorporated into the averaged current density equation shown above. The averaged crack tip current density could then be used in the model.

In conclusion, the application of the model to predicting the electrochemical conditions in cracks should not be difficult. The only complexity lies in the definition of the crack tip region and obtaining the necessary data for electrode reaction kinetics

on both passivated and possibly bare metal surface. With the aid of experimentalists, sensible judgements can be made concerning the description of the crack tip current. The model developed in this thesis can then be applied in a rigorous manner.

6.3 REFERENCES

(1) P.L. Andresen, paper #566, Corrosion/89, NACE, Houston.

(2) P.L. Andresen, in Environmental Degradation of Materials in Nuclear Power Systems - Water Reactors, G.J. Thews and J.R. Weeks, eds., TMS, 1988.

(3) F.P. Ford, paper given at "Environment-Induced Cracking of Metals", Kohler, Wisconsin, 1988.

(4) P.M. Scott,Corrosion Science, vol. 25 (819), 1985, pp. 583-606

(5) P.M. Scott, in Environmental Degradation of Materials in Nuclear Power Systems - Water Reactors, G.J. Thews and J.R. Weeks, eds., TMS, 1988, pp. 15-29.

(6) J.H. Bulloch, in Environmental Degradation of Materials in Nuclear Power Systems - Water Reactors, G.J. Thews and J.R. Weeks, eds., TMS, 1988, pp. 261-268.

(7) P. Combrade, M. Faucault, and G. Slame, in Environmental Degradation of Materials in Nuclear Power Systems - Water Reactors, G.J. Thews and J.R. Weeks, eds., TMS, 1988, pp. 261-268.

(8) J.M. Bulloch, Res. Mechanica, vol. 26, 1989, pp. 95-172.

CHAPTER 7

CONCLUSIONS AND FUTURE WORK

7.1 INTRODUCTION

A model which can predict the local electrochemistry within cracks and crevices has been developed. Both transient and steady-state conditions can be calculated. The model incorporates the important transport, electrochemical and chemical processes, and is designed for application to a wide range of alloy systems. It is thereby unique in its combination of fundamental rigor and flexibility. The model can be applied to any crack or crevice in light water reactor environments, provided that the appropriate data are available. Results from modeling of the electrochemistry within crevices are presented. Of particular interest are the results from the study of a crevice in the high temperature, low conductivity aqueous environment characteristic of BWR light water reactor recirculation systems. The extreme conditions characterizing this case produce electrochemical responses not predicted by a consideration of room temperature, high conductivity electrochemistry. The conclusions drawn from this work are presented in Section 7.2.

Analysis of the above results has generated a wide range of ideas for further application of the model, and for complementary experimental work. The most important ideas in these two areas are summarized in Section 7.3.

7.2 CONCLUSIONS

Much information pertinent to both general crevice modeling and a crevice in a BWR environment has been obtained in the course of this work. The most important portions of this information are summarized below.

- Both cathodic reactions and solubility limits on metal ions must be incorporated into the model in order to predict accurate electrochemistry within occluded regions.

- Dissolution of manganese sulfide to form H_2S can, in principle, cause a rise in the potential within the crevice without lowering the pH. This process may explain some experimental crevice measurements.

- Dissolution of completely soluble cations could cause polarization and acidification within the crevice.

- Dissolution of partially soluble metal species, such as Ni^{2+} and Mn^{2+}, does not cause polarization in the crevice. Indeed, the potential reached within the crevice is the corrosion potential for the local crevice environment.

- Excursions in bulk conductivity drastically change the electrochemistry within the crevice causing polarization, acidification and a large

increase in the crevice conductivity. The change is irreversible using realistic reduction kinetics.

- Lowering the bulk oxygen concentration and, therefore, lowering the external metal potential by the addition of dissolved hydrogen does reduce the severity of conditions generated within the crevice during and after an excursion. The conditions developed within the crevice are less likely to induce stress corrosion cracking.

- The BWR recirculation inlet safe end crevice should not crack under normal operating conditions.
    - -- Mns inclusions should be already consumed; thus, no H2S will be produced.
    - -- Excursions in bulk conductivity are, ideally, very limited in time. An aggressive environment does not have sufficient time to develop under these conditions.

- The results obtained from crevice modeling can be broadly applied to the understanding of cracking behavior.
    - -- The understanding of crack electrochemistry as culled from previous quantitative models is flawed for the following reasons
        - -- It is based in part on inaccurate experiments.
        - -- Assumption of constant potential in the crack (fixed at the corrosion potential) is inaccurate. Modeling has

shown that once polarization occurs large changes in potential will follow.

-- Another possible factor in low alloy steel cracking is the stimulation of cathodic processes at the crack tip and subsequent rise in potential resulting from the dissolution of MnS to form H_2S.

The model has revealed many important features of electrochemistry in occluded regions exposed to high temperature water. These features are not only of academic interest, but are of practical importance.

7.3 FUTURE WORK

This section is divided into two parts. The first part suggests future applications of the model. The second part indicates experimental work that should be carried out in order to broaden the data base and confirm the predictions made by the model.

7.3.1 Future Applications of the Model

In the future, the model will be applied to realistic cracking problems in nuclear power plants. The details of the application to cracking was discussed briefly in Chapter 5. As suggested, the importance of the crack tip relative to the crack walls should be assessed. Also presented were three cracking problems that should be investigated.

(1) Low alloy (pressure vessel) steels

(2) Stainless steels

(3) Inconels

It is recommended that these three cases be evaluated. It should be noted that the model developed can, in principle, be applied to any cracks or crevices exposed to a liquid inorganic aqueous environment. Hence, the possibilities for future application are great in number.

7.3.2 Suggested Experimental Work

Emphasized throughout this thesis is the importance of accurate and reliable input data. Without accurate input data, accurate predictions of electrochemistry within cracks and crevices **cannot** be made. In the field of high temperature chemistry and electrochemistry there is a dearth of reliable data and in many cases there are no data at all. Thus, it is recommended that the following data be obtained :

- High temperature polarization data (both anodic and cathodic) in the appropriate media. In the case of anodic polarization data, the appropriate media would include various concentrations of ionic species in order to correctly simulate the chemistry within the occluded region. Modeling like that presented in this thesis, could help evaluate the conditions for experimental testing. Good anodic polarization data are needed for every alloy of interest and, in the case of sensitized materials, for material typical of the grain boundary region. The solution should be deaerated as it is within a cavity. This is especially important for the cathodic polarization data. In both cases, the oxygen

concentration should be monitored in order to better assess the condition of the experiment. Cathodic polarization is needed for H^+, H_2O, O_2, H_2O_2, H_2S, and HSO_4^-, all of which play a critical role in the development of local electrochemistry within cavities.

- High temperature ionic diffusion coefficients

- High temperature equilibrium constants or free energies of formation in the appropriate media and temperature range.

- Solubility limits for all alloying elements and impurities. This information should be obtained as a function of pH and potential. Some precipitation processes are actually oxidation processes and should be evaluated accordingly.

- Potential-conductivity curves delineating regions of stress corrosion cracking susceptibility and immunity (as shown in Figure 4-1) for sensitized and non-sensitized Inconel 600 and other alloys.

In the case of the BWR recirculation inlet safe-end, it has not been experimentally demonstrated that stress corrosion cracking is induced by the buildup of an aggressive environment within the crevice. Unless convective motion dominates within the region, some chemistry change will occur. However, this change may not be necessarily sufficient to induce cracking within the safe-end crevice. In order to establish whether or not a sufficiently aggressive develops, a number of experiments and evaluations must be made under plant conditions. The necessary work includes :

- Accurate crevice experiments using the correct dimensions (i.e., L^2/h), and low conductivity solutions to access whether the conditions developed within the crevice are sufficient to cause cracking.

- The effect of a long term outage on the cracking behavior must be evaluated and the reversibility of the conditions developed during an outage to benign high temperature conditions must be demonstrated.

- Evaluation of the role of manganese sulfide inclusions.

- In-plant assessment of crud buildup in crevices is vital. The extent of crevice blockage and the nature of the crud must be determined.

- The extent of flushing within a realistic safe-end (i.e, with crud blockage) must be determined.

Once these experiments and in-plant observations have been carried out, further recommendations can be made concerning these crevice regions.

Appendix A

RECIPE FOR MODELING OF THE LOCAL ELECTROCHEMICAL CONDITIONS IN CRACKS AND CREVICES

The development of an appropriate model to predict the local electrochemistry in cracks and crevices requires a range of information regarding the mass transport and reactions in these regions. In order to focus attention on the detailed requirements for the development and successful application of such a model, a compilation of the necessary information is presented in this appendix (*1*). This list of necessary information is separated into three sections : information needed or questions that must be answered to physically describe the problem; information concerning the mathematical description of the problem, and necessary data.

Physical Description of Problem

The first step in the modeling of any problem is the physical description of the problem. A detailed understanding of the physical requirements of the problem is necessary for the development of an appropriate model. This physical description includes the following information.

- Is the cavity to be modeled as a crack or a crevice? If the former, is it a stress corrosion crack or a corrosion fatigue crack?

- The alloys involved must be known.

- The geometry of the cavity must be specified.

- Any reactions that could be occurring within the region must be listed. This includes homogeneous equilibrium and radiolysis reaction and heterogeneous electrochemical reactions (both anodic and cathodic), chemical dissolution reactions and precipitation reactions.

- The initial and boundary conditions must be specified (i.e., the bulk environment)

- Fluid flow in the cavity region may occur as a consequence of natural convection, motion of the bulk solution past the mouth of the cavity and cyclic displacement of the cavity walls. An understanding of the convective motion within the occluded region must be developed.

Mathematical Description of Problem

Once a physical description of the problem is known, the mathematical description and model can be developed. This involves using the physical description of the model to decide which mathematical terms must be used and the reasonable approximations that can be made. It must be noted that any assumptions or simplifications made will limit the application of the model. Great care must be taken in order to ensure that the assumption made do not restrict the model application to the point of it being inappropriate for use on the problem which you are trying to model. The following information is needed :

- Specific geometry must be chosen for the model (i.e., parallel-sided, tapered, or wedge shaped)

- A geometry for the cavity tip region must be specified (i.e., blunt or rounded tip)

- An expression for the width of the crevice as a function of position, and, possibly, time is necessary. In the case of corrosion fatigue modeling, this requires expressions for CMOD (crack mouth opening displacement) and CTOD (crack tip opening displacement) as a function of all necessary parameters (time, frequency, crack length, positions of load line, etc.)

- It is usually necessary to reduce the problem to a one dimensional form. This requires the assumption that the sides of the region are sealed in the through-thickness direction and that the cavity is sufficiently narrow to permit averaging across the width.

- The use of dilute solution theory will greatly simplify the problem. The validity of this assumption should be assessed. In practice, full treatment of concentrated solute theory for a number of species reactions can be prohibitively complex.

- A descision must be made as to whether steady state analysis is sufficient. Attention must be given to the possibility of multiple steady states (as described in this thesis).

- To develop the mathematical model, a choice must be made as to what transport terms should be included and what type of reaction processes should be included in the mass balance formula of the model.

  -- Diffusion and ion migration are always necessary in modeling electrochemistry within cracks or crevices (except in very limited circumstances).

  -- If convection is included as a necessary mode of transport, the velocity of the fluid as a function of time and position must be specified.

- The range homogeneous equilibrium reactions or radiolysis reactions must be identified.

- Heterogeneous reactions occurring on the walls such as electrochemical reaction (both anodic and cathodic are important), chemical dissolution or precipitation must be considered.

- The mathematical equations which describe the above conditions must be developed.

- Boundary conditions must be specified at both the cavity mouth and tip. It is usually reasonable to neglect the moving boundary nature of the system except at very high growth rates in cracks.

- Initial conditions for the cavity must be specified for transient problems.

- A robust numerical scheme is necessary to solve the equations that have been developed. This scheme should be tested using initially simple conditions and applied progressively.

Input Data

A reliable data base is necessary for any model. The more accurate and reliable the input data are, the more 'realistic' the predictions of the model will be. The output of any model is only as good as the assumptions that have been made and the data that is put into the model. The following input data will be needed.

- Bulk chemistry to which the cavity is exposed.

- The composition of the alloy.

- Diffusion coefficients for all dissolved species.

- Rate constants for homogeneous reactions. These can be chosen from equilibrium data and the assumption of fast reaction kinetics.

- Solubility limits for appropriate species. Kinetics for precipitation must be decided but may artificially set to give $\Omega \cong 1$, where Ω is the degree of supersaturation..

- Kinetics of electrochemical reactions including (both anodic and cathodic)

- concentration dependence
- potential dependence

It must be noted that the kinetics of processes occurring on the walls of the cavity may be significantly different from those occurring at the tip, and, therefore, must be specified separately. Also, the kinetics of electrochemical reactions occurring at the tip may be time dependent because the metal at the tip may go through cycles of being bare then building up a film which ruptures repeating the cycle.

- Kinetics of any chemical dissolution processes that may be occurring.

- The rate of production of species by radiolysis as a function of dose rate and type of radiation.

- The possible effect of temperature on any of the above data.

Thus, by following the above recipe it is possible to develop a rigorous and appropriate model for the prediction of the local electrochemical conditions within any occluded region. It cannot be emphasized enough that any approximations or assumptions made will limit the application of the model, and, therefore, must be made with great care. Also, after the model has been developed and is being applied, the quality of the input data will also limit the accuracy of the predictions.

References

[A-1] M. Psaila-Dombrowski and A. Turnbull, MIT Memo dated February 1989.

Appendix B

IMPLICATIONS OF THE NONLINEARITY OF THE FLUX EQUATION

The flux of the species i in one dimension (ignoring convection) is given by

$$J_i = - D_i \frac{\partial C_i}{\partial x} - z_i \mu_i F C_i \frac{\partial \phi}{\partial x} \qquad (B-1)$$

where J_i = flux of species i

D_i = diffusion coefficient of species i

C_i = concentration of species i

z_i = charge of species i

μ_i = ionic mobility of species i

F = Faraday's Constant

ϕ = potential

For the case of dilute solutions, the Nernst-Einstein equation, as described by

$$D_i = \frac{\mu_i}{R T} \qquad (B-2)$$

(where R is the gas constant and T is temperature) holds, and the flux equation becomes

$$J_i = - D_i \frac{\partial C_i}{\partial x} - \frac{z_i D_i F}{R T} C_i \frac{\partial \phi}{\partial x} \qquad (B-3)$$

Many authors use the equation to solve for the steady state concentration profile for non-reacting species, e.g. Na^+ and Cl^- ions (*1-9*). Their approach is as follows. First, at steady state, species that are not being produced or consumed in solution or on the walls or tip of the occluded region, have a flux equal to zero. Thus, Equation A-3 becomes

$$0 = - D_i \frac{\partial C_i}{\partial x} - \frac{z_i D_i F}{R T} C_i \frac{\partial \phi}{\partial x} \qquad (B-4)$$

The diffusion term is brought to the left hand side of the equation and the total equation is divided by the diffusion coefficient, D_i, resulting in the following equation

$$\frac{\partial C_i}{\partial x} = - \frac{z_i F}{R T} C_i \frac{\partial \phi}{\partial x} \qquad (B-5)$$

The partial derivatives are changed to total derivatives and the equation is divided by C_i giving

$$\frac{dC_i}{C_i} = - \frac{z_i F}{R T} d\phi \qquad (B-6)$$

Equation A-6 is integrated with the boundary condition

$$x = L \qquad \begin{matrix} C_i = C_{i,bulk} \\ \phi_i = 0 \end{matrix} \qquad (B-7)$$

to yield

$$C_i = C_{i,bulk} \exp\left[- \frac{z_i F \phi}{R T} \right] \qquad (B-8)$$

Thus, the concentration of non-reacting species is expected to have an exponential dependence on f.

The approach is invalid because the implicit assumption in going from Equation A-5 to A-6 is that ϕ is <u>only</u> a function a function of x. In truth, ϕ is a complex function of the concentration of all species in solution and the total current density. It is through these unknowns that ϕ is a function of x. Since ϕ is a function of the concentrations of all species in solution, Equation A-5 is <u>nonlinear</u> and, therefore, one cannot integrate Equation A-6 as is done by these modelers. This is easier to see if one examines the equation for the total current density in solution

$$i = F \sum_j z_j J_i = - F \left[\sum_j z_j D_j \frac{\partial C_j}{\partial x} + \sum_j \frac{z_j^2 F D_j}{R T} C_j \frac{\partial \phi}{\partial x} \right] \qquad (B-9)$$

Rearranging this equation and solving for $\partial\phi/\partial x$ results in

$$\frac{\partial \phi}{\partial x} = - \left[\frac{i + F \sum_j z_j D_j \frac{\partial C_j}{\partial x}}{\frac{F^2}{R T} \sum_j z_j^2 D_j C_j} \right] \qquad (B-10)$$

Equation A-9 shows the complex dependence of ϕ on the concentration and the concentration profiles of all the species in solution. This equation can be substituted into equation A-5 giving

$$\frac{\partial C_i}{\partial x} = \frac{z_i F}{R T} C_i \left[\frac{i + F \sum_j z_j D_j \frac{\partial C_j}{\partial x}}{\frac{F^2}{R T} \sum_j z_j^2 D_j C_j} \right] \qquad (B\text{-}11)$$

which clearly shows nonlinearity. For the same reason the flux equation is also nonlinear. Thus the Equation A-8 was derived ignoring this nonlinearity and is not generally valid. It may be a reasonable approximation in cases where concentration gradients are not great and the current is primarily carried by ion migration, though this has not been proven.

REFERENCES

(1) R.A.H. Edwards, PhD Thesis, Dept. of Metallurgy, Delft Univ. of Tech., Netherlands

(2) D.D. MacDonald and M. Urquidi-MacDonald, "Modeling of the Electrochemistry of Stress Corrosion Cracks in Sensitized Type 304 SS in Boiling Water Reactors", presented at 4th Int. Symposium on Environmental Degradation of Materials in Nuclear Power Systems - Water Reactors, 6-10 August, 1989, Jekyll Island, GA, USA, D. Cubicotti, chairman.

(3) M.J. Danielson, C.A. Oster, and R.H. Jones, Corrosion Chemistry within Pits, Crevices and Crack", A. Turnbull, ed., HMSO, 1987, p. 213-242.

(4) C.A. Oster and M.J. Danielson, PNL-5821, 1986

(5) S.M. Gravano and J.R. Galvele, Corr. Sci., vol. 24, p. 517, 1984

(6) A. Turnbull and J.G.N. Thomas, J. Electrochem. Soc., vol. 129, p. 1412, 1982.

(7) B.G. Ateya and H.W. Pickering, J. Electrochem. Soc., vol. 122, p. 1018, 1975.

(8) D.A. Vermilyea and C.S. Tedmon, Jr., J. Electrochem. Soc., vol. 117, p. 437, 1970.

(9) T.R. Beck and E.A. Grens II, J. Electrochem. Soc., vol. 116, p. 177, 1969.

Appendix C

DERIVATION OF AVERAGED CONSERVATION OF MASS EQUATION

To simplify the numerical and computational aspects of solving the coupled set of nonlinear transport equations necessary to model the electrochemistry within cracks and crevices the multidimensional governing mass conservation equation (for a crack or crevice with closed sides) is averaged. In order to average the velocity and the governing mass transport equations. The averaging described in this thesis follows that derived by Turnbull et al (*1,2*).

VELOCITY

For incompressible fluids, the continuity equation can be given by

$$\frac{\partial v_x}{\partial x} + \frac{\partial v_y}{\partial y} = 0 \qquad (C-1)$$

where v_x = velocity in x direction and v_y = velocity in y direction,so

$$\int_{-h}^{h} \left(\frac{\partial v_x}{\partial x} + \frac{\partial v_y}{\partial y} \right) dy = 0 \qquad (C-2)$$

Using Leibnitz's rule,

$$\frac{\partial}{\partial x}\int_{-h}^{h} v_x \, dy = \int_{-h}^{h} \frac{\partial v_x}{\partial x} dy + (v_x)_h \frac{\partial h}{\partial x} + (v_x)_{-h} \frac{\partial h}{\partial x} \qquad (C-3)$$

substituting Equation C-3 into Equation C-2 yields

$$\frac{\partial}{\partial x}\int_{-h}^{h} v_x \, dy - \frac{\partial h}{\partial x}[(v_x)_h + (v_x)_{-h}] + (v_x)_h - (v_x)_{-h} = 0 \qquad (C-4)$$

From symmetry

$$\begin{aligned} (v_y)_h &= -(v_y)_{-h} \\ (v_x)_h &= (v_x)_{-h} \end{aligned} \qquad (C-5)$$

therefore

$$\frac{\partial}{\partial x}\int_{-h}^{h} v_x \, dy - 2(v_x)_h \frac{\partial h}{\partial x} + 2(v_x)_h = 0 \qquad (C-6)$$

From the geometry of the model cavity

$$\begin{aligned} x &= r\cos[\theta(t)] \\ y &= h_0(t)\ r\sin[\theta(t)] \end{aligned} \qquad (C-7)$$

Using these relationships the velocities can be derived,

$$(v_x)_h = \dot{x} = r\,\dot{\theta}(t)\sin\theta(t)$$
$$(v_y)_h = \dot{y} = \dot{h}_0(t) + r\dot{\theta}(t)\cos\theta(t) \qquad \text{(C-8)}$$

These velocities can then be substituted into the later part of Equation C-6 to give

$$(v_y)_h - (v_x)_h \frac{\partial h}{\partial x} = \dot{h}_0 + r\,\dot{\theta}(t)\cos\theta(t) + \tan\theta(t)\left(r\,\dot{\theta}(t)\sin\theta(t)\right)$$
$$= \dot{h}_0 + \frac{r\,\dot{\theta}(t)}{\cos\theta(t)} = \dot{h}_0 + \frac{x\,\dot{\theta}(t)}{\cos^2\theta(t)} \qquad \text{(C-9)}$$

Since θ is very small

$$(v_y)_h - (v_x)_h \frac{\partial h}{\partial x} \approx \dot{h}_0 + x\,\dot{\theta}(t) \qquad \text{(C-10)}$$

By defining the average velocity as

$$\bar{v}_x = \frac{1}{2h}\int_{-h}^{h} v_x\,dy \qquad \text{(C-11)}$$

Equation C-6 becomes

$$\frac{\partial}{\partial x} 2h\,\bar{v}_x - 2\left(\dot{h}_0 + x\,\dot{\theta}\right) = 0 \qquad \text{(C-12)}$$

Since $\dot{h}_0$(dot) and $\dot{\theta}$(dot) did not vary with x, the Equation C-2 can be integrated to give the average velocity,

$$\bar{v}_x = \frac{\dot{h}_0 + x\,\dot{\theta}(t)}{h} \qquad (C\text{-}13)$$

MASS CONSERVATION EQUATIONS

In general, the basic mass conservation equation for a dissolved species is given by

$$\frac{\partial C}{\partial t} = -\nabla \cdot J + \sum_j R_j \qquad (C\text{-}14)$$

where C = concentration

J = flux

t = time

R = homogeneous reaction rate

In a crack or crevice with the sides sealed, this equation is reduced to two dimensions as shown in Figure C-1. The governing equation becomes

$$\frac{\partial C}{\partial t} = -\frac{\partial J_x}{\partial x} - \frac{\partial J_y}{\partial y} + \sum_j R_j \qquad (C\text{-}15)$$

This equation can be averaged over the y dimension as shown below

$$\int_{-h}^{h} \frac{\partial C}{\partial t} = -\int_{-h}^{h} \frac{\partial J_x}{\partial x}\,dy - \int_{-h}^{h} \frac{\partial J_x}{\partial x}\,dy + \int_{-h}^{h} \sum_j R_j\,dy \qquad (C\text{-}16)$$

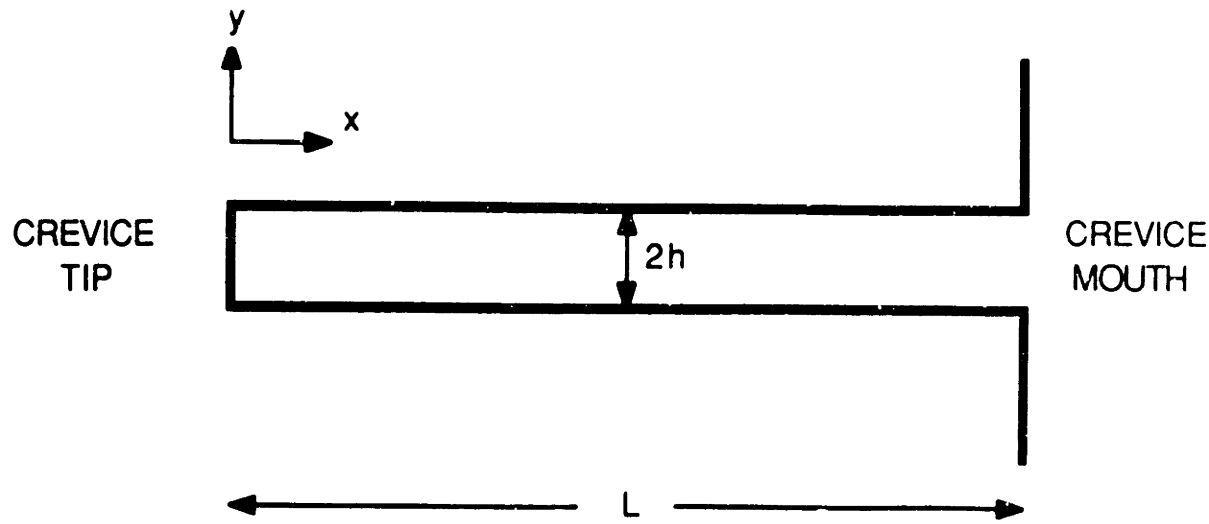

(a) Model crevice.

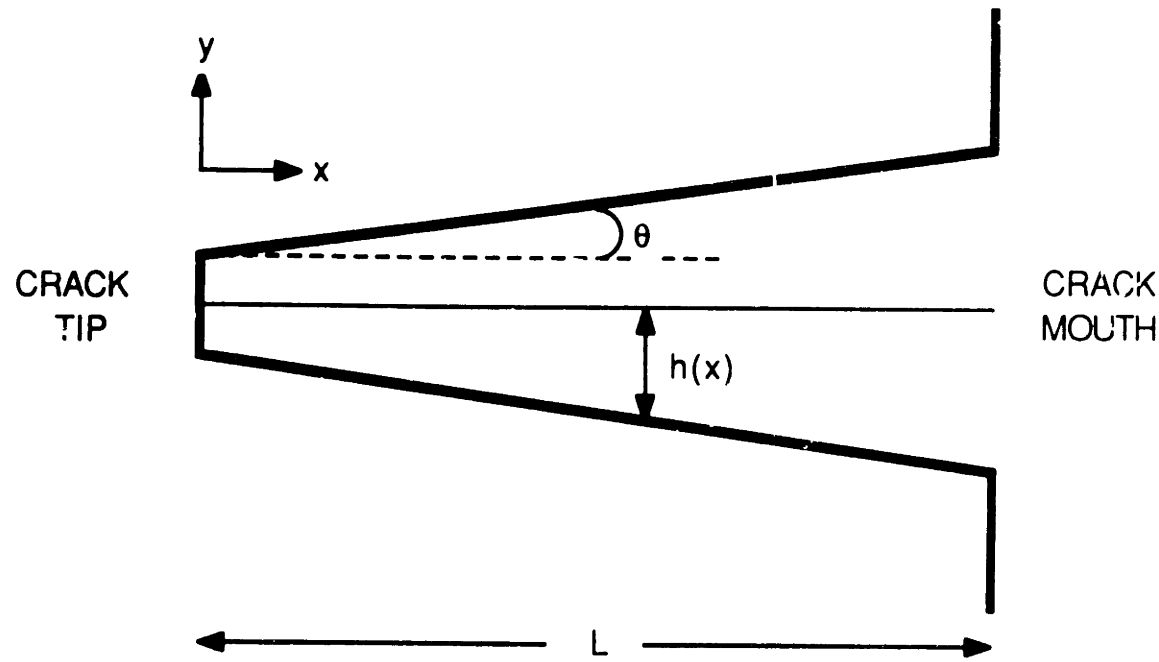

(b) Model crack.

Figure C-1. Geometry used by model for (a) crevice and (b) crack.

Now, using Leibnitz's rule,

$$\frac{\partial}{\partial t}\int_{-h}^{h} C\,dy = \int_{-h}^{h} \frac{\partial C}{\partial t}\,dy + \dot{h}\,[C_h + C_{-h}]$$

$$\frac{\partial}{\partial x}\int_{-h}^{h} J_x\,dy = \int_{-h}^{h} \frac{\partial J_x}{\partial x}\,dy + \frac{\partial h}{\partial x}[(J_x)_h + (J_x)_{-h}] \qquad (C\text{-}17)$$

Rearranging these equations and substituting into Equation C-6 results in

$$\frac{\partial}{\partial t}(2h\bar{C}) - \dot{h}\,[C_h + C_{-h}] = -\frac{\partial}{\partial x}(2h\bar{J}_x) + \frac{\partial}{\partial x}[(J_x)_h + (J_x)_{-h}]$$

$$- (J_y)_h + (J_y)_{-h} + 2h\sum_j \bar{R}_j \qquad (C\text{-}18)$$

where $\bar{R}_j$ is the homogeneous reaction rates based on the average concentration and average concentrations and fluxes defined by

$$\bar{C} = \frac{1}{2h}\int_{h}^{h} C\,dy$$

$$\bar{J}_x = \frac{1}{2h}\int_{-h}^{h} J_x\,dy \qquad (C\text{-}19)$$

From symmetry

$$C_h = C_{-h}$$
$$(J_y)_h = -(J_y)_{-h} \qquad (C\text{-}20)$$
$$(J_x)_h = (J_x)_{-h}$$

These relationships, given by Equations C-20, are substituted into Equation C-18. The resulting mass transport equation is

$$\frac{\partial}{\partial t}(h\bar{C}) - \dot{h}C_h = -\frac{\partial}{\partial x}(h\bar{J}_x) + (J_x)_h\frac{\partial h}{\partial x} - (J_y)_h + h\sum_j R_j \qquad (C\text{-}21)$$

The fluxes on the walls of the crack or crevice are given by

$$(J_x)_h = (Cv_x)_h - D\left(\frac{\partial C}{\partial x}\right)_h - \frac{z\,D\,F}{R\,T}\left(C\frac{\partial \phi}{\partial x}\right)_h$$
$$(J_y)_h = (Cv_y)_h - D\left(\frac{\partial C}{\partial y}\right)_h - \frac{z\,D\,F}{R\,T}\left(C\frac{\partial \phi}{\partial y}\right)_h \qquad (C\text{-}22)$$

Substituting these equations into equations C-21 results in

$$\frac{\partial}{\partial t}(h\bar{C}) - \dot{h}C_h = -\frac{\partial}{\partial x}(h\bar{J}_x) + \frac{\partial h}{\partial x}\left[(Cv_x)_h - D\left(\frac{\partial C}{\partial x}\right)_h - \frac{z\,D\,F}{R\,T}\left(C\frac{\partial \phi}{\partial x}\right)_h\right] \qquad (C\text{-}23)$$
$$- (Cv_y)_h + D\left(\frac{\partial C}{\partial y}\right)_h + \frac{z\,D\,F}{R\,T}\left(C\frac{\partial \phi}{\partial y}\right)_h + h\sum_j R_j$$

Since

$$\frac{\partial}{\partial x}\int_{-h}^{h} v_x\, dy = 2\left[(v_x)_h\frac{\partial h}{\partial x} - (v_y)_h\right] \qquad (C\text{-}24)$$

Equation C-23 becomes

$$\frac{\partial}{\partial t}(h\bar{C}) - hC_h = -\frac{\partial}{\partial x}(h\bar{J}_x) + C_h\frac{\partial}{\partial x}(h\bar{v}_x)$$

$$-\frac{\partial h}{\partial x}\left[D\left(\frac{\partial C}{\partial x}\right)_h + \frac{z\,D\,F}{R\,T}\left(C\frac{\partial \phi}{\partial x}\right)_h\right] \qquad (C\text{-}25)$$

$$+ D\left(\frac{\partial C}{\partial y}\right)_h + \frac{z\,D\,F}{R\,T}\left(C\frac{\partial \phi}{\partial y}\right)_h + h\sum_j R_j$$

The average flux $\bar{J}_x$ is given by

$$\bar{J}_x = \frac{1}{2h}\int_{-h}^{h}\left[Cv_x - D\frac{\partial C}{\partial x} - \frac{z\,D\,F}{R\,T}\left(C\frac{\partial \phi}{\partial x}\right)\right]dy$$

$$= \bar{C}\,\bar{v}_x - \frac{D}{2h}\left[\int_{-h}^{h}\frac{\partial C}{\partial x}\,dy + \frac{z\,D\,F}{R\,T}\bar{C}\int_{-h}^{h}\frac{\partial \phi}{\partial x}dy\right] \qquad (C\text{-}26)$$

Assuming $\bar{C}(x) \approx C(x,y)$. Using Leibnitz's rule

$$\frac{\partial}{\partial x}\int_{-h}^{h} C\,dy = \int_{-h}^{h}\frac{\partial C}{\partial x}\,dy + \frac{\partial h}{\partial x}[C_h + C_{-h}] \qquad (C\text{-}27)$$

and

$$\frac{\partial}{\partial x}\int_{-h}^{h}\phi\,dy = \int_{-h}^{h}\frac{\partial\phi}{\partial x}\,dy + \frac{\partial h}{\partial x}\left[\phi_h + \phi_{-h}\right] \qquad (C\text{-}28)$$

So, from symmetry

$$\bar{J}_x = \bar{C}\,\bar{v}_x - \frac{D}{2h}\left[\frac{\partial}{\partial x}\int_{-h}^{h} C\,dy - \frac{\partial h}{\partial x}\left[C_h + C_{-h}\right]\right] - \frac{zDF}{2hRT}\bar{C}\left[\frac{\partial}{\partial x}\int_{-h}^{h}\phi\,dy - \frac{\partial h}{\partial x}\left[\phi_h + \phi_{-h}\right]\right] \qquad (C\text{-}29)$$

or, using the definition for $\bar{C}$ and $\bar{\phi}$,

$$\bar{J}_x = \bar{C}\,\bar{v}_x - \frac{D}{2h}\left[\frac{\partial}{\partial x}(2h\bar{C}) - 2C_h\frac{\partial h}{\partial x}\right] - \frac{zDF}{2hRT}\bar{C}\left[\frac{\partial}{\partial x}(2h\phi) - 2\phi_h\frac{\partial h}{\partial x}\right] \qquad (C\text{-}30)$$

Assuming $C_h \approx \bar{C}$,

$$\bar{J}_x = \bar{C}\,\bar{v}_x - \frac{D}{h}\left[\bar{C}\frac{\partial h}{\partial x} + h\frac{\partial\bar{C}}{\partial x} - \bar{C}\frac{\partial h}{\partial x}\right] - \frac{zDF}{hRT}\bar{C}\left[\bar{\phi}\frac{\partial h}{\partial x} + h\frac{\partial\bar{\phi}}{\partial x} - \bar{\phi}\frac{\partial h}{\partial x}\right] \qquad (C\text{-}31)$$

resulting in

$$\bar{J}_x = \bar{C}\,\bar{v}_x - D\frac{\partial \bar{C}}{\partial x} - \frac{zDF}{RT}\bar{C}\frac{\partial \bar{\phi}}{\partial x} \qquad (C\text{-}32)$$

Substituting Equation C-31 into Equation C-28 and assuming

$$C_h \approx \bar{C}$$

$$\frac{\partial h}{\partial x}\left(\frac{\partial C}{\partial x}\right)_h \approx \frac{\partial h}{\partial x}\left(\frac{\partial \bar{C}}{\partial x}\right) \qquad (C\text{-}33)$$

$$\frac{\partial h}{\partial x}\left(\frac{\partial \phi}{\partial x}\right)_h \approx \frac{\partial h}{\partial x}\left(\frac{\partial \bar{\phi}}{\partial x}\right)$$

gives

$$\frac{\partial}{\partial t}(h\bar{C}) - hC_h = -h\frac{\partial \bar{J}_x}{\partial x} - \frac{\partial h}{\partial x}\left[\bar{C}\,\bar{v}_x - D\frac{\partial \bar{C}}{\partial x} - \frac{zDF}{RT}\bar{C}\frac{\partial \bar{\phi}}{\partial x}\right]$$

$$+ C_h\left[h\frac{\partial \bar{v}_x}{\partial x} + \bar{v}_x\frac{\partial h}{\partial x}\right] - \frac{\partial h}{\partial x}\left[D\left(\frac{\partial C}{\partial x}\right)_h + \frac{zDF}{RT}\left(C\frac{\partial \phi}{\partial x}\right)_h\right] \qquad (C\text{-}34)$$

$$+ D\left(\frac{\partial C}{\partial y}\right)_h + \frac{zDF}{RT}\left(C\frac{\partial \phi}{\partial y}\right)_h + h\sum_j R_j$$

Simplifying this equation gives

$$\frac{\partial \bar{C}}{\partial t} = - \frac{\partial \bar{J}_x}{\partial x} + \bar{C} \frac{\partial \bar{v}_x}{\partial x} + \frac{D}{h}\left(\frac{\partial C}{\partial y}\right)_h + \frac{z D F}{h R T}\left(C \frac{\partial \phi}{\partial y}\right)_h + \sum_j R_j \qquad (C\text{-}35)$$

In general the flux normal to the wall is given by

$$D \frac{\partial C}{\partial d_n} + \frac{zDF}{RT} \bar{C} \frac{\partial \phi}{\partial d_n} = R_{het} \qquad (C\text{-}36)$$

where R_{het} = rate of heterogeneous reactions

d_n = direction normal to the surface

Thus,

$$D\left(\frac{\partial C}{\partial y}\right)_h + \frac{zDF}{RT} \bar{C}\left(\frac{\partial \phi}{\partial y}\right)_h = \frac{R_{het}}{\cos\theta} + \tan\theta\left[D \frac{\partial C}{\partial x} + \frac{zDF}{RT} \bar{C} \frac{\partial \phi}{\partial x}\right] \qquad (C\text{-}37)$$

and, since the angle θ is small and assuming $C \approx \bar{C}$ Equation C-33 becomes

$$\frac{\partial \bar{C}}{\partial t} = - \frac{\partial \bar{J}_x}{\partial x} + \bar{C} \frac{\partial \bar{v}_x}{\partial x} + \frac{\theta D}{h} \frac{\partial \bar{C}}{\partial x} + \frac{\theta z D F}{h R T} \bar{C} \frac{\partial \bar{\phi}}{\partial x} + \sum_j R_j + \sum_j \frac{R_{j,het}}{h} \qquad (C\text{-}38)$$

In the text of this thesis $\bar{C}$ is C.

REFERENCES

(1) A. Turnbull, Mat. Sci. and Tech., vol. 1, pp. 700-710, 1985.

(2) A. Turnbull and D.H. Ferris, Corr. Sci., vol. 27, pp. 1323-1350, 1987.

APPENDIX D

DIFFERENCING OF GOVERNING TRANSPORT EQUATION

The governing mass transport equation used in this model is given by

$$\frac{\partial C}{\partial t} = D\frac{\partial^2 C}{\partial x^2} + \frac{zDF}{RT}\frac{\partial}{\partial x}\left(C\frac{\partial \phi}{\partial x}\right) - \frac{\partial}{\partial x}(Cv) + C\frac{\partial v_x}{\partial x} + \frac{\theta D}{h}\frac{\partial C}{\partial x} + \frac{\theta zDF}{hRT}C\frac{\partial \phi}{\partial x} + \sum_j R_j + \sum_j \frac{R_{j,wall}}{h} \qquad (D-1)$$

With Poisson's equation

$$\frac{\partial^2 \phi}{\partial x^2} = \frac{F}{\varepsilon}\sum_j z_j C_j \qquad (D-2)$$

and the total current density equation

$$I = F\sum_j z_j J_j = -F\left[\sum_j z_j D_j \frac{\partial C_j}{\partial x} + \sum_j \frac{z_j D_j F}{RT} C_j \frac{\partial \phi}{\partial x}\right] \qquad (D-3)$$

for the second and first derivatives of ϕ, respectively. As described in chapter three, the numerical method of lines is employed which converts the time dependent partial differential equations into time dependent ordinary differential equations by spatial

discretization of the right hand side of Equation D-1. This spatial discretization is the topic of this appendix.

Finite difference techniques are employed to convert the spatial partial differential equations into algebraic equations. This differencing takes the standard form of a central difference for the second order spatial partial derivative,

$$\frac{\partial^2 C}{\partial x^2} = \frac{C_{i+1} - 2C_i + C_{i-1}}{(\Delta x)^2} \qquad (D-4)$$

where i is the node number and Δx is the spatial increment. The first order spatial derivatives are differenced using an upwind-difference scheme which ensures convergence (*1*). Thus , the partial differential equation can be upwinded using a forward difference scheme,

$$\frac{\partial C}{\partial x} = \frac{C_{i+1} - C_i}{\Delta x} \qquad (D-5)$$

or a backward difference scheme,

$$\frac{\partial C}{\partial x} = \frac{C_i - C_{i-1}}{\Delta x} \qquad (D-6)$$

depending on the coefficient in front of the derivative. Using these differencing techniques, Equation D-1 can be converted to the following ordinary differential equation

$$\left(\frac{\partial C}{\partial t}\right)_{x=i} = D\left[\frac{C_{i+1} - 2C_i + C_{i-1}}{(\Delta x)^2}\right] - v_i\left(\frac{C_{i+1} - C_i}{\Delta x}\right)$$

$$+ \frac{zDF}{RT}\left[C_i\frac{F}{\varepsilon}\sum_j z_j C_j + \left(\frac{C_{i+1} - C_i}{\Delta x}\right)\left(\sum_j\left[Fz_jD_j\left(\frac{C_{i+1,j} - C_{i,j}}{\Delta x}\right)\right] - i\right)\right] \qquad (D-7)$$

$$+ \frac{\theta D}{h}\left(\frac{C_{i+1} - C_i}{\Delta x}\right) + \frac{\theta zDF}{hRT}C_i\left(\frac{\phi_{i+1} - \phi_i}{\Delta x}\right)$$

$$+ \sum_k R_{i,k} + \sum_k \frac{R_{i,k,wall}}{h}$$

In this equation all first order derivatives were upwinded using a forward difference scheme. Equation D-7 was used in LSODI to solve the system of nonlinear differential equations.

REFERENCE

(1) S.V. Patankar, Numerical Heat Transfer and Fluid Flow, McGraw-Hill, NY, 1980.

Appendix E

CALCULATIONS AND DATA

HOMOGENEOUS REACTION RATE CONSTANTS

Very few homogeneous reaction rate constants are known, especially at the temperature of interest in this thesis (ie. ≈ 300°C). Therefore it is necessary to assume reaction rate constants in order to predict the local electrochemistry using this model. The assumption used is based on fast reaction rate kinetics; the reactions are assumed to proceed at a rate which is sufficient to produce equilibrium in a short period of time. The only restriction is that the ratio of the forward reaction rate constant to the backward rate constant must be equal to the equilibrium constant, ie. for the reaction

$$A + B \underset{k_b}{\overset{k_f}{=}} C + D \qquad (E-1)$$

where A,B,C,D = species

k_f = forward rate constant

k_b = backward rate constant

the equilibrium constant is equal to

$$K_{eq} = \frac{k_f}{k_b} \qquad (E-2)$$

where K_{eq} is the equilibrium constant for the reaction shown in Equaiton E-1. Thus, in order to assume values for the forward and backward rate constants, the equilibrium constant for each reaction must be known.

Equilibrium constants can be calculated from the free energy change for the reaction using the following relationship (*1,2*)

$$\Delta G^{\circ} = -RT \ln K_{eq} \qquad (E-3)$$

where ΔG° = free energy change for the reaction,

R = gas constant,

T = temperature (K).

The free energy change for the general reaction

$$A + B + \ldots \underset{k_b}{\overset{k_f}{=}} a + b + \ldots \qquad (E-4)$$

is given by

$$\Delta G^{\circ}_{reaction} = \left(\Delta G^{\circ}_{f,a} + \Delta G^{\circ}_{f,b} + \ldots\right) - \left(\Delta G^{\circ}_{f,A} + \Delta G^{\circ}_{f,B} + \ldots\right) \qquad (E-5)$$

where $\Delta G_f°_i$ is the free energy of formation for species i. Thus the standard free energy change for the reaction is given by the sum of the free energies of formation of the products **minus** the free energies of formation of the reactants, or

$$\Delta G^{o}_{reaction} = \sum_{i} \Delta G^{o}_{f,i\ products} - \sum_{i} \Delta G^{o}_{f,i\ reactants} \qquad (E-6)$$

Some free energies of interest are given in Table E-1.

DIFFUSION COEFFICIENTS

There are no measured diffusion coefficients available for ionic species at 300°C. Diffusion coefficients have been calculated using a number of methods. The diffusion coefficients used in this thesis were calculated using the Stokes-Einstein equaiton, as given by

$$D_T = D_{25°C} \frac{\eta_{25°C}}{\eta_T} \left(\frac{T}{298.15}\right) \qquad (E-7)$$

where D_T = diffusion coefficient at temperature T

η_T = viscosity of solution at temperature T

T = temperature

This equation gives a rough estimate of the diffusion coeffients in high temperature waters (*3*). This equation assumes no change in the ionic radius (ie. hydration of the ion) as temperature increases. Table E-2 the diffusion coefficients used in the

Table E-1. Free Energies of Formation

Species	Free Energies of Formation (kcal/mole) 25 °C	300 °C	Ref.
Fe (s)	0	2.936	2
$Fe(OH)_2$ (aq)	-116.4	-98.7	1
Fe^{2+} (aq)	-18.8	-17.3	1
Fe_2O_3 (s)	-177.4	-159.8	1
$FeOH_+$ (aq)	-66.3	-57.2	1
H^+ (aq)	0	-2.928	2
H_2O (l)	-56.7	-46.8	1
H_2S (aq)	-16.1	-10.6	1
HS^- (aq)	-6.6	9.7	1
Mn (s)	0	0	1
Mn^{2+} (aq)	-54.5	-55.9	1
MnO (s)	-86.7	-81.9	1
$MnOH^+$ (aq)	-96.8	-88.0	1
Ni (s)	0	3.186	2
Ni^{2+} (aq)	-10.9	-9.6	1
$NiOH^+$ (aq)	-54.4	-43.0	1
NiO (s)	-50.6	-44.6	1
O_2	3.9	5.8	1
OH^- (aq)	-37.6	-17.3	1
S (s)	-9.5	-4.6	1
S^{2-} (aq)	11.0	28.7	1
$S_2O_4^{2-}$ (aq)	-162.5	-114.6	1
$S_2O_3^{2-}$ (aq)	-143.0	-95.2	1
SO_4^{2-} (aq)	-187.5	-138.8	1

Table E-2. Diffusion Coefficients

Species	Diffusion coefficients (dm^2/sec) 25 °C	300 °C	Ref.
H^+	9.34×10^{-7}	1.76×10^{-5}	5,6
OH^-	5.23×10^{-7}	9.8×10^{-6}	5,6
Na^+	1.35×10^{-7}	2.5×10^{-6}	5,6
Cl^-	2.03×10^{-7}	3.8×10^{-6}	5
Ni^{2+}	0.69×10^{-7}	1.3×10^{-6}	5
Mn^{2+}	0.681×10^{-7}	1.3×10^{-6}	6
SO_4^{2-}	1.065×10^{-7}	2.0×10^{-6}	6

modeling presented in this thesis (note : $\eta \approx 2.18$ lbm/hr ft and $\eta \approx .223$ lbm/hr ft (*4*).

SOLUBILITY LIMITS

The solubility reaction, which is assumed to take place on the walls of the cavity region, is given by

$$M^{2+} + 2\,OH^{-} \rightarrow MnO + H_2O \qquad (E-8)$$

or

$$M^{2+} + 2\,OH^{-} \rightarrow Mn(OH)_2 \qquad (E-9)$$

Thus the solubility of the metal ion can be expressed as

$$K_s = [M^{2+}][OH^{-}]^2 \qquad (E-10)$$

where Ks is the solubility product of the reaction. Some standard solubility limits are shown in Table E-3.

Table E-3. Metal ion solubility limit

Species	K_S at 300 °C	Ref.
Ni^{2+}	2.25×10^{-20}	2
Mn^{2+}	2.3×10^{-16}	2

CONDUCTIVITY

The conductivity of the solution is dependent on the amount of ions and type of ions present in the solution. The conductivity can be given by

$$\kappa = \frac{F^2}{RT} \sum_j z_j^2 D_j C_j \qquad (E-11)$$

where κ = conductivity of the solution,

z_i = the charge of species i

F = Faraday's constant

D_i = diffusion coefficient of species i

C_i = concentration of species i

R = gas constant

T = temperature

This equation assumes dilute solution theory.

REFERENCES

(1) H.E. Banner and R.V. Scheuerman, Handbook of Thermodynamical Data for Compounds and Aqueous Species, John Wiley & Sons, New York, 1978.

(2) D.D. Macdonald , T.E. Rummery, and M. Tomlinson, "Stability of Metal Oxides in High-Temperature Water", IAEA-SM-190/19.

(3) W.T. Linsday, Water Technology for Thermal Power Systems, P. Cohen, ed., ASME, New York, in press.

(4) M.M. El-Wakil, Nuclear Heat Transport, Internaional Textbook Co., Scranton, 1971.

(5) R. Parsons, Handbook of Electrochemical Constants, Academic Press, New York, 1959.

(6) R. Mills and V.M.M. Lobo, Self-diffusion in Electrolyte Solutions,

(7) P.R. Tremaine and LeBlanc, J. Chem. Therm., Vol. 12, pp. 521-538, 1988.

Appendix F

SAMPLE SYSTEM OF EQUATIONS

In this appendix, a sample system of equations will be presented in order to give a better understanding for the nature of the governing equations (i.e., Equations 3-7). A simple system of species will be considered consisting of six species : H^+, OH^-, Na^+, Cl^-, Ni^{2+}, and $NiOH^+$. The geometry of the cavity considered will be a crevice in order to simplify the equations somewhat. The following homogeneous and precipitation reactions will be considered

$$\begin{aligned} &(1)\ H^+ + OH^- = H_2O \\ &(2)\ Ni^{2+} + H_2O = NiOH^+ + H^+ \\ &(3)\ Ni^{2+} + H_2O = NiO + H_20 \end{aligned} \qquad (F-1)$$

The resulting set of governing equations is given by

$$\begin{aligned} \frac{\partial C_{H^+}}{\partial t} = D_{H^+}\frac{\partial^2 C_{H^+}}{\partial x^2} + \frac{Z_{H^+}D_{H^+}F}{RT}\frac{\partial}{\partial x}\left(C_{H^+}\frac{\partial \phi}{\partial x}\right) \\ - k_{f,1}C_{H^+}C_{OH^-} + k_{b,1} \\ + k_{f,2}C_{N^{2+}} - k_{b,2}C_{H^+}C_{NiOH^+} \end{aligned} \qquad (F-2)$$

$$\frac{\partial C_{OH^-}}{\partial t} = D_{OH^-}\frac{\partial^2 C_{OH^-}}{\partial x^2} + \frac{Z_{OH^-}D_{OH^-}F}{RT}\frac{\partial}{\partial x}\left(C_{OH^-}\frac{\partial \phi}{\partial x}\right) - k_{f,1}C_{H^+}C_{OH^-} + k_{b,1} - \frac{k_{f,3}}{h}\left(C_{Ni^{2+}}C_{OH^-}^2 - k_{s,3}\right) \quad (F-3)$$

$$\frac{\partial C_{Na^+}}{\partial t} = D_{Na^+}\frac{\partial^2 C_{Na^+}}{\partial x^2} + \frac{Z_{Na^+}D_{Na^+}F}{RT}\frac{\partial}{\partial x}\left(C_{Na^+}\frac{\partial \phi}{\partial x}\right) \quad (F-4)$$

$$\frac{\partial C_{Cl^-}}{\partial t} = D_{Cl^-}\frac{\partial^2 C_{Cl^-}}{\partial x^2} + \frac{Z_{Cl^-}D_{Cl^-}F}{RT}\frac{\partial}{\partial x}\left(C_{Cl^-}\frac{\partial \phi}{\partial x}\right) \quad (F-5)$$

$$\frac{\partial C_{Ni^{2+}}}{\partial t} = D_{Ni^{2+}}\frac{\partial^2 C_{Ni^{2+}}}{\partial x^2} + \frac{Z_{Ni^{2+}}D_{Ni^{2+}}F}{RT}\frac{\partial}{\partial x}\left(C_{Ni^{2+}}\frac{\partial \phi}{\partial x}\right) - k_{f,2}C_{Ni^{2+}} + k_{b,2}C_{H^+}C_{NiOH^+} - \frac{k_{f,3}}{h}\left(C_{Ni^{2+}}C_{OH^-}^2 - k_{s,3}\right) \quad (F-6)$$

$$\frac{\partial C_{NiOH^+}}{\partial t} = D_{NiOH^+}\frac{\partial^2 C_{NiOH^+}}{\partial x^2} + \frac{Z_{NiOH^+}D_{NiOH^+}F}{RT}\frac{\partial}{\partial x}\left(C_{NiOH^+}\frac{\partial \phi}{\partial x}\right) + k_{f,2}C_{Ni^{2+}} - k_{b,2}C_{H^+}C_{NiOH^+} \quad (F-7)$$

Equations F-2 through F-7 represent the set of governing equations used to solve for the unknown concentrations.

This page is intentionally blank.

Page 302

APPENDIX G

PROGRAM

In this appendix the program used to obtain the data presented in Chapter 4 is presented. The first section contains the program listing. The following two sections contain a sample input and a sample output from the program. It should be noted that the crack model has been developed separately and the two programs are presently being merged together to form a localized chemistry model package which is 'user friendly'. This package and an accompanying users manual with be available in the next few months.

PROGRAM LISTING

```
            PROGRAM CREVICE
C
C*************************************************************************C
C     WRITTEN BY : MAUREEN J. PSAILA-DOMBROWSKI
C     REVISION DATE : AUGUST 31, 1989
C*************************************************************************C
C   DESCRIPRTION
C
C     DIRENP4 IS A CODE WHICH MODELS THE LOCAL CHEMISTRY WITHIN A
C     STRESS CORROSION CRACK EXPOSED TO AN AQUEOUS ENVIRONMENT.
C     THE DRIVING ROUTINE DIRENP CALLS ALL THE NECESSARY SUBROUTINES
C     TO INPUT THE DATA, SOLVE THE PROBLEM, AND OUTPUT THE RESULTS
C     AND ANY ERROR MESSAGES. IN DIRENP NO POTENTIAL IS USED IN THE
C     MIGRATION TERM. POISSON'S EQUATION AND AN EQUATION FOR THE
C     TOTAL CURRENT IS USED INSTEAD. THE POTENTIAL IS CALCULATED AND
C     THEN USED TO CALCULATE THE TIP AND WALL CURRENTS.
C
C*************************************************************************C
C   DESCRIPTION OF SUBROUTINES IN DIRENP3
C
C     ADDAP       CALLED BY LSODI. SEE LSODI WRITEUP FOR COMPLETE
C                 DESCRIPTION.( FOR PARALLEL SIDED CRACK OR CREVICE)
C
C     LSODI       THIS SOLVER WAS DEVELOPED AT LAWRENCE LIVERMORE LABS.
C                 BY ALAN HINDMARSH AND JEFF PAINTER. IT CONSISTS OF A
C                 SET OF ROUTINES THAT CAN SOLVE A SET OF STIFF
C                 NONLINEAR ORDINARY DIFFERENTIAL EQUATIONS USING GEARS
C                 METHOD. IT CAN SOLVE A GENERAL PROBLEM OF THE FORM:
C                           a(i,j) YDOT(i) = g(i,j) Y(i)
C
C     OUT1        OUTPUTS ALL THE INITIAL INPUT DATA.
C
C     OUT2        OUTPUTS ALL THE INITIAL LSODI DATA.
C
C     OUT3        OUTPUTS CONCENTRATIONS AND POTENTIAL EVERY OUTPUT
C                 TIME.
C
C     REACT       SETS UP HOMOGENOUS REACTION TERMS
C
C     RESP        CALLED BY LSODI. SETS UP RESIDUAL EQUATIONS FOR
C                 SOLUTION. SEE LSODI WRITEUP FOR MORE COMPLETE
C                 DESCRIPTION.( FOR PARALLEL SIDED CRACK OR CREVICE)
C
C     SREACT      SETS UP SOLUBILITY REACTION TERMS.
C
C     TIP_I       CALCULATES THE INITIAL CURRENT AND POTENTIAL
C                 DISTRIBUTION USING BISECTION.
C
C     TREACT      SETS UP TIP REACTION TERMS.
C
C     WREACT      SETS UP WALL REACTION TERMS.
C
C     YINIT       INITIALIZES THE UNKNOWN ARRAY.
C
C*************************************************************************C
C   VAX VMS FILES CALLED:
C
C        SET.FIL:CONTAINS THE NAMES OF THE INPUT, OUTPUT, AND
C                PLOT FILES (CHANNEL 5, 6 AND 8, RESPECTIVELY)
C
```

```
C*****************************************************************C
C  VARIABLES:
C
C     A
C     ATOL        ABSOLUTE TOLERANCE FOR LSODI
C        ARS      ARRAY OF SPECIES NAMES
C     CK          STRESS INTENSITY FACTOR FOR TRAP. CRACK
C     CKMAX       CONSTANT FOR TRAP. CRACK (DUGDALE)
C     CM          POISON'S RATIO
C     CON2,3      CONSTANTS FOR TRAP. CRACK (DUGDALE)
C     C_TYPE      TELLS TYPE OF CRACK
C                          =          PARALLEL
C                          =          TRAPEZOIDAL
C     DCK         DELTA STRESS INTENSITY FACTOR TRAP.CRACK (DUGDALE)
C     DK          "      "      "      "      "          "(PARALLEL)
C     DKCON2      CONSTANT TRAP.CRACK (DUGDALE)
C     DIF         DIFFUSION COEFFICIENT
C     DCON        DIFFUSION COEFFICIENT DIVIDED BY DX*DX
C        DSRATE   DOSE RATE (RAD/S)
C        DHRATE   DOSE RATE FOR HIGH-LET PARTICLES (RAD/S)
C     E           YOUNG'S MODULUS (DUGDALE)
C     EA          ACTIVATION ENERGY (KJ/MOLE-K)
C     ETA         CONSTANT FOR VELOCITY CALCULATION (PARALLEL)
C     FCON        FARADAY'S CONSTANT
C     FILES       ARRAY CONTAINING THE NAMES OF SPECIES OUTPUT FILES
C     FLAG
C     FREQ        CRACK PUMPING FREQUENCY
C     FR(T)       CONSTANT FC/RGAS(TEM)
C        G        G-VALUE (# SPECIES/100 ev)
C        GH       G-VALUE FOR HIGH-LET PARTICLES (# SPECIES/100 ev)
C     GAMMA       CONSTANT FOR VELOCITY CALCULATION (PARALLEL)
C     H           ARRAY - CRACK HALF WIDTH
C     HCUR        STEP SIZE TO BE NEXT USED BY LSODI
C     HU          STEP SIZE LAST USED BY LSODI
C     I,II,J,K LOOP COUNTERS
C     IDERV       INDEX TO SEE IF DERIVATIVE SHOULD BE CALCULATED
C     IDIV
C     IFILES      UNIT NUMBERS FOR OUTPUT FILES
C     ITFLAG      FLAG FOR OUTPUT TIME STEPPING METHOD
C                          = 0
C                          = 1
C     IMXER       INDEX OF COMPONENT OF LARGEST MAGNITUDE IN ERROR VECTOR
C        INFIL    INPUT FILE NAME
C     IWORK       INTEGER WORKING ARRAY (LSODI)
C     KM          MEAN STRESS INTENTISTY FACTOR
C     KMAX        MAXIMUM "   "          "
C     KMIN        MINIMUM "   "          "
C     LENIW       LENGTH OF IWORK ACTUALLY REQUIRED BY LSODI
C     LENRW       LENGTH OF RWORK ACTUALLY REQUIRED BY LSODI
C     LYH
C     MF          METHOD FLAG FOR LSODI
C     MESHPTS     NUMBER OF MESH POINTS
C     MULTIME MULTIPLIER FOR OUTPUT TIME STEP
C        NEQ      NUMBER OF SPECIES
C     NJE         NUMBER OF JACOBIAN EVALUATIONS DONE SO FAR BY LSODI
C     NODEOUT     OUTPUT NODE
C     NPTS        NUMBER OF POINTS USED BY LSODI = NEQ*MESHPTS
C     NQU         METHOD ORDER LAST USED BY LSODI
C     NQUR        METHOD ORDER NEXT USED BY LSODI
C     NRE         NUMBER OF RESIDUAL EVALUATIONS DONE SO FAR BY LSODI
```

```
C        NRTN     NUMBER OF REACTIONS
C     NST         NUMBER OF STEPS TAKEN SO FAR BY LSODI
C     NWRTN       NUMBER OF WALL REACTIONS
C        MULTIME TIME MULTIPLIER FOR NEXT SOLUTION TIME
C     OTFILE      FULL OUTPUT FILE
C     P_TYPE      TELLS WHAT KIND OF PROBLEM IS BEING SOLVED
C                 P_TYPE=     1 : DIFF/I-MIGRATION
C                             2 : DIFF/I-M/CONVECTION (TRAP. CRACK)
C                             3 : DIFF/I-M/CONV (PARALLEL CRACK)
C        RGAS     UNIVERSAL GAS CONSTANT (VARIOUS UNITS)
C     RTOL        RELATIVE TOLERANCE FOR LSODI
C     RWORK       REAL WORKING ARRAY (LSODI)
C     SIGMA       YIELD STRESS (DUGDALE)
C     SR          STRESS RATIO = KMIN/KMAX
C     T           TIME
C     TCUR        CURRENT VALUE OF T
C        TDOSE    TOTAL DOSE (RADS)
C     TDOSEH
C        TEM      TEMPERATURE (KELVIN)
C        TEMR     REFERENCE TEMPERATURE FOR RATE CONSTANTS (KELVIN)
C        TFINAL   FINAL SOLUTION TIME (SEC)
C     TOLSF       TOLERANCE SCALE FACTOR USED BY LSODI
C     VAFEPP      CONSTANT FOR TRAP.CRACK (DUGDALE)
C     W
C     XHIGH       MAXIMUM POSITION
C     XLOW        MINIMUM POSITION
C     XLONG       CRACK LENGTH = XHIGH-XLOW
C     XINC        DELTA X
C     XINCSQ      XINC*XINC
C        Y        SPECIES CONCENTRATION VECTOR (LSODI)
C     YDOTI       TIME DERIVATIVE OF Y (LSODI)
C
C        LSODE VARIABLES ARE DEFINED IN THE LSODE WRITE-UP
C
C*************************  ***************************************C
C  DESCRIPTION OF NAMELIST
C
C     F           GIVES THE OUTPUT FILES FOR THE PROBLEM
C     L           GIVES PARAMETERS FOR LSODI
C     NAMES       CONTAINS NAMES OF SPECIES AND THEIR PARAMETERS
C     OUTPUT      CONTAINS OUTPUT FILES AND THEIR UNIT NUMBERS
C     SIZE        SIZES THE PROBLEM
C     STATE
C     TYPE        GIVES THE TYPE OF PROBLEM
C     TCURC       PARAMETERS FOR CRACK TIP CURRENT CALCULATION
C
C*********************************************************************C
C  FILE UNIT NUMBERS
C
C     5 = INPUT
C     6 = FULL OUTPUT
C     7 = HOMOGENOUS REACTION INPUT FILE
C     8 = WALL REACTION INPUT FILE
C     9 = TIP REACTION INPUT FILE
C     10 = SOLUBILITY REACTION INPUT FILE
C     IFILES(IS) = DATA OUTPUT FILES WHERE 'IS' IS THE SPECIES NUMBER
C                           NOTE : IFILES MUST BE >10
C
C*********************************************************************C
C  FUNCTIONS CALLED:
```

```
C
C       DEXP, DFLOTJ, DLOG10
C
C       LSODE FUNCTION CALLS ARE DEFINED IN THE LSODE WRITE-UP
C
C*********************************************************************C
C
      INCLUDE 'P.BLK'
      INCLUDE 'D.BLK'
      EXTERNAL RESP,ADDAP
C
C*********************************************************************C
C
      DIMENSION FILES(MNEQP2),IFILES(MNEQP2)
      DIMENSION RWORK(LRW),IWORK(LIW),ATOL(MNEQ*MNDX),ATOLI(MNEQ)
C     DIMENSION TDOSE(MA)
      DIMENSION Y(MA),YDOTI(MA),DKY(MA),ARS(0:MNEQ),YM(MNEQ),
     *                                  YM2(MNEQ)
C
      CHARACTER*8 ARS
      CHARACTER*35 INFILE,OTFILE,FILES
      INTEGER FLAG, P_TYPE, C_TYPE
      REAL*8 MULTIME
      REAL*8 KM,KMAX,KMIN
C
C*********************************************************************C
C  NAMELISTS
C
      NAMELIST/L/ IOPT,ITASK,RTOL,ITOL,ATOLI,RWORK,IWORK,IDERV,
     *                                  ISTATE,MF
      NAMELIST/STATE/ TEM,TEMR,DSRATE,DHRATE,EPS,EM
      NAMELIST/NAMES/ ARS,Z,TIPJ,DIF,G,GH
      NAMELIST/OUTPUT/ TOUT,TFINAL,TSTEP,MULTIME,TADD,TOUTCH
      NAMELIST/SIZE/ NS,NRTN,NWRTN,NTRTN,NSRTN,MESHPTS,XHIGH,XLOW,
     *                                  HIN
      NAMELIST/TOL/ RFACT,PFACT,PDLIM
      NAMELIST/TYPE/ P_TYPE,C_TYPE
      NAMELIST/F/ FILES,IFILES,OTFILE
      NAMELIST/TCURC/ PT1,CLAMBDA
      NAMELIST/SULPHUR/WALLF,TIPF,WALLT,TIPT,NSP1,P1,NSP2,P2,NSP3,P3
C
C*********************************************************************C
C  DEFAULT DATA FOR NAMELISTS
C
C     NOTE: MUST FIX THIS SECTION !!!!!!!!!!!!!!!!!!!!!!!!!!
C
      DATA TEM,TEMR/298.D0,289.D0/,DSRATE,DHRATE/0.0D0,0.0D0/
      DATA EPS/7.0D-9/
      DATA TSTEP/1.D-5/,TFINAL/100.D0/
      DATA MF/12/,ITOL/1/,ISTATE/1/,ITASK/1/,RTOL/1.D-5/
      DATA IDERV/0/,MULTIME/3.16227D0/
      DATA ITFLAG/0/
C
C*********************************************************************C
C  CONSTANTS
C
      DATA RGAS/8.314D0/,FR/11605.364D0/,FC/96487.D0/
C
C*********************************************************************C
C  OPEN FILE WHICH CONTAINS THE NAME OF THE INPUT FILE
```

```
C*************************************************************************C
C
C     PRINT*, 'DIRENP4'
C
      OPEN (5,FILE='DIRENP4.SET',STATUS='OLD',ERR=90)
      READ(5,100)INFILE
 90   CLOSE(5)
 100  FORMAT(A35)
C
C*************************************************************************C
C     OPEN FILE THAT CONTAINS NAMELISTS AND READ IN TYPE AND SIZE
C     NAMELIST
C*************************************************************************C
C
      OPEN (5,FILE=INFILE,STATUS='OLD')
C
      READ (5,NML=TYPE)
      READ (5,NML=SIZE)
C
C*************************************************************************C
C     READ IN OTHER NAMESLISTS
C*************************************************************************C
C
      READ (5,NML=F)
                READ (5,NML=STATE)
                READ (5,NML=OUTPUT)
      READ (5,NML=NAMES)
      READ (5,NML=TOL)
      READ (5,NML=TCURC)
      READ (5,NML=SULPHUR)
C
C*************************************************************************C
C     OPEN REACTION DATA FILES
C*************************************************************************C
C
      OPEN (7, FILE = 'REACT.DAT', STATUS = 'OLD')
      OPEN (8, FILE = 'WREACT.DAT', STATUS = 'OLD')
      OPEN (9, FILE = 'TREACT.DAT', STATUS = 'OLD')
C
C*************************************************************************C
C     CALCULATE CONSTANTS
C*************************************************************************C
C
      NEQ = NS + 1
C
      PDLIM = DABS(PDLIM)
      XLONG = XHIGH - XLOW
      XINC = XLONG/DFLOAT(MESHPTS-1)
      XINCSQ = XINC**2.0D0
      NPTS = NEQ*MESHPTS
      DO 130 I = 1,NEQ-1
          DCON(I) = DIF(I)/XINCSQ
 130  CONTINUE
C
      DO 140 I = 1,MESHPTS
C
          H(I) = HIN
C
 140  CONTINUE
C
```

```
      IDIV = MESHPTS/15
C
C     PRINT*, ' '
      PRINT*, 'NODES USED FOR OUTPUT'
      DO 150 I = 1,MESHPTS/IDIV
C
           PRINT*, (I-1)*IDIV+1
C
 150  CONTINUE
      PRINT*, MESHPTS
C
C*********************************************************************C
C     OPEN OUTPUT FILES
C*********************************************************************C
C
      OPEN (6,FILE=OTFILE,STATUS='NEW')
C
      DO 155 I = 1,NEQ
C
           OPEN (IFILES(I),FILE=FILES(I),STATUS='NEW')
C
 155  CONTINUE
C
C*********************************************************************C
C     CALL SUBROUTINE THAT OUTPUTS INITIAL INFORMATION
C*********************************************************************C
C
      CALL OUT1(INFILE,OTFILE,MULTIME,TFINAL,TOUT,EPS,NRTN,
     *                        NWRTN,NTRTN,NSRTN,MESHPTS,XLOW,XHIGH,TEM,TEMR,ARS,
     *                        Z,TIPJ,DIF,FILES,G,GH,NEQ,HIN,NS,EM,XINC,TOUTCH,TADD)
C
C*********************************************************************C
C     CONSTANTS FOR MIGRATION AND CRACK TIP CURRENT
C*********************************************************************C
C
      FC2 = FC*FC
      PCON = FC/EPS
      FRT = FR/(TEM)
      DO 160 II = 1,NEQ-1
           PCD(II) = Z(II)*DCON(II)
           PCM1(II) = PCD(II)*FRT*Z(II)
           PCM(II) = DIF(II)*FRT*Z(II)
C          PRINT*, PCD(II),' ',PCM1(II)
C
C*********************************************************************C
C       CONVERT G-VALUES FROM # spec/100 ev  TO  moles/l-rad
C*********************************************************************C
C
              GH(II) = GH(II)*1.033D-9
           G(II) = G(II)*1.033D-9
C
 160  CONTINUE
C
C*********************************************************************C
C     CALL SUBROUTINE THAT READS THE REACTION DATA AND SETS UP
C     REACTION COEFFICIENTS AND ORDER MATRICIES FOR THE HOMOGENEOUS
C     REACTIONS
C*********************************************************************C
C
      CALL REACT(NPTS,NEQ,ARS,TEM,TEMR)
```

```
C
C*****************************************************************C
C     CALL SUBROUTINE THAT READS THE REACTION DATA AND SETS UP
C     REACTION COEFFICIENTS AND ORDER MATRICIES FOR THE WALL
C     REACTIONS
C*****************************************************************C
C
      CALL WREACT(NPTS,NEQ,ARS,EM,FRT)
C
      DO 170 I = 1,NWRTN
C
          WALPHA(I) = WALPHA(I)*FRT
C
 170  CONTINUE
C
C*****************************************************************C
C     CALL SUBROUTINE THAT READS THE REACTION DATA AND SETS UP
C     REACTION COEFFICIENTS AND ORDER MATRICIES FOR THE CRACK TIP
C     REACTIONS
C*****************************************************************C
C
      CALL TREACT(NPTS,NEQ,ARS,EM,FRT)
C
      DO 180 I = 1,NTRTN
C
          TALPHA(I) = TALPHA(I)*FRT
C
 180  CONTINUE
C
C*****************************************************************C
C     CALL SUBROUTINE THAT READS THE REACTION DATA AND SETS UP
C     REACTION COEFFICIENTS AND ORDER MATRICIES FOR THE SOLUBILTY
C     REACTIONS
C*****************************************************************C
C
      CALL SREACT(NPTS,NEQ,ARS,TEM,TEMR)
C
C*****************************************************************C
C     OUTPUT CHEMICAL DISSOLUTION TERMS
C*****************************************************************C
C
      WRITE(6,185) WALLF,WALLT,TIPF,TIPT,NSP1,P1,NSP2,P2,NSP3,P3
 185  FORMAT(///10X,'CHEMICAL DISSOLUTION',
     *                    /15X,'WALLF = ',E10.2,5X,' WALLT = ',E10.2,
     *                    /15X,'TIPF = ',E10.2,5X,' TIPT = ',E10.2,
     *                    /15X,'NSP1 = ',I2,5X,' P1 = ',E10.2,
     *                    /15X,'NSP2 = ',I2,5X,' P2 = ',E10.2,
     *                    /15X,'NSP3 = ',I2,5X,' P3 = ',E10.2)
C
C*****************************************************************C
C     CALL SUBROUTINE THAT SETS INITIAL CONDITIONS
C*****************************************************************C
C
      CALL YINIT(Y,YDOTI,YM,TCH,EMCH,YM2,TCH2,EMCH2)
C
C*****************************************************************C
C     SET PARAMETERS FOR LSODI
C*****************************************************************C
C
      ITOL = 1
```

```
      RTOL = 1.0D-6
      DO 190 IS = 1,NEQ
          ATOL(IS) = 1.0D-6
  190 CONTINUE
      ITASK = 3
      ISTATE = 0
      IOPT = 0
      MF = 22
      RWORK(5) = 0.0D0
      RWORK(6) = 0.0D0
      RWORK(7) = 0.0D0
      RWORK(8) = 0.0D0
      RWORK(9) = 0.0D0
      RWORK(10) = 0.0D0
      IWORK(5) = 0
      IWORK(6) = 0
      IWORK(7) = 0
      IWORK(8) = 0
      IWORK(9) = 0
      IWORK(10) = 0
      RFACT = 1.0D-8
C
C*********************************************************************C
C     READ IN CHANGES TO LSODI INPUT PARAMETERS
C*********************************************************************C
C
      READ (5,NML = L)
      CLOSE(5)
      DO 210 IX = 1,MESHPTS
          DO 200 IN = 1,NEQ
                K = NEQ*(IX-1)
                ATOL(K+IN) = ATOLI(IN)
C               PRINT*, K,IN,K+IN,ATOL(K+IN),ATOLI(IN)
  200     CONTINUE
  210 CONTINUE
C
C*********************************************************************C
C     OUTPUT LSODI DATA
C*********************************************************************C
C
      CALL OUT2(ITOL,RTOL,ATOLI,ITASK,ISTATE,IOPT,MF,IWORK,RWORK,NEQ)
C
C*********************************************************************C
C     OUTPUT INITIAL CONCENTRAIONS AND POTENTIAL DISTRIBUTION
C*********************************************************************C
C
      TOLD = 0.0D0
      CALL OUT3(T,Y,RWORK,IWORK,IFILES,IDIV,TOLD,NEQ,MESHPTS,
     *                        Z,DIF,FRT,FC,ARS,TIPJ,XINC,EM,H)
C
C*********************************************************************C
C     CALL SOLVER
C*********************************************************************C
C
  280 CALL LSODI(RESP,ADDAP,JAC,NPTS,Y,YDOTI,T,TOUT,ITOL,RTOL,
     *                        ATOL,ITASK,ISTATE,IOPT,RWORK,LRW,IWORK,LIW,MF)
C
C*********************************************************************C
C       PRINT RESULTS OF PREVIOUS TIME STEP AND INCREMENT
C       THE TIME OR STOP AND PRINT FINAL RESULTS
```

```
C*********************************************************************C
C       CALCULATE THE TOTAL DOSE (TDOSE), AND PRINT THE RESULTS OF
C       THE LAST ITERATION
C*********************************************************************C
C
C     TDOSEL = DSRATE*T
C     TDOSEH = DHRATE*T
C
C*********************************************************************C
C     OUTPUT CONCENTRATIONS AND POTENTIAL
C*********************************************************************C
C
      CALL OUT3(T,Y,RWORK,IWORK,IFILES,IDIV,TOLD,NEQ,MESHPTS,
     *                      Z,DIF,FRT,FC,ARS,TIPJ,XINC,EM,H)
C
C*********************************************************************C
C     CHANGE MOUTH CONCENTRATIONS : EXCURSION IN CONCENTRATION OR
C     POTENTIAL
C*********************************************************************C
C
      IF(T.GE.TCH.AND.T.LT.TCH*5.0D0)THEN
C
          EM = EMCH
          ISTATE = 1
C
          DO 300 I = 1,NEQ
                 K = NEQ*(MESHPTS-1)
                 Y(K+I) = YM(I)
 300      CONTINUE
C
          DO 310 IT = 1,NTRTN
                 TCIO(IT) = TKCIO(IT)*DEXP(-TALPHA(IT)*EM)
 310      CONTINUE
C
          DO 320 IW = 1,NWRTN
                 WCIO(IW) = WKCIO(IW)*DEXP(-WALPHA(IW)*EM)
 320      CONTINUE
C
      ENDIF
C
      IF(T.GE.TCH2.AND.T.LT.TCH2*5.0D0)THEN
C
          EM = EMCH2
          ISTATE = 1
C
          DO 325 I = 1,NEQ
                 K = NEQ*(MESHPTS-1)
                 Y(K+I) = YM2(I)
 325      CONTINUE
C
          DO 330 IT = 1,NTRTN
                 TCIO(IT) = TKCIO(IT)*DEXP(-TALPHA(IT)*EM)
 330      CONTINUE
C
          DO 335 IW = 1,NWRTN
                 WCIO(IW) = WKCIO(IW)*DEXP(-WALPHA(IW)*EM)
 335      CONTINUE
C
      ENDIF
C
```

```
C*************************************************************************C
C     DETERMINE ERROR CONDITION OR END OF RUN AND TAKE APPROPRIATE
C     ACTION
C*************************************************************************C
C
      IF (ISTATE.LT.-1) GO TO 380
C
      IF (T.GE.TFINAL) GO TO 380
C
C*************************************************************************C
C       INCREMENT THE TIME WITH ADDITIVE TERM OR MULTIPLICATIVE TERM
C*************************************************************************C
C     TSTEP<0.0  ADDITIVE    ITFLAG=1
C     TSTEP>= 0.0            MULTIPLICATIVE         ITFLAG = 0
C*************************************************************************C
C
      IF(T.GE.TOUTCH) THEN
                 TOUT = T + TADD
      ELSE
                            TOUT=TOUT*MULTIME
      ENDIF
C
CCCCC             DON'T OVERSHOOT FINAL TIME REQUESTED
C
      IF(TOUT.GT.TFINAL)TOUT=TFINAL
C
CCCCC             IF TOO MANY STEPS RESET ISTATE AND CONTINUE CALCULATION
C
      IF (ISTATE.EQ.-1) ISTATE = 2
C
CCCCC             CONTINUE INTEGRATION
C
      PRINT*, ISTATE
      GO TO 280
C
C*************************************************************************C
C     PRINT OUT LSODI PARAMTERS FOR ANALYSIS
C*************************************************************************C
C
  380 HU = RWORK(11)
      HCUR = RWORK(12)
      TCUR = RWORK(13)
      TOLSF = RWORK(14)
      NST = IWORK(11)
      NRE = IWORK(12)
      NJE = IWORK(13)
      NQU = IWORK(14)
      NQUR = IWORK(15)
      IMXER = IWORK(16)
      LENRW = IWORK(17)
      LENIW = IWORK(18)
         WRITE (6,382)
  382 FORMAT (/80(1h_),/)
      WRITE (6,381)
  381 FORMAT(29X,'RUN STATISTICS')
      WRITE (6,382)
      WRITE (6,389) HU,HCUR,TCUR,TOLSF
  389 FORMAT(5X,/25H STEP SIZE LAST USED   =,E12.5,
     *                      5X,/25H STEP SIZE FOR NEXT     =,E12.5,
     *                      5X,/25H CURRENT VALUE OF T     =,E12.5,
```

```
     *                        5X,/25H TOLERANCE SCALE FACTOR=,E12.5)
      WRITE (6,390) LENRW,LENIW,NST,NRE,NJE,NQU,NQUR
  390 FORMAT(5X,/25H REQUIRED RWORK SIZE    = ,I10,
     *                        5X,/25H IWORK SIZE              = ,I10,
     *                        5X,/25H NUMBER OF STEPS         = ,I10,
     *                        5X,/25H # OF FUNC.- EVALS.      = ,I10,
     *                        5X,/25H # OF JACOB.- EVALS      = ,I10,
     *                        5X,/25H METHOD ORDER USED       = ,I10,
     *                        5X,/25H ORDER FOR NEXT STEP     = ,I10)
       WRITE (6,400) ISTATE
  400  FORMAT (///22H ERROR HALT...ISTATE =,I3)
C
C*********************************************************************C
C     OUTPUT Y IF ISTATE LT 0 (IE. FOR ERROR CONDITION)
C*********************************************************************C
C
      IF(ISTATE.LT.0)PRINT*, 'ERROR ISTATE < 0  :','Y   :',Y,
     *                                  'YDOTI   :',YDOTI
C
C*********************************************************************C
C     CLOSE OUTPUT FILE
C*********************************************************************C
C
      CLOSE(6)
C
C*********************************************************************C
C     END OF PROGRAM
C*********************************************************************C
C
      STOP
      END
C
C*********************************************************************C
C
C
C
      SUBROUTINE OUT1(INFILE,OTFILE,MULTIME,TFINAL,TOUT,EPS,NRTN,
     *                        NWRTN,NTRTN,NSRTN,MESHPTS,XLOW,XHIGH,TEM,TEMR,ARS,
     *                        Z,TIPJ,DIF,FILES,G,GH,NEQ,HIN,NS,EM,XINC,TOUTCH,TADD)
C
C*********************************************************************C
C     WRITTEN BY : MAURSEN J. PSAILA-DOMBROWSKI
C     REVISION DATE : JULY 22, 1989
C*********************************************************************C
C     LIST OF VARIABLES
C*********************************************************************C
C
      INCLUDE 'P.BLK'
C
      DIMENSION ARS(0:MNEQ),DIF(MNEQ),Z(MNS),FILES(MNEQP2),G(MNEQ),
     *                                  GH(MNEQ),TIPJ(MNS)
C
      REAL*8 MULTIME
      CHARACTER*8 ARS
      CHARACTER*9 TDATE,TTIME
      CHARACTER*35 INFILE,OTFILE,FILES
C
C*********************************************************************C
C
      CALL DATE(TDATE)
```

```
      CALL TIME(TTIME)
C
                WRITE (6,10)
 10     FORMAT(
     *           15X,    '*********************************************************',
     *           ,/ ,15X,'*                                                       *',
     *           ,/ ,15X,'*                DIRENP4 CODE OUTPUT                    *',
     *           ,/ ,15X,'*                                                       *',
     *           ,/,15X, '*********************************************************')
                WRITE (6,130)
      WRITE (6,105)TDATE,TTIME
                WRITE (6,130)
                WRITE (6,140)
                WRITE (6,130)
                WRITE (6,120) INFILE, OTFILE
C
      DO 50 I = 1,NEQ
C
          WRITE(6,300) ARS(I),FILES(I)
C
 50   CONTINUE
C
                WRITE (6,110) NS,NEQ,NRTN,NWRTN,NTRTN,NSTRTN,MESHPTS,XLOW,
     *                                 XHIGH,HIN,XINC,MESHPTS*NEQ+1
 105  FORMAT(10X, 38H                RUN DATE                = ,A9,
     *                 /10X, 38H                RUN TIME                = ,A9)
 110              FORMAT (/10X,'GENERAL DATA :',//,
     *            15X,38H  NUMBER OF SPECIES BEING EVALUATED = ,I5,/,
     *            15X,38H  NUMBER OF EQUATIONS EVALUATED     = ,I5,/,
     *                      15X,38H  NUMBER OF CHEMICAL REACTIONS      = ,I5,/,
     *            15X,38H  NUMBER OF WALL REACTIONS          = ,I5,/,
     *            15X.38H  NUMBER OF TIP REACTIONS           = ,I5,/,
     *            15X,38H  NUMBER OF SOLUBILITY REACTIONS    = ,I5,//,
     *                      15X,38H  NUMBER OF UNIFORM MESH POINTS     = ,I5,/,
     *          15X,38H  LEFT COORDINATE                     = ,D10.3,/,
     *          15X,38H  RIGHT COORDINATE                    = ,D10.3,/,
     *          15X,38H  INITIAL HALF WIDTH                  = ,D10.3,/,
     *          15X,38H  DELTA X                             = ,D10.3,/,
     *          15X,38H  NPTS + 1                            = ,I5,/)
 120              FORMAT( /10X,'FILES :',//,
     *                      16X,    ' INPUT FILE NAME                    = ',A20,/
     *            16X,   ' OUTPUT FILE NAME                  = ',A20,/)
 130              FORMAT(/80(1H=)/)
 140              FORMAT(37X,'INPUT')
C
                WRITE(6,200)TEM,TEMR,EM
 200            FORMAT(15X,  38H  TEMPERATURE                          = ,D10.3,
     *    /  15X,  38H  REFERENCE TEMPERATURE              = ,D10.3,
     *    /  15X,  38H  INITIAL BULK METAL POTENTIAL       = ,D10.3,/)
C
                WRITE (6,230) DSRATE,DHRATE,TFINAL,TOUT,EPS
 230            FORMAT (15X,38H  LOW LET DOSE RATE                  = ,D10.3,
     *           /15X,       38H  HIGH LET DOSE RATE                 = ,D10.3,
     *           //15X,      38H  FINAL TIME EVALUATION              = ,D10.3,
     *           /15X,      38H  INITIAL TIME STEP                  = ,D10.3,
     *           /15X,      38H  EPSILON                            = ,D10.3)
C
C*********************************************************************C
C      WRITE TIME STEP INCREMENT
C*********************************************************************C
```

```
C
               WRITE(6,270)MULTIME,TOUTCH,TADD
 270           FORMAT(15X,38H  TIME MULTIPLE                          = ,D10.3,/,
     *        15X,38H  TIME TO CHANGE FROM MULT. TO ADD  = ,D10.3,/,
     *        15X,38H  TIME ADDED TO TIME STEP           = ,D10.3)
C
 300 FORMAT(16X,' FILE FOR ',A8,16X,'= ',A10)
C
C    WRITE(6,540)
     DO 500 IS = 1,NEQ-1
C
         WRITE (6,550) ARS(IS),Z(IS),TIPJ(IS),DIF(IS),G(IS),GH(IS)
C
 500 CONTINUE
C
 540 FORMAT('1')
 550 FORMAT(/10X,'SPECIES : ',A8,/25X,'CHARGE   :  ',E10.3,
     *                      /25X,'CRACK TIP FLUX  :  ',E10.3,
     *                      /25X,'DIFFUSION COEFFICIENT : ',E10.3,
     *                      /25X,'G  : ',E10.3,
     *                      /25X,'GH : ',E10.3)
C
     RETURN
     END
C
C
C
C*********************************************************************C
C
     SUBROUTINE OUT2(ITOL,RTOL,ATOLI,ITASK,ISTATE,IOPT,MF,IWORK,
     *                                  RWORK,NEQ)
C
C*********************************************************************C
C    WRITTEN BY : MAUREEN J. PSAILA-DOMBROWSKI
C    REVISION DATE : JULY 22, 1989
C*********************************************************************C
C    THIS SUBROUTINE OUTPUTS THE LSODI PARAMTERS USED FOR RUN
C*********************************************************************C
     INCLUDE 'P.BLK'
C
     DIMENSION IWORK(LIW),RWORK(LRW),ATOLI(MNEQ)
C
     REAL*8 MULTIME
C*********************************************************************C
C      WRITE TIME CONTROL PARAMETERS
C*********************************************************************C
C
               WRITE(6,250) ITOL,RTOL
     DO 10 IS = 1,NEQ
         WRITE(6,260)ATOLI(IS)
 10  CONTINUE
     WRITE(6,270)ITASK,ISTATE,IOPT,MF
 250           FORMAT('1',//10X,'LSODI PARAMETERS : ',/
     *          /10X,38H  TOLERANCE FACTOR                    = ,I5,
     *          /10X,38H  RELATIVE TOLERANCE                  = ,D14.5)
C
 260 FORMAT(10X,38H  ABSOLUTE TOLERANCE                = ,D14.5)
C
 270 FORMAT(10X,38H  ITASK                             = ,I5,
     *          /10X,38H  ISTATE                           = ,I5,
```

```
     *          /10X,38H  IOPT                                  = ,I5,
     *          /10X,38H  MF                                    = ,I5)
C
     WRITE(6,300) RWORK(5),RWORK(6),RWORK(7),IWORK(5),IWORK(6),
     *                  IWORK(7)
 300 FORMAT(10X,38H  FIRST TIME STEP                    = ,E10.3,
     *               /10X,38H  MAX TIME STEP                         = ,E10.3,
     *               /10X,38H  MIN TIME STEP                         = ,E10.3,
     *               /10X,38H  MAX ORDER ALLOWED                     = ,I5,
     *               /10X,38H  MAX NUMBER OF INTERNAL STEPS          = ,I5,
     *               /10X,38H  MAX NUMBER OF MESSAGES                = ,I5,
     *                    /,'1')

     RETURN
     END
C
C
C
C*********************************************************************C
C
     SUBROUTINE OUT3(T,Y,RWORK,IWORK,IFILES,IDIV,TOLD,NEQ,MESHPTS,
     *                  Z,DIF,FRT,FC,ARS,TIPJ,XINC,EM,H)
C*********************************************************************C
C    WRITTEN BY : MAUREEN J. PSAILA-DOMBROWSKI
C    REVISION DATE : JULY 22, 1989
C*********************************************************************C
C    THIS SUBROUTINE OUTPUTS THE CONCENTRATIONS AND POTENTIAL AT
C    OUTPUT TIME
C*********************************************************************C
C    LIST OF VARIABLES
C
C    ARS                   ARRAY CONTAINING UNKNOWN NAMES
C    DIF                   DIFFUSION COEFFICIENTS FOR SPECIES I
C    FC                    FARADAY'S CONSTANT
C    FRT                   CONSTANT = F/RT
C    IDIV                  INTEGER USED TO CALCULATE OUTPUT NODES
C    IFILES                OUTPUT FILE UNIT NUMBERS FOR CONCENTRATIONS
C    IWORK                 INTEGER WORK ARRAY FOR LSODI
C    MESHPTS               NUMBER OF MESHPOINTS
C    NEQ                   NUMBER OF EQUATIONS
C    PT                    POTENTIAL ARRAY
C    RWORK                 REAL WORK ARRAY USED BY LSODI
C    T                     PRESENT TIME
C    TOLD                  OLD TIME FOR OUTPUT
C    Y                     UNKNOWN CONCENTRATION
C    Z                     CHARGE OF SPECIES I
C*********************************************************************C
     INCLUDE 'P.BLK'
C
     DIMENSION Y(1),RWORK(LRW),IWORK(LIW),IFILES(MNEQP2),
     *                  Z(MNS),DIF(MNEQ),ARS(0:MNEQ),TIPJ(MNS),H(MNDX)
C
     COMMON/TIP/ NTRTN,TALPHA(MNTR),TCIO(MNTR),KT(MNTR),TPOW(MNTR),
     *                  KOEFT(MNTR,MNEQ),TKCIO(MNTR),CTT(MNTR),ST(MNTR,0:MNEQ)
C
     COMMON/WALL/ NWRTN,WALPHA(MNWR),WCIO(MNWR),KW(MNWR),WPOW(MNWR),
     *                  KOEFW(MNWR,MNEQ),WKCIO(MNWR),CTW(MNWR),SW(MNWR,0:MNEQ)
C
     CHARACTER*8 ARS
C
```

```
C*********************************************************************C
C
      IF(T.GT.0.0D0)THEN
          ATS = (T-TOLD)/DFLOAT(IWORK(11))
          TOLD = T
      ENDIF
C
      COND = 0.0D0
C
      DO 50 IS = 1,NEQ-1
C
          COND = COND + Z(IS)*Z(IS)*DIF(IS)*FRT*FC*Y(IS)
C
 50   CONTINUE
C
C
      WRITE (6,500) T,RWORK(11),IWORK(11),ATS,COND,EM
      WRITE(6,550) (ARS(I),TIPJ(I),I=1,NEQ-1)
C
      IWORK(11) = 0
      DO 100 J = 1,(MESHPTS/10)
C
          K = NEQ*((J-1)*10)
          ZG=DFLOAT((J-1)*10)*XINC
C
          ELECT = 0.0D0
          DO 70 IS = 1,NEQ-1
C
                 ELECT = ELECT + Z(IS)*Y(K+IS)
C
 70       CONTINUE
C
          WRITE (6,600) ZG,Y(K+NEQ),ELECT,
     *                                    (ARS(I),Y(K+I),I=1,NEQ-1)
C
 100  CONTINUE
C
      K = NEQ*(MESHPTS-1)
      ELECT = 0.0D0
      DO 120 IS = 1,NEQ-1
C
          ELECT = ELECT + Z(IS)*Y(K+IS)
C
 120  CONTINUE
C
      ZG = DFLOTJ(MESHPTS-1)*XINC
      WRITE (6,600) ZG,Y(K+NEQ),ELECT,(ARS(I),Y(K+I),I=1,NEQ-1)
C
C
      DO 400 I = 1,NEQ
C
C         PRINT*, I,IFILES(I)
          WRITE(IFILES(I),700)T,
     *                      (Y((I+NEQ*((J-1)*IDIV))),J=1,MESHPTS/IDIV),
     *                      Y(I+((MESHPTS-1)*NEQ))
C
 400  CONTINUE
C
 500     FORMAT (1X,'TIME = ',D10.3,'  TIME STEP SIZE = ',E10.3,1X,
     *                       '  NUMBER OF STEPS = ', I5,/2X,
```

```
     *                        'AVE TIME STEP = ',E9.3,'   TIP COND. = ',E9.3,
     *                        '   EXT. METAL POT. = ',E9.3)
  550 FORMAT (1X,' TIP FLUX : ',
     *                        3(1X,A3,' = ',E9.3),/11X,4(1X,A3,' = ',E9.3),
     *                        /11X,4(1X,A3,' = ',E9.3),/11X,4(1X,A3,' = ',E9.3),
     *                        /11X,4(1X,A3,' = ',E9.3),/11X,4(1X,A3,' = ',E9.3))
  600    FORMAT (2X,3HX = ,F8.5,2X,3HP = ,D10.3,' ELECT = ',D10.3,/,
     *                        3(4X,A3,' = ',D13.6))
C
  650 FORMAT(1X,/)
C
  700 FORMAT(1X,E12.5,9(1X,E12.5),/1X,10(1X,E12.5),
     *                                  /1X,10(1X,E12.5))
C
      RETURN
      END
C
C
C*****************************************************************C
C*****************************************************************C
C
      SUBROUTINE REACT(NPTS,NEQ,ARS,TEM,TEMR)
C
C*****************************************************************C
C     WRITTEN BY : MAUREEN J. PSAILA-DOMBROWSKI
C     REVISION DATE : JULY 22, 1989
C*****************************************************************C
C        READS LOGICAL UNIT NUMBER 7 FOR THE REACTION MATRIX
C        AND REACTION RATE CONSTANTS.  REACTION RATE CONSTANTS ARE
C        ADJUSTED FOR TEMPERATURE USING AN ARRHENIUS TEMPERATURE
C        DEPENDENCE
C*****************************************************************C
C     LIST OF VARIABLES
C
C     CJP
C     I,II,
C      IJ,J,K
C     IFLG
C     IND
C     R
C     IP
C     IR
C     KOEF
C     NJ
C
C*****************************************************************C
C
      INCLUDE 'P.BLK'
C
      DIMENSION  EA(MNR),IP(MNR,4),IR(MNR,3),NJ(MNR,MNEQ),
     *                        ARS(0:MNEQ)
C
      COMMON/REACT/ NRTN,IN1(MNR),IN2(MNR),IN3(MNR),KOEF(MNR,MNEQ),
     *                        RC(MNR)
C
      CHARACTER*8 ARS
      CHARACTER*3 CJP
      DATA R/8.314D-3/
      ARS(0) = '     '
      IF(NRTN.EQ.0)GO TO 900
```

```
C
C*********************************************************************C
C       INITIALIZE THE COEFFICIENT AND ORDER MATRICIES FOR THE FUNCTION
C       EVALUATION SEGMENT OF LSODES
C*********************************************************************C
C
         DO 5 II=1,NEQ-1
            DO 5 IJ=1,NRTN
            KOEF(IJ,II)=0
            NJ(IJ,II)=0
 5          CONTINUE
C
C*********************************************************************C
C       READ THE REACTIONS ONE BY ONE AND SET UP THE COEFFICIENT
C       MATRICIES (KOEF), AND THE REACTION ORDER MATRIX (NJ)
C*********************************************************************C
C
C     PRINT*, 'REACT'
                WRITE (6,10)
10              FORMAT ('1',10X,
     +          'CHEMICAL REACTIONS : ',//
     +          26X,'REACTIONS',28X,'RATE',3X,'ACTIVATION',/62X,'CONSTANT',2X,
     +          'ENERGIES')
C
      READ (7,99)
      DO 140 I=1,NRTN
            READ(7,100)CJP,(IR(I,K),K=1,3),(IP(I,K),K=1,4),RC(I),EA(I)
C
C*********************************************************************C
C       CONVERT THE RATE CONSTANT USING AN ARRHENIUS EXPERSSION
C*********************************************************************C
C
            RC(I)=(RC(I)/DEXP(-EA(I)/(R*TEMR)))*DEXP(-EA(I)/(R*TEM))
C
            WRITE(6,110)CJP,(ARS(JIABS(IR(I,K))),K=1,3),
     *          (ARS(IP(I,K)),K=1,4),RC(I),EA(I)
 99       FORMAT(1X)
 100         FORMAT(A3,3(1X,I3),4(1X,I3),1X,D18.8,1X,D18.8)
 110         FORMAT(A3,1X,3A8,'>',4A8,D9.2,1X,D9.2)
C
C*********************************************************************C
C       SET UP THE REACTION INDICIES IR AND THE PRODUCT INDICIES IP
C       FILL THE COEFFICIENT MATRIX KOEF
C*********************************************************************C
C       CHECK FIRST TO SEE IF ANY OF THE REACTANTS ARE PRESENT
C       IN A SECOND ORDER FASHION
C*********************************************************************C
C
            IF(((IR(I,1).EQ.IR(I,2)).OR.(IR(I,2).EQ.IR(I,3)))
     *                      .AND.(IR(I,2).NE.0))THEN
               NJ(I,JIABS(IR(I,2)))=-2
               KOEF(I,JIABS(IR(I,2)))=-2
            ENDIF
C
C*********************************************************************C
C       FILL UP THE MATRIX FOR THE REACTANTS WHICH ARE FIRST ORDER
C*********************************************************************C
C
            DO 120 K=1,3
               IF((IR(I,K).NE.0).AND.(NJ(I,JIABS(IR(I,K))).NE.-2))THEN
```

```
                    NJ(I,JIABS(IP(I,K)))=-1
                    KOEF(I,JIABS(IR(I,K)))=-1
                ENDIF
  120         CONTINUE
C
C*****************************************************************C
C       CHECK FOR SECOND ORDER PRODUCTS
C*****************************************************************C
C
            IF(((IP(I,1).EQ.IP(I,2)).OR.(IP(I,2).EQ.IP(I,3)))
     *                      .AND.(IP(I,2).NE.0))THEN
                KOEF(I,JIABS(IP(I,2)))=2
            ENDIF
            IF(((IP(I,2).EQ.IP(I,3)).OR.(IP(I,3).EQ.IP(I,4)))
     *                      .AND.(IP(I,3).NE.0))THEN
                KOEF(I,JIABS(IP(I,3)))=2
            ENDIF
C
C*****************************************************************C
C       FILL UP THE PRODUCTS MATRIX FOR FIRST ORDER PRODUCTS
C*****************************************************************C
C
          DO 130 K=1,4
                IF((IP(I,K).NE.0).AND.(KOEF(I,IP(I,K)).NE.2))THEN
                    KOEF(I,IP(I,K))=1
                ENDIF
  130         CONTINUE
C
  140     CONTINUE
C
C*****************************************************************C
C       NORMALIZE CATALYTIC REACTANTS
C*****************************************************************C
C
C
          DO 150 K=1,NEQ-1
             DO 150 I=1,NRTN
C
C*****************************************************************C
C       ARE THERE PRODUCTS OF SPECIES K AS WELL AS REACTANTS OF
C       SPECIES K?
C*****************************************************************C
C
                IF((KOEF(I,K).NE.NJ(I,K)).AND.(NJ(I,K).NE.0))
     +          KOEF(I,K)=KOEF(I,K)+NJ(I,K)
C
C*****************************************************************C
C       ARE THERE ONLY PRODUCTS? (FILL NJ AFTER CHECKING FOR
C       CATALYTIC REACTIONS)
C*****************************************************************C
C
                IF((KOEF(I,K).NE.NJ(I,K)).AND.(NJ(I,K).EQ.0))
     *          NJ(I,K)=KOEF(I,K)
C
  150     CONTINUE
C
  210     FORMAT (/1X,A8,5(2X,D9.2))
  220     FORMAT(5x,D10.3,4(/5X,D10.3))
C       CLOSE (5)
C
```

```
C*****************************************************************C
C          SET UP REACTION ORDER INDICIES FOR FAST FUNCTION EVALUATION
C*****************************************************************C
C     NOTE REMOVED Y(NPTS+I) = 1.0D0 LOOP : DID NOT SEEM NECESSARY
C
         DO 300 I=1,NRTN
C
C*****************************************************************C
C          INITIAL ALL REACTANTS TO ZERO ORDER
C*****************************************************************C
C
              IN1(I)=NPTS+1
              IN2(I)=NPTS+1
              IN3(I)=NPTS+1
              IND=0
              IFLG=0
C
              DO 270 J=1,NEQ-1
C
C*****************************************************************C
C          ESTABLISH ALL FIRST ORDER REACTANTS
C*****************************************************************C
C
                  IF(NJ(I,J).EQ.-1.AND.IND.EQ.0)THEN
                       IN1(I)=J
                       IFLG=IFLG+1
                  ENDIF
                  IF(NJ(I,J).EQ.-1.AND.IND.EQ.1)THEN
                       IN2(I)=J
                       IFLG=IFLG+1
                  ENDIF
                  IF(NJ(I,J).EQ.-1.AND.IND.EQ.2)THEN
                       IN3(I)=J
                       IFLG=IFLG+1
                  ENDIF
C
C*****************************************************************C
C        DETERMINE THE SECOND ORDER REACTANTS (EITHER FIRST TWO
C        OR LAST TWO) IND IS NUMBER OF REACTANTS CHOSEN SO FAR
C*****************************************************************C
C
                  IF(NJ(I,J).EQ.-2.AND.IND.EQ.0)THEN
                       IN1(I)=J
                       IN2(I)=J
                       IFLG=IFLG+2
                  ENDIF
                  IF(NJ(I,J).EQ.-2.AND.IND.EQ.1)THEN
                       IN2(I)=J
                       IN3(I)=J
                       IFLG=IFLG+2
                  ENDIF
                  IND = IND+IFLG
                  IFLG=0
 270          CONTINUE
 300     CONTINUE
C
      WRITE(6,625)
      DO 600 I = 1,NRTN
C
           WRITE(6,650)(KOEF(I,K),K=1,NEQ-1)
```

```
C
 600 CONTINUE
C
 625 FORMAT(/10X,'KOEF(NRTN,NEQ) : ')
 650 FORMAT(10X,20(2X,I5))
C
      WRITE(6,725)
      DO 700  I = 1,NRTN
C
          WRITE(6,750)IN1(I),IN2(I),IN3(I),RC(I)
C
 700 CONTINUE
C
 725 FORMAT(/10X,' IN1    IN2    IN3          RC')
 750 FORMAT(10X,3(I4,1X),E10.3)
C
      CLOSE(7)
 900 RETURN
         END
C
C
C
C*********************************************************************C
C*********************************************************************C
C
      SUBROUTINE WREACT(NPTS,NEQ,ARS,EM,FRT)
C
C*********************************************************************C
C     WRITTEN BY : MAUREEN J. PSAILA-DOMBROWSKI
C     REVISION DATE : AUGUST 21, 1989
C*********************************************************************C
C     THIS SUBROUTINE READS IN ALL THE NECESSARY DATA FOR THE CRACK
C     WALL ELECTROCHEMICAL REACTIONS AND SETS UP THE ARRAYS
C*********************************************************************C
C     DESCRIPTION OF VARIABLES
C
C*********************************************************************C
      INCLUDE 'P.BLK'
C
      DIMENSION  IR(MNWR,3),IP(MNWR,3),ARS(0:MNEQ),ACTW(MNWR),
     *                      ISW(MNWR,6),WEN(MNWR)
C
      COMMON/WALL/ NWRTN,WALPHA(MNWR),WCIO(MNWR),KW(MNWR),WPOW(MNWR),
     *                      KOEFW(MNWR,MNEQ),WKCIO(MNWR),CTW(MNWR),SW(MNWR,0:MNEQ)
C
      CHARACTER*1 ACTW
      CHARACTER*8 ARS
      ARS(0) = '      '
      IF(NWRTN.EQ.0)GO TO 900
C*********************************************************************C
C     BEGIN PROGRAM
C
C     PRINT*, 'WREACT'
C*********************************************************************C
C        INITIALIZE THE COEFFICIENT AND ORDER MATRICIES FOR THE FUNCTION
C        EVALUATION SEGMENT OF LSODES
C*********************************************************************C
C
      DO 20 J=1,NWRTN
          SW(J,0) = 0.0D0
```

```
              DO 10 I=1,NEQ-1
                  KOEFW(J,I)=0
                  SW(J,I) = 0.0D0
 10           CONTINUE
 20        CONTINUE
C
C*****************************************************************C
C        READ THE REACTIONS ONE BY ONE AND SET UP THE COEFFICIENT
C        MATRICIES (KOEF), AND THE REACTION ORDER MATRIX (NJ)
C*****************************************************************C
C
      READ(8,40)
 40   FORMAT(1X)
                WRITE (6,50)
 50             FORMAT (//10X,'WALL REACTIONS : '//)
      WRITE(6,60)
 60   FORMAT(5X,'TYPE',3X,'#e')
C
      DO 500 I=1,NWRTN
C
            READ(8,80)ACTW(I),NW,((ISW(I,K),IR(I,K)),K = 1,3),
     *                      ((ISW(I,3+K),IP(I,K)),K = 1,3),WKCIO(I),
     *                      WALPHA(I),KW(I),WPOW(I)
C
 80         FORMAT(1X,A1,1X,I2,3(1X,I1,1X,I3),3(1X,I1,1X,I3),
     *                      1X,D14.6,1X,D5.2,1X,I2,1X,D4.1)
C
          WEN(I) = DFLOAT(NW)
          WCIO(I) = WKCIO(I)*DEXP(-WALPHA(I)*EM*FRT)
C
          DO 85 K = 1,3
                IF(IR(I,K).NE.0)
     *                                  SW(I,JIABS(IR(I,K))) = DFLOAT(ISW(I,K))
                IF(IP(I,K).NE.0)
     *                                  SW(I,JIABS(IP(I,K))) = DFLOAT(ISW(I,3+K))
 85       CONTINUE
C
C         DO 86 IK = 1,NEQ
C               PRINT*, I,IK,SW(I,IK)
C 86      CONTINUE
C
          IF (KW(I).EQ.0) KW(I) = NPTS+1
          IF (WPOW(I).EQ.0.0D0) WPOW(I) = 1.0D0
          IF(ACTW(I).EQ.'A') CTW(I) = 1.0D0
          IF(ACTW(I).EQ.'C') CTW(I) = -1.0D0
C
C*****************************************************************C
C     WRITE VALUES OF DATA TO OUTPUT FILE
C*****************************************************************C
C
            WRITE(6,100)ACTW(I),CTW(I),WEN(I),
     *                      ((SW(I,JIABS(IR(I,K))),ARS(JIABS(IR(I,K)))),K = 1,3),
     *                      ((SW(I,JIABS(IP(I,K))),ARS(JIABS(IP(I,K)))),K = 1,3)
 100        FORMAT(5X,A1,1X,F3.0,1X,F3.0,1X,3(1X,F3.0,1X,A5),' >',
     *                      3(1X,F3.0,1X,A5))
C
     PRINT*, 'STOP'
C*****************************************************************C
C        SET UP THE REACTION INDICIES IR AND THE PRODUCT INDICIES IP
C        FILL THE COEFFICIENT MATRIX KOEF
```

```
C*********************************************************************C
C
         DO 120 K = 1,3
C
                IF(IR(I,K).NE.0) KOEFW(I,JIABS(IR(I,K)))=-1
                IF(IP(I,K).NE.0) KOEFW(I,JIABS(IP(I,K)))=1
C
 120     CONTINUE
C
C*********************************************************************C
C
 500 CONTINUE
C
     DO 510 I = 1,NWRTN
         DO 510 J = 1,NEQ-1
                IF(SW(I,J).NE.0.0D0)
     *                                  SW(I,J) = SW(I,J)*DFLOAT(KOEFW(I,J))/WEN(I)
 510 CONTINUE
C
     WRITE(6,725)
     DO 520  I = 1,NWRTN
C
         WRITE(6,750)WCIO(I),WALPHA(I),KW(I),WPOW(I)
C
 520 CONTINUE
     WRITE(6,625)
     DO 600 I = 1,NWRTN
C
         WRITE(6,650)(SW(I,K),K=1,NEQ-1)
C
 600 CONTINUE
C
 625 FORMAT(/10X,'SW(NWRTN,NEQ) : ')
 650 FORMAT(10X,20(2X,F4.1))
C
C
C
 725 FORMAT(/20X,'   WCIO       WALPHA      KW     WPOW')
 750 FORMAT(20X,2(E10.3,1X),I4,1X,E10.3)
     CLOSE(8)
 900 RETURN
     END
C
C
C
C*********************************************************************C
C
     SUBROUTINE TREACT(NPTS,NEQ,ARS,EM,FRT)
C
C*********************************************************************C
C    WRITTEN BY : MAUREEN J. PSAILA-DOMBROWSKI
C    REVISION DATE : AUGUST 21, 1989
C*********************************************************************C
C    THIS SUBROUTINE READS IN ALL THE NECESSARY DATA FOR THE CRACK
C    TIP ELECTROCHEMICAL REACTIONS AND SETS UP THE ARRAYS
C*********************************************************************C
C    DESCRIPTION OF VARIABLES
C
C*********************************************************************C
     INCLUDE 'P.BLK'
```

```
C
      DIMENSION IR(MNWR,3),IP(MNWR,3),ARS(0:MNEQ),ACTT(MNTR),
     *                     IST(MNTR,6),TEN(MNTR)
C
      COMMON/TIP/ NTRTN,TALPHA(MNTR),TCIO(MNTR),KT(MNTR),TPOW(MNTR),
     *                     KOEFT(MNTR,MNEQ),TKCIO(MNTR),CTT(MNTR),ST(MNTR,0:MNEQ)
C
      CHARACTER*1 ACTT
      CHARACTER*8 ARS
      ARS(0) = '     '
      IF(NTRTN.EQ.0)GO TO 900
C*********************************************************************C
C     BEGIN PROGRAM
C     PRINT*, 'TREACT'
C*********************************************************************C
C        INITIALIZE THE COEFFICIENT AND ORDER MATRICIES FOR THE FUNCTION
C        EVALUATION SEGMENT OF LSODI
C*********************************************************************C
C
      DO 20 J=1,NTRTN
           ST(J,0) = 0.0D0
           DO 10 I=1,NEQ-1
                  KOEFT(J,I)=0
                  ST(J,I) = 0.0D0
 10        CONTINUE
 20   CONTINUE
C
C*********************************************************************C
C        READ THE REACTIONS ONE BY ONE AND SET UP THE COEFFICIENT
C        MATRICIES (KOEF), AND THE REACTION ORDER MATRIX (NJ)
C*********************************************************************C
C
      READ(9,40)
 40   FORMAT(1X)
                  WRITE (6,50)
 50               FORMAT (//10X,'TIP REACTIONS : '//)
      WRITE(6,60)
 60   FORMAT(5X,'TYPE',3X,'#e')
C
      DO 500 I=1,NTRTN
C
           READ(9,80)ACTT(I),NT,((IST(I,K),IR(I,K)),K = 1,3),
     *                     ((IST(I,3+K),IP(I,K)),K = 1,3),TKCIO(I),
     *                     TALPHA(I),KT(I),TPOW(I)
C
 80          FORMAT(1X,A1,1X,I2,3(1X,I1,1X,I3),3(1X,I1,1X,I3),
     *                     1X,D14.6,1X,D5.2,1X,I2,1X,D4.1)
C
           TEN(I) = DFLOAT(NT)
           TCIO(I) = TKCIO(I)*DEXP(-TALPHA(I)*FRT*EM)
C
           DO 85 K = 1,3
                  IF(IR(I,K).NE.0)
     *                                    ST(I,JIABS(IR(I,K))) = DFLOAT(IST(I,K))
                  IF(IP(I,K).NE.0)
     *                                    ST(I,JIABS(IP(I,K))) = DFLOAT(IST(I,3+K))
 85        CONTINUE
C
C          DO 86 IK = 1,NEQ
C                  PRINT*, I,IK,ST(I,IK)
```

```
C 86      CONTINUE
C
          IF (KT(I).EQ.0) KT(I) = NPTS+1
          IF (TPOW(I).EQ.0.0D0) TPOW(I) = 1.0D0
          IF(ACTT(I).EQ.'A') CTT(I) = 1.0D0
          IF(ACTT(I).EQ.'C') CTT(I) = -1.0D0
C
C*****************************************************************C
C     WRITE VALUES OF DATA TO OUTPUT FILE
C*****************************************************************C
C
              WRITE(6,100)ACTT(I),CTT(I),TEN(I),
     *                        ((ST(I,JIABS(IR(I,K))),ARS(JIABS(IR(I,K)))),K = 1,3),
     *                        ((ST(I,JIABS(IP(I,K))),ARS(JIABS(IP(I,K)))),K = 1,3)
 100          FORMAT(5X,A1,1X,F3.0,1X,F3.0,1X,3(1X,F3.0,1X,A5),' >',
     *                        3(1X,F3.0,1X,A5))
C
C*****************************************************************C
C        SET UP THE REACTION INDICIES IR AND THE PRODUCT INDICIES IP
C        FILL THE COEFFICIENT MATRIX KOEF
C*****************************************************************C
C
          DO 120 K = 1,3
C
                IF(IR(I,K).NE.0) KOEFT(I,JIABS(IR(I,K))) = -1
                IF(IP(I,K).NE.0) KOEFT(I,JIABS(IP(I,K))) = 1
C
 120      CONTINUE
C
C*****************************************************************C
C
 500 CONTINUE
C
      DO 510 I = 1,NTRTN
          DO 510 J = 1,NEQ-1
C
                IF(ST(I,J).NE.0.0D0)
     *                                  ST(I,J) = ST(I,J)*DFLOAT(KOEFT(I,J))/TEN(I)
C
 510 CONTINUE

      WRITE(6,725)
      DO 520   I = 1,NTRTN
C
          WRITE(6,750)TCIO(I),TALPHA(I),KT(I),TPOW(I)
C
 520 CONTINUE
C
      WRITE(6,625)
      DO 600 I = 1,NTRTN
C
          WRITE(6,650)(ST(I,K),K=1,NEQ-1)
C
 600 CONTINUE
C
 625 FORMAT(/10X,'ST(NTRTN,NEQ) : ')
 650 FORMAT(10X,20(2X,F4.1))
C
C
 725 FORMAT(/20X,'   TCIO       TALPHA      KT     TPOW')
```

```
 750 FORMAT(20X,2(E10.3,1X),I4,1X,F10.3)
C
      CLOSE(9)
 900 RETURN
      END
C
C
C
C*********************************************************************C
C*********************************************************************C
C
      SUBROUTINE SREACT(NPTS,NEQ,ARS,TEM,TEMR)
C
C*********************************************************************C
C     WRITTEN BY : MAUREEN J. PSAILA-DOMBROWSKI
C     REVISION DATE : JULY 22, 1989
C*********************************************************************C
C        READS LOGICAL UNIT NUMBER 7 FOR THE REACTION MATRIX
C        AND REACTION RATE CONSTANTS.  REACTION RATE CONSTANTS ARE
C        ADJUSTED FOR TEMPERATURE USING AN ARRHENIUS TEMPERATURE
C        DEPENDENCE
C*********************************************************************C
C     LIST OF VARIABLES
C
C     CJP
C     I,II,
C      IJ,J,K
C     IFLG
C     IND
C     R
C     IP
C     IR
C     KOEF
C     NJ
C
C*********************************************************************C
C
      INCLUDE 'P.BLK'
C
      DIMENSION IR(MNSR,3),ARS(0:MNEQ),NJ(MNSR,MNEQ)
C
      COMMON/SREACT/ NSRTN,INS1(MNSR),INS2(MNSR),INS3(MNSR),
     *                      KOEFS(MNSR,MNEQ),SRC(MNSR),SC(MNSR)
C
      CHARACTER*3 CJP
      CHARACTER*8 ARS
      DATA R/8.314D-3/
      ARS(0) = '      '
      IF(NSRTN.EQ.0)GO TO 900
      OPEN (10, FILE = 'SREACT.DAT', STATUS = 'OLD')
C
C*********************************************************************C
C        INITIALIZE THE COEFFICIENT AND ORDER MATRICIES FOR THE FUNCTION
C        EVALUATION SEGMENT OF LSODES
C*********************************************************************C
C
          DO 20 II=1,NEQ-1
             DO 10 IJ=1,NSRTN
                KOEFS(IJ,II)=0
 10       CONTINUE
```

```
 20   CONTINUE
C
C*****************************************************************C
C        READ THE REACTIONS ONE BY ONE AND SET UP THE COEFFICIENT
C        MATRICIES (KOEF), AND THE REACTION ORDER MATRIX (NJ)
C*****************************************************************C
C
C     PRINT*, 'SREACT'
      READ(10,40)
 40   FORMAT(1X)
                WRITE (6,50)
 50             FORMAT (//10X,'SOLUBILITY REACTIONS :',//)
      DO 140 I=1,NSRTN
             READ(10,100)(IR(I,K),K=1,3),SRC(I),SC(I)
C
C*****************************************************************C
C        CONVERT THE RATE CONSTANT USING AN ARRHENIUS EXPERSSION
C*****************************************************************C
C
C             RC(I)=(RC(I)/DEXP(-EA(I)/(R*TEMR)))*DEXP(-EA(I)/(R*TEM))
C
             WRITE(6,110)(ARS(JIABS(IR(I,K))),K=1,3),SRC(I),SC(I)
 100         FORMAT(3(1X,I3),2(1X,D15.10))
 110         FORMAT(3(1X,A8),2(1X,D9.2))
C
C*****************************************************************C
C        SET UP THE REACTION INDICIES IR AND THE PRODUCT INDICIES IP
C        FILL THE COEFFICIENT MATRIX KOEF
C*****************************************************************C
C        CHECK FIRST TO SEE IF ANY OF THE REACTANTS ARE PRESENT
C        IN A SECOND ORDER FASHION
C*****************************************************************C
C
             IF(((IR(I,1).EQ.IR(I,2)).OR.(IR(I,2).EQ.IR(I,3)))
     *                        .AND.(IR(I,2).NE.0))THEN
                 NJ(I,JIABS(IR(I,2)))=-2
                 KOEFS(I,JIABS(IR(I,2)))=-2
             ENDIF
C
C*****************************************************************C
C        FILL UP THE MATRIX FOR THE REACTANTS WHICH ARE FIRST ORDER
C*****************************************************************C
C
             DO 120 K=1,3
                IF((IR(I,K).NE.0).AND.(NJ(I,JIABS(IR(I,K))).NE.-2))THEN
                     NJ(I,JIABS(IR(I,K)))=-1
                     KOEFS(I,JIABS(IR(I,K)))=-1
                ENDIF
 120          CONTINUE
C
 140  CONTINUE
C
C*****************************************************************C
C          SET UP REACTION ORDER INDICIES FOR FAST FUNCTION EVALUATION
C*****************************************************************C
C     NOTE REMOVED Y(NPTS+I) = 1.0D0 LOOP : DID NOT SEEM NECESSARY
C
         DO 300 I=1,NSRTN
C
C*****************************************************************C
```

```
C          INITIAL ALL REACTANTS TO ZERO ORDER
C*************************************************************************C
C
              INS1(I)=NPTS+1
              INS2(I)=NPTS+1
              INS3(I)=NPTS+1
              IND=0
              IFLG=0
C
              DO 270 J=1,NEQ-1
C
C*************************************************************************C
C          ESTABLISH ALL FIRST ORDER REACTANTS
C*************************************************************************C
C
                  IF(NJ(I,J).EQ.-1.AND.IND.EQ.0)THEN
                      INS1(I)=J
                      IFLG=IFLG+1
                  ENDIF
                  IF(NJ(I,J).EQ.-1.AND.IND.EQ.1)THEN
                      INS2(I)=J
                      IFLG=IFLG+1
                  ENDIF
                  IF(NJ(I,J).EQ.-1.AND.IND.EQ.2)THEN
                      INS3(I)=J
                      IFLG=IFLG+1
                  ENDIF
C
C*************************************************************************C
C        DETERMINE THE SECOND ORDER REACTANTS (EITHER FIRST TWO
C        OR LAST TWO) IND IS NUMBER OF REACTANTS CHOSEN SO FAR
C*************************************************************************C
C
                  IF(NJ(I,J).EQ.-2.AND.IND.EQ.0)THEN
                      INS1(I)=J
                      INS2(I)=J
                      IFLG=IFLG+2
                  ENDIF
                  IF(NJ(I,J).EQ.-2.AND.IND.EQ.1)THEN
                      INS2(I)=J
                      INS3(I)=J
                      IFLG=IFLG+2
                  ENDIF
                  IND = IND+IFLG
                  IFLG=0
  270         CONTINUE
  300     CONTINUE
C
      WRITE(6,625)
      DO 600 I = 1,NSRTN
C
          WRITE(6,650)(KOEFS(I,K),K=1,NEQ-1)
C
  600 CONTINUE
C
  625 FORMAT(/10X,'KOEFS(NSRTN,NEQ) : ')
  650 FORMAT(10X,20(2X,I5))
C
      WRITE(6,725)
      DO 700  I = 1,NSRTN
```

```
C
         WRITE(6,750)INS1(I),INS2(I),INS3(I),SRC(I),SC(I)
C
 700 CONTINUE
C
 725 FORMAT(/10X,' INS1    INS2     INS3           SRC             SC')
 750 FORMAT(10X,3(I4,1X),2(1X,E10.3))
C
     CLOSE(10)
 900 RETURN
        END
C
C
C
C*********************************************************************C
C
     SUBROUTINE YINIT(Y,YDOTI,YM,TCH,EMCH,YM2,TCH2,EMCH2)
C
C*********************************************************************C
C    WRITTEN BY : MAUREEN J. PSAILA-DOMBROWSKI
C    REVISION DATE : JULY 22, 1989
C*********************************************************************C
C    THIS SUBROUTINE INITIALIZES THE ARRAY CONTAINING THE UNKNOWNS
C*********************************************************************C
C    LIST OF VARIABLES
C
C    CONPOT      CONSTANT USED TO CALCULATE INITIAL POTENTIAL
C                       DISTRIBUTION
C    DEL_P       SPATIAL POTENTIAL GRADIENT
C    DIST        DISTANCE FROM CRACK TIP
C    I,IS,IX,
C      J         LOOP COUNTERS
C    K,KN,L,
C      KP        COUNTERS FOR Y (L IS FOR Y = POTENTIAL)
C    TIPCUR      TOTAL CRACK TIP CURRENT
C    TOUTI       TOUT FOR CALCULATION OF YDOTI
C
C*********************************************************************C
C
     INCLUDE 'P.BLK'
     INCLUDE 'D.BLK'
C
     DIMENSION Y(MA),YDOTI(MA),YI(MNEQ),RWORK(LRW),IWORK(LIW),
     *                                YM(MNEQ),YIM(MNEQ),YMCH(MNEQ),YM2(MNEQ),
     *                                YMCH2(MNEQ)
C
     NAMELIST/VALUES/ YI,YIM,YMCH,TICH,EMICH,YMCH2,TICH2,EMICH2
C
C*********************************************************************C
C
C    PRINT*, 'YINIT'
C
     READ(5,NML=VALUES)
C
C*********************************************************************C
C    CALCULATE CONSTANTS AND INITIALIZE COUNTERS AND SET CONSTANT
C    VALUES
C*********************************************************************C
C    Y(NPTS+1) = 1.0D0 IS CONSTANT USED FOR CALCULATING REACTION
C    TERMS IN RESIDUAL EQUATION
```

```
C*****************************************************************C
C
      TCH2 = TICH2
      EMCH2 = EMICH2
      EMCH = EMICH
      TCH = TICH
      Y(NEQ*MESHPTS+1) = 1.0D0
C
C*****************************************************************C
C     SET INITIAL VALUES OF CONCENTRATION
C*****************************************************************C
C     IF CONCENTRATION GRADIENT EXISTS
C*****************************************************************C
C
C     DO 10 I = 1,MESHPTS*(NEQ-1)
C         Y(I) = YI(I)
C         PRINT*, I,YI(I),Y(I)
C
C*****************************************************************C
C     IF NO CONCENTRATION GRADIENT EXISTS
C*****************************************************************C
C
      DO 10 J=1,MESHPTS
C
          DO 5 I = 1,NEQ
C
                  K = (NEQ)*(J-1) + I
                  Y(K)=YI(I)
C
 5        CONTINUE
C
 10   CONTINUE
C
      DO 20 I = 1,NEQ
C
          Y(NEQ*(MESHPTS-1)+I) = YIM(I)
          YM(I) = YMCH(I)
          YM2(I) = YMCH2(I)
C
 20   CONTINUE
C
      IF(TCH.EQ.0.0D0)THEN
          EM = EMCH
          DO 50 I = 1,NEQ
                  K = NEQ*(MESHPTS-1)
                  Y(K+I) = YM(I)
 50       CONTINUE
      ENDIF
C
      IF(TCH2.EQ.0.0D0)THEN
          EM = EMCH2
          DO 60 I = 1,NEQ
                  K = NEQ*(MESHPTS-1)
                  Y(K+I) = YM2(I)
 60       CONTINUE
      ENDIF

C
C
      RETURN
```

```
      END
C
C
C
C*********************************************************************C
C*********************************************************************C
C
C
      SUBROUTINE RESP(NPTS,T,Y,S,R,IRES)
C
C*********************************************************************C
C     WRITTEN BY : MAUREEN J. PSAILA-DOMBROWSKI
C     REVISION DATE : JULY 22, 1989
C*********************************************************************C
C
C     THIS SUBROUTINE SETS UP THE RESIDUAL FOR LSODI. THE RESIDUAL IS
C     THE DIFFERENCE BETWEEN THE EXACT EQUATION AND THE APPROXIMATION
C     TO THE EQUATION
C
C*********************************************************************C
C    VARIABLES (IN ALPHABETIC ORDER)
C
C     A
C     CKMAX                   CONSTANT RELATED TO KMAX USED IN CTOD
C                             CALCULATIONS
C     CON2,CON3  CONSTANTS
C     COVCON                  CONSTANT USED TO DETERMINE UPWIND DIRECTION
C     DELK                    AMPLITUDE OF STRESS INTENSITY FACTOR
C     DELTA
C     DELDOT                  TIME DERIVATIVE OF DELTA
C     DCON                    DIFFUSION COEFFICIENT/DX**2
C     DIF                     DIFFUSION COEFFICIENT
C     DKCON2                  CONSTANT
C     DX                      DELTA X USED ABOVE
      H0                      CRACK TIP HALF WIDTH
C     H0DOT                   TIME DERIVATIVE OF H0
C     H(X)                    CRACK HALF WIDTH
C     KOEF(IR,IS)             COEFFICIENT ARRAY FOR REACTIONS
C     KM                      MEAN STRESS INTENSITY FACTOR
C     KMAX                    MAXIMUM STRESS INTENSITY FACTOR
C     L,I,IX,IS,IR            COUNTERS
C     R(I)                    RESIDUAL ARRAY FOR EACH EQUATION
C     RC(IR)                  REACTION RATE CONSTANT ARRAY
C     S(I)                    LSODI'S QUESS TO RESIDUAL
C     SK                      STRESS INTENSITY FACTOR
C     SR                      STRESS RATIO = Kmin/Kmax
C     T                       TIME
C     THETA                   CRACK ANGLE
C     THEDOT                  TIME DERIVATIVE OF CRACK ANGLE
C     V(X)                    VELOCITY ARRAY
C     VAFEPP                  CONSTANT
C     X                       POSITION FROM CRACK TIP
C     XINC                    DELTA X
C     XINCSQ                  DX*DX
C     Y                       UNKNOWN ARRAY
C
C*********************************************************************C
C
      INCLUDE 'P.BLK'
      INCLUDE 'D.BLK'
```

```
C
C*************************************************************************C
C    DIMENSION AND COMMON BLOCKS
C
     DIMENSION R(MA),Y(MA),S(MA)
C
C*************************************************************************C
C
     REAL*8 KM,KMAX,KMIN,KDOT
C
C*************************************************************************C
C    BEGINNING OF PROGRAM
C*************************************************************************C
C     CALCULATE CRACK TIP FLUX
C*************************************************************************C
C
     DO 50 IS = 1,NEQ-1
C
          TIPJ(IS) = 0.0D0
C
CCCCCCCCC    FROM CURRENT
C
          DO 45 IT = 1,NTRTN
C
                IF(ST(IT,IS).EQ.0.0D0)GO TO 45
C
                IF(Y(KT(IT)).GT.1.0D-14)THEN
C
                    TIPJ(IS) = TIPJ(IS) + ST(IT,IS)*TCIO(IT)
     *                                  *(Y(KT(IT))**TPOW(IT))
     *                                  *DEXP(TALPHA(IT)*Y(NEQ))/FC
C
                ENDIF
C
 45       CONTINUE
C
CCCCCCCCC    FROM CHEMICAL DISSOLUTION
C
          IF(IS.EQ.NSP1.AND.T.LT.TIPT) TIPJ(IS) = TIPJ(IS) + P1*TIPF
C
          IF(IS.EQ.NSP2.AND.T.LT.TIPT) TIPJ(IS) = TIPJ(IS) + P2*TIPF
C
          IF(IS.EQ.NSP3.AND.T.LT.TIPT) TIPJ(IS) = TIPJ(IS) + P3*TIPF
C
 50   CONTINUE
C
C*************************************************************************C
C     START CALCULATION OF CONCENTRATION
C*************************************************************************C
C
C     PRINT*, T
C
     TCURR = 0.0D0
     ASAVE = 0.0D0
C
     DO 300 IX = 1,MESHPTS-1
C
          K = (IX-1)*NEQ
          L = K + NEQ
C
```

```
      ASUM1 = 0.0D0
C
      IF(IX.EQ.1.)THEN
C
C     PRINT*, 'IX,IT,CTT(IT),TCURR'
            DO 60 IT = 1,NTRTN
C
            IF(Y(KT(IT)).GT.1.0D-14)THEN
C
                  CON1 = CTT(IT)*TCIO(IT)*DEXP(TALPHA(IT)*Y(NEQ))
                  CON2 = CON1 * (Y(KT(IT))**TPOW(IT))
                  TCURR = TCURR + CON2
C
                  ASAVE = ASAVE - CON2*S(NEQ)*TALPHA(IT)
C
                  IF(KT(IT).NE.(NPTS+1))THEN
                                    ASAVE = ASAVE - TPOW(IT)*CON1*
     *                              (Y(KT(IT))**(TPOW(IT)-1.D0))*S(KT(IT))
                  ENDIF
C
            ENDIF
C
C     PRINT*, IX,IT,CTT(IT),TCURR
 60         CONTINUE
C
      ENDIF
C
      IF(IX.EQ.1.OR.IX.EQ.MESHPTS)THEN
C
C     PRINT*, 'IX,IW,CTW(IW),TCURR'
            DO 64 IW = 1,NWRTN
C
                  IF (KW(IW).EQ.(NPTS+1)) THEN
                                    KP = NPTS+1
                  ELSE
                                    KP = K + KW(IW)
                  ENDIF
C
                  IF(Y(KP).GT.1.0D-14)THEN
C
                        CON1 = CTW(IW)*WCIO(IW)*(XINC/2.0D0)*
     *                                    DEXP(WALPHA(IW)*Y(L)),H(IX)
C
                        CON2 = CON1 * (Y(KP)**WPOW(IW))
C
                        TCURR = TCURR + CON2
C
                        ASAVE = AS. 'E - CON2 * S(NEQ) * WALPHA(IW)
C
                        IF(KW(IW).NE.(NPTS+1))THEN
C
                                    ASAVE = ASAVE - WPOW(IW)*(Y(KP)**
     *                                    (WPOW(IW)-1.D0))*S(KP)*CON1
                        ENDIF
C
                  ENDIF
C
 64         CONTINUE
C
      ELSE
```

```
C
                DO 65 IW = 1,NWRTN
C
                    IF (KW(IW).EQ.(NPTS+1)) THEN
                                        KP = NPTS+1
                    ELSE
                                        KP = K + KW(IW)
                    ENDIF
C
                    IF(Y(KP).GT.1.0D-14)THEN
C
                            CON1 = CTW(IW)*WCIO(IW)*(XINC)*
     *                                          DEXP(WALPHA(IW)*Y(L))/H(IX)
C
                            CON2 = CON1 * (Y(KP)**WPOW(IW))
C
                            TCURR = TCURR + CON2
C
                            ASAVE = ASAVE - CON2 * S(L)* WALPHA(IW)
C
                            IF(KW(IW).NE.(NPTS+1))THEN
C
                               ASAVE = ASAVE - WPOW(IW)*(Y(KP)
     *                                          **(WPOW(IW)-1.D0))*S(KP)*CON1
                            ENDIF
C
                    ENDIF
C
 65             CONTINUE
        ENDIF
C
C       PRINT*, ASAVE
        ASUM1 = ASUM1 + ASAVE
C
 66     SUM1 = 0.0D0
        SUM2 = 0.0D0
        SUM3 = 0.0D0
C
        DO 70 IS = 1,NEQ-1
C
                I = K + IS
C
                CON = Z(IS)*Z(IS)*DIF(IS)
C
                SUM1 = SUM1 + CON*Y(I)
                SUM3 = SUM3 + Z(IS)*Y(I)
C
                IF (IX.LT.MESHPTS-1)THEN
C
                  ASUM1 = ASUM1 - CON*FC*FRT*( (S(I)*(4.0D0*Y(L+NEQ)
     *                                  - 3.0D0*Y(L) - Y(L+2*NEQ))) + (Y(I)*
     *                          (4.0D0*S(L+NEQ) - 3.0D0*S(L) - S(L+2*NEQ))) )
     *                                  /(2.0D0*XINC)
C
C
                ELSE
C
                   ASUM1 = ASUM1 - CON*FC*FRT*( (S(I)*(Y(L+NEQ)
     *                                  - Y(L-NEQ))) + (Y(I)*(S(L+NEQ) - S(L-NEQ)))
     *                                  /(2.0D0*XINC)
```

```
C
                ENDIF
C
 70       CONTINUE
C
          IF (IX.EQ.1) THEN
                DO 80 IS = 1,NEQ-1
C
                    I = K + IS
C
                    CON = Z(IS)*DIF(IS)*FC/(2.0D0*XINC)
C
                    SUM2 = SUM2 + CON*(4.0D0*Y(I+NEQ)
     *                                -3.0D0*Y(I)-Y(I+2*NEQ))
C
                    ASUM1 = ASUM1 - CON*(4.0D0*S(I+NEQ)
     *                                -3.0D0*S(I)-S(I+2*NEQ))
C               PRINT*, 'I: ',I,ASUM1
C
 80             CONTINUE
          ELSE
                DO 90 IS = 1,NEQ-1
C
                    I = K + IS
C
                    CON = Z(IS)*DIF(IS)*FC/(2.0D0*XINC)
C
                    SUM2 = SUM2 + CON*(Y(I+NEQ)-Y(I-NEQ))
C
                    ASUM1 = ASUM1 - CON*(S(I+NEQ)-S(I-NEQ))
C               PRINT*, 'I: ',I,ASUM1
C
 90           CONTINUE
          ENDIF
C
          R(L) = ASUM1
C
          CKAP = SUM1*FC*FRT
          DP = (-TCURR-SUM2)/CKAP
          DDP = -PCON*SUM3
C
 95       DO 200 IS = 1,NEQ-1
C
                I = K + IS
C
CCCCCCCC        INITIALIZE ARRAY R
C
                R(I) = 0.0D0
C
CCCCCCCCC       NOTE : REACTIONS AND TRANSPORT TERMS ARE
CCCCCCCCC       NOT ADDED AT CRACK MOUTH
C
CCCCCCCCC       ADD REACTION TERMS
C
                RR = 0.0D0
 100            DO 120 IR = 1,NRTN
C
                    IF(KOFF(IR,IS).EQ.0)GO TO 120
                    KPIN1 = K+IN1(IR)
                    KPIN2 = K+IN2(IR)
```

```
                    KPIN3 = K+IN3(IR)
                    IF(KPIN1.GT.NPTS) KPIN1 = NPTS+1
                    IF(KPIN2.GT.NPTS) KPIN2 = NPTS+1
                    IF(KPIN3.GT.NPTS) KPIN3 = NPTS+1
C
                    RR = RR + DFLOTJ(KOEF(IR,IS))*RC(IR)*
     *                                        Y(KPIN1)*Y(KPIN2)*Y(KPIN3)
C
 120            CONTINUE
C
                RWR = 0.0D0
                DO 130 IW = 1,NWRTN
C
                    IF(SW(IW,IS).EQ.0.0D0)GO TO 130
C
                    IF (KW(IW).EQ.(NPTS+1)) THEN
                                KP = NPTS+1
                    ELSE
                                KP = K + KW(IW)
                    ENDIF
C
                   IF(Y(KP).GT.1.0D-14)THEN
C
                           RWR = RWR + SW(IW,IS)*WCIO(IW)
     *                                        *(Y(KP)**WPOW(IW))*
     *                                        DEXP(WALPHA(IW)*Y(L))/(H(IX)*FC)
C
                   ENDIF
C
 130            CONTINUE
C
                RSR = 0.0D0
                DO 150 IR = 1,NSRTN
C
                    IF(KOEFS(IR,IS).EQ.0)GO TO 150
                    KPIN1 = K+INS1(IR)
                    KPIN2 = K+INS2(IR)
                    KPIN3 = K+INS3(IR)
                    IF(KPIN1.GT.NPTS) KPIN1 = NPTS+1
                    IF(KPIN2.GT.NPTS) KPIN2 = NPTS+1
                    IF(KPIN3.GT.NPTS) KPIN3 = NPTS+1
C
                    RSR = RSR + DFLOTJ(KOEFS(IR,IS))*SRC(IR)*
     *                        DMAX1((Y(KPIN1)*Y(KPIN2)*Y(KPIN3)-SC(IR)),0.0D0)
     *                                        /H(IX)
C
C
 150            CONTINUE
C
CCCCCCCCC       CHEMICAL DISSOLUTION
C
                RSD = 0.0D0
C
                IF(IS.EQ.NSP1.AND.T.LT.WALLT)
     *                          RSD = RSD + P1*WALLF/H(IX)
C
                IF(IS.EQ.NSP2.AND.T.LT.WALLT)
     *                          RSD = RSD + P2*WALLF/H(IX)
C
                IF(IS.EQ.NSP3.AND.T.LT.WALLT)
```

```
     *                                  PSD = PSD + P3*WALLF/H(IX)
C
CCCCCCCCCC        RADIOLYSIS REACTIONS
C
C                 DIST = (NDX-IX)*XINC
C                 RR = RR + G(IS)*DSRATE*DEXP(ATTG*DIST)
C     *                                          + GH(IS)*DHRATE*DEXP(ATTN*DIST)
C
CCCCCCCCCC        FOR CRACK TIP APPLY BOUNDARY CONDITIONS
C
                  R(I) = R(I) + RR + RWR + RSR + RSD
C
                  IF(IX.EQ.1) THEN
C
CCCCCCCCCC            CALCULATE Y-NEQ
C
                      YMNEQ = Y(I+NEQ) + (2.0D0*XINC/DIF(IS))*(TIPJ(IS)
     *                                          + Y(I)*PCM(IS)*DP)
C
CCCCCCCCCC            ADD TRANSPORT TERMS : DIFFUSION
C
                      R(I) = R(I)
     *                              + DCON(IS)*(Y(I+NEQ) - 2.0D0*Y(I) + YMNEQ)
C
C                     PRINT*, 'R(1) ', R(I)
C
CCCCCCCCCC            MIGRATION
C
                      CVCONM = -PCM(IS)*DP
                      RM = PCM(IS)*Y(I)*DDP
D                     PRINT*, ' RM FIRST', RM
C
                      IF (CVCONM.GT.0.0D0) THEN
C
                             YM1 = Y(I) - YMNEQ
                             RM = RM + PCM(IS)*DP*YM1/(XINC)
D                            PRINT*, '<0   YM1 ',YM1
C
                      ELSE
C
                             YP1 = Y(I+NEQ) - Y(I)
                             RM = RM + PCM(IS)*DP*YP1/(XINC)
D                            PRINT*, '>0   YP1 ',YP1
C
                      ENDIF
C
CCCCCCCCC             ADD MIGRATION TERM AND REACTIONS AND SUBTRACT
CCCCCCCCC             GUESS
C
                      R(I) = R(I) + RM  - S(I)
C
                      GO TO 200
C
                  ENDIF
C
CCCCCCCCCC        TRANSPORT TERMS FOR REST OF CRACK OR CREVICE
C
                  R(I) = R(I)
C
CCCCCCCCCC        DIFFUSION
```

```
C
     *                        + DCON(IS)*( Y(I+NEQ) - 2.0D0*Y(I) + Y(I-NEQ) )
C
D                 PRINT*, ' R DIFF ',R(I)
C
CCCCCCCCC         MIGRATION
C
                  CVCONM = -PCM(IS)*DP
                  RM = PCM(IS)*Y(I)*DDP
D                 PRINT*, ' RM FIRST', RM
C
                  IF (CVCONM.GT.0.0D0) THEN
C
                      YM1 = Y(I) - Y(I-NEQ)
                      RM = RM + PCM(IS)*DP*YM1/(XINC)
C
                  ELSE
C
                      YP1 = Y(I+NEQ) - Y(I)
                      RM = RM + PCM(IS)*DP*YP1/(XINC)
C
                  ENDIF
C
C
                  R(I) = R(I) + RM
C
CCCCCCCCC         SUBTRACT APPROXIMATE TERM FROM LSODI
C
                  R(I) = R(I) - S(I)
C
 200      CONTINUE
C
 300 CONTINUE
C
      DO 400 IS = 1,NEQ
                  I = NEQ*(MESHPTS-1)+IS
                  R(I) = R(I) - S(I)
 400 CONTINUE
C
C
      RETURN
      END
C
C
C
C*********************************************************************C
C
      SUBROUTINE ADDAP(NPTS, T, Y, ML, MU, P, NROWP)
C
C*********************************************************************C
C     WRITTEN BY : MAUREEN J. PSAILA-DOMBROWSKI
C     REVISION DATE : JULY 22, 1989
C*********************************************************************C
C
      INCLUDE 'P.BLK'
      INCLUDE 'D.BLK'
C
      DIMENSION Y(MA),P(NROWP,MA)
C
C     PRINT *, 'ADDA'
```

```
C     PRINT*, NROWP,NEQ
C
C*************************************************************************C
C     POTENTIAL TERMS
C*************************************************************************C
C
      DO 300 IX = 1,MESHPTS-1
C
          K = (IX-1)*NEQ
          L = K + NEQ
C
C         PRINT*, 'IX : ',IX,K,L
          DO 70 IXX = 1,IX
C
             KX = (IXX-1)*NEQ
             LX = KX + NEQ
C
C         PRINT*, 'IXX : ',IXX,KX,LX
             IF(IXX.EQ.1)THEN
                 DO 60 IT = 1,NTRTN
C
                     IF(Y(KT(IT)).GT.1.0D-14)THEN
C
                             CON1 = CTT(IT)*TCIO(IT)*DEXP(TALPHA(IT)*Y(LX))
                             CON2 = CON1 * (Y(KT(IT))**TPOW(IT))
C
                             P(L,LX) = P(L,LX) + CON2*TALPHA(IT)
C
                             IF(KT(IT).NE.(NPTS+1))THEN
                                 P(L,KT(IT)) = P(L,KT(IT)) + TP[illegible] *CON1*
     *                                        (Y(KT(IT))**([illegible]-1.D0))
                             ENDIF
C
                     ENDIF
C
 60              CONTINUE
C
          ENDIF
C
             IF(IXX.EQ.1.OR.IXX.EQ.MESHPTS)THEN
C
                 DO 64 IW = 1,NWRTN
C
                     IF (KW(IW).EQ.(NPTS+1)) THEN
                                     KP = NPTS+1
                     ELSE
                                     KP = KX + KW(IW)
                     ENDIF
C
                     IF(Y(KP).GT.1.0D-14)THEN
C
                             CON1 = CTW(IW)*WCIO(IW)*(XINC/2.0D0)*
     *                                        DEXP(WALPHA(IW)*Y(LX))/H(IXX)
C
                             CON2 = CON1             * (Y(KP)**WPOW(IW))
C
                             P(L,LX) = P(L,LX) + CON2 *WALPHA(IW)
C
                             IF(KW(IW).NE.(NPTS+1))THEN
C
```

```
                P(L,KP) = P(L,KP) + (Y(KP)**(WPOW(IW)-1.D0))
     *                                          *WPOW(IW)*CON1
                        ENDIF
C
                    ENDIF
C
 64             CONTINUE
        ELSE
                DO 65 IW = 1,NWRTN
C
                    IF (KW(IW).EQ.(NPTS+1)) THEN
                                KP = NPTS+1
                    ELSE
                                KP = KX + KW(IW)
                    ENDIF
C
                    IF(Y(KP).GT.1.0D-14)THEN
C
                            CON1 = CTW(IW)*WCIO(IW)*(XINC)*
     *                                         DEXP(WALPHA(IW)*Y(LX))/H(IXX)
C
                            CON2 = CON1 *(Y(KP)**WPOW(IW))
C
                            P(L,LX) = P(L,LX) + CON2*WALPHA(IW)
C
                            IF(KW(IW).NE.(NPTS+1))THEN
C
                     P(L,KP) = P(L,KP) + (Y(KP)**(WPOW(IW)-1.D0))
     *                                          *CON1*WPOW(IW)
                            ENDIF
C
                    ENDIF
C
 65             CONTINUE
        ENDIF
C
 70     CONTINUE
C
C       PRINT*, P(L,L)
C
        DO 200 IS = 1, NEQ-1
C
                I = K + IS
C
                CON3 = Z(IS)*DIF(IS)*FC/(2.0D0*XINC)
C
                IF (IX.LT.MESHPTS-1)THEN
C
                CON1 = Z(IS)*Z(IS)*DIF(IS)*FC*FRT/(2.0D0*XINC)
                CON2 = CON1*Y(I)
C
                    P(L,I) = P(L,I) + CON1*(4.0D0*Y(L+NEQ)
     *                                                  - 3.0D0*Y(L) - Y(L+2*NEQ))
C
                    P(L,L) = P(L,L) - CON2*3.0D0
C
                    P(L,L+NEQ) = P(L,L+NEQ) + CON2*4.0D0
C
                    P(L,L+2*NEQ) = P(L,L+2*NEQ) - CON2
C
```

```
C
C
C
                    P(L,I+NEQ) = P(L,I+NEQ) + CON3*4.0D0
C
                    P(L,I) = P(L,I) - CON3*3.0D0
C
                    P(L,I+2*NEQ) = P(L,I+2*NEQ) - CON3
C
C
                ELSE
C
                CON1 = Z(IS)*Z(IS)*DIF(IS)*FC*FRT/(XINC)
                CON2 = CON1*Y(I)
                    P(L,I) = P(L,I) + CON1*(Y(L+NEQ) - Y(L))
C
                    P(L,L+NEQ) = P(L,L+NEQ) + CON2
C
                    P(L,L-NEQ) = P(L,L-NEQ) - CON2
C
C
                    P(L,I+NEQ) = P(L,I+NEQ) + CON3
C
                    P(L,I-NEQ) = P(L,I-NEQ) - CON3
C

C
                ENDIF
C
C
C
C*********************************************************************C
C               CONCENTRATION TERMS
C*********************************************************************C
C
 95             P(I,I) = P(I,I) + 1.0D0
C
C               PRINT*, I,P(I,I)
C
 200     CONTINUE
C
 300 CONTINUE
C
     DO 400 IS = 1,NEQ
         K = (MESHPTS-1)*NEQ +IS
         P(K,K) = P(K,K) + 1.0D0
 400 CONTINUE
C
C    DO 500 IX = 1,MESHPTS
C    DO 500 IS = 1, NEQ
C               K = (IX-1)*NEQ+IS
C               PRINT*, IX,IS,K,P(K,K)
C 500           CONTINUE
C
     RETURN
     END
C
C
C
C*********************************************************************C
```

```
C
      SUBROUTINE TIP_I(T,Y,PFACT)
C
C*************************************************************************C
C     WRITTEN BY : MAUREEN J. PSAILA-DOMBROWSKI
C     REVISION DATE : JULY 22, 1989
C*************************************************************************C
C     THIS SUBROUTINE USES OHM'S LAW TO CALCULATE AN INITIAL FLUXES
C     AND POTENTIAL AT THE CRACK TIP.
C*************************************************************************C
C     LIST OF VARIABLES
C
C
C
C*************************************************************************C
C
      INCLUDE 'P.BLK'
C
      DIMENSION Y(MA),SUM1S(MNDX),SUM2S(MNDX),YSAVE(MNDX)
C
      COMMON/SPECS/ Z(MNS),DIF(MNEQ),DCON(MNEQ)
C
      COMMON/POT/ PCD(MNS),PCM1(MNS),FRT,TIPJ(MNS),CLAMBDA,
     *                                PCON,FC,PCM(MNS),PDLIM
C
      COMMON/CRACK/ XLONG,XINC,XINCSQ,MESHPTS,NEQ,H(MNDX)
C
      COMMON/TIP/ NTRTN,TALPHA(MNTR),TCIO(MNTR),KT(MNTR),TPOW(MNTR),
     *                    KOEFT(MNTR,MNEQ),TKCIO(MNTR),CTT(MNTR),ST(MNTR,0:MNEQ)
C
      COMMON/WALL/ NWRTN,WALPHA(MNWR),WCIO(MNWR),KW(MNWR),WPOW(MNWR),
     *                    KOEFW(MNWR,MNEQ),WKCIO(MNWR),CTW(MNWR),SW(MNWR,0:MNEQ)
C
C*************************************************************************C
C     START PROGRAM
C*************************************************************************C
C     CALCULATE PL AND PR
C*************************************************************************C
C
      IC = 0
 5    Y(MESHPTS*NEQ) = 0.0D0
      NPTS = MESHPTS*NEQ
      COND = 0.0D0
      TCURRS = 0.0D0
      IALPHA = 0
      DO 7 IX = 1,MESHPTS
          L = NEQ*IX
          YSAVE(IX)= Y(L)
 7    CONTINUE
      IC = IC + 1
C
C*************************************************************************C
C     CALCULATE TOTAL CURRENT DOWN CRACK
C*************************************************************************C
C
      DO 10 IT = 1,NTRTN
C
          IF(TALPHA(IT).NE.0.0D0)IALPHA=1
          IF(Y(KT(IT)).GT.1.0D-14)
     *                TCURRS = TCURRS + CTT(IT)*TCIO(IT)*(Y(KT(IT))**TPOW(IT))
```

```
     *                                   *DEXP(TALPHA(IT)*Y(NEQ))
C
 10  CONTINUE
C    PRINT*, 'TCURRS',TCURRS
C
     DO 25 IX = 1,MESHPTS-1
          K = NEQ*(IX-1)
          DO 20 IW = 1,NWRTN
C
                IF (KW(IW).EQ.(NPTS+1)) THEN
                          KP = NPTS+1
                ELSE
                          KP = K + KW(IW)
                ENDIF
C
                IF(Y(KP).GT.1.0D-14)THEN
C
                          IF(WALPHA(IW).NE.0.0D0)IALPHA=1
C
                TCURRS = TCURRS + CTW(IW)*WCIO(IW)*XINC/H(IX)
     *                               *(Y(KP)**WPOW(IW))
     *                               *DEXP(WALPHA(IW)*Y(K+NEQ))
C
                ENDIF
C
 20       CONTINUE
 25  CONTINUE
C
C*************************************************************************C
C    START POSITION LOOP
C*************************************************************************C
C
     DO 450 IX = MESHPTS-1,1,-1
C
          K = (IX-1)*NEQ
          L = K + NEQ
C
C******              SUBTRACT OFF CURRENT OF LAST DX FROM TOTAL CURRENT
C
          TCURR = TCURRS
C
          DO 60 IW = 1,NWRTN
C
                    IF (KW(IW).EQ.(NPPTS+1)) THEN
                                   KP = NPTS+1
                    ELSE
                                   KP = K + KW(IW)
                    ENDIF
                   IF(Y(KP).GT.1.0D-14)THEN
C
                    TCURR = TCURR - CTW(IW)*WCIO(IW)*XINC/H(IX)
     *                               *(Y(KP)**WPOW(IW))
     *                               *DEXP(WALPHA(IW)*Y(L))
C
C
                    ENDIF
C
 60       CONTINUE
C
 66       SUM1 = 0.0D0
```

```
      SUM2 = 0.0D0
C
      DO 70 IS = 1,NEQ-1
C
            I = K + IS
C
            SUM1 = SUM1 + Z(IS)*Z(IS)*DIF(IS)*Y(I)
C
 70   CONTINUE
C
      IF (IX.EQ.1) THEN
            DO 80 IS = 1,NEQ-1
C
                I = K + IS
C
                SUM2 = SUM2 + Z(IS)*DIF(IS)*(4.0D0*Y(I+NEQ)
     *                            -3.0D0*Y(I)-Y(I+2*NEQ))/(2.0D0*XINC)
C
 80         CONTINUE
      ELSE
            DO 90 IS = 1,NEQ-1
C
                I = K + IS
C
                YP1 = Y(I+NEQ)
                YM1 = Y(I-NEQ)
C
                SUM2 = SUM2 + Z(IS)*DIF(IS)*(YP1-YM1)
     *                                      /(2.0D0*XINC)
C
 90       CONTINUE
      ENDIF
C
      CKAP = FC*SUM1*FRT
      COND = CKAP/XINC
C
      IF (TCURR.GE.0.0D0)THEN
            PR = Y(L+NEQ) + (TCURR+SUM2)/COND
            PL = Y(L+NEQ)
            IF(T.EQ.0.0D0.AND.IALPHA.EQ.1)PR = PDLIM
      ELSE
            PR = Y(L+NEQ)
            PL = Y(L+NEQ) + (TCURR+SUM2)/COND
            IF(T.EQ.0.0D0.AND.IALPHA.EQ.1)PL = PDLIM
C     *                                     PL = Y(L)
      ENDIF
C
C*************************************************************************C
C     CALCULATE F(PL) AND F(PR)
C*************************************************************************C
C
      ITERL = 0
 200                  TCURRL = TCURR
            TCURRR = TCURR
C     ENDIF
      ITERL = ITERL + 1
C
      DO 250 IW = 1,NWRTN
C
            IF(WCIO(IW).EQ.0.0D0)GO TO 250
```

```
C
                    IF (KW(IW).EQ.(NPTS+1)) THEN
                                        KP = NPTS+1
                    ELSE
                                        KP = K + KW(IW)
                    ENDIF
C
                   IF(Y(KP).GT.1.0D-14)THEN
C
                TCURRL = TCURRL + CTW(IW)*WCIO(IW)*(Y(KP)**WPOW(IW))
     *                              *DEXP(WALPHA(IW)*PL)*XINC/H(IX)
C
                TCURRR = TCURRR + CTW(IW)*WCIO(IW)*(Y(KP)**WPOW(IW))
     *                              *DEXP(WALPHA(IW)*PR)*XINC/H(IX)
C               ENDIF
C
                ENDIF
C
 250      CONTINUE
CC
          IF(IX.EQ.1)THEN
            DO 260 IT = 1,NTRTN
C
                   IF(Y(KP).GT.1.0D-14)THEN
C
                TCURRR = TCURRR + CTT(IT)*TCIO(IT)*(Y(KT(IT))**TPOW(IT))
     *                              *DEXP(TALPHA(IT)*PR)

                TCURRL = TCURRL + CTT(IT)*TCIO(IT)*(Y(KT(IT))**TPOW(IT))
     *                              *DEXP(TALPHA(IT)*PL)
C
                    ENDIF
C
 260        CONTINUE
          ENDIF
C
          IF (TCURRL.EQ.TCURRR)THEN
                IF(TCURR.GE.0.0D0)Y(L) = PR
                IF(TCURR.LT.0.0D0)Y(L) = PL
                GO TO 420
          ENDIF
C
          FPL = (TCURRL + SUM2)/COND + (Y(L+NEQ)-PL)
          FPR = (TCURRR + SUM2)/COND + (Y(L+NEQ)-PR)
C
          IF (FPL*FPR.LT.0.0D0) THEN
C
                IF(PR.NE.0.0D0)PTOL = DABS((PR-PL)/PR)
                IF(PR.EQ.0.0D0.AND.PL.NE.0.0D0)PTOL = DABS((PR-PL)/PL)
C               PRINT*, 'LT 0 ',PTOL
                IF(PTOL.LT.(2.0D0*PFACT)) GO TO 400
C
                PSTORE = PL
                PL = (PL+PR)/2.0D0
C               PRINT*, 'PL',PL,'PR',PR
                GO TO 200
C
          ELSE
C
                IF(PR.NE.0.0D0)PTOL = DABS((PR-PL)/PR)
```

```
                IF(PR.EQ.0.0D0.AND.PL.NE.0.0D0)PTOL = DABS((PR-PL)/PL)
C               PRINT*, 'GT 0 ',PTOL
                IF(PTOL.LT.(2.0D0*PFACT)) GO TO 400
C
                PR = PL
                PL = PSTORE
                PL = (PL+PR)/2.0D0
C               PRINT*, 'PL',PL,'PR',PR
                GO TO 200
C
        ENDIF
C
 400    Y(L) = (PL+PR)/2.0D0
C
 420    DO 440 IW = 1,NWRTN
C
                IF (KW(IW).EQ.(NPTS+1)) THEN
                        KP = NPTS+1
                ELSE
                        KP = K + KW(IW)
                ENDIF
C
                IF(Y(KP).GT.1.0D-14)THEN
C
                        TCURRS = TCURRS - CTW(IW)*WCIO(IW)*XINC
     *                                          *(Y(KP)**WPOW(IW))*
     *                                          DEXP(WALPHA(IW)*Y(L))/H(IX)
C
                ENDIF
C
 440    CONTINUE
C
 450 CONTINUE
C
     IF(IC.LE.1) GO TO 5
     DO 500 IX = 1, MESHPTS-1
C
        L = IX*NEQ
        IF (DABS((YSAVE(IX)-Y(L))/YSAVE(IX)).GT.PFACT) GOTO 5
C
 500 CONTINUE
C
C
     RETURN
     END
```

SAMPLE INPUT

```
THINGS TO REMEMBER:
     1) THERE ARE TWO PLACES TO SET EM : STATE AND VALUES(EICH=EM
                              AFTER TICH)

 $TYPE
  P_TYPE = 0,
  C_TYPE = 0
 $END
  VERIFY = 'Y'


 $SIZE
  NS = 6,
  NRTN = 4,
  NWRTN = 4,
  NTRTN = 4,
  NSRTN = 1,
  MESHPTS = 31,
  XLOW  = 0.0D0,
  XHIGH = 1.0D-2,
  HIN = 1.709D-7
 $END

 $F
  FILES(1) = 'H86',
  FILES(2) = 'OH86',
  FILES(3) = 'NA86',
  FILES(4) = 'HSO486',
  FILES(5) = 'MN86',
  FILES(6) = 'MNOH6',
  FILES(7) = 'P86',
  IFILES(1) = 41,
  IFILES(2) = 42,
  IFILES(3) = 43,
  IFILES(4) = 44,
  IFILES(5) = 45,
  IFILES(6) = 46,
  IFILES(7) = 47,
  OTFILE = 'CREV86'
 $END


 $STATE
  DSRATE = 0.0D0
  DHRATE = 0.0D0
  TEM = 573.0D0
  TEMR = 573.0D0
  EPS = 7.0D-11
  EM = 0.0D0
 $END

 $OUTPUT
  TOUT = 1.0D-2
  TFINAL = 9.0D2,
  TSTEP = 1.0D-6,
  MULTIME = 1.8D0,
  TADD = 25.0D,
  TOUTCH = 300.0D0
 $END
```

```
$NAMES
 ARS= ' ','H','OH','NA','HSO4','MN','MNOH','P',
 Z = 1.0D0,-1.0D0,1.0D0,-1.0D0,2.D0,1.D0,0.0D0
 TIPJ = 0.0D0,0.0D0,0.0D0,0.D0,0.D0,0.0D0,0.D0
 DIF = 1.86D-5,1.0D-5,2.36D-6,1.89D-6,1.4D-6,1.4D-6,0.D0
 G = 0.0D0,0.0D0,0.0D0,0.0D0,0.0D0,0.D0,0.D0
 GH = 0.0D0,0.0D0,0.0D0,0.0D0,0.0D0,0.D0,0.D0
$END


$TOL
 PDLIM = 1.5D0
 RFACT = 1.0D-15
 PFACT = 1.0D-5
$END


$VELPAR
 ETA = 1.26D-4
 GAMMA = 8.66D-4
 A = 0.18D0
 CK = 0.1932503D0
 DCK = 0.3162277D0
 FREQ = 1.0D0
$END

$VELDUG
 DK = 0.6324555D0
 SR = 0.1D0
 W = 0.32D0
 E = 2.0D3
 CM = 0.3D0
 FREQ = 0.1D0
 SIGMA = 3.4D0
$END


$TCURC
 PT1 = 1.0D0
 CLAMBDA = 0.5D0
$END

$SULPHUR
 WALLF = 1.0D-11
 TIPF = 1.0D-11
 WALLT = 0.0D0
 TIPT = 0.0D0
 NSP1 = 20
 NSP2 = 20
 P1 = 1.0
 P2 = 1.0
$END

$VALUES
 YI = 2.239D-6,2.239D-6,2.51D-6,2.51D-6,0.D0,0.D0,0.742747D0,
 YIM = 2.239D-6,2.238D-6,2.51D-6,2.51D-6,0.D0,0.D0,0.0D0
 YMCH = 2.961D-5,1.689D-7,2.51D-6,2.961D-5,0.D0,0.D0,0.0D0
 YMCH2 = 2.239D-6,2.239D-6,2.51D-6,2.51D-6,0.D0,0.D0,0.0D0
 TICH = 450.0D0
 EMICH = 0.0D0
```

```
 TICH2 = 450.25D0
 EMICH2 = 0.0D0
$END


$L
 MF = 22
 ITOL = 2
 ATOLI(1) = 1.0D-12
 ATOLI(2) = 1.0d-12
 ATOLI(3) = 1.0d-12
 ATOLI(4) = 1.0d-12
 ATOLI(5) = 1.0d-20
 ATOLI(6) = 1.0d-20
 ATOLI(7) = 1.0d-12
 RTOL = 1.0D-6
 ISTATE = 0
 IOPT = 1
 ITASI = 3
 RWORK(5) = 0.0D0
 RWORK(6) = 0.0D0
 RWORK(7) = 0.0D0
 RWORK(8) = 0.0D0
 RWORK(9) = 0.0D0
 RWORK(10) = 0.0D0
 IWORK(5) = 0.0D0
 IWORK(6) = 5000
 IWORK(7) = 0
 IWORK(8) = 0
 IWORK(9) = 0
 IWORK(10) = 0
 IDERV = 0
$END
```

```
CJP| 1 | 2 | 3 | 4 | 5 | 6 | 7 |                               |                  |
 W    1   2                          1.00D12               12.6
 W                   1   2          5.012D0                12.6
Mn    5              6   1          1.698d3                12.6
Mn    6   1          5              1.0d9                  12.6
H2S   5              6   1          1.818D3                12.6
H2S   6   1          5              1.0D10                 12.6
NI    5              6   1          6.026D3                12.6
NI    6   1          5               1.D9                  12.6
CJP| 1 | 2 | 3 | 4 | 5 | 6 | 7 |                               |                  |
REACTF3_2.DAT
```

```
| 1 | 2 | 3 |       SRC       |       SC        |
  2   2   5       1.0D8           2.3D-16                 MN
  2   2   5       1.0D14          2.25D-20                NI
  2   2   7       1.0D12          1.9857D-11
  2   6           1.0D14          3.765E-14
SREACT.DAT
```

	#e	R1	R2	R3	P1	P2	P3	TKCIO	TALPH	KT	TPOW	
A	2				2 1			7.4844D-4	0.0	0	0.0	
C	1				1 2			4.545D-8	0.6	0	0.0	H2O
C	1	1 1						2.03D-2	0.6	1	1.0	H+
A	2				1 5			7.16D-6	0.0	0	0.0	MN
C	8	1 4	9 1		1 5			2.03D-2	0.6	4	1.0	HSO4
C	1	1 5			1 6			2.03D-2	0.6	5	1.0	H2S
C	1				1 2			1.5D-6	0.6	0	0.0	
C	1	1 1						6.71D-1	0.6	1	1.0	
A	2				1 5			7.56D-4	0.0	0	0.0	
C	1	1 5			1 6			6.71D-1	0.6	5	1.0	
A	8				9 1	1 4		9.65D-7	0.0	0	0.0	
C	4	1 6			4 2			171.1364D0	0.5	6	1.0	
	#e	R1	R2	R3	P1	P2	P3	TKCIO	TALPH	KT	TPOW	

TREACT.DAT

	#e	R1	R2	R3	P1	P2	P3	WKCIO	WALPH	KW	WPOW	
A	2				2 1			7.4844D-4	0.0	0	0.0	
C	1				1 2			4.545D-8	0.6	0	0.0	H2O
C	1	1 1						2.03D-2	0.6	1	1.0	H+
A	2				1 5			7.56D-6	0.0	0	0.0	MN
C	8	1 4	9 1		1 5			2.03D-2	0.6	4	1.0	HSO4
C	1	1 5			1 6			2.03D-2	0.6	5	1.0	H2S
C	1				1 2			1.5D-6	0.6	0	0.0	
C	1	1 1						6.71D-1	0.6	1	1.0	
A	2				1 5			7.56D-4	0.0	0	0.0	
C	1	1 5			1 6			6.71D-1	0.6	5	1.0	
A	8				9 1	1 4		9.65D-7	0.0	0	0.0	
C	4	1 6			4 2			171.1364D0	0.5	6	1.0	
	#e	R1	R2	R3	P1	P2	P3	WKCIO	WALPH	KW	WPOW	

WREACT.DAT

SAMPLE OUTPUT

```
**************************************************
*                                                *
*              DIRENP4 CODE OUTPUT               *
*                                                *
**************************************************

================================================================================

                    RUN DATE              = 16-NOV-89
                    RUN TIME              = 22:07:46

================================================================================

                                  INPUT

================================================================================

      FILES :

            INPUT FILE NAME                   = DIRENP4.DAT
            OUTPUT FILE NAME                  = CREV86

            FILE FOR H                        = H86
            FILE FOR OH                       = OH86
            FILE FOR NA                       = NA86
            FILE FOR HSO4                     = HSO486
            FILE FOR MN                       = MN86
            FILE FOR MNOH                     = MNOH6
            FILE FOR P                        = P86

      GENERAL DATA :

            NUMBER OF SPECIES BEING EVALUATED =      6
            NUMBER OF EQUATIONS EVALUATED     =      7
            NUMBER OF CHEMICAL REACTIONS      =      4
            NUMBER OF WALL REACTIONS          =      4
            NUMBER OF TIP REACTIONS           =      4
            NUMBER OF SOLUBILITY REACTIONS    =      0

            NUMBER OF UNIFORM MESH POINTS     =     31
            LEFT COORDINATE                   =  0.000D+00
            RIGHT COORDINATE                  =  0.100D-01
            INITIAL HALF WIDTH                =  0.171D-06
            DELTA X                           =  0.333D-03
            NPTS + 1                          =    218

            TEMPERATURE                       =  0.573D+03
            REFERENCE TEMPERATURE             =  0.573D+03
            INITIAL BULK METAL POTENTIAL      =  0.000D+00

            LOW LET DOSE RATE                 =  0.000D+00
            HIGH LET DOSE RATE                =  0.000D+00

            FINAL TIME EVALUATION             =  0.900D+03
            INITIAL TIME STEP                 =  0.100D-01
            EPSILON                           =  0.700D-10
            TIME MULTIPLE                     =  0.180D+01
            TIME TO CHANGE FROM MULT. TO ADD  =  0.300D+03
            TIME ADDED TO TIME STEP           =  0.250D+02
```

```
SPECIES : H
          CHARGE  :   0.100E+01
          CRACK TIP FLUX  :   0.000E+00
          DIFFUSION COEFFICIENT :  0.166E-04
          G  :  0.000E+00
          GH :  0.000E+00

SPECIES : OH
          CHARGE  :  -0.100E+01
          CRACK TIP FLUX  :   0.000E+00
          DIFFUSION COEFFICIENT :  0.100E-04
          G  :  0.000E+00
          GH :  0.000E+00

SPECIES : NA
          CHARGE  :   0.100E+01
          CRACK TIP FLUX  :   0.000E+00
          DIFFUSION COEFFICIENT :  0.236E-05
          G  :  0.000E+00
          GH :  0.000E+00

SPECIES : HSO4
          CHARGE  :  -0.100E+01
          CRACK TIP FLUX  :   0.000E+00
          DIFFUSION COEFFICIENT :  0.189E-05
          G  :  0.000E+00
          GH :  0.000E+00

SPECIES : MN
          CHARGE  :   0.200E+01
          CRACK TIP FLUX  :   0.000E+00
          DIFFUSION COEFFICIENT :  0.140E-05
          G  :  0.000E+00
          GH :  0.000E+00

SPECIES : MNOH
          CHARGE  :   0.100E+01
          CRACK TIP FLUX  :   0.000E+00
          DIFFUSION COEFFICIENT :  0.140E-05
          G  :  0.000E+00
          GH :  0.000E+00
```

CHEMICAL REACTIONS :

	REACTIONS	RATE CONSTANT	ACTIVATION ENERGIES
W H OH	;	0.10D+13	0.13D+02
W	>H OH	0.50D+01	0.13D+02
n MN	>MNOH H	0.17D+04	0.13D+02
n MNOH H	>MN	0.10D+10	0.13D+02

KOEF(NRTN,NEQ) :

-1	-1	0	0	0	0
1	1	0	0	0	0
1	0	0	0	-1	1
-1	0	0	0	1	-1

IN1	IN2	IN3	RC
1	2	218	0.100E+13
218	218	218	0.501E+01
5	218	218	0.170E+04
1	6	218	0.100E+10

WALL REACTIONS :

TYPE	#e								
A	1.	2.	0.	0.	0.	>	2. H	0.	0.
C	-1.	1.	0.	0.	0.	>	1. OH	0.	0.
C	-1.	1.	1. H	0.	0.	>	0.	0.	0.
A	1.	2.	0.	0.	0.	>	1. MN	0.	0.

WCIO	WALPHA	KW	WPOW
0.748E-03	0.000E+00	218	0.100E+01
0.455E-07	0.600E+00	218	0.100E+01
0.203E-01	0.600E+00	1	0.100E+01
0.756E-05	0.000E+00	218	0.100E+01

SW(NWRTN,NEQ) :

1.0	0.0	0.0	0.0	0.0	0.0
0.0	1.0	0.0	0.0	0.0	0.0
-1.0	0.0	0.0	0.0	0.0	0.0
0.0	0.0	0.0	0.0	0.5	0.0

TIP REACTIONS :

TYPE	#e								
A	1.	2.	0.	0.	0.	>	2. H	0.	0.
C	-1.	1.	0.	0.	0.	>	1. OH	0.	0.
C	-1.	1.	1. H	0.	0.	>	0.	0.	0.
A	1.	2.	0.	0.	0.	>	1. MN	0.	0.

TCIO	TALPHA	KT	TPOW
0.748E-03	0.000E+00	218	0.100E+01
0.455E-07	0.600E+00	218	0.100E+01
0.203E-01	0.600E+00	1	0.100E+01
0.756E-05	0.000E+00	218	0.100E+01

ST(NTRTN,NEQ) :

```
   1.0    0.0    0.0    0.0    0.0    0.0
   0.0    1.0    0.0    0.0    0.0    0.0
  -1.0    0.0    0.0    0.0    0.0    0.0
   0.0    0.0    0.0    0.0    0.5    0.0

SOLUBILITY REACTIONS :

OH      OH      MN          0.10D+09  0.23D-15

KOEFS(NSRTN,NEQ) :
        0      -2       0       0      -1       0

 INS1   INS2     INS3          SRC              SC
   2      2     5   0.100E+09  0.230E-15


CHEMICAL DISSOLUTION
     WALLF =   0.10E-10       WALLT =   0.00E+00
     TIPF =    0.10E-10       TIPT =    0.00E+00
     NSP1 = 20        P1 =    0.10E+01
     NSP2 = 20        P2 =    0.10E+01
```

```
LSODI PARAMETERS :

  TOLERANCE FACTOR                  =      2
  RELATIVE TOLERANCE                =    0.10000D-05
  ABSOLUTE TOLERANCE                =    0.10000D-11
  ABSOLUTE TOLERANCE                =    0.10000D-11
  ABSOLUTE TOLERANCE                =    0.10000D-11
  ABSOLUTE TOLERANCE                =    0.10000D-11
  ABSOLUTE TOLERANCE                =    0.10000D-19
  ABSOLUTE TOLERANCE                =    0.10000D-19
  ABSOLUTE TOLERANCE                =    0.10000D-11
  ITASK                             =      3
  ISTATE                            =      0
  IOPT                              =      1
  MF                                =     22
  FIRST TIME STEP                   =  0.000E+00
  MAX TIME STEP                     =  0.000E+00
  MIN TIME STEP                     =  0.000E+00
  MAX ORDER ALLOWED                 =      0
  MAX NUMBER OF INTERNAL STEPS      =   5000
  MAX NUMBER OF MESSAGES            =      0
```

```
TIME =  0.000D+00  TIME STEP SIZE =  0.000E+00   NUMBER OF STEPS =     0
 AVE TIME STEP = 0.000E+00   TIP COND. = 0.146E-03   EXT. METAL POT. = 0.000E+00
 TIP FLUX :  H   = 0.000E+00 OH  = 0.000E+00 NA  = 0.000E+00
           HSO = 0.000E+00 MN  = 0.000E+00 MNO = 0.000E+00
 X = 0.00000  P = 0.743D+00 ELECT =  0.000D+00
   H   =  0.223900D-05    OH  =  0.223900D-05    NA  =  0.251000D-05
   HSO =  0.251000D-05    MN  =  0.000000D+00    MNO =  0.000000D+00
 X = 0.00333  P = 0.743D+00 ELECT =  0.000D+00
   H   =  0.223900D-05    OH  =  0.223900D-05    NA  =  0.251000D-05
   HSO =  0.251000D-05    MN  =  0.000000D+00    MNO =  0.000000D+00
 X = 0.00667  P = 0.743D+00 ELECT =  0.000D+00
   H   =  0.223900D-05    CH  =  0.223900D-05    NA  =  0.251000D-05
   HSO =  0.251000D-05    MN  =  0.000000D+00    MNO =  0.000000D+00
 X = 0.01000  P = 0.000D+00 ELECT =  0.100D-08
   H   =  0.223900D-05    OH  =  0.223800D-05    NA  =  0.251000D-05
   HSO =  0.251000D-05    MN  =  0.000000D+00    MNO =  0.000000D+00


TIME =  0.100D-01  TIME STEP SIZE =  0.692E-03   NUMBER OF STEPS =   117
 AVE TIME STEP = 0.859E-04   TIP COND. = 0.163E-03   EXT. METAL POT. = 0.000E+00
 TIP FLUX :  H   = 0.512E-08 OH  = 0.519E-08 NA  = 0.000E+00
           HSO = 0.000E+00 MN  = 0.392E-10 MNO = 0.000E+00
 X = 0.00000  P = 0.766D+00 ELECT = -0.671D-13
   H   =  0.113894D-05    OH  =  0.442708D-05    NA  =  0.250995D-05
   HSO =  0.251004D-05    MN  =  0.983177D-06    MNO =  0.132187D-05
 X = 0.00333  P = 0.766D+00 ELECT = -0.386D-13
   H   =  0.113944D-05    OH  =  0.442513D-05    NA  =  0.251008D-05
   HSO =  0.250994D-05    MN  =  0.982525D-06    MNO =  0.132050D-05
 X = 0.00667  P = 0.766D+00 ELECT = -0.386D-13
   H   =  0.113944D-05    OH  =  0.442513D-05    NA  =  0.251008D-05
   HSO =  0.250994D-05    MN  =  0.982525D-06    MNO =  0.132050D-05
 X = 0.01000  P = 0.000D+00 ELECT =  0.100D-08
   H   =  0.223900D-05    OH  =  0.223800D-05    NA  =  0.251000D-05
   HSO =  0.251000D-05    MN  =  0.000000D+00    MNO =  0.000000D+00


TIME =  0.187D-01  TIME STEP SIZE =  0.735E-03   NUMBER OF STEPS =   139
 AVE TIME STEP = 0.619E-04   TIP COND. = 0.199E-03   EXT. METAL POT. = 0.000E+00
 TIP FLUX :  H   = 0.573E-08 OH  = 0.581E-08 NA  = 0.000E+00
           HSO = 0.000E+00 MN  = 0.392E-10 MNO = 0.000E+00
 X = 0.00000  P = 0.775D+00 ELECT = -0.655D-13
   H   =  0.778752D-06    OH  =  0.647933D-05    NA  =  0.250995D-05
   HSO =  0.251005D-05    MN  =  0.142195D-05    MNO =  0.285677D-05
 X = 0.00333  P = 0.775D+00 ELECT = -0.439D-13
   H   =  0.779144D-06    OH  =  0.647602D-05    NA  =  0.251014D-05
   HSO =  0.250989D-05    MN  =  0.142126D-05    MNO =  0.285410D-05
 X = 0.00667  P = 0.775D+00 ELECT = -0.443D-13
   H   =  0.779144D-06    OH  =  0.647602D-05    NA  =  0.251014D-05
   HSO =  0.250989D-05    MN  =  0.142126D-05    MNO =  0.285410D-05
 X = 0.01000  P = 0.000D+00 ELECT =  0.100D-08
   H   =  0.223900D-05    OH  =  0.223800D-05    NA  =  0.251000D-05
   HSO =  0.251000D-05    MN  =  0.000000D+00    MNO =  0.000000D+00


TIME =  0.330D-01  TIME STEP SIZE =  0.115E-02   NUMBER OF STEPS =   163
 AVE TIME STEP = 0.878E-04   TIP COND. = 0.269E-03   EXT. METAL POT. = 0.000E+00
 TIP FLUX :  H   = 0.630E-08 OH  = 0.638E-08 NA  = 0.000E+00
           HSO = 0.000E+00 MN  = 0.392E-10 MNO = 0.000E+00
 X = 0.00000  P = 0.783D+00 ELECT = -0.557D-13
```

```
   H    =  0.509516D-06     OH   =  0.990968D-05     NA   =  0.251003D-05
   HSO  =  0.251000D-05     MN   =  0.183930D-05     MNO  =  0.572153D-05
 X = 0.00333   P = 0.783D+00 ELECT = -0.231D-13
   H    =  0.509778D-06     OH   =  0.990452D-05     NA   =  0.251021D-05
   HSO  =  0.250983D-05     MN   =  0.183869D-05     MNO  =  0.571698D-05
 X = 0.00667   P = 0.783D+00 ELECT = -0.250D-13
   H    =  0.509777D-06     OH   =  0.990453D-05     NA   =  0.251022D-05
   HSO  =  0.250983D-05     MN   =  0.183869D-05     MNO  =  0.571699D-05
 X = 0.01000   P = 0.000D+00 ELECT =  0.100D-08
   H    =  0.223900D-05     OH   =  0.223800D-05     NA   =  0.251000D-05
   HSO  =  0.251000D-05     MN   =  0.000000D+00     MNO  =  0.000000D+00


TIME =  0.590D-01  TIME STEP SIZE =  0.132E-02   NUMBER OF STEPS =   340
 AVE TIME STEP = 0.767E-04   TIP COND. = 0.294E-03   EXT. METAL POT. = 0.000E+00
 TIP FLUX :  H    = 0.644E-08 OH   = 0.652E-08 NA   = 0.000E+00
           HSO = 0.000E+00 MN   = 0.392E-10 MNO  = 0.000E+00
 X = 0.00000   P = 0.785D+00 ELECT =  0.862D-15
   H    =  0.453624D-06     OH   =  0.111319D-04     NA   =  0.251027D-05
   HSO  =  0.250980D-05     MN   =  0.185921D-05     MNO  =  0.695939D-05
 X = 0.00333   P = 0.785D+00 ELECT = -0.218D-13
   H    =  0.453619D-06     OH   =  0.111320D-04     NA   =  0.251031D-05
   HSO  =  0.250975D-05     MN   =  0.185919D-05     MNO  =  0.695940D-05
 X = 0.00667   P = 0.785D+00 ELECT = -0.215D-13
   H    =  0.453619D-06     OH   =  0.111320D-04     NA   =  0.251030D-05
   HSO  =  0.250975D-05     MN   =  0.185919D-05     MNO  =  0.695940D-05
 X = 0.01000   P = 0.000D+00 ELECT =  0.100D-08
   H    =  0.223900D-05     OH   =  0.223800D-05     NA   =  0.251000D-05
   HSO  =  0.251000D-05     MN   =  0.000000D+00     MNO  =  0.000000D+00


TIME =  0.109D+00  TIME STEP SIZE =  0.446E-02   NUMBER OF STEPS =   360
 AVE TIME STEP = 0.140E-03   TIP COND. = 0.294E-03   EXT. METAL POT. = 0.000E+00
 TIP FLUX :  H    = 0.644E-08 OH   = 0.652E-08 NA   = 0.000E+00
           HSO = 0.000E+00 MN   = 0.392E-10 MNO  = 0.000E+00
 X = 0.00000   P = 0.785D+00 ELECT = -0.655D-16
   H    =  0.453617D-06     OH   =  0.111321D-04     NA   =  0.251050D-05
   HSO  =  0.250961D-05     MN   =  0.185915D-05     MNO  =  0.695928D-05
 X = 0.00333   P = 0.785D+00 ELECT = -0.218D-13
   H    =  0.453613D-06     OH   =  0.111321D-04     NA   =  0.251049D-05
   HSO  =  0.250961D-05     MN   =  0.185914D-05     MNO  =  0.695931D-05
 X = 0.00667   P = 0.785D+00 ELECT = -0.231D-13
   H    =  0.453606D-06     OH   =  0.111323D-04     NA   =  0.251084D-05
   HSO  =  0.250954D-05     MN   =  0.185908D-05     MNO  =  0.695921D-05
 X = 0.01000   P = 0.000D+00 ELECT =  0.100D-08
   H    =  0.223900D-05     OH   =  0.223800D-05     NA   =  0.251000D-05
   HSO  =  0.251000D-05     MN   =  0.000000D+00     MNO  =  0.000000D+00


TIME =  0.190D+00  TIME STEP SIZE =  0.772E-02   NUMBER OF STEPS =   373
 AVE TIME STEP = 0.217E-03   TIP COND. = 0.294E-03   EXT. METAL POT. = 0.000E+00
 TIP FLUX :  H    = 0.644E-08 OH   = 0.652E-08 NA   = 0.000E+00
           HSO = 0.000E+00 MN   = 0.392E-10 MNO  = 0.000E+00
 X = 0.00000   P = 0.785D+00 ELECT = -0.825D-16
   H    =  0.453608D-06     OH   =  0.111323D-04     NA   =  0.251079D-05
   HSO  =  0.250936D-05     MN   =  0.185907D-05     MNO  =  0.695913D-05
 X = 0.00333   P = 0.785D+00 ELECT = -0.218D-13
   H    =  0.453604D-06     OH   =  0.111323D-04     NA   =  0.251078D-05
   HSO  =  0.250937D-05     MN   =  0.185907D-05     MNO  =  0.695917D-05
 X = 0.00667   P = 0.785D+00 ELECT = -0.504D-13
```

```
   H    =  0.453461D-06     OH   =  0.111358D-04     NA   =  0.251675D-05
   HSO  =  0.250721D-05     MN   =  0.185790D-05     MNO  =  0.695703D-05
 X = 0.01000   P = 0.000D+00 ELECT =  0.100D-08
   H    =  0.223900D-05     OH   =  0.223800D-05     NA   =  0.251000D-05
   HSO  =  0.251000D-05     MN   =  0.000000D+00     MNO  =  0.000000D+00


TIME =  0.353D+00  TIME STEP SIZE =  0.200E-01   NUMBER OF STEPS =   385
 AVE TIME STEP = 0.424E-03   TIP COND. = 0.294E-03   EXT. METAL POT. = 0.000E+00
 TIP FLUX :  H    = 0.644E-08 OH   = 0.652E-08 NA   = 0.000E+00
           HSO = 0.000E+00 MN   = 0.392E-10 MNO = 0.000E+00
 X = 0.00000   P = 0.785D+00 ELECT = -0.778D-16
   H    =  0.453589D-06     OH   =  0.111328D-04     NA   =  0.251138D-05
   HSO  =  0.250869D-05     MN   =  0.185892D-05     MNO  =  0.695885D-05
 X = 0.00333   P = 0.785D+00 ELECT = -0.218D-13
   H    =  0.453585D-06     OH   =  0.111328D-04     NA   =  0.251138D-05
   HSO  =  0.250890D-05     MN   =  0.185892D-05     MNO  =  0.695888D-05
 X = 0.00667   P = 0.785D+00 ELECT = -0.579D-13
   H    =  0.452871D-06     OH   =  0.111504D-04     NA   =  0.254086D-05
   HSO  =  0.249745D-05     MN   =  0.185306D-05     MNO  =  0.694796D-05
 X = 0.01000   P = 0.000D+00 ELECT =  0.100D-08
   H    =  0.223900D-05     OH   =  0.223800D-05     NA   =  0.251000D-05
   HSO  =  0.251000D-05     MN   =  0.000000D+00     MNO  =  0.000000D+00


TIME =  0.637D+00  TIME STEP SIZE =  0.406E-01   NUMBER OF STEPS =   395
 AVE TIME STEP = 0.718E-03   TIP COND. = 0.294E-03   EXT. METAL POT. = 0.000E+00
 TIP FLUX :  H    = 0.644E-08 OH   = 0.652E-08 NA   = 0.000E+00
           HSO = 0.000E+00 MN   = 0.392E-10 MNO = 0.000E+00
 X = 0.00000   P = 0.785D+00 ELECT = -0.803D-16
   H    =  0.453557D-06     OH   =  0.111336D-04     NA   =  0.251241D-05
   HSO  =  0.250807D-05     MN   =  0.185866D-05     MNO  =  0.695836D-05
 X = 0.00333   P = 0.785D+00 ELECT = -0.228D-13
   H    =  0.453541D-06     OH   =  0.111339D-04     NA   =  0.251295D-05
   HSO  =  0.250796D-05     MN   =  0.185856D-05     MNO  =  0.695821D-05
 X = 0.00667   P = 0.785D+00 ELECT = -0.309D-13
   H    =  0.452261D-06     OH   =  0.111654D-04     NA   =  0.256992D-05
   HSO  =  0.249143D-05     MN   =  0.184806D-05     MNO  =  0.693854D-05
 X = 0.01000   P = 0.000D+00 ELECT =  0.100D-08
   H    =  0.223900D-05     OH   =  0.223800D-05     NA   =  0.251000D-05
   HSO  =  0.251000D-05     MN   =  0.000000D+00     MNO  =  0.000000D+00


TIME =  0.114D+01  TIME STEP SIZE =  0.846E-01   NUMBER OF STEPS =   404
 AVE TIME STEP = 0.123E-02   TIP COND. = 0.294E-03   EXT. METAL POT. = 0.000E+00
 TIP FLUX :  H    = 0.644E-08 OH   = 0.652E-08 NA   = 0.000E+00
           HSO = 0.000E+00 MN   = 0.392E-10 MNO = 0.000E+00
 X = 0.00000   P = 0.785D+00 ELECT = -0.364D-15
   H    =  0.453498D-06     OH   =  0.111350D-04     NA   =  0.251432D-05
   HSO  =  0.250661D-05     MN   =  0.185818D-05     MNO  =  0.695745D-05
 X = 0.00333   P = 0.785D+00 ELECT = -0.245D-13
   H    =  0.453382D-06     OH   =  0.111378D-04     NA   =  0.251950D-05
   HSO  =  0.250538D-05     MN   =  0.185725D-05     MNO  =  0.695577D-05
 X = 0.00667   P = 0.785D+00 ELECT = -0.216D-13
   H    =  0.451974D-06     OH   =  0.111725D-04     NA   =  0.259179D-05
   HSO  =  0.249678D-05     MN   =  0.184572D-05     MNO  =  0.693410D-05
 X = 0.01000   P = 0.000D+00 ELECT =  0.100D-08
   H    =  0.223900D-05     OH   =  0.223800D-05     NA   =  0.251000D-05
   HSO  =  0.251000D-05     MN   =  0.000000D+00     MNO  =  0.000000D+00
```

```
TIME =  0.209D+01  TIME STEP SIZE =  0.124E+00   NUMBER OF STEPS =   413
 AVE TIME STEP = 0.232E-02   TIP COND. = 0.294E-03   EXT. METAL POT. = 0.000E+00
 TIP FLUX :  H   = 0.644E-08 OH  = 0.652E-08 NA  = 0.000E+00
           HSO = 0.000E+00 MN  = 0.392E-10 MNO = 0.000E+00
 X = 0.00000  P = 0.785D+00 ELECT = -0.204D-14
   H   =  0.453331D-06     CH  =  0.111391D-04     NA  =  0.252061D-05
   HSO =  0.250333D-05     MN  =  0.185681D-05     MNO =  0.695489D-05
 X = 0.00333  P = 0.785D+00 ELECT = -0.239D-13
   H   =  0.453011D-06     OH  =  0.111469D-04     NA  =  0.253662D-05
   HSO =  0.250121D-05     MN  =  0.185421D-05     MNO =  0.695006D-05
 X = 0.00667  P = 0.785D+00 ELECT = -0.216D-13
   H   =  0.451777D-06     OH  =  0.111774D-04     NA  =  0.261370D-05
   HSO =  0.250737D-05     MN  =  0.184411D-05     MNO =  0.693107D-05
 X = 0.01000  P = 0.000D+00 ELECT =  0.100D-08
   H   =  0.223900D-05     OH  =  0.223800D-05     NA  =  0.251000D-05
   HSO =  0.251000D-05     MN  =  0.000000D+00     MNO =  0.000000D+00


TIME =  0.358D+01  TIME STEP SIZE =  0.282E+00   NUMBER OF STEPS =   420
 AVE TIME STEP = 0.354E-02   TIP COND. = 0.295E-03   EXT. METAL POT. = 0.000E+00
 TIP FLUX :  H   = 0.644E-08 OH  = 0.652E-08 NA  = 0.000E+00
           HSO = 0.000E+00 MN  = 0.392E-10 MNO = 0.000E+00
 X = 0.00000  P = 0.785D+00 ELECT = -0.299D-14
   H   =  0.452937D-06     OH  =  0.111488D-04     NA  =  0.253788D-05
   HSO =  0.249796D-05     MN  =  0.185357D-05     MNO =  0.694882D-05
 X = 0.00333  P = 0.785D+00 ELECT = -0.231D-13
   H   =  0.452546D-06     OH  =  0.111584D-04     NA  =  0.256119D-05
   HSO =  0.249903D-05     MN  =  0.185039D-05     MNO =  0.694290D-05
 X = 0.00667  P = 0.785D+00 ELECT = -0.219D-13
   H   =  0.451489D-06     OH  =  0.111845D-04     NA  =  0.263786D-05
   HSO =  0.251498D-05     MN  =  0.184176D-05     MNO =  0.692665D-05
 X = 0.01000  P = 0.000D+00 ELECT =  0.100D-08
   H   =  0.223900D-05     OH  =  0.223800D-05     NA  =  0.251000D-05
   HSO =  0.251000D-05     MN  =  0.000000D+00     MNO =  0.000000D+00


TIME =  0.659D+01  TIME STEP SIZE =  0.434E+00   NUMBER OF STEPS =   428
 AVE TIME STEP = 0.704E-02   TIP COND. = 0.295E-03   EXT. METAL POT. = 0.000E+00
 TIP FLUX :  H   = 0.644E-08 OH  = 0.652E-08 NA  = 0.000E+00
           HSO = 0.000E+00 MN  = 0.392E-10 MNO = 0.000E+00
 X = 0.00000  P = 0.785D+00 ELECT = -0.242D-14
   H   =  0.452083D-06     OH  =  0.111699D-04     NA  =  0.258082D-05
   HSO =  0.249185D-05     MN  =  0.184658D-05     MNO =  0.693569D-05
 X = 0.00333  P = 0.785D+00 ELECT = -0.227D-13
   H   =  0.451763D-06     OH  =  0.111777D-04     NA  =  0.260490D-05
   HSO =  0.249774D-05     MN  =  0.184399D-05     MNO =  0.693086D-05
 X = 0.00667  P = 0.785D+00 ELECT = -0.218D-13
   H   =  0.450964D-06     OH  =  0.111976D-04     NA  =  0.267248D-05
   HSO =  0.251938D-05     MN  =  0.183747D-05     MNO =  0.691857D-05
 X = 0.01000  P = 0.000D+00 ELECT =  0.100D-08
   H   =  0.223900D-05     OH  =  0.223800D-05     NA  =  0.251000D-05
   HSO =  0.251000D-05     MN  =  0.000000D+00     MNO =  0.000000D+00


TIME =  0.120D+02  TIME STEP SIZE =  0.990E+00   NUMBER OF STEPS =   435
 AVE TIME STEP = 0.124E-01   TIP COND. = 0.296E-03   EXT. METAL POT. = 0.000E+00
 TIP FLUX :  H   = 0.644E-08 OH  = 0.652E-08 NA  = 0.000E+00
           HSO = 0.000E+00 MN  = 0.392E-10 MNO = 0.000E+00
 X = 0.00000  P = 0.785D+00 ELECT = -0.127D-14
```

```
   H    =  0.450801D-06     OH   =  0.112017D-04     NA   =  0.265117D-05
   HSO  =  0.248845D-05     MN   =  0.183611D-05     MNO  =  0.691597D-05
 X = 0.00333  P = 0.785D+00 ELECT = -0.221D-13
   H    =  0.450628D-06     OH   =  0.112059D-04     NA   =  0.266866D-05
   HSO  =  0.249617D-05     MN   =  0.183472D-05     MNO  =  0.691339D-05
 X = 0.00667  P = 0.785D+00 ELECT = -0.215D-13
   H    =  0.450227D-06     OH   =  0.112153D-04     NA   =  0.271514D-05
   HSO  =  0.251960D-05     MN   =  0.183146D-05     MNO  =  0.690724D-05
 X = 0.01000  P = 0.000D+00 ELECT =  0.100D-08
   H    =  0.223900D-05     OH   =  0.223800D-05     NA   =  0.251000D-05
   HSO  =  0.251000D-05     MN   =  0.000000D+00     MNO  =  0.000000D+00


TIME =  0.209D+02  TIME STEP SIZE =  0.147E+01   NUMBER OF STEPS =   442
 AVE TIME STEP = 0.201E-01   TIP COND. = 0.297E-03   EXT. METAL POT. = 0.000E+00
 TIP FLUX :  H   = 0.645E-08 OH  = 0.653E-08 NA  = 0.000E+00
           HSO = 0.000E+00 MN  = 0.392E-10 MNO = 0.000E+00
 X = 0.00000  P = 0.785D+00 ELECT =  0.345D-16
   H    =  0.449325D-06     OH   =  0.112386D-04     NA   =  0.273428D-05
   HSO  =  0.248651D-05     MN   =  0.182409D-05     MNO  =  0.689327D-05
 X = 0.00333  P = 0.785D+00 ELECT = -0.215D-13
   H    =  0.449321D-06     OH   =  0.112386D-04     NA   =  0.274225D-05
   HSO  =  0.249446D-05     MN   =  0.182408D-05     MNO  =  0.689329D-05
 X = 0.00667  P = 0.785D+00 ELECT = -0.211D-13
   H    =  0.449388D-06     OH   =  0.112369D-04     NA   =  0.276225D-05
   HSO  =  0.251831D-05     MN   =  0.182463D-05     MNO  =  0.689432D-05
 X = 0.01000  P = 0.000D+00 ELECT =  0.100D-08
   H    =  0.223900D-05     OH   =  0.223800D-05     NA   =  0.251000D-05
   HSO  =  0.251000D-05     MN   =  0.000000D+00     MNO  =  0.000000D+00


TIME =  0.393D+02  TIME STEP SIZE =  0.378E+01   NUMBER OF STEPS =   449
 AVE TIME STEP = 0.411E-01   TIP COND. = 0.297E-03   EXT. METAL POT. = 0.000E+00
 TIP FLUX :  H   = 0.645E-08 OH  = 0.653E-08 NA  = 0.000E+00
           HSO = 0.000E+00 MN  = 0.392E-10 MNO = 0.000E+00
 X = 0.00000  P = 0.785D+00 ELECT =  0.142D-14
   H    =  0.447755D-06     OH   =  0.112780D-04     NA   =  0.282358D-05
   HSO  =  0.248514D-05     MN   =  0.181135D-05     MNO  =  0.686912D-05
 X = 0.00333  P = 0.785D+00 ELECT = -0.208D-13
   H    =  0.447930D-06     OH   =  0.112735D-04     NA   =  0.282121D-05
   HSO  =  0.249309D-05     MN   =  0.181279D-05     MNO  =  0.687189D-05
 X = 0.00667  P = 0.785D+00 ELECT = -0.207D-13
   H    =  0.448492D-06     OH   =  0.112594D-04     NA   =  0.281267D-05
   HSO  =  0.251704D-05     MN   =  0.181735D-05     MNO  =  0.688055D-05
 X = 0.01000  P = 0.000D+00 ELECT =  0.100D-08
   H    =  0.223900D-05     OH   =  0.223800D-05     NA   =  0.251000D-05
   HSO  =  0.251000D-05     MN   =  0.000000D+00     MNO  =  0.000000D+00


TIME =  0.679D+02  TIME STEP SIZE =  0.448E+01   NUMBER OF STEPS =   456
 AVE TIME STEP = 0.626E-01   TIP COND. = 0.298E-03   EXT. METAL POT. = 0.000E+00
 TIP FLUX :  H   = 0.645E-08 OH  = 0.653E-08 NA  = 0.000E+00
           HSO = 0.000E+00 MN  = 0.392E-10 MNO = 0.000E+00
 X = 0.00000  P = 0.785D+00 ELECT =  0.209D-14
   H    =  0.446908D-06     OH   =  0.112974D-04     NA   =  0.286776D-05
   HSO  =  0.248495D-05     MN   =  0.180514D-05     MNO  =  0.685732D-05
 X = 0.00333  P = 0.785D+00 ELECT = -0.204D-13
   H    =  0.447249D-06     OH   =  0.112907D-04     NA   =  0.286029D-05
   HSO  =  0.249283D-05     MN   =  0.180728D-05     MNO  =  0.686143D-05
 X = 0.00667  P = 0.785D+00 ELECT = -0.206D-13
```

```
   H    =  0.448053D-06     OH   =  0.112704D-04     NA   =  0.283764D-05
   HSO  =  0.251664D-05     MN   =  0.181379D-05     MNO  =  0.687379D-05
 X = 0.01000   P = 0.000D+00 ELECT =  0.100D-08
   H    =  0.223900D-05     OH   =  0.223800D-05     NA   =  0.251000D-05
   HSO  =  0.251000D-05     MN   =  0.000000D+00     MNO  =  0.000000D+00


TIME =  0.126D+03  TIME STEP SIZE =  0.711E+01   NUMBER OF STEPS =   466
 AVE TIME STEP = 0.124E+00   TIP COND. = 0.298E-03   EXT. METAL POT. = 0.000E+00
 TIP FLUX :  H    = 0.645E-08 OH   = 0.653E-08 NA   = 0.000E+00
           HSO = 0.000E+00 MN   = 0.392E-10 MNO = 0.000E+00
 X = 0.00000   P = 0.785D+00 ELECT =  0.228D-14
   H    =  0.446767D-06     OH   =  0.113030D-04     NA   =  0.288066D-05
   HSO  =  0.248510D-05     MN   =  0.180336D-05     MNO  =  0.685393D-05
 X = 0.00333   P = 0.785D+00 ELECT = -0.203D-13
   H    =  0.447054D-06     OH   =  0.112956D-04     NA   =  0.287170D-05
   HSO  =  0.249294D-05     MN   =  0.180570D-05     MNO  =  0.685842D-05
 X = 0.00667   P = 0.785D+00 ELECT = -0.205D-13
   H    =  0.447926D-06     OH   =  0.112736D-04     NA   =  0.284493D-05
   HSO  =  0.251662D-05     MN   =  0.181276D-05     MNO  =  0.687184D-05
 X = 0.01000   P = 0.000D+00 ELECT =  0.100D-08
   H    =  0.223900D-05     OH   =  0.223800D-05     NA   =  0.251000D-05
   HSO  =  0.251000D-05     MN   =  0.000000D+00     MNO  =  0.000000D+00


TIME =  0.225D+03  TIME STEP SIZE =  0.114E+02   NUMBER OF STEPS =   477
 AVE TIME STEP = 0.208E+00   TIP COND. = 0.298E-03   EXT. METAL POT. = 0.000E+00
 TIP FLUX :  H    = 0.645E-08 OH   = 0.653E-08 NA   = 0.000E+00
           HSO = 0.000E+00 MN   = 0.392E-10 MNO = 0.000E+00
 X = 0.00000   P = 0.785D+00 ELECT =  0.229D-14
   H    =  0.446755D-06     OH   =  0.113033D-04     NA   =  0.288139D-05
   HSO  =  0.248513D-05     MN   =  0.180326D-05     MNO  =  0.685374D-05
 X = 0.00333   P = 0.785D+00 ELECT = -0.203D-13
   H    =  0.447043D-06     OH   =  0.112959D-04     NA   =  0.287234D-05
   HSO  =  0.249296D-05     MN   =  0.180561D-05     MNO  =  0.685826D-05
 X = 0.00667   P = 0.785D+00 ELECT = -0.205D-13
   H    =  0.447919D-06     OH   =  0.112738D-04     NA   =  0.284534D-05
   HSO  =  0.251663D-05     MN   =  0.181271D-05     MNO  =  0.687174D-05
 X = 0.01000   P = 0.000D+00 ELECT =  0.100D-08
   H    =  0.223900D-05     OH   =  0.223800D-05     NA   =  0.251000D-05
   HSO  =  0.251000D-05     MN   =  0.000000D+00     MNO  =  0.000000D+00


TIME =  0.434D+03  TIME STEP SIZE =  0.618E+02   NUMBER OF STEPS =   483
 AVE TIME STEP = 0.433E+00   TIP COND. = 0.298E-03   EXT. METAL POT. = 0.000E+00
 TIP FLUX :  H    = 0.645E-08 OH   = 0.653E-08 NA   = 0.000E+00
           HSO = 0.000E+00 MN   = 0.392E-10 MNO = 0.000E+00
 X = 0.00000   P = 0.785D+00 ELECT =  0.229D-14
   H    =  0.446755D-06     OH   =  0.113033D-04     NA   =  0.288139D-05
   HSO  =  0.248514D-05     MN   =  0.180326D-05     MNO  =  0.685374D-05
 X = 0.00333   P = 0.785D+00 ELECT = -0.203D-13
   H    =  0.447043D-06     OH   =  0.112959D-04     NA   =  0.287235D-05
   HSO  =  0.249296D-05     MN   =  0.180561D-05     MNO  =  0.685826D-05
 X = 0.00667   P = 0.785D+00 ELECT = -0.205D-13
   H    =  0.447919D-06     OH   =  0.112738D-04     NA   =  0.284534D-05
   HSO  =  0.251663D-05     MN   =  0.181271D-05     MNO  =  0.687174D-05
 X = 0.01000   P = 0.000D+00 ELECT =  0.100D-08
   H    =  0.223900D-05     OH   =  0.223800D-05     NA   =  0.251000D-05
   HSO  =  0.251000D-05     MN   =  0.000000D+00     MNO  =  0.000000D+00
```

```
TIME =  0.496D+03  TIME STEP SIZE =  0.618E+02   NUMBER OF STEPS =   484
 AVE TIME STEP = 0.128E+00   TIP COND. = 0.298E-03   EXT. METAL POT. = 0.000E+00
 TIP FLUX :  H   = 0.645E-08 OH  = 0.653E-08 NA  = 0.000E+00
           HSO = 0.000E+00 MN  = 0.392E-10 MNO = 0.000E+00
 X = 0.00000  P = 0.785D+00 ELECT =  0.229D-14
   H   =  0.446755D-06     OH  =  0.113033D-04     NA  =  0.288139D-05
   HSO =  0.248514D-05     MN  =  0.180326D-05     MNO =  0.685374D-05
 X = 0.00333  P = 0.785D+00 ELECT = -0.203D-13
   H   =  0.447043D-06     OH  =  0.112959D-04     NA  =  0.287235D-05
   HSO =  0.249296D-05     MN  =  0.180561D-05     MNO =  0.685826D-05
 X = 0.00667  P = 0.785D+00 ELECT = -0.205D-13
   H   =  0.447919D-06     OH  =  0.112738D-04     NA  =  0.284534D-05
   HSO =  0.251663D-05     MN  =  0.181271D-05     MNO =  0.687174D-05
 X = 0.01000  P = 0.000D+00 ELECT =  0.100D-08
   H   =  0.223900D-05     OH  =  0.223800D-05     NA  =  0.251000D-05
   HSO =  0.251000D-05     MN  =  0.000000D+00     MNO =  0.000000D+00


TIME =  0.522D+03  TIME STEP SIZE =  0.402E+01   NUMBER OF STEPS =    31
 AVE TIME STEP = 0.833E+00   TIP COND. = 0.298E-03   EXT. METAL POT. = 0.000E+00
 TIP FLUX :  H   = 0.645E-08 OH  = 0.653E-08 NA  = 0.000E+00
           HSO = 0.000E+00 MN  = 0.392E-10 MNO = 0.000E+00
 X = 0.00000  P = 0.785D+00 ELECT =  0.229D-14
   H   =  0.446744D-06     OH  =  0.113036D-04     NA  =  0.288186D-05
   HSO =  0.248495D-05     MN  =  0.180317D-05     MNO =  0.685357D-05
 X = 0.00333  P = 0.785D+00 ELECT = -0.203D-13
   H   =  0.447031D-06     OH  =  0.112962D-04     NA  =  0.287284D-05
   HSO =  0.249277D-05     MN  =  0.180552D-05     MNO =  0.685808D-05
 X = 0.00667  P = 0.785D+00 ELECT = -0.205D-13
   H   =  0.447906D-06     OH  =  0.112741D-04     NA  =  0.284590D-05
   HSO =  0.251641D-05     MN  =  0.181260D-05     MNO =  0.687153D-05
 X = 0.01000  P = 0.000D+00 ELECT =  0.000D+00
   H   =  0.223900D-05     OH  =  0.223900D-05     NA  =  0.251000D-05
   HSO =  0.251000D-05     MN  =  0.000000D+00     MNO =  0.000000D+00


TIME =  0.551D+03  TIME STEP SIZE =  0.878E+01   NUMBER OF STEPS =     6
 AVE TIME STEP = 0.489E+01   TIP COND. = 0.298E-03   EXT. METAL POT. = 0.000E+00
 TIP FLUX :  H   = 0.645E-08 OH  = 0.653E-08 NA  = 0.000E+00
           HSO = 0.000E+00 MN  = 0.392E-10 MNO = 0.000E+00
 X = 0.00000  P = 0.785D+00 ELECT =  0.229D-14
   H   =  0.446740D-06     OH  =  0.113037D-04     NA  =  0.288204D-05
   HSO =  0.248489D-05     MN  =  0.180314D-05     MNO =  0.685351D-05
 X = 0.00333  P = 0.785D+00 ELECT = -0.203D-13
   H   =  0.447028D-06     OH  =  0.112963D-04     NA  =  0.287299D-05
   HSO =  0.249271D-05     MN  =  0.180549D-05     MNO =  0.685802D-05
 X = 0.00667  P = 0.785D+00 ELECT = -0.205D-13
   H   =  0.447903D-06     OH  =  0.112742D-04     NA  =  0.284600D-05
   HSO =  0.251637D-05     MN  =  0.181258D-05     MNO =  0.687149D-05
 X = 0.01000  P = 0.000D+00 ELECT =  0.000D+00
   H   =  0.223900D-05     OH  =  0.223900D-05     NA  =  0.251000D-05
   HSO =  0.251000D-05     MN  =  0.000000D+00     MNO =  0.000000D+00


TIME =  0.593D+03  TIME STEP SIZE =  0.179E+02   NUMBER OF STEPS =     5
 AVE TIME STEP = 0.830E+01   TIP COND. = 0.298E-03   EXT. METAL POT. = 0.000E+00
 TIP FLUX :  H   = 0.645E-08 OH  = 0.653E-08 NA  = 0.000E+00
           HSO = 0.000E+00 MN  = 0.392E-10 MNO = 0.000E+00
 X = 0.00000  P = 0.785D+00 ELECT =  0.229D-14
```

```
   H    =  0.446739D-06     OH   =  0.113037D-04     NA   =  0.288208D-05
   HSO  =  0.248487D-05     MN   =  0.180313D-05     MNO  =  0.685349D-05
 X = 0.00333   P = 0.785D+00 ELECT = -0.203D-13
   H    =  0.447027D-06     OH   =  0.112963D-04     NA   =  0.287303D-05
   HSO  =  0.249270D-05     MN   =  0.180548D-05     MNO  =  0.685801D-05
 X = 0.00667   P = 0.785D+00 ELECT = -0.205D-13
   H    =  0.447903D-06     OH   =  0.112742D-04     NA   =  0.284603D-05
   HSO  =  0.251637D-05     MN   =  0.181257D-05     MNO  =  0.687148D-05
 X = 0.01000   P = 0.000D+00 ELECT =  0.000D+00
   H    =  0.223900D-05     OH   =  0.223900D-05     NA   =  0.251000D-05
   HSO  =  0.251000D-05     MN   =  0.000000D+00     MNO  =  0.000000D+00


TIME =  0.619D+03  TIME STEP SIZE =  0.253E+02   NUMBER OF STEPS =      3
 AVE TIME STEP = 0.884E+01   TIP COND. = 0.298E-03   EXT. METAL POT. = 0.000E+00
 TIP FLUX :  H    = 0.645E-08 OH   = 0.653E-08 NA   = 0.000E+00
             HSO = 0.000E+00 MN   = 0.392E-10 MNO  = 0.000E+00
 X = 0.00000   P = 0.785D+00 ELECT =  0.229D-14
   H    =  0.446739D-06     OH   =  0.113037D-04     NA   =  0.288209D-05
   HSO  =  0.248487D-05     MN   =  0.180313D-05     MNO  =  0.685349D-05
 X = 0.00333   P = 0.785D+00 ELECT = -0.203D-13
   H    =  0.447026D-06     OH   =  0.112963D-04     NA   =  0.287304D-05
   HSO  =  0.249270D-05     MN   =  0.180548D-05     MNO  =  0.685800D-05
 X = 0.00667   P = 0.785D+00 ELECT = -0.205D-13
   H    =  0.447903D-06     OH   =  0.112742D-04     NA   =  0.284603D-05
   HSO  =  0.251636D-05     MN   =  0.181257D-05     MNO  =  0.687148D-05
 X = 0.01000   P = 0.000D+00 ELECT =  0.000D+00
   H    =  0.223900D-05     OH   =  0.223900D-05     NA   =  0.251000D-05
   HSO  =  0.251000D-05     MN   =  0.000000D+00     MNO  =  0.000000D+00


TIME =  0.660D+03  TIME STEP SIZE =  0.396E+02   NUMBER OF STEPS =      3
 AVE TIME STEP = 0.136E+02   TIP COND. = 0.298E-03   EXT. METAL POT. = 0.000E+00
 TIP FLUX :  H    = 0.645E-08 OH   = 0.653E-08 NA   = 0.000E+00
             HSO = 0.000E+00 MN   = 0.392E-10 MNO  = 0.000E+00
 X = 0.00000   P = 0.785D+00 ELECT =  0.229D-14
   H    =  0.446739D-06     OH   =  0.113037D-04     NA   =  0.288209D-05
   HSO  =  0.248487D-05     MN   =  0.180313D-05     MNO  =  0.685349D-05
 X = 0.00333   P = 0.785D+00 ELECT = -0.203D-13
   H    =  0.447026D-06     OH   =  0.112963D-04     NA   =  0.287304D-05
   HSO  =  0.249270D-05     MN   =  0.180548D-05     MNO  =  0.685800D-05
 X = 0.00667   P = 0.785D+00 ELECT = -0.205D-13
   H    =  0.447903D-06     OH   =  0.112742D-04     NA   =  0.284603D-05
   HSO  =  0.251636D-05     MN   =  0.181257D-05     MNO  =  0.687148D-05
 X = 0.01000   P = 0.000D+00 ELECT =  0.000D+00
   H    =  0.223900D-05     OH   =  0.223900D-05     NA   =  0.251000D-05
   HSO  =  0.251000D-05     MN   =  0.000000D+00     MNO  =  0.000000D+00


TIME =  0.733D+03  TIME STEP SIZE =  0.714E+02   NUMBER OF STEPS =      3
 AVE TIME STEP = 0.242E+02   TIP COND. = 0.298E-03   EXT. METAL POT. = 0.000E+00
 TIP FLUX :  H    = 0.645E-08 OH   = 0.653E-08 NA   = 0.000E+00
             HSO = 0.000E+00 MN   = 0.392E-10 MNO  = 0.000E+00
 X = 0.00000   P = 0.785D+00 ELECT =  0.229D-14
   H    =  0.446739D-06     OH   =  0.113037D-04     NA   =  0.288209D-05
   HSO  =  0.248487D-05     MN   =  0.180313D-05     MNO  =  0.685349D-05
 X = 0.00333   P = 0.785D+00 ELECT = -0.203D-13
   H    =  0.447026D-06     OH   =  0.112963D-04     NA   =  0.287304D-05
   HSO  =  0.249270D-05     MN   =  0.180548D-05     MNO  =  0.685800D-05
 X = 0.00667   P = 0.785D+00 ELECT = -0.205D-13
```

```
   H    =  0.447903D-06     OH   =  0.112742D-04     NA   =  0.284603D-05
   HSO  =  0.251636D-05     MN   =  0.181257D-05     MNO  =  0.687148D-05
 X = 0.01000   P = 0.000D+00 ELECT =  0.000D+00
   H    =  0.223900D-05     OH   =  0.223900D-05     NA   =  0.251000D-05
   HSO  =  0.251000D-05     MN   =  0.000000D+00     MNO  =  0.000000D+00


TIME =  0.979D+03  TIME STEP SIZE =  0.245E+03   NUMBER OF STEPS =      3
 AVE TIME STEP = 0.822E+02   TIP COND. = 0.298E-03   EXT. METAL POT. = 0.000E+00
 TIP FLUX :  H    = 0.645E-08 OH  = 0.653E-08 NA  = 0.000E+00
           HSO = 0.000E+00 MN  = 0.392E-10 MNO = 0.000E+00
 X = 0.00000   P = 0.785D+00 ELECT =  0.229D-14
   H    =  0.446739D-06     OH   =  0.113037D-04     NA   =  0.288209D-05
   HSO  =  0.248487D-05     MN   =  0.180313D-05     MNO  =  0.685349D-05
 X = 0.00333   P = 0.785D+00 ELECT = -0.203D-13
   H    =  0.447026D-06     OH   =  0.112963D-04     NA   =  0.287304D-05
   HSO  =  0.249270D-05     MN   =  0.180548D-05     MNO  =  0.685800D-05
 X = 0.00667   P = 0.785D+00 ELECT = -0.205D-13
   H    =  0.447903D-06     OH   =  0.112742D-04     NA   =  0.284603D-05
   HSO  =  0.251636D-05     MN   =  0.181257D-05     MNO  =  0.687148D-05
 X = 0.01000   P = 0.000D+00 ELECT =  0.000D+00
   H    =  0.223900D-05     OH   =  0.223900D-05     NA   =  0.251000D-05
   HSO  =  0.251000D-05     MN   =  0.000000D+00     MNO  =  0.000000D+00
```

RUN STATISTICS

```
STEP SIZE LAST USED    =, 0.24517E+03
STEP SIZE FOR NEXT     =, 0.24517E+03
CURRENT VALUE OF T     =, 0.97938E+03
TOLERANCE SCALE FACTOR=, 0.00000E+00

REQUIRED RWORK SIZE    =       49064
IWORK SIZE             =         237
NUMBER OF STEPS        =           0
# OF FUNC.- EVALS.     =         439
# OF JACOB.- EVALS     =           2
METHOD ORDER USED      =           1
ORDER FOR NEXT STEP    =           1


ERROR HALT...ISTATE =  1
```